Neural Correlates of Gain Control in Drosophila and Humans

Sultan Ahmed H Alamri

PhD in Cognitive Neuroscience and Neuroimaging

University of York

Psychology

March 2016

Abstract

Previous research has shown that visual sensitivity in human epilepsy patients is abnormal – characterized by increased responses at high contrast levels. These abnormalities have been linked to changes in neuronal gain control. Using animal models to study these changes is a useful approach. In this thesis, we used a steady-state visually evoked potential (SSVEP) technique similar to that used in humans to study photoreceptor-level and neuronal gain control in wild type (w⁻) Drosophila across a range of ages. We then compared these responses to those obtained from Drosophila carrying the *kcc* potassium channel mutation that renders young flies susceptible to light and shock-induced seizures. By taking into account the age and temperature dependence of the mutant (kcc^{DHS1}) flies, we were able to identify increased neural activity that recovers to the normal profile as they get older. We also found that these kcc^{DHS1} flies are hypersensitive to light, particularly when young. These two findings are consistent with the fact that the level of the KCC protein increases with age. In addition, we found that kcc^{DHS1} flies generate high frequency oscillations in their ERGs in response (50 – 100 Hz) to abrupt light onsets and offsets – a phenomenon that might be linked to abnormal changes in the gain control of neuronal feedback circuits.

Studying visual abnormalities in Drosophila can reveal important information but eventually we need to link any visual abnormalities observed in animal models to humans. We therefore, attempted to measure subtle changes in gain control in humans due to adaptation, and at the same time make use of the human mental ability to measure another measure of gain control, attention, using an fMRI technique. Although our data did not show any interaction between adaptation and attention, it suggests that attention in early visual pathways largely affects the level of suppression in non-stimulated regions around the adaptor rather than responses to the probe itself. This is a manipulation that links to our work on adaptation in Drosophila in Chapter 6.

Overall, the results presented in this thesis showed that fly models of epilepsy can be useful for studying changes in visual gain control, and showed that this work might be extended to humans.

Table of Contents

5

List of Figures

9

13

List of Tables

15

16

17

Dedication

I dedicate this humble effort to my sweet and loving father and mother, whose affection, love, encouragement and prays of day and night able me to get such success and honor.

Acknowledgements

The work in this thesis could have not been completed without my supervisors Prof. Alex Wade and Dr. Chris Elliott. They were always reassuring and providing excellent advice and guidance.

I would also like to extend my thanks to Heidi Basler being a member of my thesis advisory panel. I always felt nervous before meetings but they were a great opportunity for personal growth and feedback, and I'm glad to have had your knowledge and advice during the course of my PhD.

The research contained within this thesis could not have been completed without the numerous people who helped me to collect data, design tasks, and pilot the stimuli. Those individuals helped to lift great weights off my shoulders and allow me to focus my efforts towards more pressing matters!

A special mention goes to my wife Nada Alqarni, and my sons Ahmed and Meshal who were always there to provide encouragement and a motivating kick whenever I felt overwhelmed. I would also like to thank my friends for providing that little escape from academia, particularly Mohammed Alharbi, Magbool Alelyani, Ali Alghamdi, Anwar Aljadaani and Swailim Alotawi.

Finally I would like to express my sincere gratitude to the participants. Without their contributions none of this research could have been conducted.

Declaration

I hereby declare that this thesis contains original work completed solely by myself under the supervision of Prof. Alex Wade and Dr. Chris Elliott, with the exception of the experiments presented in **Chapter 6**. These experiments were conducted in collaboration with an MSc student (Jonathon Robinson) who was supervised by supervised by Prof. Alex Wade, Dr. Chris Elliott and myself.

The data reported in **Chapter 4** were accepted for poster publication as:

Wade, A.R., Afsari, F., Alamri, S., Robertson, J., Elliott, C.J.H., 2013. Steady state visually-evoked responses in Drosophila models of neurological disease. J. Vis. 13, P38–P38. doi:10.1167/13.15.73.

The data reported in **Chapter 4** and **Chapter 6** were accepted for poster publication as:

Alamri, S; Wade, A; Robertson, J; Elliott, C., 2014. Steady state visually-evoked responses in Drosophila models of epilepsy. Applied Vision Association Spring Meeting, York, UK 11 April 2014, 2014. . Perception 43, 469–480. doi:10.1068/ava14

The data reported in **Chapter 4**, **Chapter 5** and **Chapter 6** were presented as:

S.A.H. Alamri, A.R. Wade, C.J.H. Elliott. Abnormal steady-state visual responses in a Drosophila model of epilepsy. Poster presented at the Society for Neuroscience, Chicago, USA, 2015.

This work has not previously been presented for an award at this, or any other, university. All sources are acknowledged as References.

1 Chapter 1

1.1 Introduction

Vision is often considered the most important of the five human senses, as 80% of information and knowledge collected from the outside world enters via the visual pathway (Holtzschue, 2011). Vision is stimulated by light, a form of electromagnetic radiation emitted from sources like the sun, electric bulbs, lamps, etc.

A considerable body of literature has described the importance of the retina in facilitating the complex task of pattern recognition and spatial localization performed by the brain, including some early computations on the visual input delivered from the eye. One of these computations is neuronal gain control. Gain control is a key feature present in almost all information processing systems. Such systems are required to control the relationship between the input, which depends on the surrounding environment and thus can vary dramatically, and the output, which is always required to remain within the limited dynamic range of such systems. Some forms of gain control that can be found in man-made devices are the volume control on a radio and the brightness control on a computer monitor. Even though these forms of gain control are not the most exciting technological features, such devices would be rendered useless without them.

Gain control mechanisms have been found to regulate many processes, including hearing (Schneider et al., 2011), olfaction (Finger, 2009) vision (Bex et al., 2007; Bonds, 1991; Busse et al., 2009; Hou et al., 2013; Ohzawa et al., 1982; Wilson and Kim, 1998). In the visual system, gain control appears to occur at all stages of processing. The retina modulates the relationship between light input and neural response. This function is essential to vision, since light intensity can range across more than ten orders of magnitude, while photoreceptors have a limited dynamic range of only two orders of magnitude. The retina uses the rod and cone photoreceptors located in the retina, as well as the pupil, as anatomical solutions to this problem. The rods respond to low light levels (night vision), whereas the cones respond to high light levels (daylight vision). This form of gain control is called light adaptation (also called luminance gain

control). Light adaptation occurs predominantly in the retina and modifies the retinal response to match the local luminance.

Most visual signals do not originate from changes in luminance, but rather, as a response to changes in the *variance* of local luminance, or as it is more commonly called, spatial contrast (Fig. 1-1) (Mante et al., 2005). Gain control is commonly plotted as a contrast response function (CRF) having a typical sigmoidal shape, i.e. weak neural responses at low contrast levels, increasing monotonically with contrast before saturating at high contrast levels (Albrecht and Hamilton, 1982). Two types of gain control mechanisms have been considered as a response to changes in contrast: contrast gain and response gain (Fig. 1-2) (Sclar et al., 1989). The signature of contrast gain modulation is a horizontal shift in the CRF curve. This reflects a change in the neural contrast sensitivity. Another type of gain control, 'response gain' is shown by an increase in neuronal firing in response to increased contrast, reflecting a multiplicative change acting on the output rather than the input.
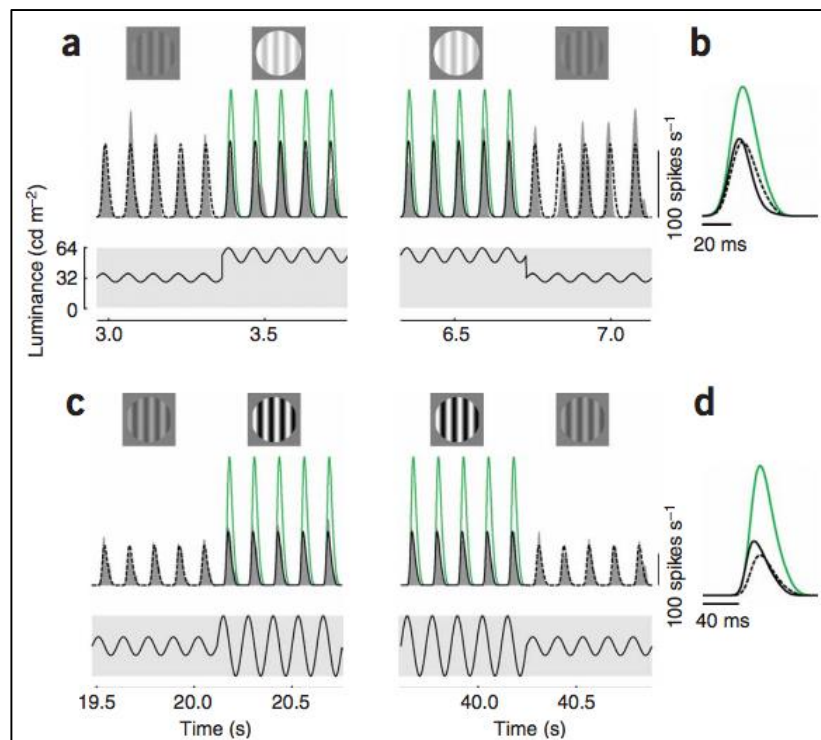
Figure 1-1: The effect of changes in luminance and contrast on the early visual system (LGN). (a) and (b) show the response to drifting gratings of constant contrast and an increase in luminance. (c) and (d) show the response to drifting gratings of constant luminance and an increase in contrast. Note that in (a) and (b), there was no change in the response of the LGN neurons. (c) and (d) show a weak effect from changes in contrast. Low luminance is indicated by the dashed line, high luminance in black and the response expected in the absence of gain control is in green, adopted from Mante et al (2005).
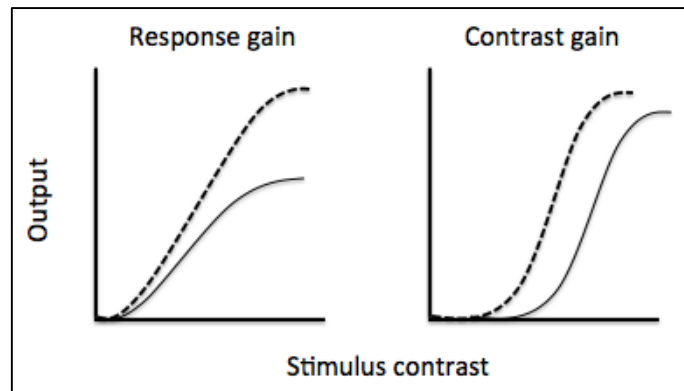
Figure 1-2: The effects of contrast on the contrast response functions. Response gain (left) refers to an increase in the firing with increasing contrast. Contrast gain (right) refers to the horizontal shift of the contrast response function curve.

1.1.1 Contrast gain control (CGC)

Because the visual system is more sensitive to contrast than it is to luminance, neurons continually adjust their sensitivity based on the mean level of contrast present in the visual environment (Priebe and Ferster, 2002). Thus, maintaining the best sensitivity to contrast in the environment is an important task of the visual system. Contrast gain control starts in the retina (Demb, 2002; Shapley and Victor, 1981) and becomes more prominent in the lateral geniculate nucleus (LGN) (Bonin et al., 2005) and the visual cortex (Ohzawa et al., 1982).

Neurons in the visual system must simultaneously process information from multiple sources. Individual neurons provide information about restricted areas of visual space called receptive fields, but can nevertheless be modulated by the visual properties of neighbouring neurons.

An example of this effect is overlay masking (Busse et al., 2009; Tsai et al., 2012), a form of gain control that can rapidly modify neuronal firing, with an approximate response time of 100 milliseconds (Petrov et al., 2005).

1.1.2 Contrast adaptation

In addition to contrast gain control based on the integration of spatial inputs, neurons show an analogous effect in the time domain, when their responses change after a sustained presentation to a stimulus. This temporal aspect of contrast gain control is called contrast adaptation. Single-unit studies on anesthetized cats showed that adaptation to contrast causes a horizontal shift in the CRF curve, recentring it to the contrast of the adapting stimulus (Bonds, 1991; Ohzawa et al., 1982; Sclar et al., 1985). The same effect was also seen in monkey (Sclar et al., 1989) and human studies (Gardner et al., 2005). In general, contrast adaptation allows the alteration of visual sensitivity to match the most recent stimulus conditions (Fig. 1-3), and represents the relatively long-term changes of contrast gain control taking place over seconds to minutes.
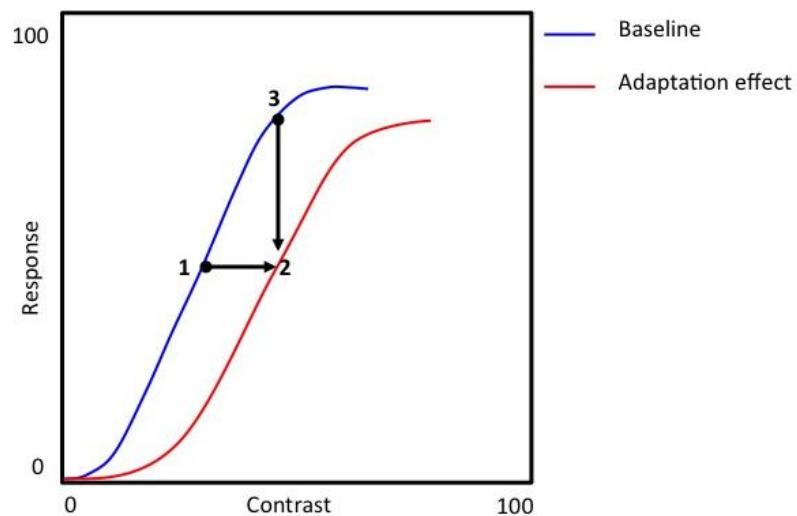
Figure 1-3: The effects of adaptation on the contrast response function. Adaptation affects the neurons in two ways: (1) the CRF is shifted to the right direction (point 1 to 2). (2) Neural response to the mean contrast in the environment is decreased after adaptation (point 3 to 2) but the steepness of the curve at that point is increased. This means that the neuron can discriminate a smaller change in contrast around this mean. Adopted from Pestilli et al. (2007).

1.1.3 Attention

The large amount of information entering the retina at any given time cannot be processed simultaneously due to the brain's limited processing capacity. Attentional mechanisms are required to overcome this problem by allowing the selective processing of incoming stimuli. As such, spatial attention has been shown to influence neural responses in human V1 neurons (Gandhi et al., 1999) as well as in the lateral geniculate nucleus (LGN) (O'Connor et al., 2002). Thus, the directing of one's attention to a particular spatial location activates neural gain control mechanisms (Carrasco et al., 2004). However, the nature of this control has been a subject of considerable debate. Some previous research has indicated that attention acts by increasing neuronal responses multiplicatively via *response gain* mechanisms (Lee and Maunsell, 2010), whereas others (Martínez-Trujillo and Treue, 2002; Reynolds et al., 2000) have shown that attention acts by increasing the effective contrast via *contrast gain* mechanisms.

1.1.4 The normalization model

Divisive normalization is an important neural computation widely used to describe contrast gain control. Normalization models consist of two stages: 1) The receptive field acts as a spatiotemporal filter to generate stimulus selectivity, such as orientation and motion, and 2) non-selective contrast gain control arises from neighbouring neurons (a gain pool). The response of the cells is the result of dividing the input from the first stage by the summed activity of a pool of neurons (the second stage) (Heeger, 1992). Although the normalization model, established in the early 1990s, was first used to explain the non-linearity of neurons in the primary visual

cortex (Albrecht and Geisler, 1991; Carandini et al., 1997; Foley, 1994; Heeger, 1992), it is now believed to operate throughout the visual system. This model offers an explanation for several physiological results, including response saturation at high contrast levels, the rightward shift of the response after prolonged exposure to a stimulus (Ohzawa et al., 1982), cross-orientation suppression (Brouwer and Heeger, 2011), surround-suppression (Tanaka and Ohzawa, 2009), edge detection (Hammett et al., 2003), motion selectivity (Albrecht and Geisler, 1991), suppression in the LGN (Bonin et al., 2005) and modulation of neural responses by attention (Hara et al., 2014; Reynolds and Heeger, 2009).

In recent years, there has been increased interest in the biophysical and cellular mechanisms underlying contrast gain control (Beaudoin et al., 2007; Carandini et al., 2002; Katzner et al., 2011). However, due to the complexity of the underlying circuits, these processes have been difficult to resolve. Various mechanisms have been studied to account for the changes in contrast response functions, including feedforward and feedback connections (Smith et al., 2006), shunting inhibition (Mitchell and Silver, 2003; Prescott and De Koninck, 2003), synaptic depression (Abbott et al., 1997) and synaptic noise (Chance et al., 2002; Prescott and De Koninck, 2003).

1.1.5 Clinical relevance

Gain control may have clinical relevance, as CRFs have been found to be abnormal in a host of conditions, including epilepsy (Porciatti et al., 2000; Tsai et al., 2011), Parkinson's disease (Afsari et al., 2014), schizophrenia (Dakin et al., 2005; Yoon et al., 2010), amblyopia (Heimel et al., 2010), aging (Betts et al., 2009), depression (Bubl et al., 2009) and likely, autism (Smith and Matson, 2010; Tuchman and Rapin, 2002). Abnormalities in visual gain control may therefore be useful both as biomarkers for disease and as a way of studying the neuronal deficits causing these diseases. Here we will focus on the relationship between epilepsy and visual gain control.

1.1.5.1   Epilepsy

Epilepsy is a prevalent neurological disorder, affecting more than 65 million people around the world (Ngugi et al., 2010); the majority of these people (approximately 80%) live in the developing countries (Mbuba and Newton, 2009). In the United States, epilepsy is more common than Parkinson's disease, autism, multiple sclerosis, and cerebral palsy combined (Hirtz et al., 2007).

Epileptic patients are at risk of death from a number of problems. The first problem is status epilepticus (SE) (Boggs, 2004). Individuals with this life threatening condition suffer from a continuous seizure. The second problem is suicide as a consequence of depression (Adelöw et al., 2012). The third issue is serious injury resulted from seizures (Bowman et al., 2010). The fourth problem is sudden, unexpected death in epilepsy (SUDEP) commonly caused by respiratory failure or cardiac arrest (Shorvon and Tomson, 2011). Moreover, epileptic patients are susceptible to specific diseases, such as anxiety, migraine and infertility. In addition, attention deficit and hyperactivity disorders affect children with epilepsy more than normal children (Plioplys et al., 2007). Finally, evidence has shown that children with epilepsy are more prone to autism and severe cognitive impairment than others (Gabis et al., 2005).

1.1.5.1.1   Epidemiology

There are two main types of measures to describe the epidemiology of epilepsy: prevalence and incidence. The worldwide prevalence is variable depending on the socioeconomic status (SES), and estimated to be 5 - 10 per 1000. The SES is strongly associated with epilepsy prevalence (Steer et al., 2014), in which epilepsy is more common in areas of high SES deprivation. This relationship is not well understood. Incidence, which is the occurrence of new cases, is approximately 50 per 100,000 per year (Sander, 2003).

1.1.5.1.2   Etiology

Most forms of epilepsy are known to occur spontaneously. However, some epilepsy syndromes require a specific precipitant or trigger to induce seizures. This type of epilepsy is known as reflex epilepsy. For instance, people with primary reading epilepsy have seizures induced by reading, whereas patients with photosensitive epilepsy have seizures triggered by

flashing lights. In addition, other triggers or precipitants can induce epileptic seizures in patients who are prone to spontaneous seizures. For instance, children with childhood absence epilepsy can have seizures triggered by hyperventilation. In actuality, both hyperventilation and flashing lights are used in clinical EEG to induce seizures, and thus, help in the diagnosis. Other triggers can assist the progress of, rather than induce, seizures. These precipitants include: emotional stress, heat stress, alcohol, sleeps deprivation and febrile illness (Frucht et al., 2000). Moreover, menstrual cycles in epileptic women can induce seizures. Catamenial epilepsy involves seizures associated with the menstrual cycle (Herzog et al., 2004).

The causes of epilepsy can be divided into four main groups:

- Idiopathic epilepsy: this is defined as epilepsy caused predominately by genetics, and is not associated with significant neuroanatomical or neuropathological changes.
- Symptomatic epilepsy: this is defined as epilepsy of either an acquired or genetic origin, and is associated with neuroanatomical or neuropathological abnormality.
- Provoked epilepsy: this is defined as epilepsy caused predominately by environmental factors. The reflex epilepsies (which are usually genetic) are part of this category.
- Cryptogenic epilepsy: this is defined as epilepsy with an expected symptomatic nature, where the cause has not been identified. Although the number of such cases is decreasing, cryptogenic epilepsy is still an important group, accounting for at least 40% of adults (Shorvon, 2011). This is attributed to either insufficient investigation or lack of findings.

Clearly, there are some limitations with this categorization, owing to the fact that epilepsy is often multi-factorial. Even in the presence of a main cause, other causes (genetic or environmental) can play a role in its clinical manifestations. The range of etiology changes in different age groups, patient groups and geographical location. Generally, the most common causes of childhood epilepsy are congenital and perinatal conditions, while in adult life, epilepsy is largely caused by external non-genetic causes, but this distinction is not at all absolute. Vascular diseases are the most common cause in late adult life. In particular regions of the world, endemic infections are major causes. These include: tuberculosis (TB), cysticerosis, human immunodeficiency virus (HIV) and viral diseases (Shorvon et al., 2009).

1.1.5.1.3 Idiopathic epilepsy

Heredity plays an important role in the generation of epilepsy. Idiopathic epilepsies are known to have a strong genetic basis (polygenic or oligogenic). Gene expression can be inconstant and affected by developmental and environmental factors, and epilepsies are usually age dependent. Single gene disorders form approximately 1-2% of all epilepsies, and there are usually additional neurological characteristics (Shorvon, 2011).

Idiopathic epilepsies result mainly from mutations in the genes coding for ion channels – both voltage-gated ion channels, which are important for the generation and control of action potentials, and ligand-gated ion channels, which are predominantly associated with synaptic transmission. Studies have identified mutations in specific types of channels leading to idiopathic epilepsy, including voltage-gated potassium (Biervert et al., 1998; Charlier et al., 1998), sodium (Escayg et al., 2000; Wallace et al., 1998) and chloride (Haug et al., 2003) channels, as well as ligand-gated receptors such as $GABA_A$ (Baulac et al., 2001; Wallace et al., 2001).

Ion channels are directly involved in both membrane excitability and neurotransmitter release. In principle, seizures can result from either an increase in excitatory stimuli or an impairment of inhibitory mechanisms. For example, the mechanism of inhibition can be disturbed directly via a mutation in the $GABA_A$ receptor, or indirectly through a mutation in a voltage-gated chloride channel. The voltage-gated chloride channel is important for $GABA_A$'s inhibitory response, as it has a fundamental role in the chloride efflux pathway and thus the generation of action potential. Mutations in the chloride channel have been reported to be involved in childhood absence epilepsy (CAE), juvenile absence epilepsy (JAE), juvenile myoclonic epilepsy (JME) and epilepsy with grand mal seizures on awakening (EGMA) (Haug et al., 2003). In addition, drugs that increase GABA function, such as benzodiazepines, phenobarbital and vigabatrin, effectively treat nearly all types of seizures (Wong, 2010).

1.1.5.1.4   Brain development and epilepsy

It is essential to consider developmental changes in the brain during all stages of life to be able to understand the neurobiology of epilepsies, both idiopathic and symptomatic. This is due to the fact that a number of epilepsies have particular onset and offset ages. Generally, the immature brain is more prone to seizures than the mature brain. Changing density of different neurotransmitter receptors and synaptic pruning, transform the activity of $GABA_A$ receptor from excitatory in the immature brain to inhibitory in the adult brain, as well as changes in the glutamate receptors (their structures and functions). As mentioned before, epilepsies are usually age dependent. This indicates that the abnormal genes are particularly critical when the epilepsy syndrome is active, or/and that the brain is more prone to the abnormal genes at that time. Certain syndromes of idiopathic epilepsy have a featured onset in the neonatal period, other syndromes in the infantile or late childhood, and some in adolescence or even adult life.

1.1.6   Gain control and epilepsy

Gain control has been described as a canonical neural computation that operates throughout the brain to maintain the input-output relationships of neurons (Carandini and Heeger, 2012). In addition, any imbalance between neural excitation and inhibition may impact gain control (Morrone et al., 1987). Thus, one might expect that gain control could inform the nature of hyperexcitability in patients with epilepsy. Some forms of epilepsy have been shown to be caused by abnormal gain control, e.g. photosensitive epilepsy (Porciatti et al., 2000). Also, patients with other forms of epilepsy, such as idiopathic generalized epilepsy, show abnormal gain control as well (Tsai et al., 2011). In both studies, observed changes in gain control were characterized by a lack of response saturation at high contrast levels. These changes were best described by a combination of contrast gain and response gain mechanisms (Fig. 1-4), and were thought to relate to reduced GABAergic inhibition by surrounding neurons (i.e. the gain pool) (Tsai et al., 2011).
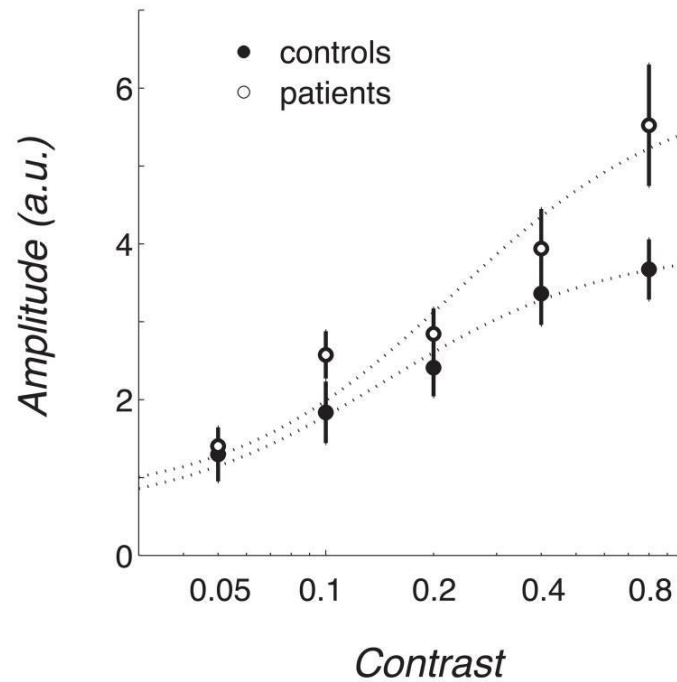
Figure 1-4: Contrast response functions (CRFs) of patients with idiopathic generalized epilepsy (open circles) and control subjects (filled circles). IGE patients show lack of response saturation at the high contrast levels, adopted from Tsai et al. (2011).

Despite an enormous amount of interest in contrast gain control, there are still some aspects of it that remain poorly understood. One major aim of this thesis is to investigate further into the underlying mechanisms of contrast gain control and its relationship to epilepsy, in particular. To do this, we used a 'steady state' electrophysiological technique similar to that employed by other researchers studying epilepsy in humans (Porciatti et al., 2000; Tsai et al., 2011). Since both masking and contrast adaptation depend on contrast gain control, we performed our experiments by looking at contrast response functions (CRFs) in Drosophila models carrying mutations in the gene encoding the voltage-gated chloride channel, *kcc*.

Animals and Drosophila share hundreds of common genetic diseases, and as a consequence, animals can be used as models to study human diseases. The main purpose of using fly models is to examine the effects of specific genes and then manipulate the effects of those genes both

genetically and pharmacologically. Using fly models allow us to measure the beneficial and harmful effects of a specific experiment before it can be tested on human patients.

1.2 Drosophila as a model of disease

Following the discovery of the white eye mutant by Thomas Morgan (Morgan, 1910), *Drosophila melanogaster*, also known as the fruit fly, has been heavily used in genetic research. There are many important features of the insect that make it a very attractive model for studying human disease. The fruit fly genome has been entirely sequenced, and encodes about 14,000 genes on four chromosomes (Adams et al., 2000), with the fourth chromosome often ignored because of its small size. It is estimated that approximately 77% of genes involved in human diseases have a fruit fly gene counterpart (Reiter et al., 2001). Furthermore, the expression of human genes into flies often causes phenotypes that resemble human diseases. Another advantage is the rapid life cycle of the fly; it only takes about 12 days at 25 °C for a single fertile mating pair to produce hundreds of eggs (Powell, 1997). Thus fruit fly research progresses rapidly (Fig 1-5). In addition, the fly genome has low redundancy; mutations in a single gene often lead to a phenotype, a situation that is not true in other animal models. Finally, the availability of powerful tools for genetic manipulations, e.g. the GAL4 and UAS system (Brand and Perrimon, 1993), enables the selective expression of transgenes in a desired set of neurons.
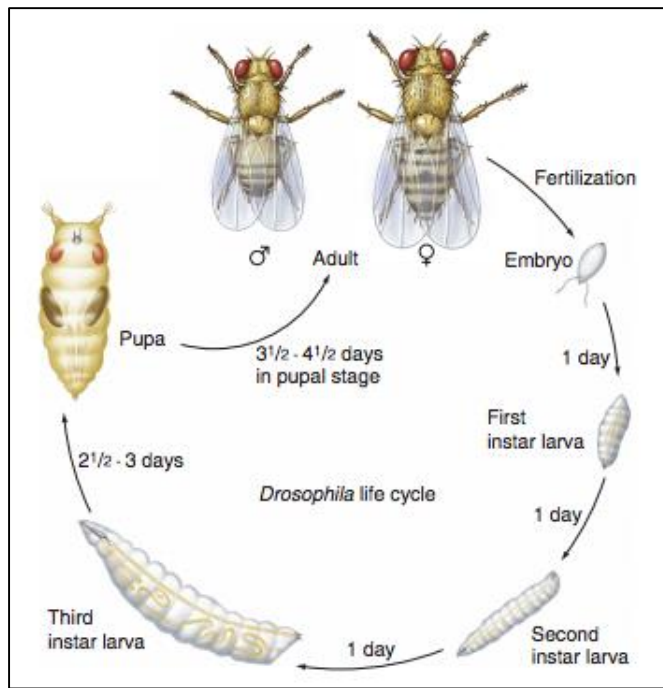
Figure 1-5: The Drosophila life cycle. Adopted from Powell (1997).

1.2.1 The GAL4-UAS system

As mentioned before, one of the major advantages of using Drosophila in genetic research is the creation of the GAL4-UAS system for targeted gene expression by Brand and Perrimon in 1993. The GAL4 part of the system encodes a protein of 881 amino acids, identified as a regulator of genes. GAL4 activates gene transcription by directly binding to an UAS (upstream activation sequence) site. In this system, expression of the gene of interest, 'responder', is governed by the presence of the USA element. In order to activate the transcription of the responder, flies carrying GAL4 in a particular set of cells, called the driver, are mated with the flies carrying the UAS-responder (Fig. 1-6) (Duffy, 2002). The expression patterns of thousands of GAL4 constructs are now categorised meaning that Drosophila geneticists can express almost any gene in a well-defined cell- or tissue-specific manner.
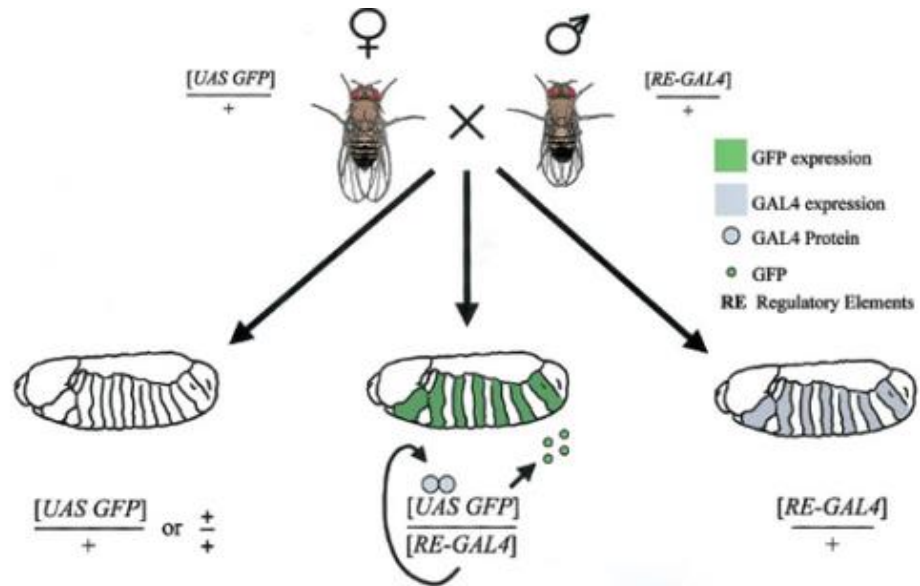
Figure 1-6: The GAL5-UAS system in Drosophila. *A* female carrying a UAS-responder (GFP) is mated with a male carrying the GAL4 driver. The resulting progeny that only expresses the UAS and GAL4 would demonstrate the GFP in the cells. Adopted from Duffy (2002).

1.3 Drosophila Visual System

1.3.1 Fly eyes

The visual system of Drosophila (Fig. 1-7) is comprised of three simple eyes (ocelli) located in the front of the head, compound eyes, and four visual ganglia termed the lamina, the medulla, the lobula and the lobula plate. Each one of the three simple eyes consists of a simple lens and a light-sensitive layer of cells (Shorrocks, 1972). The role of the ocelli is not for image formation but for light detection (Montell, 2012), and will not be discussed in detail here.
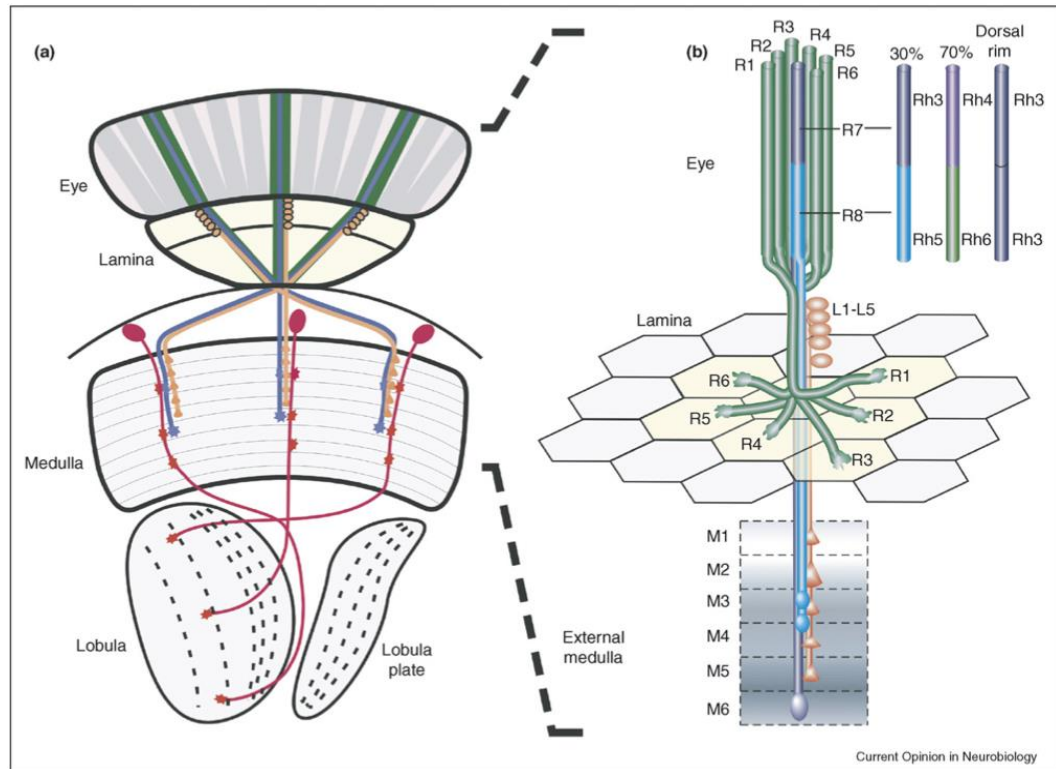
Figure 1-7: The visual system of fly. (a) Cross sectional anatomy showing the positions of the eye, lamina, medulla and lobula. (b) Connections of the neural photoreceptor cells (R1-R8) showing their projections to different sites in the lamina and medulla. Adopted from Ting and Lee (2007).

1.3.2 Receptors

The compound eyes are composed of between 750-800 units called ommatidia. Each ommatidium possesses its own lens and contains a collection of eight neural photoreceptor cells (labelled 'R' 1 through 8) that are responsible for light signal transduction. The ommatidium also contains non-neural supporting cells and pigment cells (Shorrocks, 1972). The pigment cells produce the red pigment (also called drosopterin) that optically isolates each ommatidium from its neighbour. This red pigment stops the light from entering through the sides of the ommatidium and therefore enhances visual acuity. The brown pigment (also called ommochrome) is also produced by the pigment cells. Eye colour is determined by the amount

and distributions of the two pigments. It is worth noting that the white-eyed mutants typically used as background in Drosophila research do not express the red and brown pigments (Offner, 1996).

Each individual ommatidium appears on the surface of the eye as a single dome, called a facet, and these ommatidia are arranged in a hexagonal array so that the surface of the eye contains the highest number of facets. Ommatidia are covered by crystalline corneal lenses, which focus light onto the light-sensitive structure underneath (Fig. 1-8) (Belusic, 2011a; Kumar, 2001). Photoreceptors have three distinct regions: the light-sensitive structure (rhabdomere), the soma, and the axon. The rhabdomere consists of approximately 30,000 microvilli. The microvillar membrane (the membrane of the rhabdomere) is filled with approximately 1000 visual pigment molecules termed rhodopsin, which are responsible for light absorption (Fig. 1-9) (Belusic, 2011b; Kumar, 2001; Ting and Lee, 2007). Photoreceptor neurons can express a variety of rhodopsin genes but only one gene is expressed in each cell. The outer photoreceptor neurons, R1-R6, express rhodopsin1 (Rh1), which absorbs maximally in the blue region of the visible spectrum (480 nm). R1-R6 photoreceptors, which are required for motion detection and image formation (Salcedo et al., 1999), have rod-like properties and thus function well in dim light (Cook and Desplan, 2001). The inner photoreceptor neurons, R7 and R8, have more complex expression of rhodopsin. R7 (positioned distally in the ommatidium) expresses either Rh3 or Rh4, which absorb maximally at 331 and 355 nm, respectively. R8 (positioned proximally in the ommatidium) expresses either the blue-sensitive Rh5 or the green-sensitive Rh6, absorbing at 442 and 515 nm, respectively (Salcedo et al., 1999). Approximately 30% of central ommatidia have R7 that expresses Rh3 and R8 that expresses Rh5. The remaining 70% have R7 that expresses Rh4 and R8 that expresses Rh6. These two types of ommatidia are randomly distributed throughout the eye. It is likely that the presence and distribution of these two subclasses allow the system to achieve proper colour perception (Cook and Desplan, 2001). Finally, Rh2 is another UV-sensitive rhodopsin and is expressed in the ocelli (Salcedo et al., 1999).

The content of rhodopsin in the Drosophila eye depends greatly on the amount of carotenoids present in their diet. The elimination of carotenoids can result in rhodopsin reduction in the eyes

(Goldsmith et al., 1964). In contrast, large amounts of carotenoid in the feeding media increase the sensitivity of R1-R6 in the ultra-violet range.
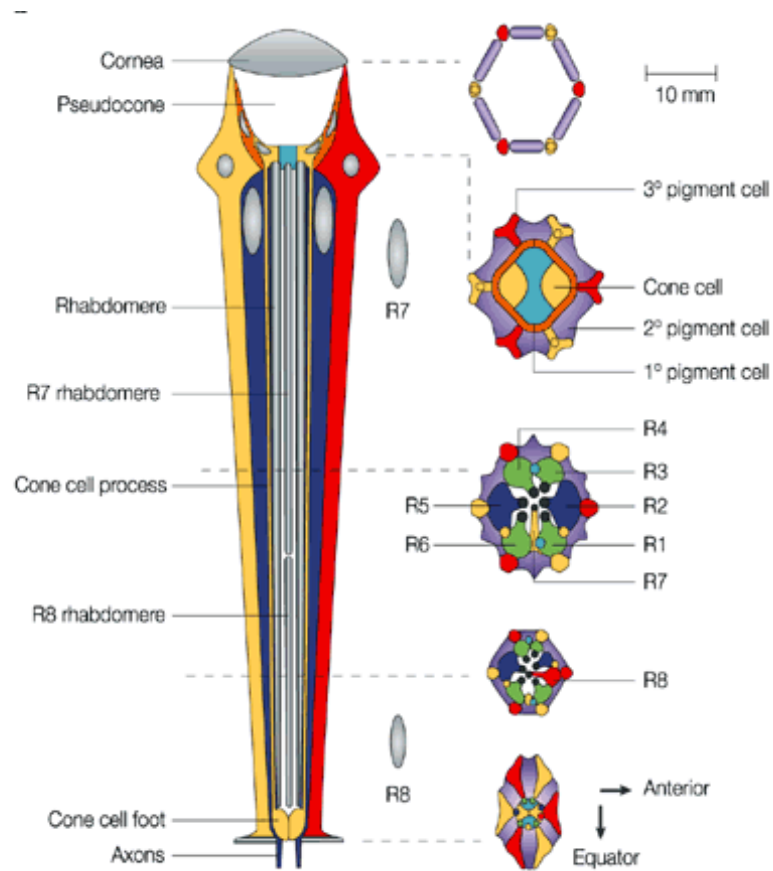
Figure 1-8: The Drosophila ommatidium. Each individual ommatidium appears on the surface of the eye as a single dome, called a facet. Crystalline corneal lenses cover ommatidia. Underneath the cornea are the inner photoreceptors (R1-R6) and the outer photoreceptors (R7-R8), adopted from Kumar (2001).
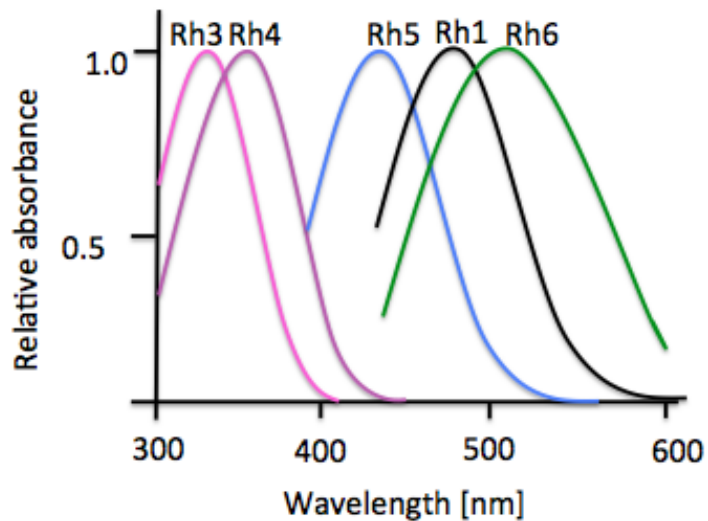
Figure 1-9: Relative absorbance of photoreceptors (R1-R6: Rh1), (R7&R8: Rh3, Rh4, Rh5 and Rh6), adopted from Belusic (2011). For comparison, the human eye is sensitive between approximately 400 to 700nm.

1.3.3 Photo-transduction

Phototransduction is the process by which light is converted into electrical signals by the photoreceptors in the retina, a process occurring via rhodopsin, a G-protein coupled receptor containing the chromophore 11-cis 3-hydroxyretinal. When the chromophore is struck by a photon, 11-cis 3-hydroxyretinal undergoes photoisomerisation to all-trans-retinal. This conformational change creates an activated form of rhodopsin − metarhodopsin − and subsequently activates a G-protein isoform, G_α, which then activates a phospholipase C isoform (PLCβ4). This leads to the opening of the Ca^{2+}-permeable channels TRP and TRPL, and subsequently, to depolarization (Hardie and Raghu, 2001).

Phototransduction in the fruit fly is, to some extent, similar to that of humans. Shared functional attributes include low dark noise (the spontaneous fluctuations in electrical signal in the absence of light), mediation by graded potential, and the presence of light adaption mechanisms. However, there are also some differences underlying the phototransduction mechanism between humans and flies. First, fruit fly photoreceptors *depolarize* because the

transduction channels open in response to light, whereas in human photoreceptors, the channels close, leading to *hyperpolarization*. Second, fruit fly phototransduction, which possesses the fastest known G-protein signalling pathways, is ten times faster than that of humans. Finally, human rods saturate rapidly as light intensity increases, limiting their ability to adapt, whereas fruit fly photoreceptors can adapt over the entire environmental range, up to 10^6 photons per second (Hardie and Raghu, 2001).

1.3.4 The fly eye pigmentation

Eye pigmentation in Drosophila is influenced by a number of different genes. Mutations in these genes will result in altered eye color. Pigmentation of the Drosophila eye is due to mixing two pigments: drosopterins and ommachromes, in appropriate proportion in the pigment cells of the eye. Drosopterins are red pigments synthesized from guanine. Ommochromes are brown pigments synthesized from tryptophan. The pigment precursors are transported into the pigment cells by the so-called 'ABC transporter' system encoded by three genes, white (*w*), scarlet (*st*) and brown (*bw*). The white and scarlet genes work together to produce tryptophan transporter, and the white and brown genes together to produce guanine transporter (Mackenzie et al., 1999). For example, knocking out the brown gene (encoding drosopterins) with a mutation results in the inability of the fly to produce the red pigment, and thus the fly will have brown eyes (Fig. 10). Similarly, knocking out the scarlet gene (encoding ommochromes) results in the inability of the fly to produce the brown pigment, and thus the fly will have red eyes.
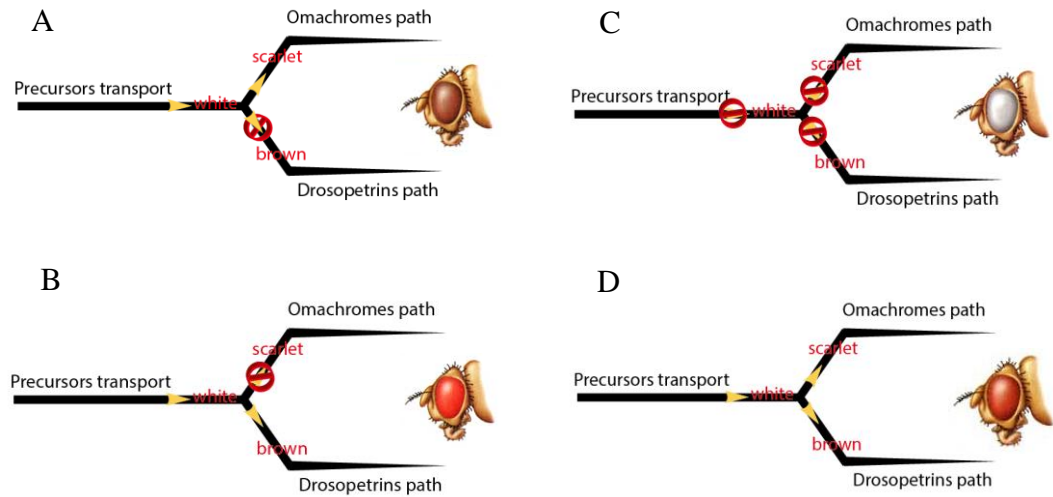
Figure 1-10: The fly eye pigmentation.

1.3.5 Central Processing

1.3.5.1 Anatomy

After photoreceptor transduction, the neural signal is conveyed in the optic lobes. The first optic lobe following the retina is the lamina. Besides the photoreceptor axons, the lamina consists of amacrine cells (Lai), the feed-forward monopolar cells, L1-L5, the two GABAergic feedback cells, C2 and C3, and the functionally mysterious T1 cell type (Fig. 1-11) (Tuthill et al., 2013). The outer photoreceptors (R1-R6) from different ommatidia synapse directly on L1-L3 neurons in a single cartridge. Owing to the curvature of the compound eye that matches the diffraction of the lens, six outer photoreceptors from six neighbouring ommatidia detect light from the same point in space and project their signals to the same laminar cartridge (Fig. 1-12) (Morante and Desplan, 2005; Ting and Lee, 2007). This arrangement of neural superposition increases the signal to noise ratio of phototransduction and thus improves visual acuity (Sanes and Zipursky, 2010).

The next component of the Drosophila visual system is the medulla, which is divided into 10 layers, M1-M10. The inner photoreceptors (R7-R8) and L1-L5 form synapses in one or a few of the outer layers (M1-M6). To maintain retinotopic mapping of visual information in the

40

higher visual areas, connections from R7 and R8 of a single ommatidium, and lamina neurons L1-l5 from a single cartridge, are restricted to a single medullar column (Sanes and Zipursky, 2010). Since the inner photoreceptors, which are important for colour vision, project to the medulla, it is thought that the medulla is likely to be involved in the processing of colour perception (Morante and Desplan, 2008).
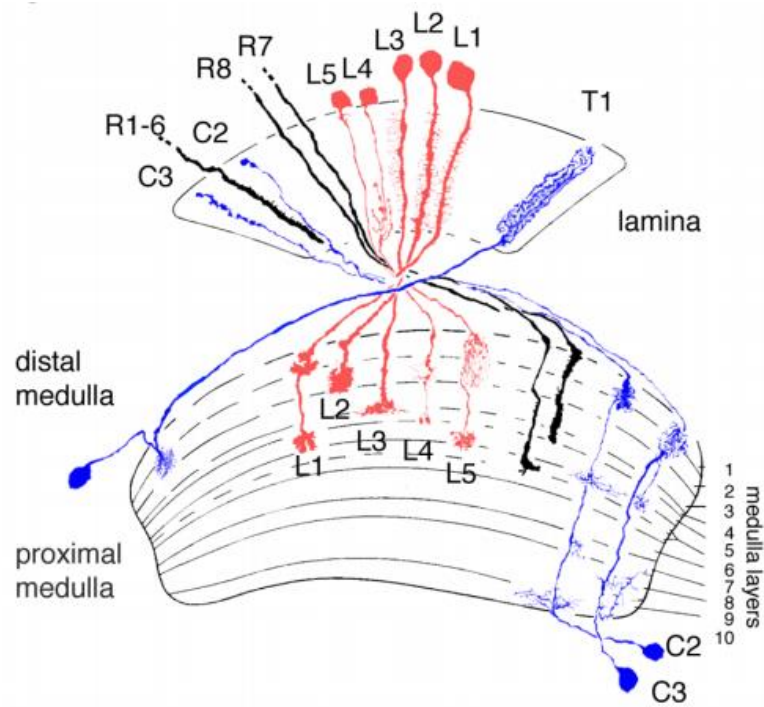
Figure 1-11: The lamina and medulla of the Drosophila visual system. The laminar output neurons L1-L5 are shown in red, and the feedback neurons C2, C3 and T1 are shown in blue. The photoreceptor axons are shown in black. Note that the cell bodies of C2, C3 and T1 are located in the medulla and send their axons back to the lamina, adopted from Tuthill et al. (2013).
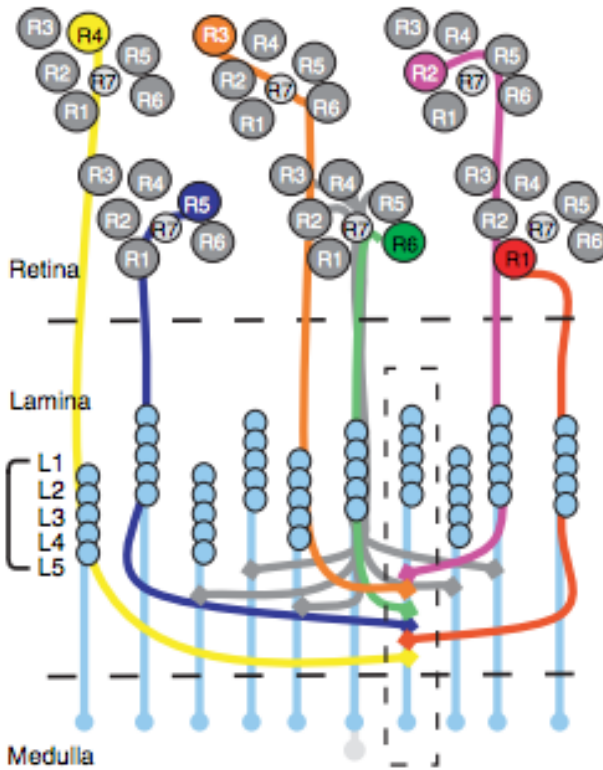
Figure 1-12: Neural superposition: The six outer photoreceptors from six neighboring ommatidia share the same visual field and project to the same laminar cartridge, adopted from Morante and Desplan (2005).

1.3.6 Electrical signaling in the nervous system in humans and flies

The function of the nervous system is based on the balance between synaptic excitation and inhibition. GABA and glycine are the primary inhibitory neurotransmitters in the adult central nervous system, while glutamate is the primary excitatory neurotransmitter. Glutamate meditates synaptic excitation by opening ionotropic glutamate receptors, which are channels of high sodium-selective conductance. This leads to an inward sodium current and hence to a depolarization of the postsynaptic membrane. In contrast, GABA and glycine mediate synaptic inhibition by opening of ligand-gated anion channels. Depending of the intracellular concentration of chloride in the particular cell, GABA and glycine can lead to a hyperpolarization or a depolarization of the cell. When the intracellular chloride concentration

42

is below or at the equilibrium, GABA and glycine will result in synaptic inhibition. However, it is important to note that when the chloride concentration is above equilibrium, GABA and glycine will be excitatory. Therefore, changing the intracellular concentration of chloride provides a way to control GABA and glycine.

In the embryonic and early postnatal development, the intracellular chloride concentration is above equilibrium and therefore both GABA and glutamate are mostly excitatory. It is believed that the excitatory GABA actions during these times are important for the development of the nervous system, including neurogenesis and synaptogenesis, through the activation of voltage-gated calcium channels (VGCCs) (Cherubini et al., 1991; Owens et al., 1996). During the CNS maturation, there is a decrease in the chloride concentration, which is eventually below equilibrium. Thus, opening of $GABA_A$ or glycine receptors results in an inflow of Cl^- and an inhibitory effect. The essential players in this phenomenon are probably members of the cation-chloride cotransporter gene family.

1.3.6.1   GABA and GABA receptors

Gamma-aminobutyric acid (GABA) is the primary inhibitory neurotransmitter in the brain. Decreased GABA activity can cause several disorders including epilepsy, Parkinson's disease, anxiety and Huntington's disease (Bettler et al., 2004). In Drosophila, GABA plays a role in a number of processes including vision (Raghu et al., 2013).

GABA is synthesized in cells containing glutamic acid decarboxylase (GAD), an enzyme that converts glutamate to GABA. Increased GABA levels in the brain inactivate GAD and subsequently GABA synthesis is reduced. After the release of GABA into the synaptic cleft, it binds to specific receptors in the postsynaptic membrane. Different GABA transporters (GATs) in both neurons are responsible for the reuptake of GABA. There are also $GABA_B$ receptors found on the presynaptic membrane that act as feedback regulators (Squire, 2008).

There are two types of GABA receptors, the ionotropic receptor ($GABA_A$) and metabotropic receptors ($GABA_B$). Ionotropic GABA receptors ($GABA_A$), the main mediator of inhibitory synaptic transmissions, are abundant in both vertebrate and invertebrate nervous systems. In Drosophila, GABA is exclusively found in the central nervous system (Enell et al., 2007). When

43

GABA binds to these receptors, a conformational change will occur causing chloride ions to flow into the cell, leading to hyperpolarization of the postsynaptic membrane. Vertebrates have two main classes of ionotropic GABA receptors, $GABA_A$ and $GABA_C$. $GABA_A$ receptors are widely spread in the central nervous system. Unlike $GABA_C$ receptors, $GABA_A$ receptors are antagonized by bicuculline. Ionotropic GABA receptors are composed of five subunits; α, β, γ, δ and ρ. $GABA_A$ receptors are composed of α, β, γ and δ subunits, whereas $GABA_C$ receptors are composed of ρ subunits (Hosie et al., 1997). Nowadays, $GABA_C$ receptors are described as a variant within the $GABA_A$ subunit family and designated as the ρ subfamily of the $GABA_A$ receptors ($GABA_A$- ρ) (Enell et al., 2007).

To date, only three subunits have been identified in Drosophila; RDL, GRD and LCCH3, and these three subunits are encoded by the three genes: *Rdl* (resistant to dieldrin) (Ffrench-Constant and Roush, 1991), *Grd* (GABA- and glycine-like receptor of Drosophila) (Harvey et al., 1994) and *Lcch3* (ligand-gated chloride channel homologue 3) (Henderson et al., 1993), respectively. RDL is the most studied subunit because it is considered to be a suitable model of ionotropic GABA receptors and for its role in insecticide resistance. RDL has been found throughout the central nervous system at both the synapses and the neuronal cell bodies (Buckingham et al., 2005).

The metabotropic receptors are indirectly linked with ion channels through a signal transduction mechanism, often G-protein. Three subtypes of G-protein-coupled $GABA_B$ receptors were identified in Drosophila. However, only two subtypes have been identified in vertebrates (Bettler et al., 2004).

1.3.6.2 Cation-Chloride Cotransporters (CCCs)

Electrical signaling in the nervous system is based on two types of molecules, ion channels and ion transporters. Ion channels are used to move ions down their concentration gradient (from high concentration to low concentration). In contrast, ion transporters move ions against their concentration gradient (from low concentration to high concentration). This operation requires energy, supplied by ATP, which results in a conformational change in the pump and pushes the ions to the other side of the membrane (Gadsby, 2009).

CCCs are expressed in all organs and hence play many roles in both non-neuronal and neuronal cells. In the non-neuronal cells, for example, they are crucial for blood pressure regulation (Flatman, 2008) The main focus here will be on the neuronal CCCs, especially potassium chloride (K-Cl) cotransporters (KCC2), and only some basic aspects of the other members of CCCs will be touched upon.

In vertebrate, the CCC family comprises nine members encoded by the genes *Slc12a1-9.* Two members are Na-K-Cl cotransporters, NKCC1 and NKCC2 encoded by *Slc12a2* and *Slc12a1,* respectively, one is Na-Cl (NCC) cotransporter encoded by *Slc12a3,* and four are K-Cl cotransporters (KCC1-4), encoded by *Slc12a4-7.* The remaining two members, CIPI encoded by *Slc12a8 and* CCC9 encoded by *Slc12a9,* have not been described yet (Blaesse et al., 2009). NKCC and NCC are mainly expressed in the kidney (Clayton et al., 1998), while all other CCCs are expressed in the central nervous system (CNS) (Kaila et al., 2014).

KCC2, which is encoded by the gene *Slc12a5,* is exclusively expressed in the central nervous system (CNS) (Williams et al., 1999). KCC2 is the primary chloride extruder to promote fast postsynaptic inhibition in the brain (Kahle KT et al., 2014; Kaila et al., 2014). The decrease in KCC2 levels in model organisms bring about neuronal hyperexcitability (Hekmat-Scafe et al., 2006; Hübner et al., 2001; Tanis et al., 2009). KCC2 down-regulation has been shown to be involved in some neurological diseases featuring GABAergic disinhibition (Kahle et al., 2008). Complete loss of *kcc2* in knockout mice is lethal, suggesting this is an essential gene (Lee et al., 2005).

Under normal conditions, the opening of GABA$_A$ receptors allows chloride ions to flow into the intracellular space, causing hyperpolarization and thus inhibiting postsynaptic neurons from firing (Rivera et al., 1999). However, when GABA$_A$ receptors and glycine receptors are stimulated during embryonic development (Ben-Ari, 2002), or in certain pathophysiological conditions (e.g. epilepsy) (Cohen et al., 2002), chloride ions flow out the cells. This effect is due to low KCC2 levels that result in a higher intracellular concentration of chloride, making the internal environment less negative (more depolarized) (Payne et al., 2003) (Fig. 1-13).

45
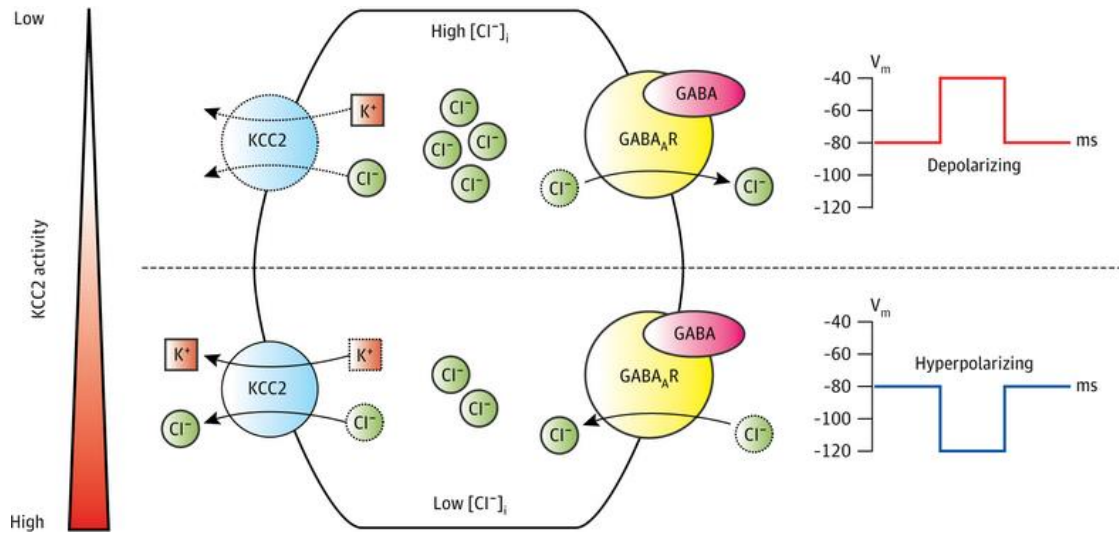
Figure 1-13: The level of KCC2 controls the excitability of neurons. When the level of KCC2 is high, the opening of GABA$_A$ receptors allows chloride ions to flow into the intracellular space, causing hyperpolarization. However, when KCC2 level is low, chloride ions flow out the cell, causing depolarization. Adopted from Kahle KT et al. (2014).

1.4 Drosophila as a model of epilepsy

Fly models of human epilepsy recapitulate several features of the human disease: Firstly, seizure thresholds, which are the minimum amount of electrical energy necessary to generate a generalized seizure, are present in both species and these can be modulated by several different types of mutations. In addition, Electroconvulsive shock treatment (ECT) raises the seizure threshold. The significance of using this model is supported by the fact that seizures can spread through the central nervous system (CNS) and can be spatially segregated into particular areas of the CNS (Pandey and Nichols, 2011). Furthermore, seizure thresholds can be raised using antiepileptic drugs (AEDs), such as sodium valproate, phenytoin, gabapentin, and potassium bromide. Finally, mutations in the sodium channels can suppress seizures (Kuebler et al., 2001; Kuebler and Tanouye, 2002, 2000; Reynolds et al., 2004; Song and Tanouye, 2008; Tan et al., 2004).

Transient electrical shocks delivered to the Drosophila brain can elicit seizure-like activity (Lee and Wu, 2002). This, along with excellent genetic control and relatively simple neurophysiology, makes fruit flies an attractive model for studying seizure disorders. Since epilepsy causes visual gain control abnormalities in humans (Porciatti et al., 2000; Tsai et al., 2011), one might expect to see the same effect in Drosophila models of epilepsy. This would give us the opportunity to examine genetic changes that give rise to altered visual processing. Furthermore, once the visual deficit is identified, these genetic models can be used to test potential therapeutic treatments.

The gene *kcc*, which is homologous to the mammalian *kcc2*, encodes the K+/Cl- co-transporter in *Drosophila melanogaster* (Hekmat-Scafe et al., 2006a). A *kcc* mutation was identified by Hekmat-Scafe et al. (2006) on the second chromosome. Drosophila *kcc* mutants are more sensitive to seizure-inducing stimuli, e.g. being banged on a table ('bang sensitive') or illuminated with a bright light source. The seizure susceptibility of the Drosophila *kcc* mutants shows an age and temperature dependence, mimicking some human chloride co-transporter–based juvenile epilepsies (Haug et al., 2003; Renganathan and Delanty, 2003).

1.4.1 *kcc* mutation

Mutations of a number of genes in Drosophila result in a distinct seizure behavior during mechanical stimulation (banging). Mutants that show seizure and paralysis, well known as bang-sensitive mutants, including *bang sensitive (bas), bang-sensless (bss), easily-shocked* (Ganetzky and Wu, 1982) and *kazachoc (kcc)* , provide valuable model systems for research into the neural basis of a seizure behavior. Drosophila bang-sensitive mutants exhibit seizure and paralysis following a mechanical or electrical shock. This is followed by a refractory period, during which the mutants are no longer sensitive to mechanical disturbances (Lee and Wu, 2002). This bang-sensitive behavior is interestingly similar to some forms of vertebrate epilepsy and seizure.

Epileptic seizures are caused by defects of substantial genetic and molecular heterogeneity (Stafstrom and Tempel, 2000) and have not been explained by a single mechanism (Shorvon, 2014).

kcc (kazachoc) is a gene encoding the K+/Cl- co-transporter in *Drosophila melanogaster*. The location of the *kcc* gene is in the 57 kb segment at region 60A near the distal end of chromosome 2R. The *kcc* gene has two major alternative splicing forms: the B form, which is seen in adult heads, and the D form seen in embryos. The *kcc* gene has different forms of recessive alleles, including: *kcc^{EY08304}, kcc^{ML1}, kcc^{DHS1} and kcc^{KG02390}* (Hekmat-Scafe et al., 2006). The *kcc^{EY08304}* is an allele results from a P-element insertion into the last exon of the *kcc* gene. It is a lethal allele when expressed homozygously. However, over 40% of *kcc^{EY08304}/ kcc^{DHS1}* or *kcc^{EY08304} / kcc^{ML1}* adults are bang sensitive. The *kcc^{KG02390}* results from a P-element insertion outside the coding sequence of the *kcc* gene and so can be thought of as the wild type. The *kcc^{ML1}* is produced by imprecise excision of P{SUPor-P)*kcc^{KG02390}* that has deleted 88bp of genomic sequence. The KCC protein in *kcc^{ML1}* mutants is about half the size of that in the wild type flies. The *kcc^{DHS1}* is produced by the insertion of 13 bp (ACTATGCTACTGT) after the seventh base pair in intron 11 of the *kcc* gene (Fig. 1-14). The activity of the KCC protein in *kcc^{DHS1}* mutants is reduced about four fold compared to the wild type flies (Hekmat-Scafe et al., 2006).
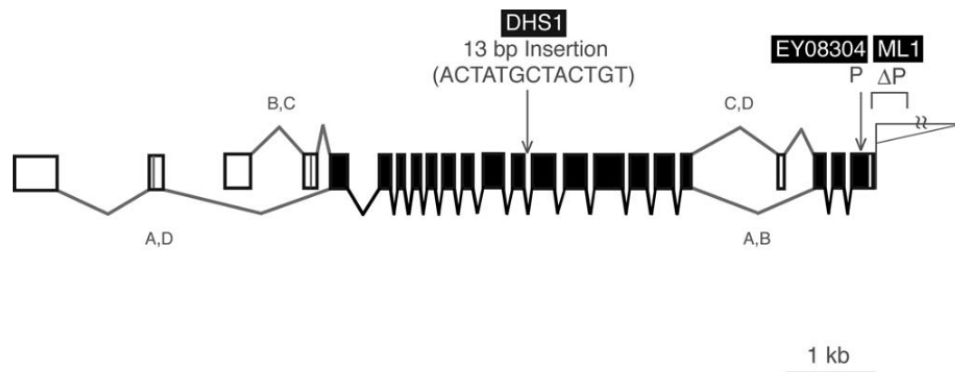
Figure 1-14: The *kcc* gene. Adopted from Hekmat-Scafe et al. (2006).

The *kcc^{DHS1}* mutation shows bang sensitive paralytic phenotype, a behavioral indication of seizure sensitivity. The penetrance of the homozygous *kcc^{DHS1}/ kcc^{DHS1}* BS phenotype is 27%. This BS phenotype appears to be a stochastic phenomenon: the phenotype seems to appear and

disappear randomly at different times. Other BS mutants, such as *sda*, *eas* and *bss,* show 100% penetrance of the BS phenotype. Moreover, the kcc^{DHS1} mutants show a recovery time of about 19 seconds (14 seconds of paralysis followed by 5 seconds of recovery seizures). *sda, eas* and *bss* mutants show significantly longer recovery times 37, 52, and 198 seconds, respectively of (Hekmat-Scafe et al., 2006).

The KCC protein in the head of kcc^{DHS1} mutants increases as the age of the fly increases. The level of the KCC protein increases approximately 13 times by four days after eclosion, compared to just 1.9 fold in the wild type flies. The increase in the KCC protein levels is related to the decrease the in bang sensitivity of the kcc^{DHS1} mutants. Furthermore, kcc^{DHS1} mutation shows temperature dependence, with the phenotype being more severe at lower temperature (Hekmat-Scafe et al., 2006).

The seizure threshold is significantly lower in kcc^{DHS1} flies: about one-third that of wild type flies. The BS mutants, sda, eas and bss have even lower seizure thresholds, about 5 to 10 fold lower than the wild type. The seizure phenotype observed in kcc^{DHS1} flies depends on $GABA_A$ receptor signaling, assuming that the seizure is attributable to the disruption in the Cl- gradients that are responsible for GABAergic inhibition in the central nervous system. This assumption was tested by Hekmat-Scafe et al. (2006) by using picrotoxin (PTX), a $GABA_A$ blocker and an established chemioconvulsant in animal models (Stilwell et al., 2006). In kcc^{DHS1} mutants, PTX acts as an anticonvulsant by reducing the BS phenotype. Therefore, blocking $GABA_A$ receptors by PTX clearly shows that the seizures seen in the kcc^{DHS1} flies result from the lack of inhibitory signaling from GABAergic neurons. Moreover, *Rdl* (a gene encoding $GABA_A$ receptors) mutation results in a significant reduction in the seizure sensitivity in the homozygous kcc^{DHS1}/kcc^{DHS1}. Similarly, Gad^{L352F} (a mutation in the enzyme producing GABA, GAD) causes a reduction in the seizure sensitivity (Hekmat-Scafe et al., 2006).

The KCC protein is expressed intensely in the brain neuropil, including the four optic neuropils of the optic lobe: lamina, medulla, lobula and lobula plate (Fig. 1-15). Little or no KCC protein was found in the mushroom body (MB), an important structure in memory and learning. The expression of *Rdl* $GABA_A$ receptor is also similar to that of the KCC expression except that *Rdl* is also expressed in the mushroom body (MB) (Hekmat-Scafe et al., 2006).
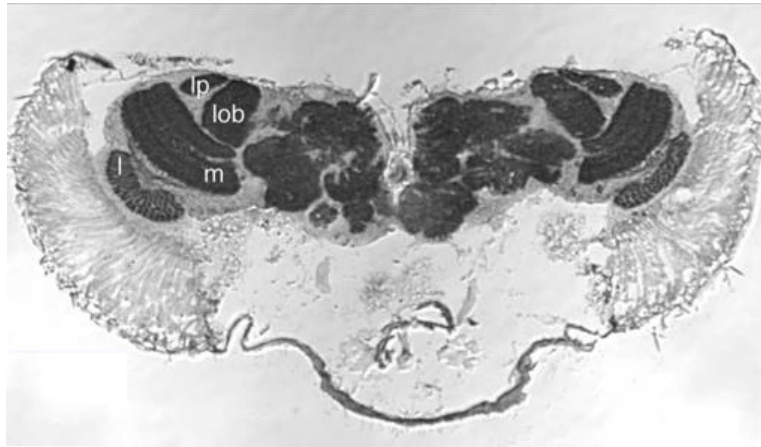
Figure 1-15: Immunohistochemical staining shows *kcc* expression in the fruit fly eye. Adopted from Hekmat-Scafe et al. (2006).

Studying changes to contrast gain control in animal models is informative but linking these changes to those observed in humans is essential, particularly if they are to have clinical relevance. Because *Drosophila melanogaster* is used as a common model for human genetic diseases, we sought to draw parallels between visual gain control in flies and humans via a common measure of neuronal gain control: Contrast adaptation. Contrast adaptation can be measured in both species: In flies using EEG and in humans using functional magnetic resonance imaging (fMRI).

In flies, we are able to measure the effects of contrast gain control in normal controls as well as in animals carrying mutations in the *kcc* gene. Based on earlier work in humans, we expected to find abnormal (reduced) gain control and therefore potentially reduced or abnormal contrast adaptation.

In our human experiments, we took advantage of the human's ability to perform behavioural tasks, in order to examine the neural interaction between adaptation and attention – something no other group has done in the field of human neuroimaging, to our knowledge. A similar type of attentional experiment would be extremely difficult, although perhaps not impossible in flies (Van Swinderen, 2012; Wiederman and O'Carroll, 2013).

1.5 Measuring early vision in humans using fMRI

Most findings about the contrast sensitivity of brain regions have come from electrophysiological studies in animals. Studies measuring the effect of contrast adaptation on contrast response functions (Albrecht and Hamilton, 1982; Carandini et al., 1997; Heeger, 1992; Ohzawa et al., 1985, 1982, Sclar et al., 1989, 1985) have found that contrast adaptation results in a horizontal shift of the contrast response functions (CRFs) so as to centre the steepest part of the curve at or near the adapting contrast. Similarly, studies measuring the effect of attention on CRFs (Reynolds et al., 2000a; Williford and Maunsell, 2006) have shown that attention acts by either increasing contrast sensitivity, thus shifting the CRFs along the horizontal axis, or by increasing the neural responses, thus shifting the CRFs along the vertical axis.

Due to the high spatial resolution of the method, the number of human visual studies using functional magnetic resonance imaging (fMRI) has increased tremendously since the advent of the technique in 1990 (Ogawa et al., 1990). These studies have shown that the blood oxygen level dependent (BOLD) responses increase with stimulus contrast (Avidan et al., 2002; Boynton et al., 1999; Geoffrey M. Boynton et al., 1996; S. A. Engel et al., 1994; Tootell et al., 1995), increasing the confidence that the fMRI signal reflects neuronal activity. More importantly, these studies have shown similar effects, to some extent, with regards to contrast adaptation (Gardner et al., 2005) and attention (Boynton, 2009; Buracas and Boynton, 2007; Murray, 2008). However, too little attention has been paid to the interaction between contrast adaptation and attention. In this thesis, we will use fMRI to examine the way in which these two interact. Our ultimate goal is to develop novel assays for gain control in humans, which could be used to study neurological diseases such as epilepsy.

1.5.1 Human visual system

When light rays hit the eye, they first pass through the cornea, to the aqueous humour, the iris, the lens, the vitreous humour and finally, the retina. In the retina, the light rays are detected and converted into electrical signals by the photoreceptor cells, rods and cones. The bipolar cells receive the input from the photoreceptors and then send it to the retinal ganglion cells. The information is then sent to the brain by the optic nerves, which are made up from the axons of

the ganglion cells. The optic nerves from each eye cross at a point known as the optic chiasm. After this point, the optic nerves are collectively known as the optic tract. The majority of the axons of the optic tract terminate at the lateral geniculate nucleus (LGN) of the thalamus. The axons of the LGN cells form the optic radiation, which terminates in the primary visual cortex (V1). Besides V1, other cortical regions (e.g. V2 and V3) are involved in processing visual information.

1.5.1.1 Projections from the retina to the brain

The axons of the retinal ganglion cells that originate at the temporal side of the retina continue to the same side of the hemisphere, whereas axons originate at the nasal side cross over to the opposite hemisphere (Fig. 1-16). This means that axons from the temporal side of the retina of the left eye and from the nasal side of the right eye send their information to the left hemisphere, forming the right visual field. On the other hand, axons from the nasal side of the left eye and from the temporal side of the right eye send their information to the right hemisphere, forming the left visual field.

Most of the optic tract axons terminate in the LGN. The human LGN is a bilateral complex structure of six layers. The mapping of the retina into the LGN is very precise: adjacent points in the retina correspond to adjacent points in each layer of the LGN. Axons from the eye on the same side of the LGN (ipsilateral) terminate in layers 5, 3 and 2, whereas axons from the opposite side (contralateral) terminate in layers 6, 4 and 1.
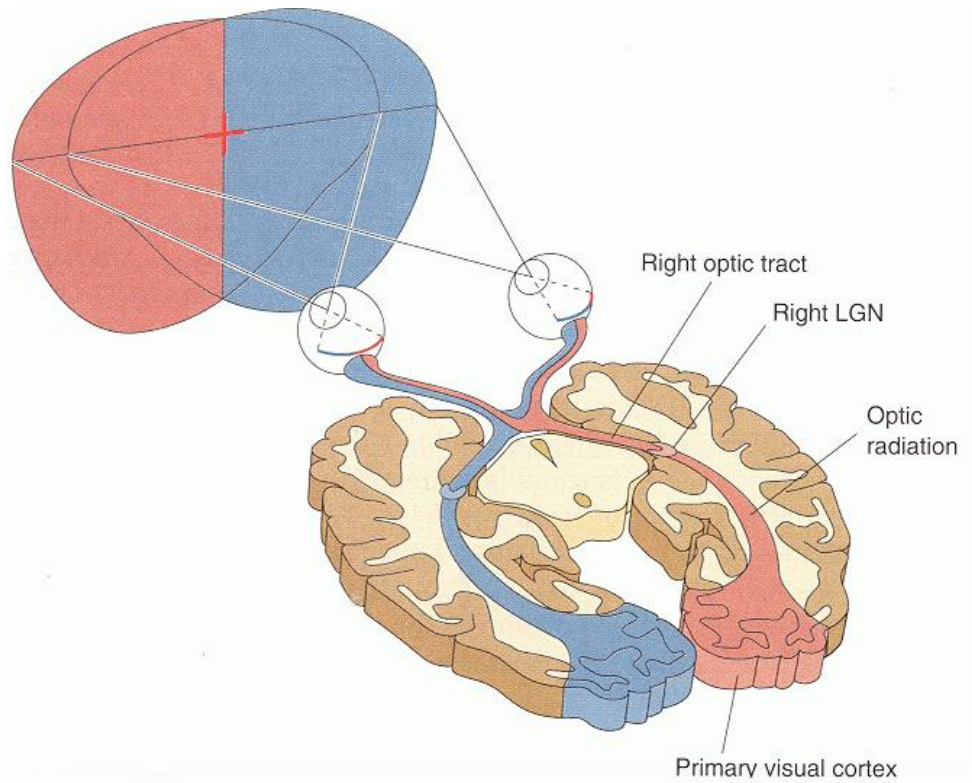
Figure 1-16: Projections from the retina to the brain, adopted from Wang (2013).

The LGN layers contain different types of neurons. Layer 1 and 2, known as magnocellular layers, contain neurons with large cell bodies, whereas layer 3, 4 5 and 6, known as parvocellular layers, contain small cell bodies. An additional type of layers (konio layer) is located at the base of each parvocellular and magnocellular layers (Wang, 2013).

The distribution of axons from the retinal ganglion cells within the LGN is highly regulated. This means that different types of ganglion cells send information to specific types of LGN neurons. Parasol retinal ganglion cells project their axons to the magnocellular layers, forming the magnocellular pathway, and midget cells project their axons to the parvocellular layers, forming the parvocellular pathway. The magnocellular pathway is, broadly speaking, sensitive to low contrast, low resolution and motion, while the parvocellular pathway is sensitive to high resolution and the perception of color (Agarwal et al., 2011).

The axons of the LGN neurons send their information to the primary visual cortex via the optic radiation. The primary visual cortex, known as striate cortex or V1, receives the visual information from the ipsilateral LGN in a point-to-point manner. This means that each cortex represents the opposite visual field, and the adjacent points in the retina are mapped at adjacent points in the primary visual cortex, in the same way as in the LGN. This organized retinal projection on visual cortex is known as retinotopic mapping.

1.5.1.2   Retinotopic maps in the visual cortex

The field of neuroscience has made remarkable progress in defining individual visual areas *in vivo*. The sizes and anatomical locations of these visual regions varies slightly between subjects (Dougherty et al., 2003; Engel et al., 1997a), thus defining these regions for each subject is crucial in the experimental studies of human brain. The main technique used for obtain retinotopic mapping is functional magnetic resonance imaging (fMRI). The details about the actual experiment are described later.

1.5.1.3   The primary visual cortex (V1)

This is located within the calcarine sulcus in the occipital lobe. V1 is the first cortical region to process visual information and has been studied extensively since the seminal works of Hubel and Wiesel (1968, 1962, 1959).

Cells in the primary visual cortex can be divided into simple, complex and hypercomplex. Simple cells have distinct regions of inhibition and excitation within the receptive field. Complex cells have no distinct inhibitory and excitatory regions within their receptive field (Hubel and Wiesel, 1962, 1959). Hypercomplex cells are sensitive to the length of the stimulus (Hubel and Wiesel, 1965).

Another feature of cortical neurons is the orientation selectivity (Hubel and Wiesel, 1962, 1959). Orientation-selective neurons are important in detecting edges, and they are spatially organized in the cortex. They are arranged in orientation columns, each one consisting of cells of single preferred orientation. The preferred orientation changes gradually across the cortical surface resulting in stereotypical 'pinwheel' domains of orientation selectivity (Bonhoeffer and Grinvald, 1991; Hubel and Wiesel, 1977).

Moreover, cortical cells are selective to spatial frequency (Campbell et al., 1969). The selectivity of spatial frequency and orientation are related. Neurons that are narrowly tuned for spatial frequency show tendency towards narrow tuning for orientation (Webster and De Valois, 1985).

In addition, the firing rates of neurons have a limited range. Increasing the sensitivity of neurons allows these neurons to respond to a wide range of inputs. The mechanism responsible for that is called contrast normalization (Heeger, 1992). It results in a non-linear sigmoidal shape in response to a stimulus of increasing contrast levels. V1 cells also process motion, color and many other perceptual features; however, these features are outside the scope of this thesis.

1.5.1.4   Visual cortical pathways

The idea that two pathways of the visual information, starting from V1 and traveling to different direction was suggested by Mishkin et al., (1983). The occipital-temporal pathway, also known as ventral stream, is responsible for object recognition, whereas the occipital-parietal pathway, dorsal stream, is responsible for spatial vision and visually guided actions.

It is believed that the LGN pathways, parvocellular and magnocellular, remain segregated in V1; however, there is evidence of a crosstalk between the pathways - neurons in the higher visual cortical areas represent information that reflects integration across multiple pathways (Casagrande et al., 2005).

1.5.1.5   Biomarkers of disease

Previous work in human epilepsy using SSVEPs showed changes in CRFs (Porciatti et al., 2000; Tsai et al., 2011). In these studies, the abnormal gain control was characterized as a lack of response saturation at high contrast levels. They suggested that these changes in neural sensitivity may give rise to hyperexcitability underlying epilepsy. Using fMRI to measure changes in CRFs in normal subjects is our aim as these changes have mostly been measured using EEG or psychophysics.

1.6 Conclusion

Gain control is a universal mechanism that regulates input-output relationships. It has been found in different regions of the brain in several animal models. While animal models are useful in investigating the physiological mechanisms of gain control, they are not sufficient to understand its clinical relevance in human diseases such as epilepsy. Research in humans, using techniques such as fMRI, will allow the study of more complex forms of gain control, e.g. attention-mediated gain control.

In this thesis, I attempt to show that Drosophila models of epilepsy can be used to investigate gain control abnormalities, followed by the testing of pharmacological and genetic treatments to rescue the visual deficits. In order to apply this to humans, we have started by looking at the effect of contrast adaptation and attention on contrast response functions. This may allow us to further understand the mechanisms underlying gain control, particularly in epileptic patients.

2 Chapter 2: Methodology (SSVEPs)

This chapter provides an overview of the major methodologies used during the PhD. Due to the nature of this thesis; two methodology chapters are presented here and in the next chapter. The first one is dedicated to the Drosophila experiments (Chapter 4, 5 and 6) using steady state visually evoked potentials (SSVEPs). The second one is specific to the human experiment (Chapter 7) using functional magnetic resonance imaging (fMRI).

First, I will discuss the Drosophila culture, including the food medium, organisms attacking Drosophila, and the adult fly (section 1). Then, I will describe the technique used to measure the visual responses, SSVEP (section 2). Finally, I will describe the stimuli used and analyses performed.

2.1 Drosophila culture

2.1.1 The food medium

As mentioned before (see Chapter 1), the fly's diet is crucial when trying to measure responses from the visual system because the amount of carotenoid in the food is responsible for the rhodopsin concentration in the eye (Goldsmith et al., 1964). Mashed bananas were the first food material to be used for fruit flies in the laboratory. Nowadays, we use a standard mixture of maize, agar, sugar and yeast. The ingredients are mixed together after adding warm water. When cooking for about one hour, the food can be poured into half-pint bottles (the traditional Drosophila home) (Sang, 1982). The flies are kept in these glass bottles where they are allowed to lay eggs. All flies were kept in the glass bottles, and upon hatching only the female flies of interest were transferred into vials on yeast-sucrose-agar fly food so that age-specific flies were available for experiments.

2.1.2 Organisms attacking Drosophila

There are two main organisms that can affect Drosophila in the laboratory, mould and mites. Even though mould is not directly harmful to the flies, some toxic products are produced which could affect the flies. Mites however, are far more serious leading to reduction in the number of

progeny and can destroy the entire culture by eating all the eggs. Stocks affected should be discarded (Sang, 1982).

2.1.3 The adult flies

Drosophila males and females are easily distinguished. Males are smaller, with blackened tip to the abdomen. A patch of bristles on their foreleg, known as sex comb, is also found in males but not females.

It is essential to use virgin females when flies of different phenotypes are to be crossed. Because flies will not mate for about eight hours after emergence, collecting virgin females is done by emptying the culture bottle or vial, waiting for several hours, and then collecting the females that have emerged during the intervening period. Newly emerged flies are recognized by their pale color, and the presence of the meconium, a visible marker in the middle of the gut: the remains of the larval gut (Sang, 1982).

2.2 Steady state visual evoked potentials (SSVEPs)

2.2.1 Overview

The technique used to measure the Drosophila visual responses is based on steady state visual evoked potentials (SSVEPs). When stimulating the sense organs of humans or animals, electrophysiological potentials are generated. These potentials are knows as sensory evoked potentials (SEPs). These evoked potentials are different from the spontaneous potentials (the background EEG), which are detected without stimulation. The most important advantage of SEPs is that they are time-locked to the stimulus and thus can be improved using averaging techniques on several trials (Dawson, 1954). SEPs generated by visual stimuli are termed visual evoked potentials (VEPs).

Visual stimuli usually produce transient responses, but using long stimulus trains allows the visual system to produce a stable pattern of repetitive VEPs that overlap each other. These evoked EEG waves are called steady-state visual evoked potentials (SSVEPs) (Regan, 1966). In humans, SSVEPs have been used in many cognitive applications, including visual attention (Morgan et al., 1996), working memory (Silberstein et al., 2001), as well as many clinical

applications, including aging (Macpherson et al., 2009), Parkinson disease (Afsari et al., 2014; Marx et al., 1986), schizophrenia (Line et al., 1998), Alzheimer disease (Jacob et al., 2002), depression (Kemp et al., 2004), autism (Belmonte, 2000), anxiety (Gray et al., 2003) and epilepsy (Birca et al., 2008; Tsai et al., 2011; Vermeulen et al., 2008)

2.2.1.1   SSVEPs vs. transient VEPs

The main difference between SSVEPs and transient VEPs lies in the spectral characteristics of the signal. In the case of the SSVEPs, the neural responses are periodic (because the stimulus itself repeats with constant periodic oscillations). The evoked potentials therefore give rise to well-defined peaks in the frequency domain. By comparison, neural responses driven by single pulses (VEPs), do not contain isolated, well-defined peaks in the frequency spectrum (Vialatte et al., 2010).

The flickering visual stimulation can be characterized into two classes, full-field or 'pattern'. Full field (pure luminance) modulations are delivered as repeated flickering lights, while pattern stimulation (generated by an LCD monitor) can be delivered in either reversal or on/off fashion. The strength of the flash stimulus is measured in photopic candelas per square meter (cd/m^2) (Odom et al., 2004). Full field stimulation can be considered to be a special case of pattern modulation with a spatial frequency of zero cycles per degree.

Delivering a flickering light at a particular frequency, known as frequency-tagged flickering stimuli, stimulates the visual pathway, causing this frequency to radiate throughout the brain, i.e. neurons synchronize their firing to the frequency of flickering light (Hutcheon and Yarom, 2000). That means when the stimulus is modulated repeatedly over time, the evoked response produced by the stimulus has a periodic time course.

The amplitude of the SSVEP is different for each stimulation frequency or subject. In fact, the majority of SSVEP studies tend to have the stimulus frequency to be above 10 Hz (Garcia, 2008). Consequently, the responses to individual stimuli overlap owing to the decreased time interval between stimuli. Because SSVEPs are periodic, responses are restricted to a particular set of frequencies, and it is therefore easier to analyze these SSVEP responses in the frequency domain instead of the time domain. The stimulus frequency controls the content of the response

frequency, meaning that there are narrowband peaks at frequencies that are directly related to the stimulus in the response spectrum (Fig. 2-1) (Norcia et al., 2015). SSVEPs have two parameters: response amplitude and response phase. The latter is related to the processing of the visual system, and can be described as the time it takes for a response to be generated following a stimulus. Phase is a circular variable taking values over 2π radians or 360°. Both parameters can be plotted conveniently as a vector in a polar coordinate system (Fig. 2-1). The length of the vector represents the response amplitude, and the angle of the polar represents the response phase (Fig. 2-1).

SSVEP responses typically contain activity at the input frequency and multiples thereof (harmonics). Harmonics exist for two reasons: multiple temporal frequencies may be present in the stimulus (as when a square wave is used), and, in addition, the system may be non-linear (Norcia et al., 2015). As an example, a square wave modulation should give rise to response at multiple odd harmonics of the input frequency while the presence of a squaring non-linearity will generate outputs with twice the input frequency.

Harmonics occur at an exact integer multiple of the stimulus frequency, 2f, 3f, 4f and so on. The presence of the odd and even harmonics can be related to the temporal symmetry of responses to the stimulus: Odd harmonics represent responses that are asymmetric across a single stimulus cycle. For example, when the responses to onsets differ to the responses to offsets (Fig. 2-2). In comparison, when the stimulus used evokes identical responses (because the properties of the responses to both halves of the stimulus cycle are identical), it only generates even harmonics. For example, using pattern reversal stimuli generates even harmonics because such stimuli are, on average, the same in both halves of the cycle (Fig. 2-3). Thus, the repetition rate of the measured responses will be twice the stimulus frequency (Norcia et al., 2015). In our experiments, we identify different frequency components by the nomenclature: [harmonic] F [input], where input refers to either probe [1] or mask [2]. For example, the first harmonic of the probe is 1F1, while the second harmonic of the mask is 2F2. In these experiments the input frequencies are 12 Hz for the probe and 15 Hz for the mask. Because the largest responses are usually found in the first and second harmonics, we will only describe the responses corresponding to these frequency components throughout the thesis.

In addition to the fundamental (input) frequencies and harmonics, when two stimuli are presented simultaneously (masking) at different frequencies they generate response components at frequencies that are low-order sum and differences of the fundamental frequencies (Tsai et al., 2012) (Fig. 2-4 and 2-5). These so-called 'intermodulation' terms (e.g. 1F1+1F2) are signatures of signal combination after a neuronal non-linearity. In Drosophila, we associate them with signals arising in deeper structures of the visual system such as the medulla and lobular plate. Because frequency-tagged flickering stimuli generate responses that are frequency and phase-locked with a high signal to noise ratio, this technique is commonly used in electrophysiological experiments (Candy et al., 2001; Carandini and Ferster, 1997; Porciatti et al., 1999; Regan, 1966; Van Swinderen, 2012).
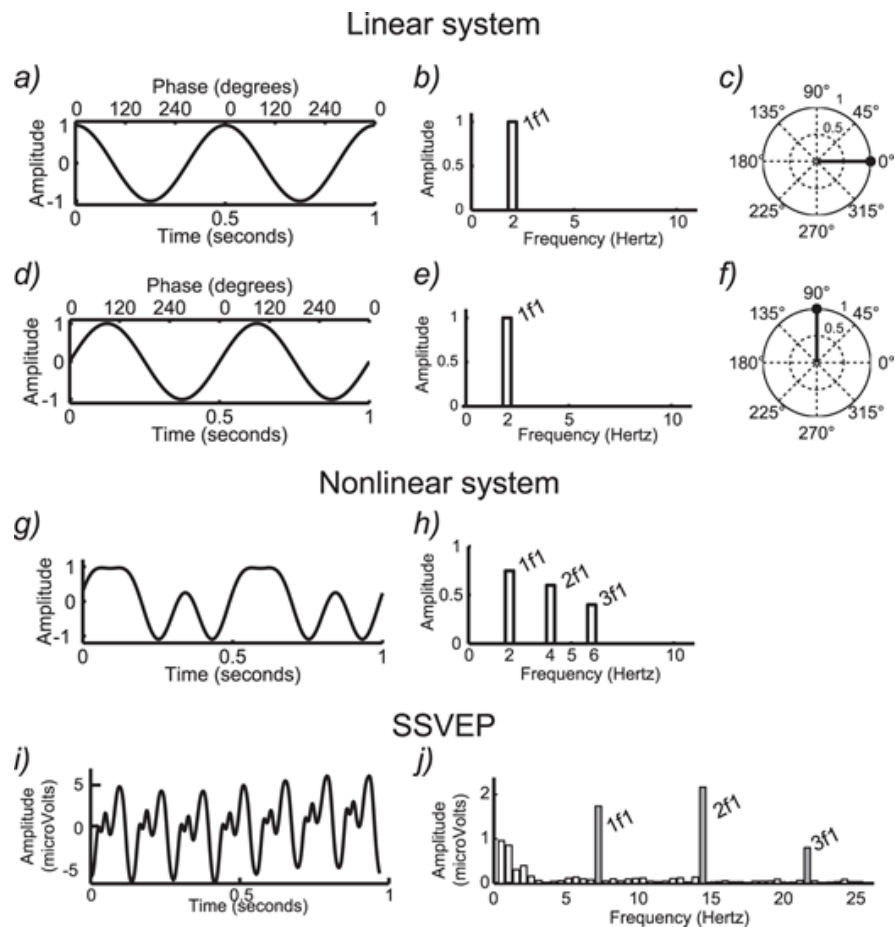
Figure 2-1: SSVEP in the time and frequency domain. a) Shows a time domain representation of a sinusoidal response from a linear system. B) Shows the frequency domain representation of (a). c) Shows a vector representation of the amplitude and phase of (a). d, e and f are the same as a, b, and c, respectively, but with a phase shift of 90 degrees. g) Shows a response from a nonlinear system in the time domain. h) Shows the frequency domain representation of (g), containing multiple harmonics. i) Shows SSVEP in the time domain with a stimulus frequency of 7.2 Hz. j) Shows the frequency domain representation of (i). Adapted from Norcia et al. (2015).
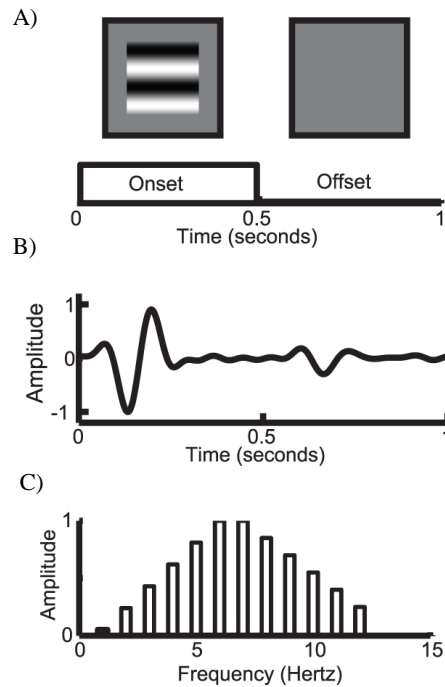
Figure 2-2: A) Schematic illustration of pattern onset/offset stimulus. B) Shows one cycle of response to the stimulus onset (large) and offset (small). (C) Shows the frequency domain containing odd and even harmonics of the stimulus frequency. Adapted from Adapted from Norcia et al. (2015).
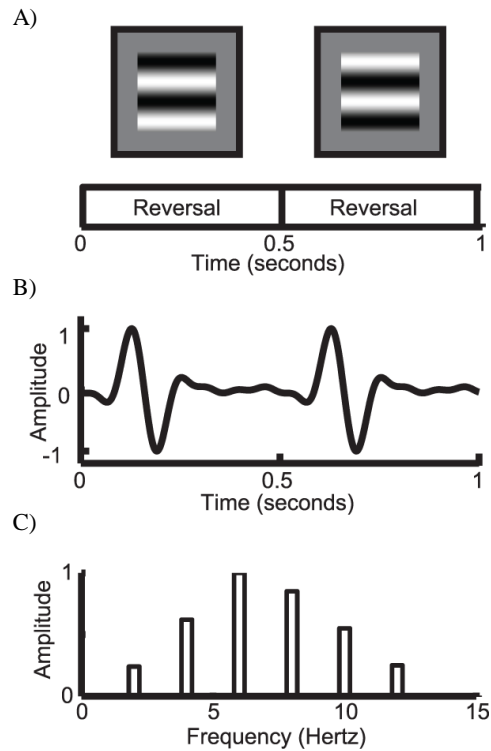
Figure 2-3: A) Schematic illustration of pattern reversal stimulus. B) Shows one cycle of response to the stimulus reversal (both are large). (C) Shows the frequency domain containing only the even harmonics of the stimulus frequency. Note that the frequency of the pattern reversal stimulus in this example is the frequency at which the stimulus returns to its original state (1 Hz), and the response harmonics are the multiple of this rate rather than the pattern alternation rate. Adapted from Norcia et al. (2015).

64

Linear Response

Summation + Random Noise

Non-Linear Early Response

Summation + Random Noise
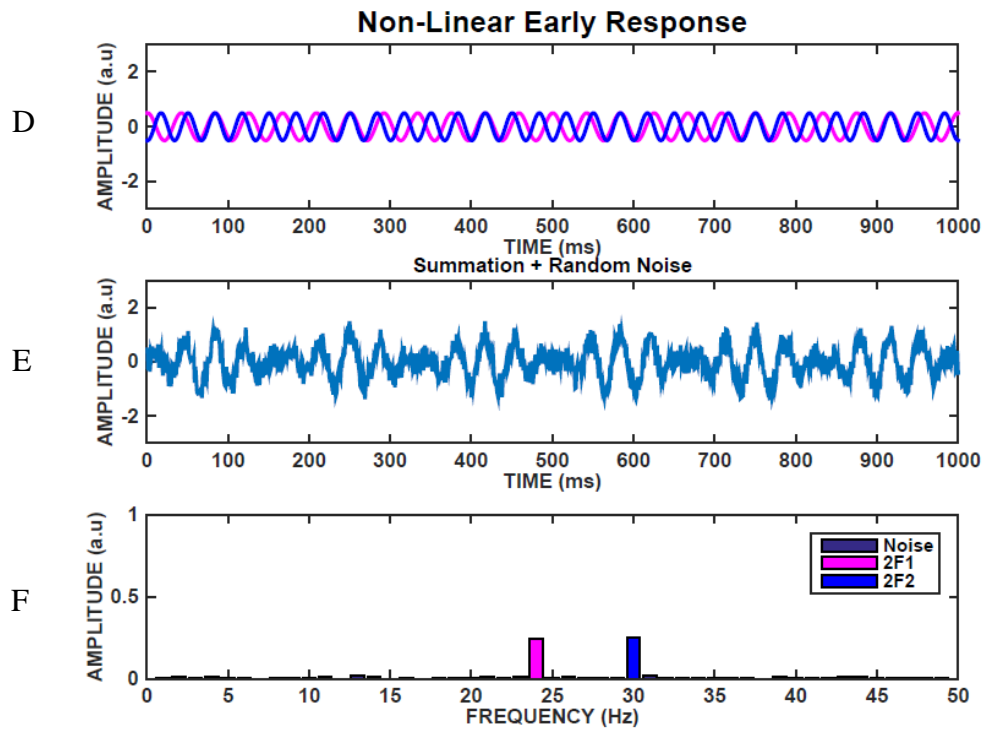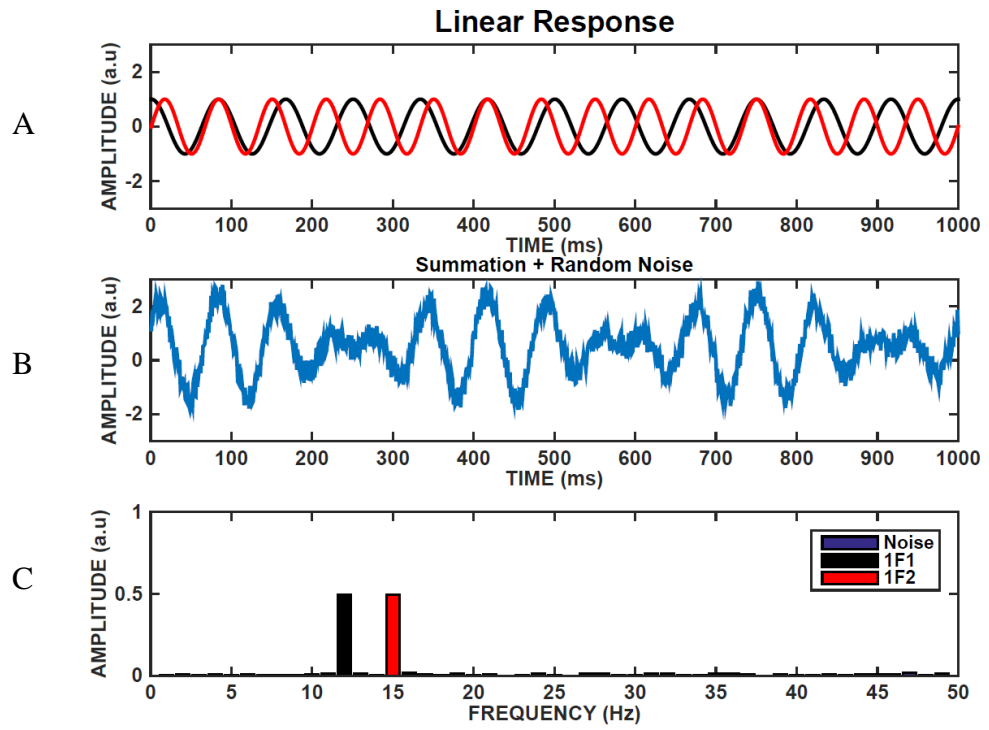
Figure 2-4: The difference between linear and non-linear system in generating different responses. The first figure shows that for a linear system, the two stimuli (probe at 12 Hz and mask at 15 Hz), (in A and B) generate only the two fundamental frequencies at the frequency domain (C). Note that the amplitude of the summed signal ranges from -2 to 2: the range is amplified by the constructive or destructive interference of the inputs. When we added a non-linearity that occurs early in the system (such as squaring then summing the input frequencies) (in D and E), the 'frequency doubled' harmonics at 24 Hz for the probe and 30 Hz for the mask were present (F).
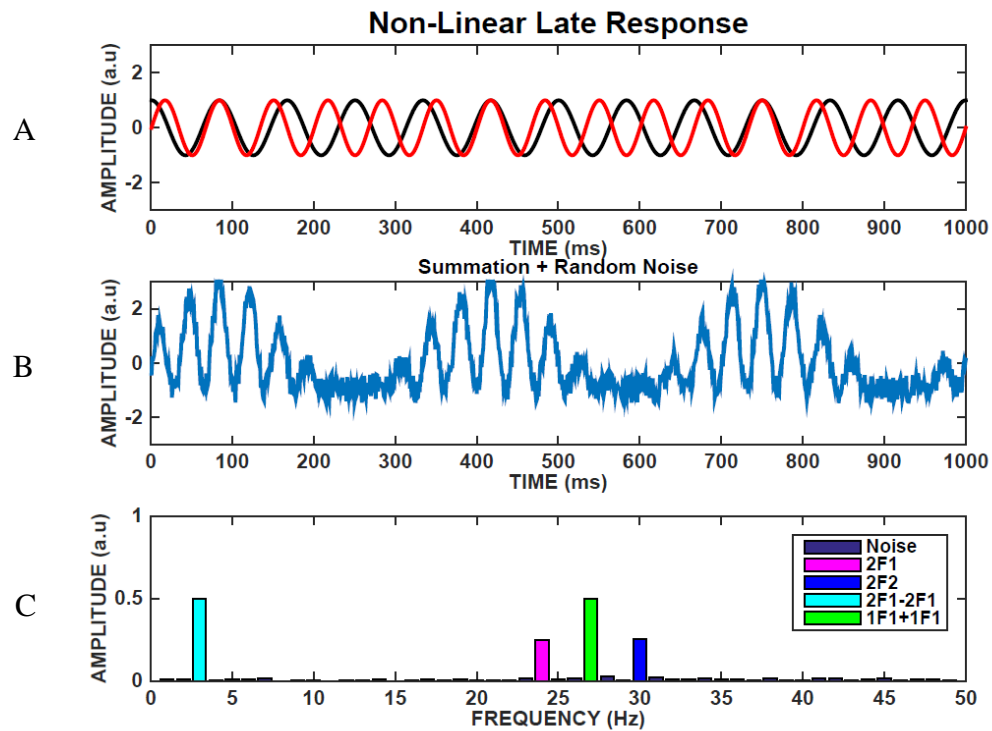
Figure 2-5: Adding a non-linearity that occurs later in the system (such as summing then squaring the input frequencies) (B) generates additional 'intermodulation' terms at sums and differences of the input frequencies (C).

2.2.2 Fourier analysis

Besides averaging, the most important technique for analyzing the SSVEP signals is the Fourier transform. The Fourier transform is a very powerful tool that converts the responses in the time domain into its components in the frequency domain (or, technically, back again). The responses detected by the electrodes (as a waveform) are a combination of the input frequency and multiples thereof, and it is difficult to identify the separate components in the time domain. Converting the responses into the frequency domain helps to separate out these components. These components, in turn, correspond to processing in different stages of the visual pathway.

In Drosophila, many neurons in the visual pathway contribute to the responses and using the Fourier transform can help to distinguish the photoreceptors (which occur at the first harmonic – tracking the mean luminance of the scene) from those of later neurons which are sensitive to onset and offset transients (Fig. 2-6). This can be verified using genetic techniques: Using transgenic flies to inactivate the histamine A receptor(e.g. $ort^{-/-}$) and thus stopping the photoreceptors from synaptic transmission into the laminar neurons and amacrine cells, confirmed that the first harmonic is a good representation of the photoreceptor responses while the second harmonic is largely due to the neural signaling (Fig. 2-7) (Afsari et al., 2014).
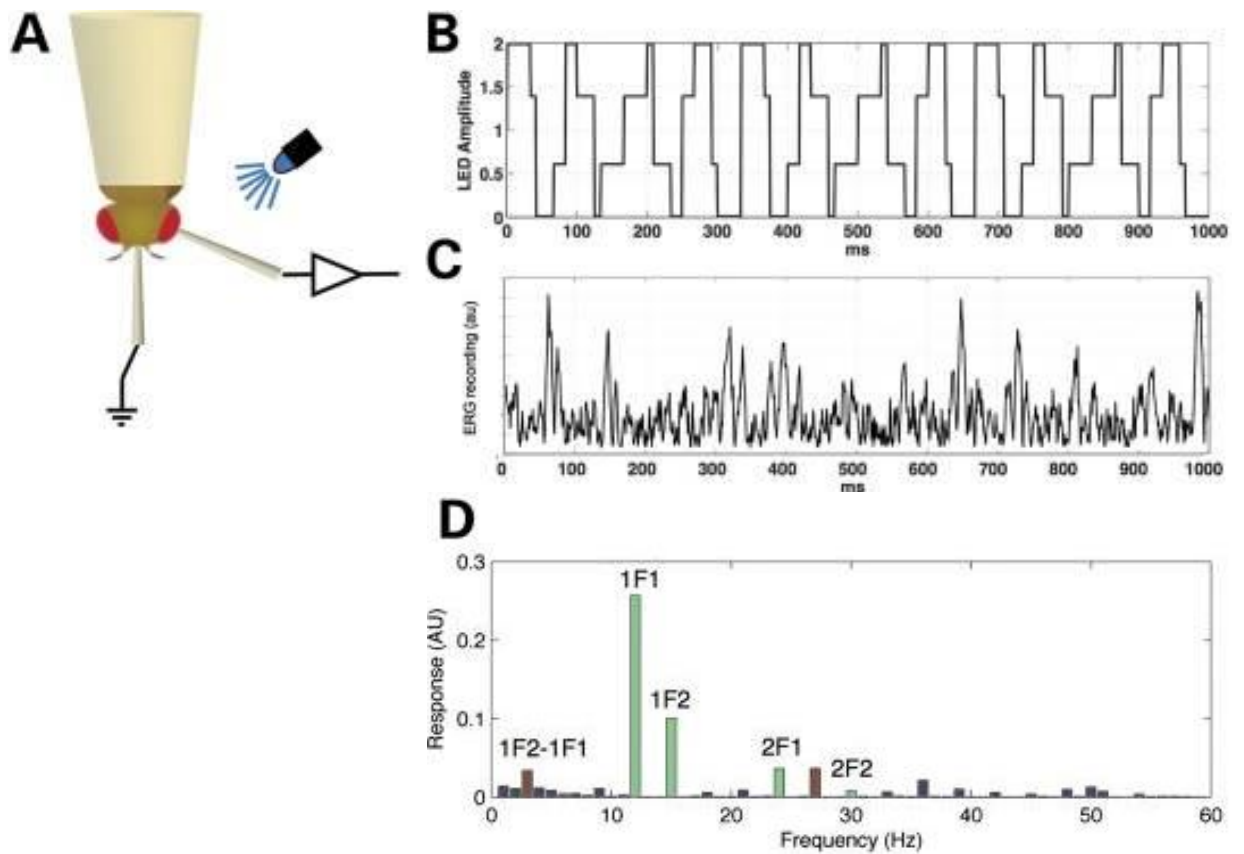
Figure 2-6: The technique used in our experiments. (A) Flies are glued in pipette tip using a droplet of nail polish, and then illuminated by a blue light. Electrodes are placed in the mouth and eye to measure the visual responses. (B) The stimulus is the sum of two square waves. (C) A response recording in the time domain. (D) The application of Fourier transform, separate out the responses according to their frequencies. Adopted from Afsari et al. (2014)
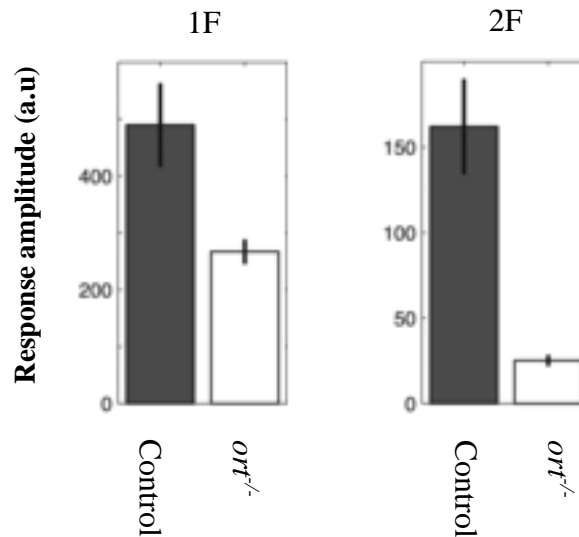
Figure 2-7: The physiological origins of the harmonics in the SSVEP responses. The ort null mutation inactivates the histamine A receptor causing the absence of photoreceptor synaptic transmission into the laminar neurons. This confirmed that the first harmonic (1F) is generated by the photoreceptors, while the second harmonic (2F) is by the neural signaling. Adopted from Afsari et al. (2014)

2.2.3 Electroretinogram (ERG)

The Drosophila electroretinogram (ERG) has been used for more than four decades (Heisenberg, 1971; Hotta and Benzer, 1969). The recording method uses an extracellular electrode to record an electrical potential from photoreceptors and downstream neurons within the fly eye in response to flashes of light (Dolph et al., 2011).

The light stimulation of the fly eye results in an initial positive 'on' transient voltage spike attributed to the hyperpolarization of the laminar neurons (L1-L2). These neurons are the synaptic targets of the photoreceptors R1-R6. Chloride-permeable ionotropic histamine receptors are opened in response to the release of histamine neurotransmitters by the photoreceptors. This is followed by a sustained negative potential reflecting the depolarization of photoreceptors. This lasts as long as the stimulus, and its amplitude is proportional to the

intensity of the stimulus. At the offset of the light stimulation, a negative 'off' transient is elicited reflecting the repolarization of the laminar neurons after photoreceptors cessation of histamine neurotransmitters (Fig. 2-8) (Hardie and Raghu, 2001). Responses from the photoreceptors R7 and R8 are weak and have no transients. However, the ERG from these photoreceptors usually has an on transient component attributed to the gap junctions between R7-R8 and the axons of R1-R6 in the lamina.
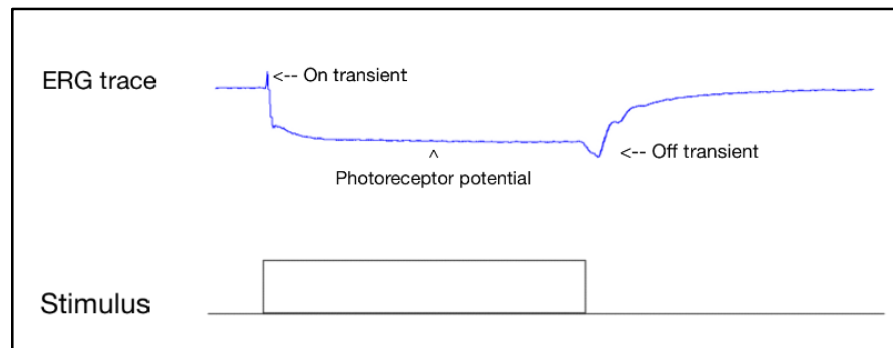
Figure 2-8: The ERG signal.

2.3 Material and methods

All flies were kept at 23 °C in a room that was dark most of the time. Keeping the flies in the dark is important because the kcc^{DHS1} flies are sensitive to light and can induce seizures in these mutants. Flies were transferred to new vials every 7 days to prevent overlapping of generations. The kcc^{DHS1} flies are sensitive to temperature (see Chapter 1), and thus controlling this factor was essential throughout the experiments.

2.3.1 Preparation

The most widely used method for anesthetizing flies for examination is the use of carbon dioxide. Flies can tolerate this state of anoxia for hours without any effects in the ERG (Agam et al., 2000). The flies quickly recover consciousness after being transferred to a CO_2-free atmosphere. Only female flies were used in our experiments for two reasons: they are larger, and to avoid possible variations in response to sex differences.

Flies were aspirated out of their vial into a shortened pipette tip. Each fly was fixed in place using a droplet of nail polish (Creative Nail Design). The movement was restricted as much as possible above the abdomen in order to avoid suffocation. Suffocation was indicated by the absence of a ERG response to a pulsed light. The responses were recorded by placing a glass electrode, filled with simple Drosophila saline (130 mM NaCl, 4.7 mM KCl, 1.9 mM CaCl2) (Heisenberg, 1971), close to the eye so that the electrode contacted the surface of the eye without damaging it. Another reference electrode was placed into the mouthparts to ensure electrical contact and also to further restrict movement. After preparation, the fly was put in the dark and allowed to recover for at least 5 minutes.

2.3.2 Visual Stimuli

To produce a SSVEP signal, flies are stimulated using a pulse of light lasting between 10 ms and 10 sec. The source of light is usually a direct current (DC) operated LED. Flies observe this as a flicker, leading to oscillations of the signal. The stimuli used in our fly experiments were either single, or summed square waves, flickering about a mean illumination at a specific frequency. The square waves were used to reflect other Drosophila ERG experiments.

Because we only want to stimulate the blue-sensitive rhodopsin (Rh1) present in R1-6 photoreceptors, peaking at 487 (Belusic, 2011), only a single LED channel centered at 467 nm (Gaussian spectral profile, FWHM 34 nm) was used (Prizmatix FC5-LED).

This wavelength is very close to that which Hindle et al. (2013) used in their study (465 nm) and was also effective to drive R1-6 photoreceptors in our experiments. The input/output linearity of the LED was verified using both a photodiode and a photospectrometer (Ocean Optics USB2000).

LED brightness was controlled using the concept of pulse width modulation (PWM). PWD is an encoding technique that is used in electronics to vary the levels of power by the oscillating the output from the microcontroller. The PWM cycle contains a time span with a signal at a high level followed by a time span with a signal at low level. One of the features of PWM is the duty cycle, which is the ratio between the pulse width and the cycle duration. By increasing or decreasing (modulating) the pulse width, we can control the light output from the LED. A duty

cycle of 50% means that the LED is on for 50% and off for 50% for the total cycle duration, and therefore it will appear half as bright (Fig. 2-9).
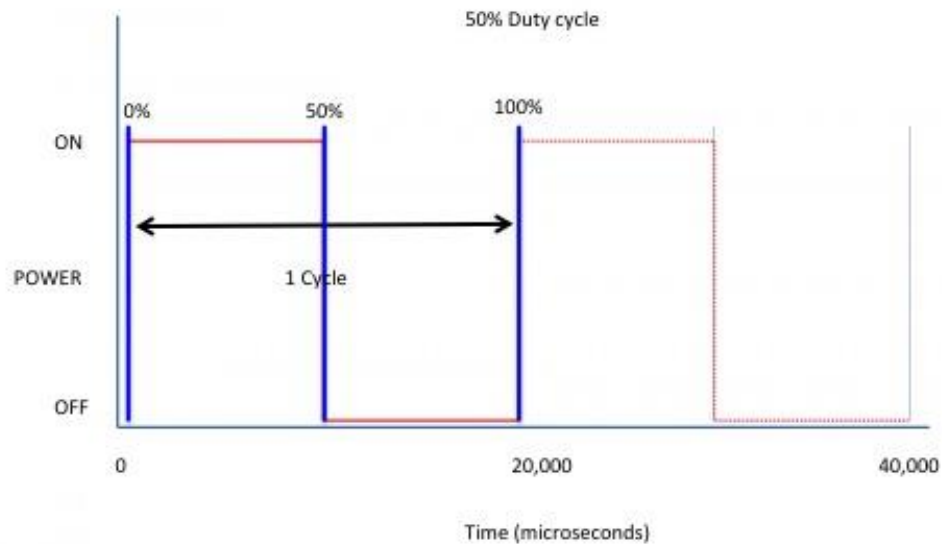
Figure 2-9: PWD. To achieve 50% LED brightness, the LED should be on for 10,000 microseconds and off for 10,000 microseconds.

The A/D convertor [National Instruments USB-6229] sampling rate was set to 1000Hz, and this limits the highest frequency we can resolve to 500Hz (1000/2) according to Nyquist Theorem. The noise in the signal can be calculated by summing up the squares of the amplitudes of every frequency component in a 1 second bin except the signal and harmonics and then take the square root of the sum of the squares (the 'root mean squared noise' - RMS). In our experiments, temporal bins whose RMS noise level is more than 2.5 standard deviations from the mean were eliminated. Following noise rejection, all bins from a single probe and mask condition were averaged in the time domain. Then, bins from all repetitions (5 repetitions) of a single condition in each fly were averaged. Evoked responses that are coherent with, or time-locked to, the stimulus, add constructively in the responses while noise that is incoherent with the stimulus, will tend to cancel out. Finally, we obtained a frequency domain representation of the data by computing Fourier transform.

72

All analyses were performed using Matlab code. The Matlab code is stored in: https://github.com/wadelab/flyCode.

2.3.3 Modeling

Most studies that have characterized CRFs in vertebrates (Albrecht et al., 1984; Sclar et al., 1990) or invertebrates (Matić and Laughlin, 1981; Minke, 1982) used the hyperbolic ratio equation of Naka and Rushton (1966):

$$R = R_{max} \frac{C^n}{C^n + C_{50}^n}$$

This equation provides values for 4 parameters; R_{max}, C_{50} and the exponent n. The R_{max} gives the maximum response observed. The C_{50} describes the contrast value at which half this maximum response was observed (also called the semi-saturation constant). The exponent n controls the nonlinearity of the slope. To produce a good fit for this type of neuronal data, the exponent n was restricted to a small range (1.5-2.5) (Busse et al., 2009) – a range that is commonly encountered in both human and animal electrophysiology.

In many of the datasets I describe below, the hyperbolic ratio function fails to fit the data well. Specifically, many of the contrast response functions that I measure with low spatial frequency stimuli do not saturate and therefore estimates of both C_{50} and R_{max} are unreliable. In these cases, it is possible to obtain a robust estimate of the maximum response amplitude by taking the average of the responses at the two or three highest contrasts.

2.4 Equipment

In most of the Drosophila studies described here, data were acquired in an electrophysiology rig sited within a Faraday cage to reduce external electrical noise (Fig. 2-10). Stimuli were generated by passing a PWM waveform to an external interface board (National Instruments USB-6229). EEG data were amplified using a dedicated custom amplifier circuit and digitized using the same NI board (see Chapter 4 and 6 for more details).

In the experiments described in Chapter 5, I used a dedicated stimulus display and acquisition system build around an Arduino microcontroller board. In this system, all data IO was controlled

by the microcontroller and datasets were accessed via an IP connection (see Chapter 5 for more details).
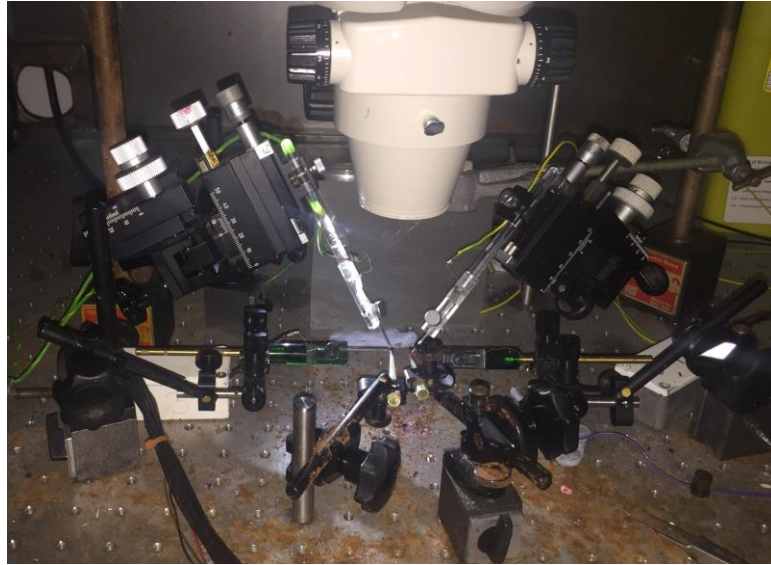
Figure 2-10: The ERG rig used in Chapter 4 and 6.

2.5 Conclusion

This chapter presented an overview of the SSVEPs used in our Drosophila experiments in Chapters 4, 5 and 6. We also summarized the preparation methods and technique used for analyzing the SSVEP signals.

In the following chapter, an overview of the technique used for the human experiment will be discussed.

3   Chapter 3: Methodology-fMRI

This chapter focuses on the fundamental principles of fMRI, including the physical principles of MRI, the preprocessing steps of the fMRI data and the fMRI data analysis used in our experiment. This chapter serves as an important background for our human study in chapter 7.

3.1 Principle of functional Magnetic Resonance Imaging

Since the advent of fMRI in 1990 (Ogawa et al., 1990), the field of neuroscience has been revolutionized. Using fMRI, we can non-invasively localize and measure neural activity. In the first part of this section, we will describe the physics of magnetic resonance technology. The second part focuses on the basics of the blood oxygenation level dependent (BOLD) response.

3.1.1 Magnetic Resonance Imaging (MRI)

The physics of MRI are complex. For simplicity we will divide this section into three parts. The first part discusses the atoms in the presence of an external magnetic field. The second part explains the state of these atoms after the application of a radiofrequency pulse. The last part explains the impact of RF pulse termination on the atoms.

3.1.1.1   Nuclear Magnetic Resonance:

Some of the basic properties of atomic nuclei are mass, charge and spin. The atomic mass is the total number of protons and neutrons. Protons and neutrons randomly spin around their axes. In nuclei with even mass number, the spins cancel each other out and thus net spin is zero. However, nuclei with odd mass number have a net spin. Following the law of electromagnetism, which states that any moving electric charge generates a magnetic field, these odd mass number nuclei also possess a magnetic field, called a magnetic moment.

Because hydrogen nuclei are abundant in the body (the body is about 60% H_2O) as well as have a relatively large magnetic moment, they are commonly used as the source of the MR signal. In the absence of an external magnetic field, the magnetic moments of hydrogen nuclei are randomly orientated, leading to no net magnetic effect. In contrast, in the presence of an external magnetic field the hydrogen nuclei align their magnetic moments with the external

magnetic field (Fig 3-1). Some nuclei align with the magnetic field (spin-up), and the others align against the magnetic field (spin-down). Spin-up nuclei have low energy and thus cannot oppose the magnetic field but spin-down nuclei have sufficient energy to oppose the magnetic field. In thermal equilibrium, there are slightly more spin-up nuclei, producing a net magnetic effect (M_0) that is aligned with the main magnetic field (B_0). Increasing the strength of the magnetic field leads to more spin-up nuclei and as a result more MR signal.

In addition to spinning around it own axes, hydrogen nuclei produce another spin under the influence of the eternal magnetic field. This secondary spin is called precession (Fig 3-2). The effect of this is a circular movement around the B_0, processional path. The speed at which these nuclei spin around the B_0 is called precessional frequency. To calculate the precessional frequency, the Larmor equation must be used:

$$\omega = B_0 \times \lambda$$

Where ω is the precessional frequency, measured in MHz, B_0 is the magnetic field, measured in tesla (T), and λ is the gyromagnetic ratio, measured in MHz/T. The gyromagnetic ratio is specific for each nucleus. For hydrogen, it is 42.57 MHz/T.
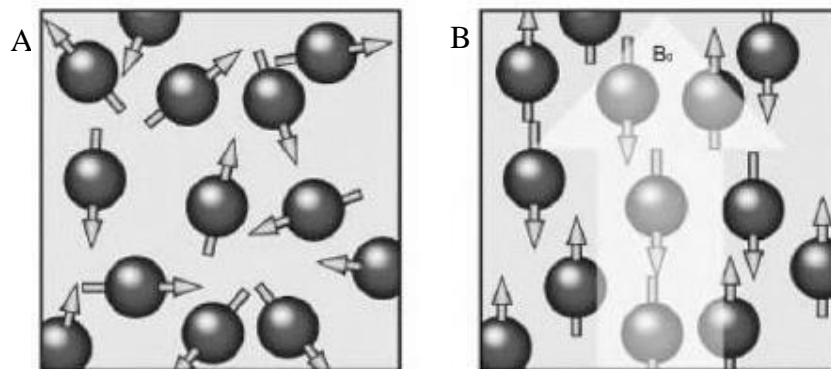
Figure 3-1: The effect of adding the external magnetic field. A) Hydrogen nuclei are randomly oriented, thus the spins cancel out each other. B) After the application of the external magnetic field, spins are either up or down. Adapted from Westbrook and Roth (2011).
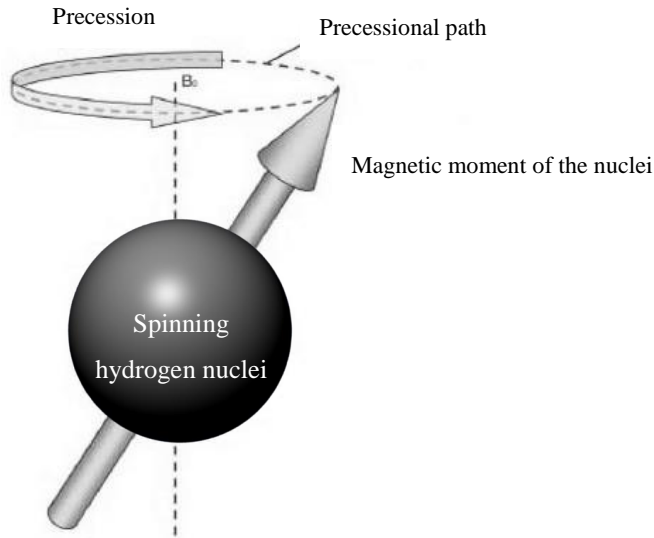
Figure 3-2: The precessional path caused by the external magnetic field. Modified from Westbrook and Roth (2011).

The spinning nuclei have different positions in the precessional path. This is described as being out-of-phase or incoherent. The importance of this will be described below.

3.1.1.2 The radiofrequency pulse (RF)

The net magnetization (M_0) is extremely weak compared to the main magnetic field (B_0), and thus cannot be observed without the application of an RF pulse. The RF pulse is an electromagnetic wave that is transmitted perpendicular to B_0. The RF pulse should have the same frequency as the precessional frequency of hydrogen nuclei. When the RF is applied, hydrogen nuclei resonate (receive energy from the RF pulse). This resonance results in energy absorption from the RF pulse leading an increase in the number of spin-down nuclei. As a result, the M_0 tips over into the transverse plane (Fig 3-3). As the effect of the RF pulse is to tip the M_0 away from the vertical axis, such pulses are usually described by the tip or flip angle they produce (e.g. 90 degrees). The duration and the amplitude of the RF pulse determine this flip angle.
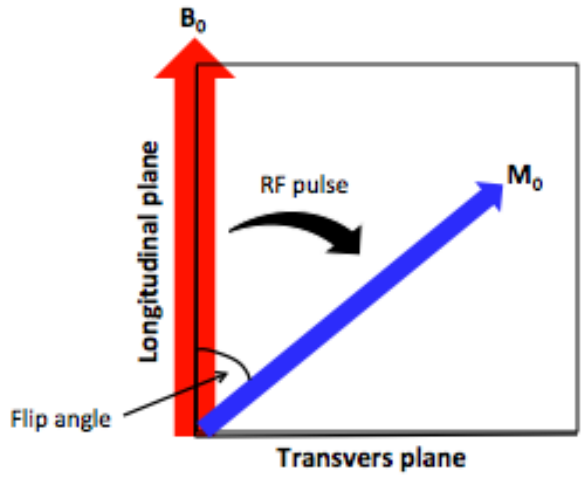
Figure 3-3: The effect of the RF pulse. The net magnetization flips onto the transverse plane.

Another RF effect is that it moves the nuclei in the M_0 into phase, i.e. have the same position (Fig 3-4). A receiver coil is placed in the transverse plane. As M_0 rotates in the transverse plane, it induces voltage in the receive coil. This voltage is the MR signal.

Out of phase (incoherent)

In phase (coherent)
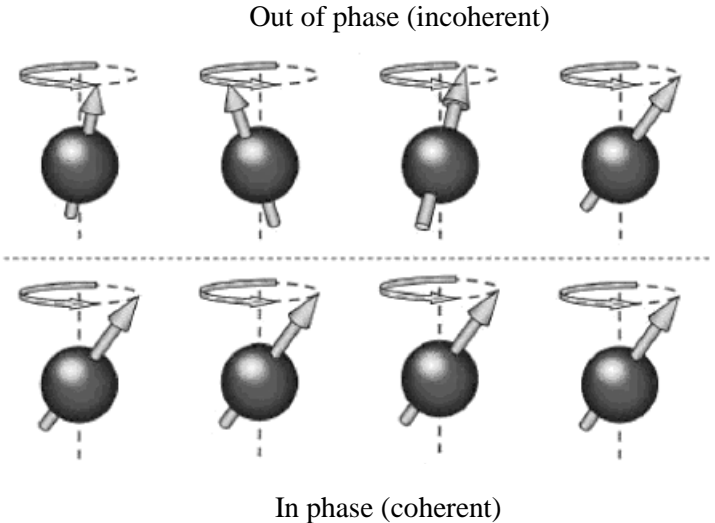
Figure 3-4: The effect of the RF pulse on the phase of the spins. A) Before the RF pulse, hydrogen nuclei are out of phase. B) The spins are in phase after the RF pulse application. Adapted from Westbrook and Roth (2011).

3.1.1.3   Relaxation:

Upon the termination of the RF pulse, the M_0 returns to its initial state. It starts to grow back in the vertical direction, and nuclei start to become out of phase. This decreases the voltage induced in the receiver coil. This is called free induction decay (FID) (Fig. 3-5).

M_0 consists of two components, Mz and Mx-y. Mx-y is M_0 in the transverse plane and thus represents the MR signal (Fig. 3-6). When the M_0 receives a 90 degrees RF pulse, the Mz component is zero as M_0 is on the x-y axis. During relaxation, Mz increases and Mx-y decreases. The time that describes losing 63% of Mx-y is called T2 relaxation time; whereas T1 relaxation time describes the time it takes the Mz to recover 63% of its longitudinal value.

T2 decay

Free induction decay
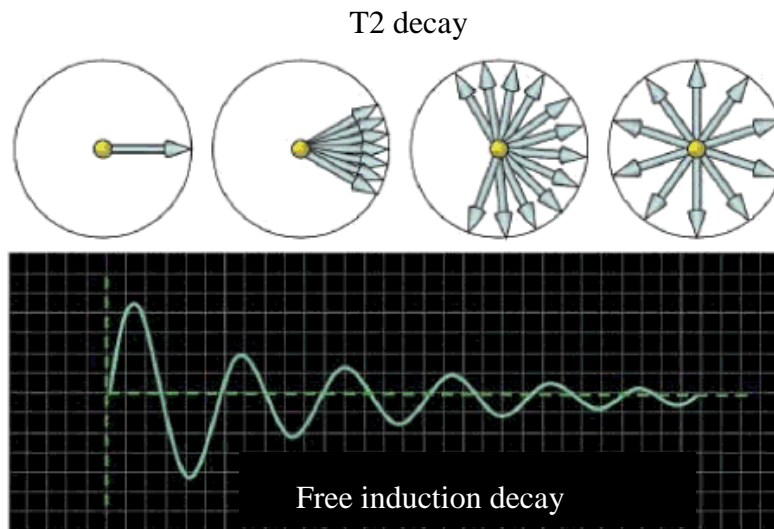
Figure 3-5: The effect of RF pulse termination. Spins in the transverse plane start to dephase causing a decay in the induced signal in the receiver coil, FID. Modified from Westbrook and Roth (2011).
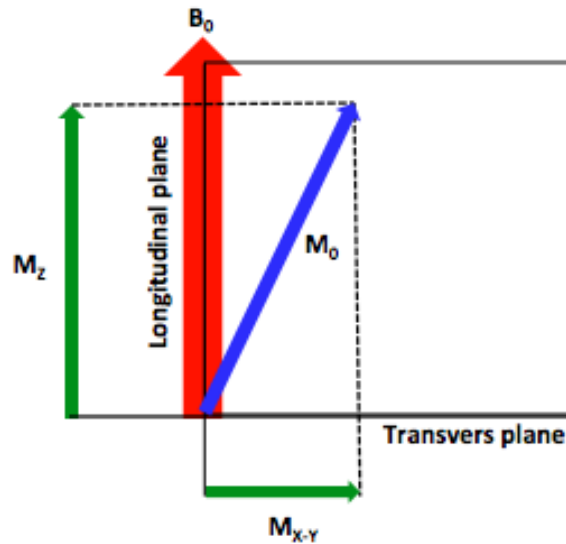
Figure 3-6: The amount of transverse magnetization vs. the signal amplitude.

T1 and T2 relaxation times are specific for each tissue. They are shorter in fat and longer in water. This allows us to obtain contrast in the MRI images. Using certain parameters (TR, TE and flip angle), it is possible to highlight the tissue of interest. T1 weighted images take advantage of the short T1 relaxation time of fat and the long T1 relaxation time of water by using short repetition times (TRs). Because T1 in fat is short, the Mz component will be higher than that of the water. Applying another 90% RF pulse produces more Mx-y component of fat compared to water. Therefore, fat in T1 weighted images appears brighter than water. T2 weighted images, however, take advantage of the short T2 relaxation of fat and the long T2 of water by using long echo times (TEs). Because fat has a shorter T2 than water, using long TE allows us to obtain more signal from water, and therefore, water appears brighter than fat in the T2 weighted images (Westbrook and Roth, 2011).

In addition to T1 and T2 relaxation times, there is a much faster relaxation process called T2*. The T2* relaxation is caused by the inhomogeneity in the magnetic field and the magnetic susceptibility of the tissues. To obtain anatomical images, T2* relaxation can be restored by applying 180 degrees RF pulses to rephase the spins in the transverse plane. In fMRI, however,

T2* is very important as the technique takes advantage of the susceptibility difference between deoxyhaemoglobin and oxyhaemoglobin.

3.1.2 Functional Magnetic Resonance Imaging (fMRI)

fMRI is when MRI is used to study the functional activity of the brain. This technique takes advantage of the positive relationship between neural activity and blood flow. Despite some limitations, the high spatial resolution (1-3 mm^3) makes fMRI the most widely used non-invasive technique to measure neural activity.

3.1.2.1   The BOLD signal

In 1990, Ogawa and his colleagues (Ogawa et al., 1990) found that image contrast is decreased following an increase in the blood flow. Rats breathing 100% oxygen had high contrast, shown as several dark lines in the image. When 10% CO_2 was introduced along with 90% oxygen, the dark lines disappeared, showing a poor contrast image. He concluded that CO_2 increased the blood flow to the brain, leading to low contrast. Because the level of blood in the brain can affect the signal intensity, this technique was called blood oxygenation level dependent (BOLD).

Neural activity requires energy, which in turn is provided by a molecule called adenosine triphosphate (ATP). The production of ATP requires oxygen and the supply of oxygen comes from the blood. Because oxygen is not soluble in water, it is transported around the body bound to an iron-containing protein called hemoglobin. When hemoglobin binds to oxygen, it is called oxyhemoglobin. When no oxygen is bound, it is called deoxyhemoglobin. The importance of this is that the magnetic properties in the oxyhemoglobin are different from that of the deoxyhemoglobin (Pauling and Coryell, 1936). Deoxyhemoglobin is a paramagnetic molecule, i.e. it is slightly attracted to a magnet. It introduces a susceptibility difference between the blood vessels and their surrounding tissues. This susceptibility difference results in dephasing of the hydrogen nuclei, leading to a reduction in the T2*. Oxyhemoglobin, on the other hand, is a diamagnetic molecule, i.e. it is slightly repelled by a magnet, and has a weak effect on the nearby magnetic field. Thus, increasing the oxyhemoglobin concentration increases the local signal (Glover, 2011; Ogawa et al., 1990). This signal is the BOLD signal.

81

3.1.2.2 The hemodynamic response function (HRF)

The typical BOLD signal time course following neural activity is called the hemodynamic response (Fig. 3-7). Immediately after the stimulus onset, the BOLD signal slightly decreases. This initial decrease is known as the initial dip, and its source is highly controversial because it has not always been observed although it is thought to be related to local deoxygenation caused by an temporary, uncompensated increase in metabolic activity (Heeger and Ress, 2002; Malonek and Grinvald, 1996). Following the initial dip is an increase in the BOLD signal, peaking at about 4-8 seconds after the stimulus onset. If the neural activity continues, the BOLD signal will plateau. After the stimulus offset, the BOLD signal starts to return to baseline 7-11 seconds later, accompanied by a signal undershoot. The physiology of this hemodynamic response (specifically, how the relationship between neural activity and blood flow is mediated) is not completely understood.
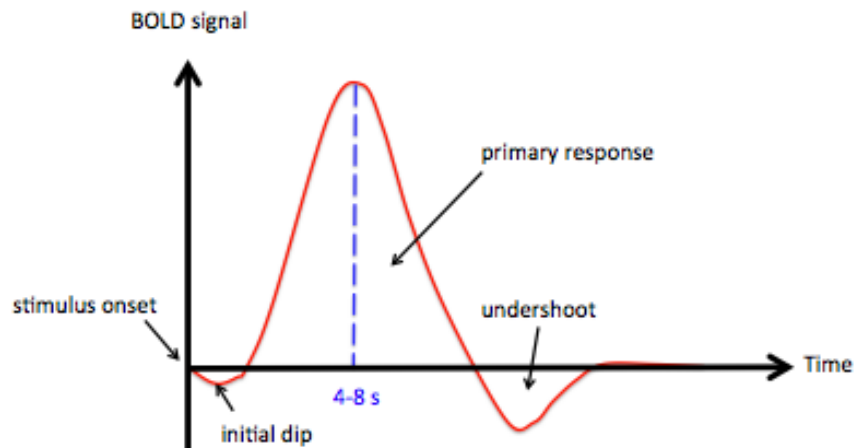
Figure 3-7: The hemodynamic response.

The BOLD signal can represent either positive BOLD responses (PBR) or negative BOLD responses (NBR). The positive BOLD has been demonstrated to correlate with increases in

neural activity indicated by local field potentials (LFP) (Logothetis et al., 2001). In contrast, the source of the negative BOLD is poorly understood. It is been shown that the NBR is caused by responses that are below the pre-stimulus baseline. The NBR is suggested to be driven by an active neural mechanism for three reasons: firstly, the hemodynamic response function cannot entirely explain it (Boas et al., 2008). Secondly, the NBR can be seen in the opposite cerebral hemisphere of the positive BOLD (Smith et al., 2004). Finally, the NBR has been found to correlate with a decrease in membrane potential corresponding to an active suppressive mechanism (Devor et al., 2007; Gouws et al., 2014; Shmuel et al., 2006; Wade and Rowland, 2010).

3.1.3 Limitations of the BOLD technique

The most obvious problem with using the BOLD technique is our poor understanding of the coupling between neural activity and the BOLD signal. Moreover, the BOLD signal has a low temporal resolution, with the signal peaks at about 4-8 seconds after the onset of the stimulus-evoked neural activity. In general, the temporal resolution of fMRI (the shortest interval that it can resolve between two events) is about 1-2 seconds.

3.2 General Methods

The cortex, composed of the grey matter, is the most prominent and most studied part of the human brain. The thickness of the cortex is in the range of 2 and 3 mm. Despite the limited size of the cranium, the brain creates folds (sulci – dips and gyri - peaks) allowing for greater surface area to be packed into a limited 3D volume. In fact, nearly 70% of the cerebral cortex is buried in sulci. Thus to extract and localize the functional information accurately several steps are required.

This section describes the general experimental methods, which were implemented during this thesis. These include the preprocessing steps (realignment, co-registration, normalization and smoothing), the techniques for retinotopic mapping and the fMRI scanning settings.

3.2.1 Preprocessing

There are several steps that are required before the statistical analysis of the data. Each of these steps provides different benefits. The theory of each step is described below.

3.2.1.1 Realignment

Motion-related artifacts are always present in fMRI images. Despite restraints on head movement, subjects show displacements of up to several millimeters (Fig. 3-8). Head movement can introduce changes in the BOLD signal that has nothing to do with the task-related activity. In addition, the statistical analysis assumes that a voxel represents a single location in the brain. Due to movement, the time course from a single voxel might represent a signal derived from another region of the brain. To reduce those false activations, algorithms are employed to correct for motion artifacts. In general, motion correction estimates the movement of the brain throughout the scan relative to a reference (usually the first slice), and then realigns the time series of the brain images to that reference. The realignment is applied by rigid body transformations. This assumes that the size and shape of the slices are the same, and that the slices can be spatially matched to another by a combination of six parameters, three translation parameters in mm (x, y and z) and three rotation parameters in degrees (pitch, roll and yaw) (Clare, 1997).

Time
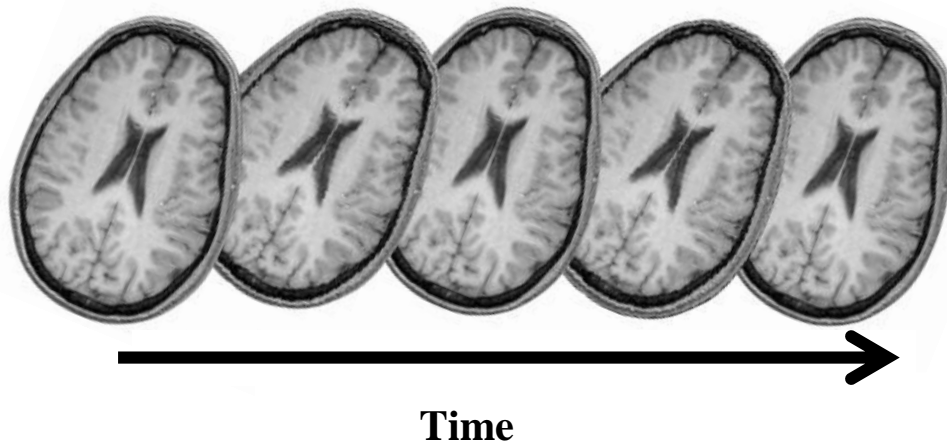
Figure 3-8: Motion correction is based on taken the first slice as a reference to align the other slices to it.

3.2.1.2   Co-registration

Despite the high spatial localization of MRI, the spatial resolution of the commonly used fMRI (EPI) is usually much lower. To overcome this problem, fMRI data is superimposed on a high resolution, T1 weighted, structural image from the same subject. In our work this occurs in two stages: fMRI data are obtained in the same reference space as a set of high-resolution T1-weighted 'inplane' images. These inplanes are then aligned to a high-resolution, full brain anatomical image in which the white and grey matter have been segmented. The same transformation can then be applied to the T2*-weighted fMRI data to bring them into alignment with the same high-resolution anatomy. Finally, the fMRI data can be restricted to the grey matter of the high-resolution data (where we know that the BOLD signal actually arises).

3.2.1.3   Spatial normalization

To compensate for the huge differences of sizes and shapes of individuals brains, a process called normalization can be used to register an individual brain to into a standard brain. The most widely used coordinate systems are the one described by Talairach and Tournoux (Talairach JT, 1988), and the Montreal Neurological Institute (MNI) space. In our experiments however, we analyze data in the space of individual subjects and no spatial normalization was used.

3.2.1.4   Spatial smoothing

Another preprocessing step is to remove the high spatial frequencies of the signal by applying a low pass filter (a blur). Although spatial smoothing results in reduced spatial resolution, it has a number of advantages including, increasing the signal to noise ratio and making the noise statistics more Gaussian and therefore amenable to parametric statistical analysis. Because our experiment depended on the analysis of very high resolution images, we did not apply spatial smoothing to our data.

3.2.2   Software package

We use mrVISTA software for presenting and analyzing the data (http://white.stanford.edu/newlm/index.php/Software). This package is optimized for surface-

85

based analysis and retinotopic mapping. Anatomical volumes were segmented into white and grey matter volumes for each hemisphere using the Freesurfer4 "autorecon" script http://surfer.nmr.mgh.harvard.edu. This was followed by manual topology checking using mrGray, part of the standard mrVISTA toolbox. Cortical surfaces (grey matter) were constructed from this segmentation of visualization using mrMesh, a tool in mrVISTA toolbox.

3.2.3 Retinotopic mapping

As discussed before, the retinal signals are projected into the visual cortex in an organized manner. This means that points that are close together on an object and on the retina activate neurons that are close together in the visual cortex. Despite the fact that the fovea (the center of the retina) accounts for only 0.01% of the retina's area, signals from the fovea account for approximately 10% of the retinotopic map on the visual cortex (Van Essen and Anderson, 1995). This is known as cortical magnification.

3.2.3.1   Phase-encoding technique

The borders of the different visual regions can be described precisely because retinotopic mapping reverses at the borders of these regions. A method to measure retinotopic mapping were introduced about 20 years ago (DeYoe et al., 1994; Stephen A. Engel et al., 1994). The method is based on checkerboard-like stimuli that change position over time, and create travelling waves of activity in the primary visual cortex (Fig. 3-9). One stimulus consists of a number of expanding rings to measure the eccentricity maps (the distance from the center of gaze). A second stimulus consists of a number of rotating wedges to measure the angle maps. This technique is called phase-encoding retinotopy or the 'traveling wave' method. The data are usually superimposed on an inflated and flattened cortex to aid interpretation. Colors in the retinotopic maps represent the response phase at each location.
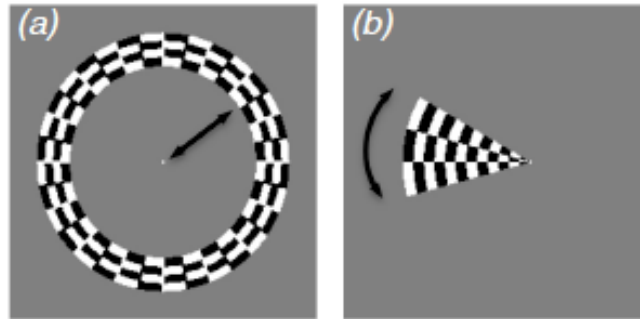
Figure 3-9: Retinotopic mapping stimuli. a) is the expanding stimulus to map the eccentricity representation of the visual field. b) is the rotating wedges to map the angular representation of the visual field.

3.2.3.1.1   Eccentricity organization

As discussed before, eccentricity organization can be measured by using an expanding ring stimulus. An example of this is seen in (Fig. 3-10). The retinotopic maps are organized in the visual cortex as follows: V1, V2 and V3 contain a foveal representation located in the occipital pole, with more peripheral representations extending into the anteromedial cortex. The foveal representation occupies a large surface compared to the peripheral representation (Brewer and Barton, 2012).
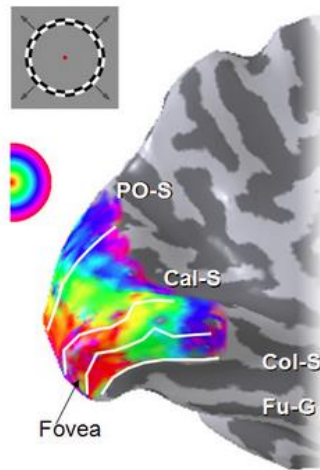
Figure 3-10: The inflated cortical surface shows the eccentricity map. Abbreviations: CC, corpus callosum; POS, parietal-occipital sulcus; CaS, calcarine sulcus. Adopted from Brewer and Barton (2012).

3.2.3.1.2   Angular organization

Angular organization can be measured by using a rotating wedge stimulus. An example of this is seen in (Fig. 3-11). Polar angle indicates the angle from the horizontal meridian. The boundaries between each map are defined by the location of vertical meridian representation. V1 contains a representation of the entire hemifield. V1/V2d border is delineated by the lower vertical meridian (red band), and the upper vertical meridian (blue band) at the V1/V2v. On the contrary, V2 and V3 contain representations of only spilt-hemifield (quarterfields), which are indicated by their positions dorsal (upper) or ventral (lower) to V1. The boundaries between the dorsal V2 and V3 are defined by the horizontal meridian, from lower vertical meridian towards the horizontal meridian for V2 and then it reverses back to the lower vertical meridian. The boundaries between the ventral V2 and V3 are defined by the horizontal meridian as well. This time V2v is represented by the upper vertical meridian to the horizontal meridian, and then reverses back towards the upper vertical meridian to represent V3v (Wandell and Winawer, 2011).

88
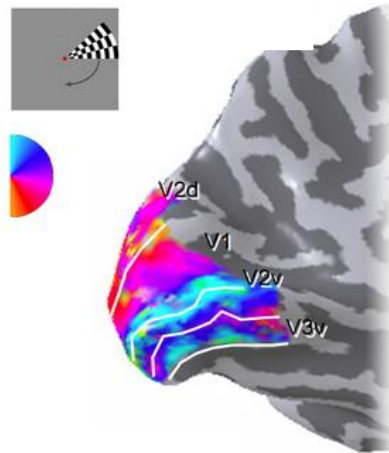
Figure 3-11: The inflated cortical surface shows the angular map. Adopted from Brewer and Barton (2012).

Retinotopic maps are an essential step in the analysis of spatial attentional modulation in V1. These maps can be obtained for each hemisphere for each participant, allowing researchers to identify visual representation of each stimuli placed in the visual field. These functionally defined regions can then be used as regions of interest (ROIs). These ROIs can be stored on disk from one session to another, meaning that those that already have retinotopic maps will not be required to do another retinotopic scan.

3.2.4 Defining region of interest (ROI)

Two methods of identifying ROIs are common in the literature: the use of anatomical landmarks and functional localization. Using anatomical landmarks is only possible for clearly defined regions such as amygdala. The majority of brain regions, however, lack these defined regions. Another problem in these structural ROIs is that the defined ROIs may have different response properties, i.e. a variety of neurons coding for different information.

By using a separate localizer scan, functional localization of ROIs can overcome these problems associated with structural ROIs. Consequently, this method has been used extensively in vision studies.

3.2.4.1 Functional localizer

The localizer we used was a 'block design' to identify four regions of interests in the primary visual cortex for further analysis. In this type of experiment, stimuli are presented one after the other in ordered blocks and each stimulus is presented for a relatively long time (several seconds). In our experiment, we presented circular stimuli in four well-separated parts of the visual field: the left ventral, left dorsal, right ventral and right dorsal. These positions were chosen carefully to generate a single stimulus representation in each quarterfield (and therefore a single response in each quadrant of V1, V2 and V3). These localizers were sinusoidal gratings of 100% contrast, 2.1° radius, spatial frequency of 2 cycles per degree (cpd) and frequency of 6 Hz. Each disc was presented for six seconds and the whole block was repeated eight times (Fig. 3-12). Localizers were generated using Psykinematix software version 1.4.3, and ran by a Macintosh computer running the Mac OS X. These localizers were rear-projected (Dukane Image Pro 8942 LCD projector) onto an acrylic screen in the bore of the MRI scanner at a viewing distance of 57 cm. Lying supine, subjects viewed the stimuli via a front-silvered mirror placed above the head coil. The participants were asked to fixate at the center of the screen throughout the scan.

A

Single stimulus block

(repeated 8 times per scan)

6 s

24 s

B

5 deg

5 deg
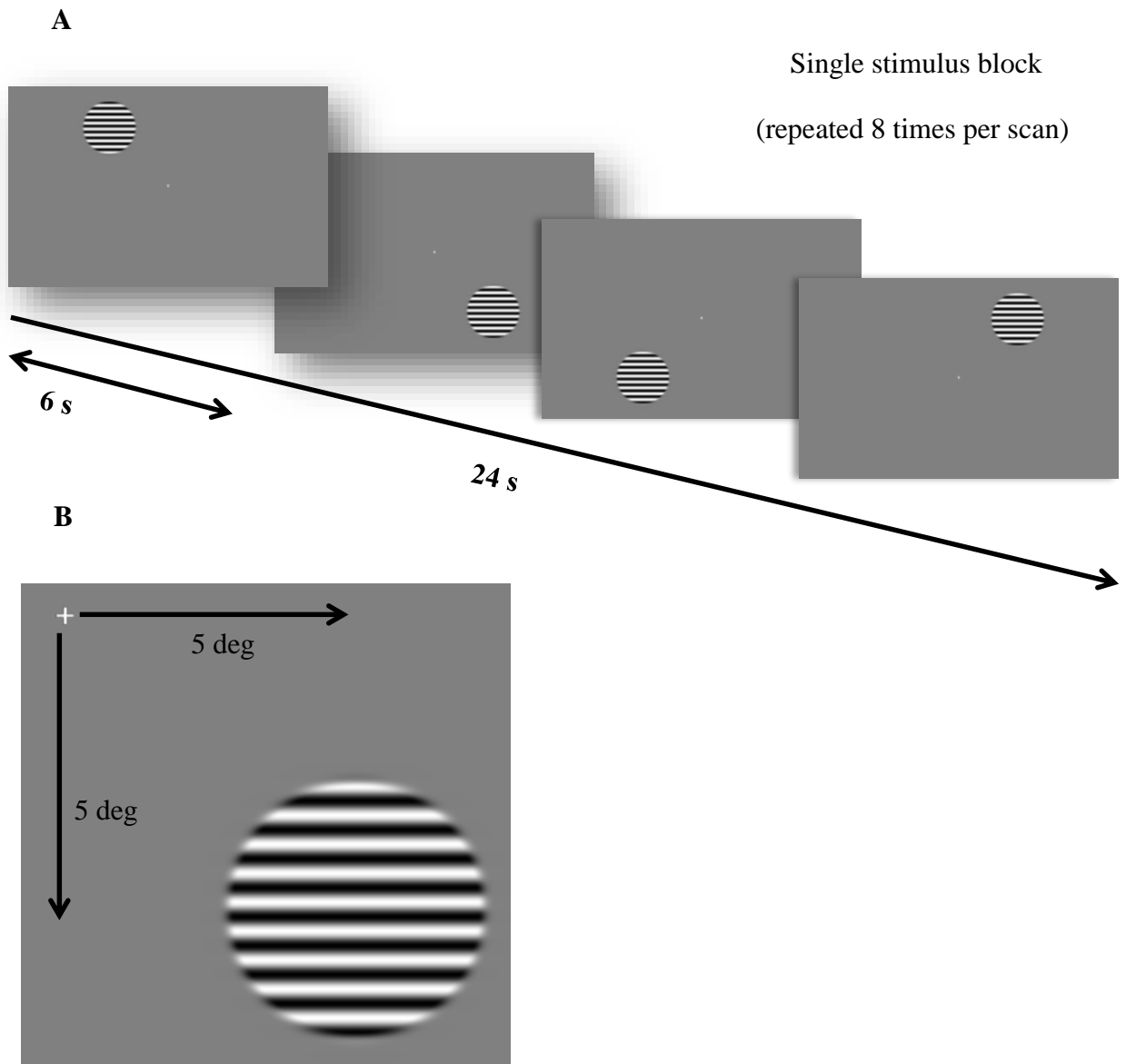
Figure 3-12: Localizer configuration and timings. A, the stimulus was presented for 6 seconds at four different positions. B, shows the exact position of the stimulus at 5 cm from the fixation point.

3.2.5 fMRI Data Analysis

3.2.5.1   General Linear Model (GLM)

The majority of fMRI studies involve either asking the participant to perform a specific task or the participant is exposed to particular stimuli at a specific time. fMRI analyses are based on the assumption that these tasks or stimuli generate activities in certain regions of the brain (see section 1.1.2). To identify the contribution of each stimulus to the signal variation, a model is created representing the task of stimulus in time convolved with the hemodynamic response function (HRF). In brief: each component of this model is assigned a weight (a 'beta value') and a least-squares solution to the model provides an estimate of the value for each beta value.

The method is called the 'general linear model' (GLM) (Friston et al., 1995) and it treats the data as a linear combination of model functions (predictors) plus noise. The model functions for each voxel are generated by convolving the model HRF with a condition matrix describing the appearance of each stimulus type. These model functions are assumed to have known curves but their amplitudes must be estimated:

$$Y = \beta_1 X_1 + \epsilon$$

Where Y is BOLD response, X_1 is the predictor (the expected shape of the BOLD response), β_1 quantifies how much each predictor (X) independently effect Y and ϵ explains the variance in the data (Fig. 3-13). The least-squares solution to this model is fully determined and provides a single number for each of the beta values at each voxel. These beta values are therefore indicators of the strength of each stimulus component at a particular voxel throughout the scan. This GLM procedure is implemented in all fMRI analysis packages including the VISTA software we used in our study.
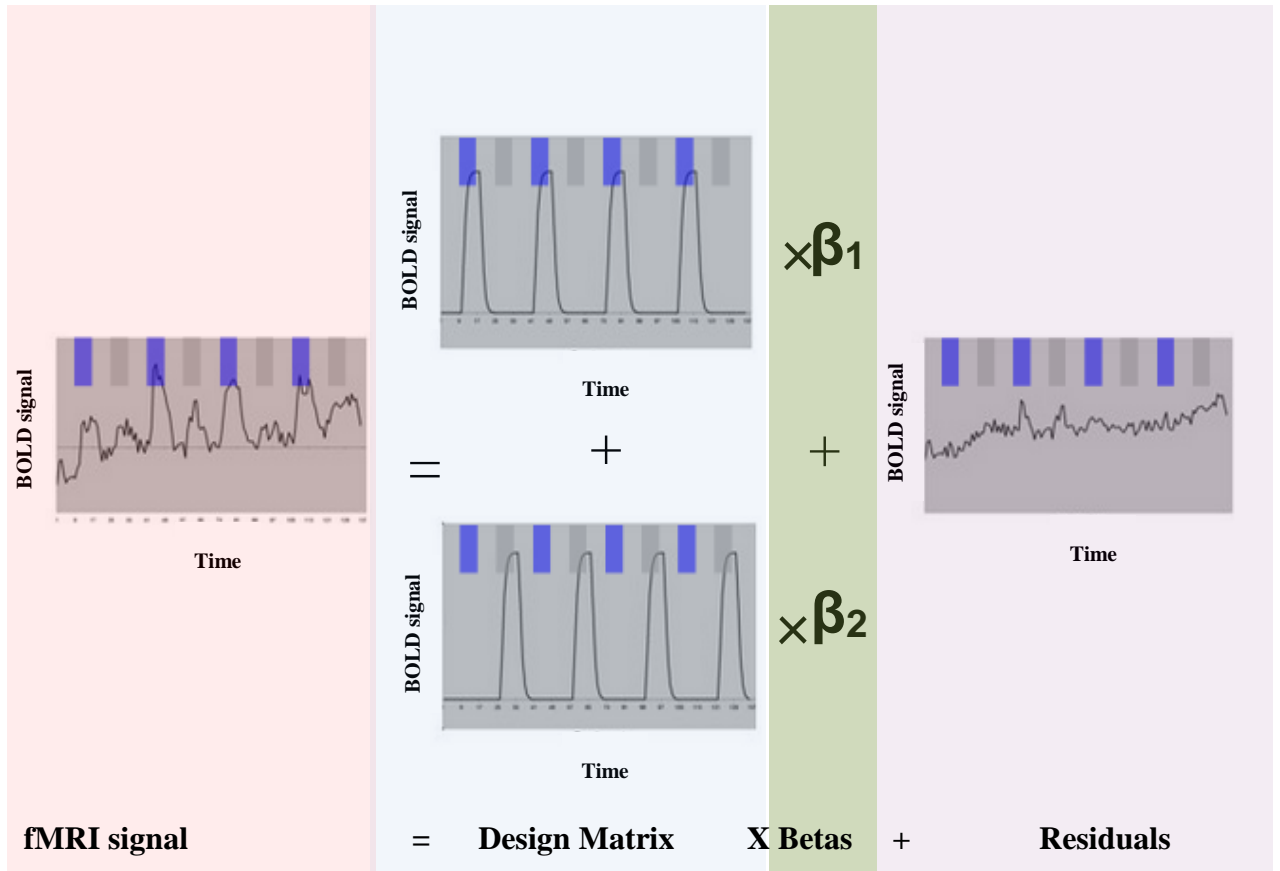
Figure 3-13: The GLM for two predictors can be explained by what we can explain (the design matrix convolved with HDR function), and the betas which are how much of the design matrix can be explained, plus the residuals which we cannot explain.

4 Chapter 4: Abnormal gain control in Drosophila mode of epilepsy

4.1 Introduction

Recent work using steady-state visually-evoked potentials (SSVEPs) has demonstrated abnormal visual gain control in human epilepsy patients (Porciatti et al., 2000; Tsai et al., 2011). In Drosophila, a mutation in the *kcc* gene (*kcc^{DHS1}*) renders young flies susceptible to light and shock-induced seizures (Hekmat-Scafe et al., 2006) and has been used as a model of human juvenile epilepsy. Here, we used SSVEPs to study the age profile of contrast-driven photoreceptor and neuronal responses in both *kcc^{DHS1}* and wild type (*w^-*) Drosophila. Then we describe the relationship between the *kcc^{DHS1}* mutation and the eye color of the fly.

4.2 Material and methods

4.2.1 Fly stocks and genetics

A list of Drosophila strains used in this experiment is given in Table 4-1. D506 female flies carrying the homozygous *kcc^{DHS1}* mutation were used in this experiment (*w^{1118}; kcc^{DHS1}/ kcc^{DHS1}*). These flies also bear the white mutation in the first chromosome. As these flies have white eyes, we used, as controls, the white-eyed wild type flies (*w^-*) to avoid any confounding effect of eye pigmentation.

Stock No.	Genotype	Abbreviation	Source
D506	*w; kcc^{DHS1}/CyO*	*kcc^{DHS1}*	*A generous gift of Mark Tanouye*
w^{1118}	*Wild type (White eyes)*	*w-*	*Elliott/Sweeney lab stock*

Table 4-1: The Drosophila stock used in the 1st part of this Chapter.

Flies were kept in glass bottles containing maize-meal fly food at 23°C, and allowed to lay eggs for 10 days. After 10 days, the adult flies were removed. The bottles were inspected daily,

and the newly hatched females homozygous for kcc^{DHS1} (kcc^{DHS1} / kcc^{DHS1}) were transferred into vials containing yeast-sucrose-agar fly food (Carpenter, 1950). For one-day-old flies, the visual responses were tested within 8-18 hours after eclosion. More flies were tested at 2, 3, 10, 20 and 30 days after eclosion. The tests were performed at approximately the same time of the day (between 5 pm and 1 am) to avoid any effect of circadian rhythms on the flies' visual responses (Nippe, 2015).

4.2.2 SSVEP methods

4.2.2.1   Stimuli

The Drosophila ERG used in this experiment was set up to accommodate two flies simultaneously to increase the efficiency and reduce between-subject variance in the results. Stimuli used in this experiment consisted of changes in illumination generated using a fiber optic light directed onto the flies' eyes at a distance of 7 cm. A diffusing screen was placed in front of the fiber optic ensuring that the ommatidia were stimulated with a relatively homogeneous light field.

Stimuli were produced by a controllable fiber-coupled multi-channel LED system (Prizmatix FC5-LED) run by a 16-bit analogue to digital converter (National Instruments USB-6229). This was performed under the control of Matlab 2011b (Mathworks, Natick, MA) with the Data Acquisition Toolbox installed.

We examined responses to 7 contrast levels ranging from 0% to 69% contrast in equal steps. We also examined the effect of adding in a mask with a constant contrast of 30%. Trials were randomized and the entire sequence of 14 trials was repeated 5 times. The total data acquisition time was approximately 12 minutes.

4.2.2.2   SSVEP recording

Signals were amplified and then digitized using the same PC and Measurement Computing DAC/ADC that ran the stimuli. The verification of the quality and stability of the electrical contacts was performed by a preliminary trace recording using DasyLAB software (Measurement Computing Corporation, 2012). The sampling rate was set to 1000 Hz.

The visual responses of the flies were checked by manually turning the LED on and off. Only the flies that showed high and maintained responses were accepted.

4.2.2.3 Analysis

The analysis is conceptually similar to that used previously (Xiao and Wade, 2010, Wang and Wade, 2011, Tsai et al., 2011) in human studies, and identical to that used by Afsari et al. (2014) in their fly study. In brief description, we computed the amplitude and phase of the SSVEP responses at the low-order multiples (termed 1F1 and 2F1 for the probe condition, and 1F2 and 2F2 for the mask condition), and the combinations (termed 1F1+1F2 for the probe condition and 2F1+2F2 for the mask condition) of the input frequencies (see Chapter 2).

To understand what the effect the kcc^{DHS1} mutation has on the visual system of the fruit flies, we analysed the responses to the mean of the two highest contrast levels. Although some of the data can be fit well with a hyperbolic ratio function, $R = R_{max} \frac{C^n}{C^n + C_{50}^n}$, some of the CRFs cannot because they do not saturate. Thus, we chose to use the mean of the two highest contrast levels to estimate the maximum response. This approach was taken instead of only taking the highest level due to the observation that the responses do not always increase monotonically and to reduce measurement noise.

4.2.2.3.1 Statistical analysis

One way to analyze these responses would be to use multivariate statistics. However, responses of 1F1 and 2F1 are not completely independent (photoreceptors synapse to the lamina neurons and the feedback responses from the lamina to the photoreceptors). For simplicity, we performed a two-way ANOVA. A multivariate approach might also yield useful information, using SPSS software (IBM SPSS Statistics, version 22).

4.3 Results

4.3.1 Contrast response functions of the *kcc^DHS1* flies

The visual response in Drosophila is mediated by the retinal photoreceptors, which synapse onto the lamina neurons. Then, the majority of the lamina neurons synapse onto the medulla neurons, only some lamina neurons synapse onto the amacrine cells to mediate the lateral interactions (Heisenberg, 1971). It is clear that all these neurons are synaptically linked. They can be disambiguated to some degree by the different components they generate in the frequency domain (Afsari et al., 2014).

Our experiments were designed to present stimuli similar to that used in previous human and animal studies (Tsai et al., 2012). As in those studies, our stimuli contained different contrast levels allowing us to generate and analyze the contrast response functions (CRFs).

We sought to examine the effect of the kcc^{DHS1} mutation on the Drosophila visual system by comparing the responses of kcc^{DHS1} flies to the white-eyed control (*w-*) flies. Because the effect of the kcc^{DHS1} mutation is age dependent (Hekmat-Scafe et al., 2006), we recorded the responses across different ages (1, 2, 3, 10, 20 and 30 days).

Performing the experiment as described above allows us to measure the responses to both the probe and mask separately even though they are presented at the same time. Based on previous studies (Afsari et al., 2014; Busse et al., 2009), we expect to see a decrease in the probe response (due to contrast gain control) when the mask is presented at the same time.

The CRFs from control flies (*w-*) at days 1, 2, and 3 are shown in (Fig. 4-1). We can see that the unmasked (probe) responses (shown in grey) from both the first (1F1) and second (2F1) harmonic components increase monotonically with contrast. Increasing probe contrast increased the responses to the probe. After the application of a mask contrast at a different frequency, the responses to the probe reduced for the 1F1 responses but it did not seem to have an effect at the 2F1 level. The effect of adding the mask contrast on the contrast response functions (CRFs) can be described as a rightward shift in the CRFs. Masking at this stage shows a pure contrast gain change. Older control flies, i.e. day 10, 20 and 30, have similar responses to the young flies except that the effect of adding the mask contrast is evident at the 2F1 level. Here, the masking

effect is best explained by both rightward shift and downward compression of the contrast response functions (CRFs) (Fig. 4-2). Masking here is a combination of both contrast gain (rightward shift) and response gain (scaling of the overall response curve).

w-
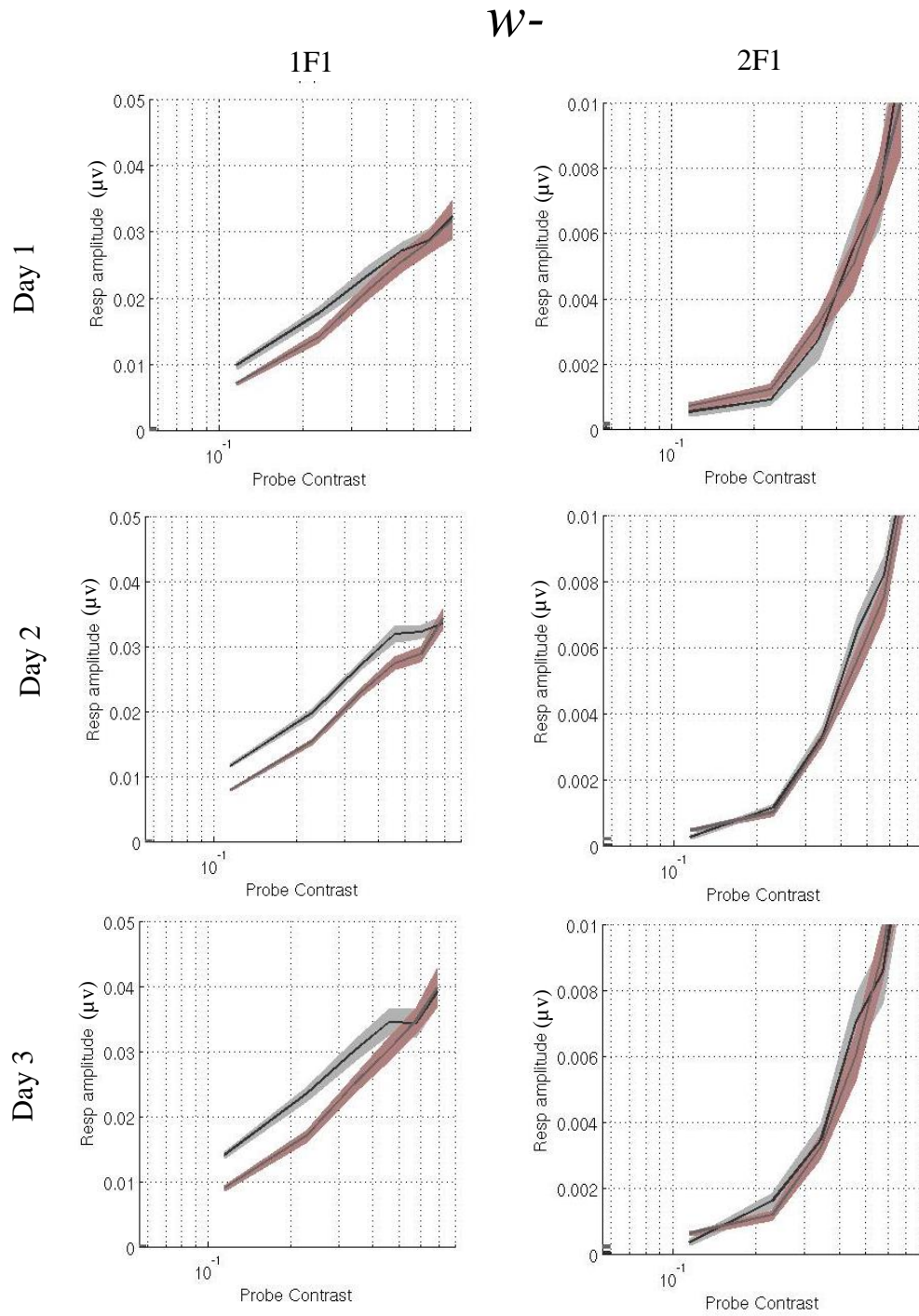
Figure 4-1: Contrast Response Functions for wild-type flies are increasing monotonic curves, with no plateau and little masking. The masked (in red) and unmasked (in grey) CRFs for *w-* flies aged 1, 2 and 3 days at the 1F1 and 2F1 levels. 2F1 curves are steeper than 1F1 curves, and the masking effect is absent. Day 1, *N*= 12; Day 2, *N*= 32; Day 3, *N*=20.

1F1

2F1

Day 10

Day 20

Day 30
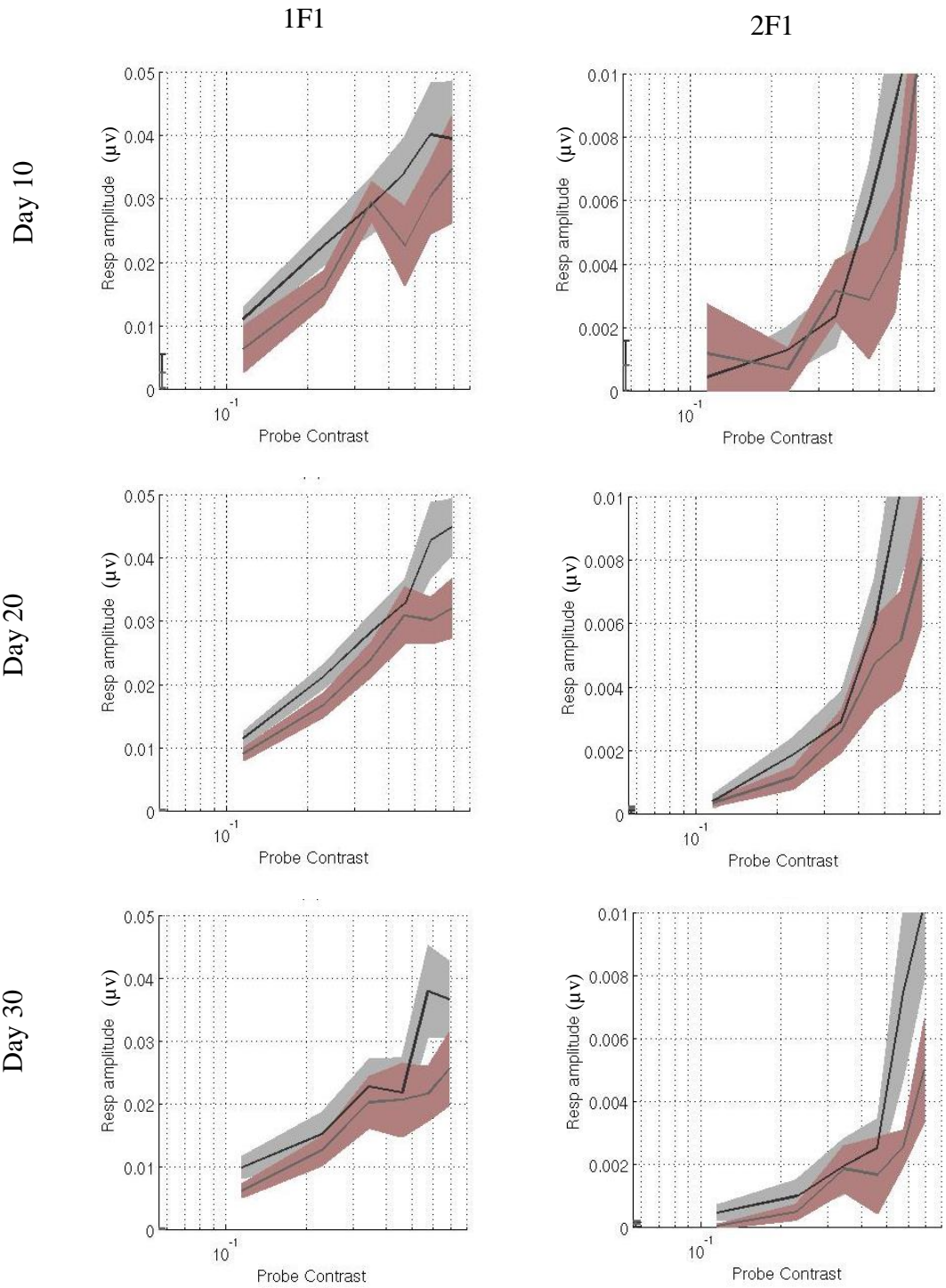
Figure 4-2: Contrast Response Functions for wild-type flies are increasing monotonic curves, with no plateau and little masking. The masked (in red) and unmasked (in grey) CRFs for *w-* flies aged 10, 20 and 30 days at the 1F1 and 2F1 levels. 2F1 curves are steeper than 1F1 curves. Day 10, *N*= 8; Day 20, *N*= 12; Day 30, *N*=9.

When we looked at the kcc^{DHS1} flies, we noticed that the responses increased with contrast but that they were weak at the photoreceptor level particularly early in life. When a mask contrast was applied, the contrast response functions (CRFs) showed predominantly a rightward shift. Therefore, the effect of masking in the kcc^{DHS1} flies can be thought of as primarily a contrast gain change. Young kcc^{DHS1} flies demonstrated noisy neural responses (Fig. 4-3), particularly at day 1 and 2. These neural responses (2F1) become more stable by day 10 and 20. The effect of adding the mask on 2F1 is best explained by the rightward shift of the contrast response functions (CRFs). On the contrary, old kcc^{DHS1} flies show weak masking especially at the neural level and its effect is best described by response gain (Fig. 4-4).

$$kcc^{DSH1}$$

1F1

2F1

Day 1

Day 2

Day 3
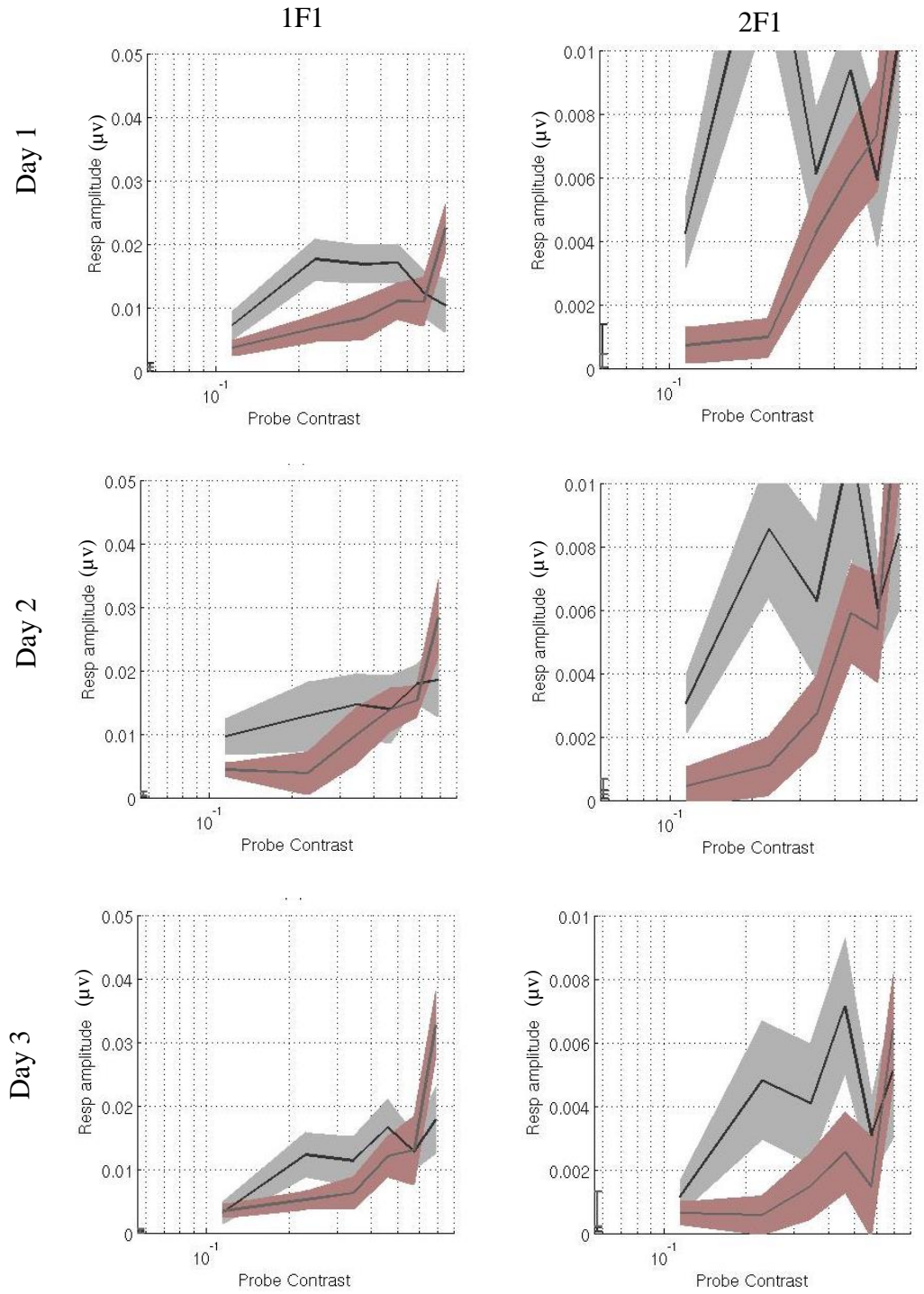
Figure 4-3: Contrast Response Functions for the kcc^{DHS1} flies showing increasing responses with contrast. The unmasked responses (in grey) are very stable at the 1F1 level but unstable at the 2F1 level. The masked (in red) responses show no saturation. 2F1 curves are steeper than 1F1 curves. Day 1, N= 16; Day 2, N= 12; Day 3, N=14.

kcc^{DSH1}

1F1

2F1

Day 10

Day 20

Day 30
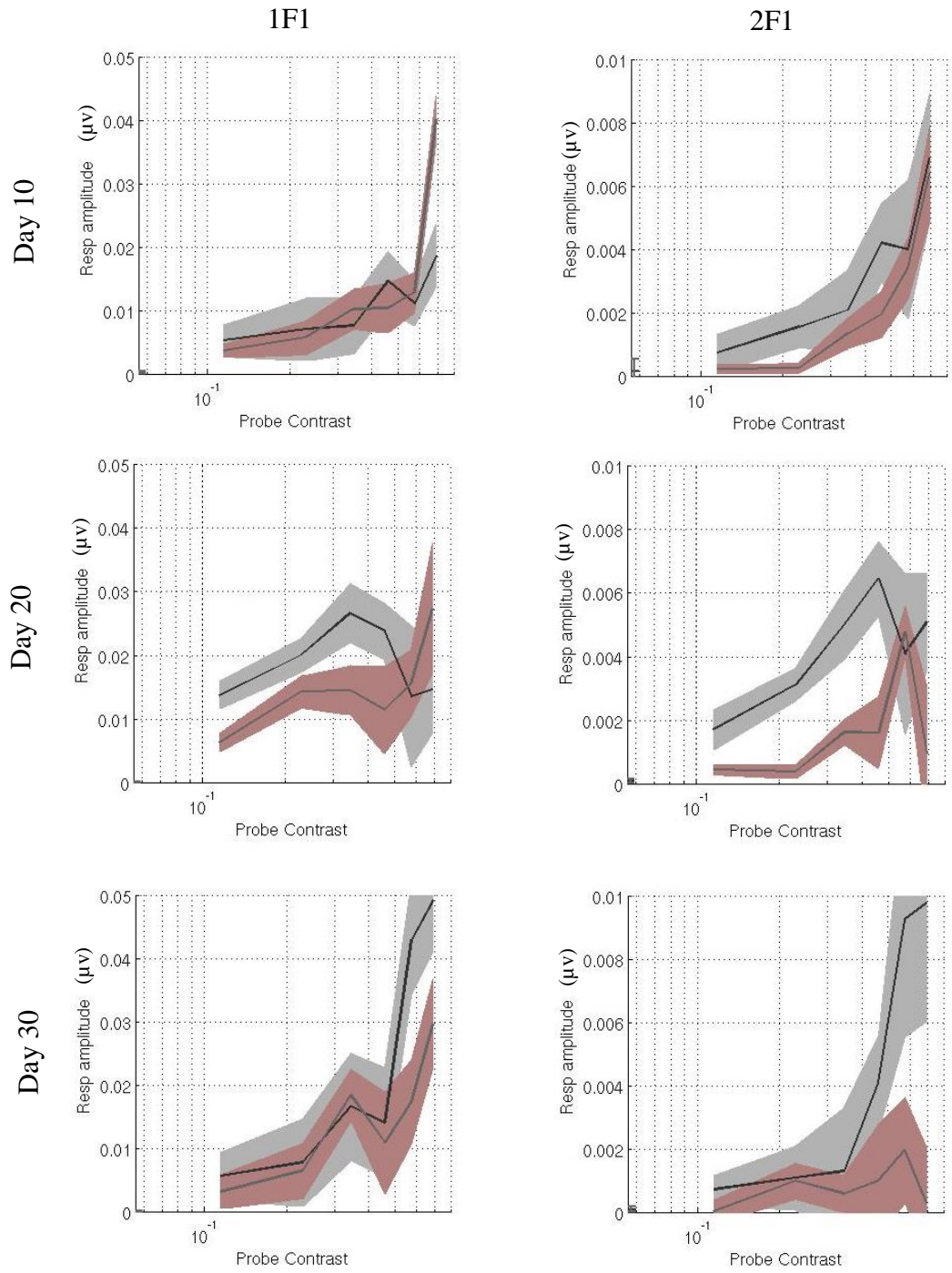
Figure 4-4: Contrast Response Functions for the kcc^{DHS1} flies showing increasing responses with contrast. The unmasked (in grey) and masked (in red) responses are stable at the 1F1 and 2F1 levels. More masking is present at the 2F level. Day 10, N= 12; Day 20, N= 12; Day 30, N=9.

4.3.2 The maximum photoreceptor (1F1) responses

Because fitting the non-saturating data with the hyperbolic ratio did not result in a good estimation of the maximum responses (R_{max})- see section 6.1.2.4 in Chapter 6, we analysed the maximum responses by taking the mean of the two highest contrast levels.

4.3.2.1 Maximum 1F1 responses of *w-* flies

First of all, we examined each phenotype individually. At the photoreceptor level (1F1), the control (*w-*) flies showed steady unmasked and masked responses at young ages (from day 1 to day 3) then peaked at around day 10 and day 20 before starting to drop by day 30 (Fig. 4-5). In addition, the effect of masking seems to be greater at old ages (day 10 to day 30). To identify the effect of age, we divided the age differences into two categories, young (day 1 to 3) and old (day 10 to 30).

Source	ANOVA Results
Age (young vs. old)	F= 14.1, df =1, *p<0.000*
Mask (unmasked vs. masked)	F= 34.3, df =1, *p<0.000*
Age * Mask	F= 30.9, df =1, *p<0.000*

Table 4-2: The results of performing a two-way ANOVA on the 1F1 responses of the w- flies.

A 2 (age: young vs. old) x 2 (mask: unmasked vs. masked) between subjects ANOVA was conducted to study the 1F1 differences between unmasked and masked responses as a function of age (Table 4-2). There was a significant main effect of age, such that the young flies ($\bar{x}$=0.068, SD= 0.01) had significantly lower 1F1 responses than old flies ($\bar{x}$=0.076, SD=0.025). The main effect of masking was also significant, such that the unmasked responses ($\bar{x}$=0.075, SD= 0.017) had significantly higher 1F1 responses compared to the masked responses ($\bar{x}$=0.066, SD= 0.015). In addition, the interaction effect was significant: the change in response due to masking depended on age as well.

Briefly, masking is present in older flies but not in younger flies. The difference between unmasked and masked responses was not significant early in life, $p > 0.05$, but was highly significant in old flies, $p < 0.001$ (Fig. 4-6).
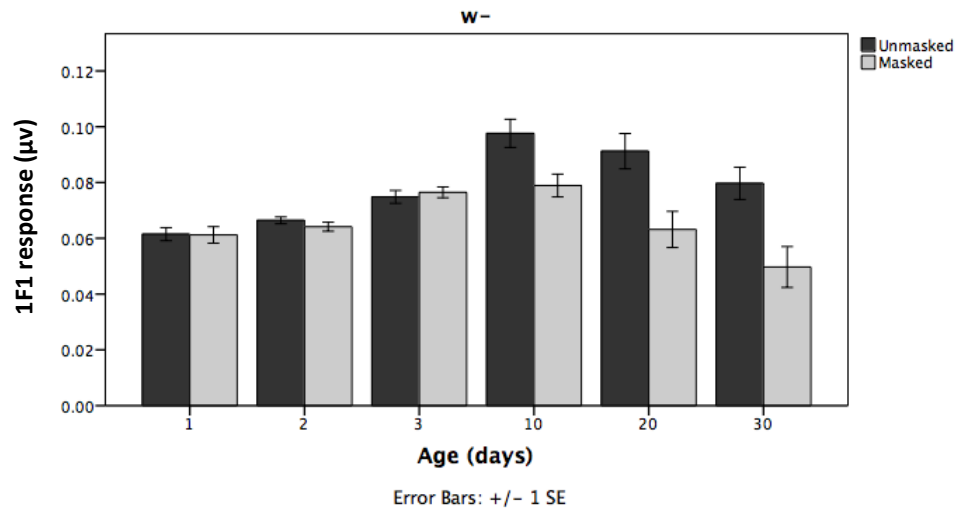
Figure 4-5: The maximum 1F1 values for the masked and unmasked responses of *w-* flies, aged 1, 2, 3, 10, 20 and 30 days. More responses and masking are present in 10, 20 and 30 days old flies.
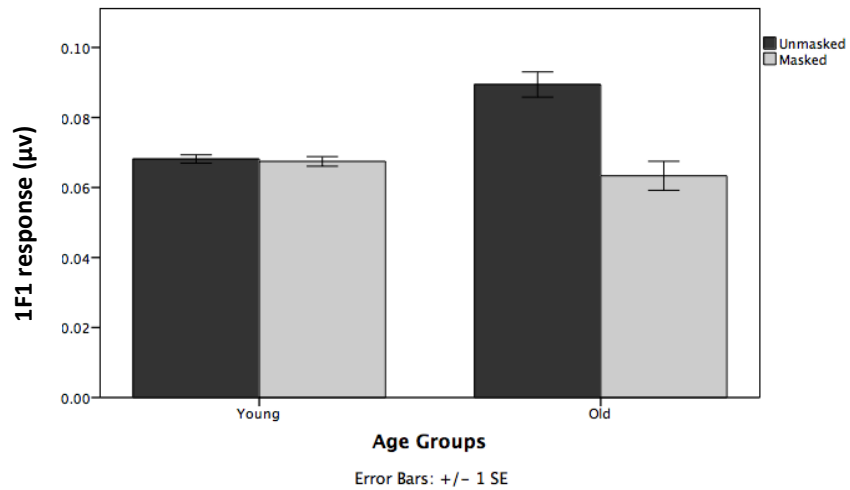
Figure 4-6: The maximum 1F1 values for the masked and unmasked responses of *w-* flies. More responses and masking are present in older flies. Young represents 1, 2 and 3 days old flies, and old represents 10, 20 and 30 days old flies.

4.3.2.2 Maximum 1F1 responses *kcc*^{DHS1} flies

First harmonic (1F1) responses in *w-* flies increase gradually with age up to around 10 days and then decrease again. In contrast, unmasked 1F1 responses for the *kcc*^{DHS1} flies increase monotonically with age peaking sharply at day 30 (Fig. 4-7). Similar to our observation for the control (*w-*) flies, the effect of masking seems to be greater at old ages (day 10 to day 30). Again, we wanted to look at the effect of age, so we divided the age differences into two categories, young (day 1 to 3) and old (day 10 to 30), and then conducted a 2x2 ANOVA (Table 4-3).

Source	ANOVA Results
Age (young vs. old)	F= 22, df =1, **p<0.001**
Mask (unmasked vs. masked)	F= 0.03, df =1, p>0.05
Age * Mask	F= 9.6, df =1, **p<0.01**

Table 4-3: The results of performing a two-way ANOVA on the 1F1 responses of the kcc^{DHS1} flies.

There was a significant main effect of age, such that the young flies ($\bar{x}$=0.036, SD= 0.014) had significantly lower 1F1 responses than old flies ($\bar{x}$=0.052, SD=0.03). However, the main effect of masking was not significant, such that the overall unmasked responses ($\bar{x}$=0.0425, SD= 0.027) and the masked responses ($\bar{x}$=0.043, SD=0.02) are not significantly different from each other. The interaction effect, however, was significant: masking increased responses in young flies but decreased it in older animals. The unmasked responses were significantly lower in the young flies compared to the old flies, $p<0.001$. The masked responses however, were not different between the two age groups, $p>0.05$. Moreover, early in life, the unmasked responses were significantly lower than that of the masked responses, $p<0.05$. At older ages, the unmasked responses were significantly greater than the masked responses, $p<0.05$ (Fig. 4-8). The increased masked responses in younger animals are curious: We hypothesize that they may result from an increase in broadband noise triggered by the increased overall contrast in the mask conditions.
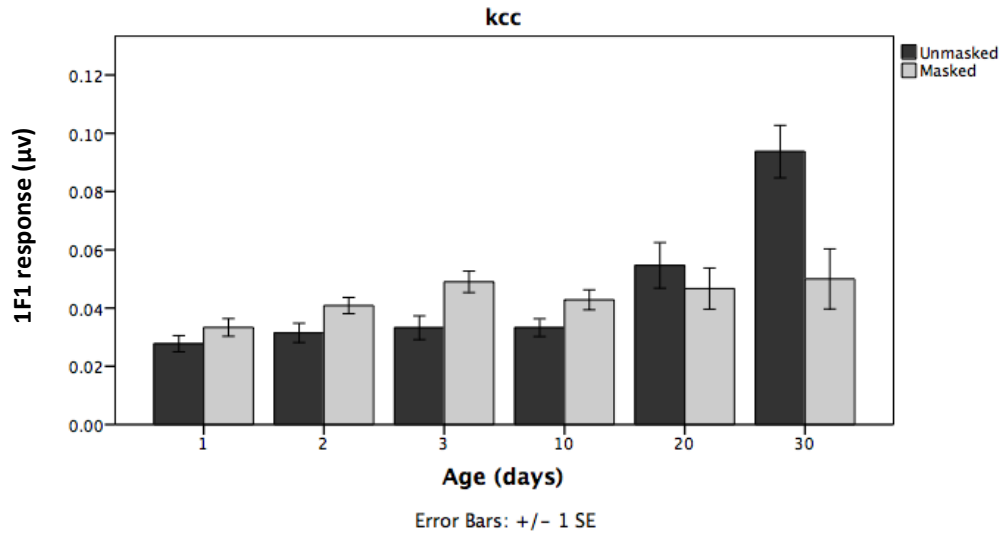
responses of *kcc^{DHS1}* flies. Aged 1, 2, 3, 10, 20 and 30 days. The 1F responses as well as masking show a gradual increase with age.
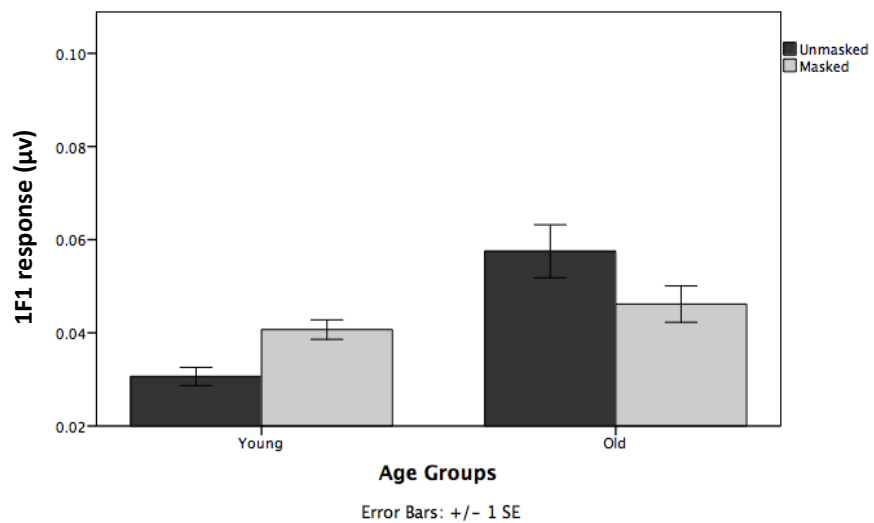
Figure 4-8: The maximum 1F1 values for the masked and unmasked responses of *kcc^{DHS1}* flies. Young flies have reduced unmasked responses compared to older flies. Young represents 1, 2 and 3 days old flies, and old represents 10, 20 and 30 days old flies.

4.3.2.3 The difference in the unmasked 1F1 responses between *w*- and *kcc^{DHS1}* flies

How do 1F1 (photoreceptor) responses differ between *w*- and *kcc^{DHS1}* flies and how do the differences depend on age?

We first examined the unmasked 1F1 responses (Fig. 4-9). A two-factor analysis of variance showed a significant effect of genotypes. The control (*w*-) flies showed significantly higher 1F1 responses ($\bar{x}$=0.075, SD=0.02) than *kcc^{DHS1}* flies ($\bar{x}$=0.04, SD=0.027). There was a significant effect of age and no significant interaction between genotype and age (Table 4-4).

Source	ANOVA Results
Genotype (*kcc^{DHS1}* vs. *w*-)	F= 133, df =1, **p<0.001**
Age (young vs. old)	F= 64.1, df =1, **p<0.001**
Genotype * Age	F= 0.9, df =1, $p>0.05$

Table 4-4: The results of performing a two-way ANOVA on the 1F1 unmasked *kcc^{DHS1}* and *w*- flies.
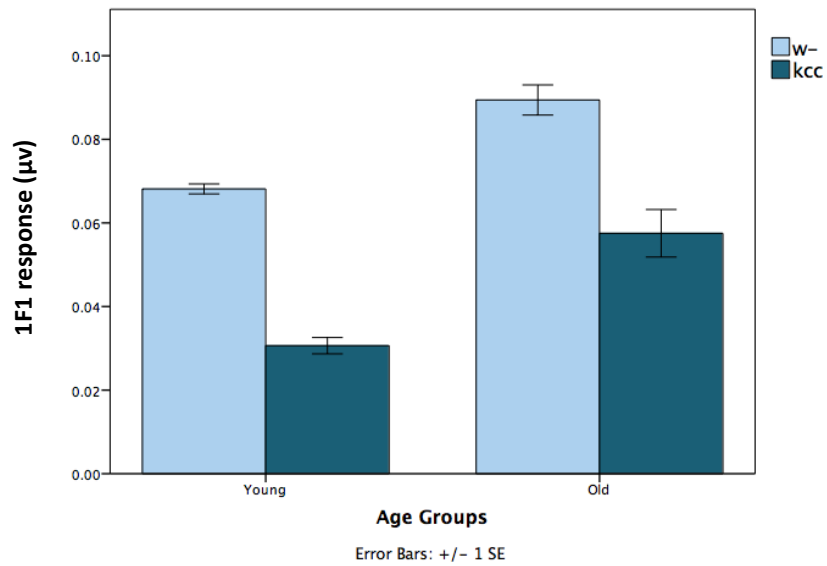
Figure 4-9: The maximum 1F1 values for unmasked responses of *w-* and *kcc^DHS1* flies as a function of age. The young and old *w-* flies show greater responses compared to the *kcc^DHS1* flies.

4.3.2.4   The difference in the masked 1F1 responses between *w-* and *kcc^DHS1* flies

Finally, we looked at the masked 1F1 responses (Fig. 4-10) and computed a two-way ANOVA. Just as in the case of the unmasked responses, ANOVA analysis revealed a significant effect of genotype: *w-* flies showed significantly higher responses ($\bar{x}$=0.07, SD=0.015) than *kcc^DHS1* flies ($\bar{x}$=0.04, SD=0.02) and there was no effect of age or a significant interaction between age and genotype (Table 4-5).

Source	ANOVA Results
Genotype (*kcc*^DHS1 vs. *w*-)	F= 67.2, df =1, *p<0.001*
Age (young vs. old)	F= 0.1, df =1, *p>0.05*
Genotype * Age	F= 3.2, df =1, *p>0.05*

Table 4-5: The results of performing a two-way ANOVA on the 1F1 masked *kcc*^DHS1 and *w*- flies.
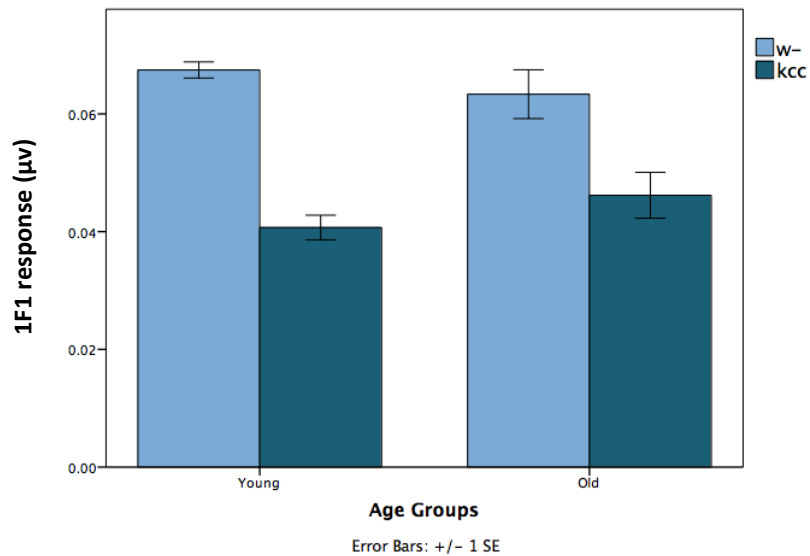
Figure 4-10: The maximum 1F1 values for the masked responses of *w*- and *kcc*^DHS1 flies. The young and old *w*- flies show greater responses compared to the *kcc*^DHS1 flies.

In general therefore, we find an overall reduction in photoreceptor responses for the *kcc*^DHS1 flies compared to the *w*- flies. This occurs both in the masked and unmasked conditions. Photoreceptor responses normalize in the *kcc*^DHS1 flies with age: the reduction in 1F1 responses is smaller both in absolute and relative terms for older animals. The cause of this reduction is unclear – it could result from a failure of feedback from deeper neural levels or a general physiological weakness in younger animals.

4.3.3 The maximum neural (2F1) responses

Until now we have considered the 1F1 responses. As mentioned previously, these reflect the contribution of the photoreceptors to the SSVEP response. We are also interested in the effect of the kcc^{DHS1} mutation on the neuronal responses of the fly. These responses are manifest in the second harmonic of the input frequency (2F1). Although we first consider the 2F1 responses in isolation, we note that neuronal responses are driven by photoreceptor responses and so it is of interest to normalize the 2F1 by the 1F1 amplitude to derive a 'pure' estimate for neuronal sensitivity.

In terms of the neural (2F1) responses, we took the same approach for analysing the maximum responses. The 2F1 for the control flies (*w-*) follow the same pattern as the 1F1, i.e. an increase in the response with age, which starts to drop later in life (at day 30). The effect of masking is identical to that of the 1F, i.e. develops with age (Fig. 4-11).

4.3.3.1 Maximum 2F1 responses of *w-* flies

Conducting a two-way ANOVA (Table 4-6) showed a significant main effect of age, such that the young flies ($\bar{x}=0.021$, SD= 0.003) had significantly higher 2F1 responses compared to old flies ($\bar{x}=0.019$, SD=0.009). The main effect of masking was also significant, such that the unmasked responses ($\bar{x}=0.02$, SD= 0.005) had significantly higher 2F1 responses compared to the masked responses ($\bar{x}=0.018$, SD= 0.006). The interaction effect between masking and age was significant. The unmasked responses were lower in the young flies compared to the old flies, p<0.001. Early in life, the masked responses were significantly higher than that at old age, *p*<0.001. Furthermore, the difference between unmasked and masked responses was not significant early in life, p=0.9, compared to old flies, p<0.001 (Fig. 4-12).

Source	ANOVA Results
Age (young vs. old)	F= 3.9, df =1, *p<0.05*
Mask (unmasked vs. masked)	F= 51, df =1, *p<0.001*
Age * Mask	F= 49.1, df =1, *p<0.001*

Table 4-6: The results of performing a two-way ANOVA on the 2F1 unmasked and masked responses of the *w-* flies.

Error Bars: +/− 1 SE
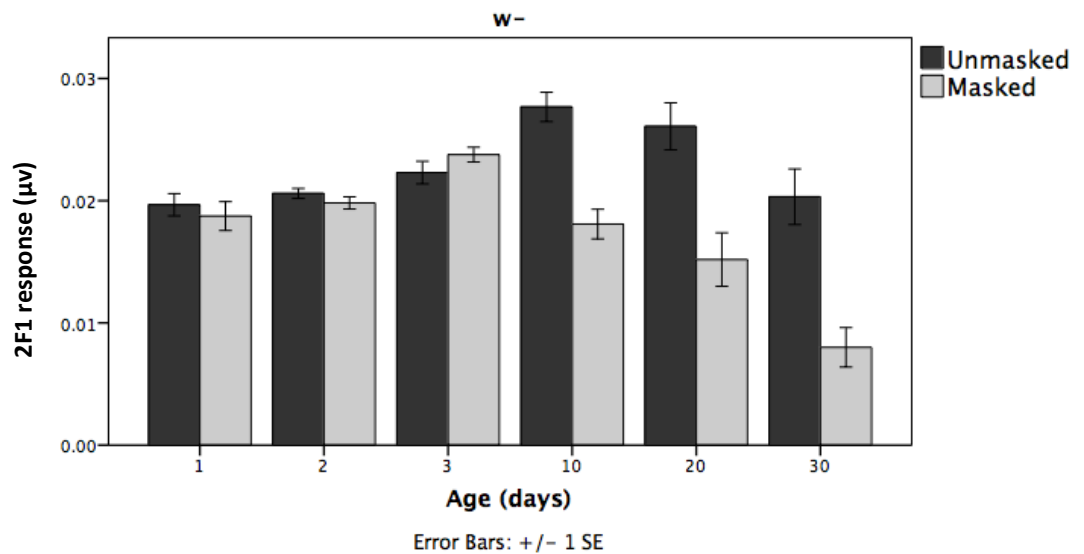
Figure 4-11: The maximum 2F1 values for the unmasked and masked responses of *w-* across all ages. Clearly more masking is present in older flies.
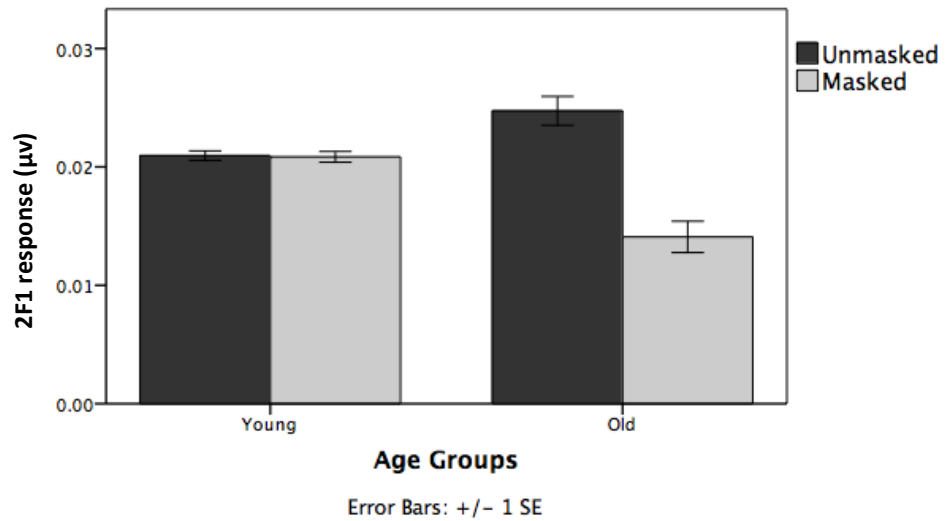
Figure 4-12: The maximum 2F1 values for the unmasked and masked responses of *w-*. More masking is evident in older flies.

4.3.3.2   Maximum 2F1 responses of *kcc^{DHS1}* flies

For *w-* flies, the neuronal responses follow the same pattern as the photoreceptor responses suggesting that neuronal sensitivity is relatively unchanged across age. Importantly, the 2F1 responses in the *kcc^{DHS1}* flies have a different pattern. For the unmasked responses, the responses are high early in life, and then drop to low levels before recovering at day 30. The masked responses, however, do not recover at all (Fig. 4-13). This is similar to our previous observation that masking is more apparent at old ages. Looking at the effect of age and masking on *kcc^{DHS1}* flies 2F1 responses using two-way ANOVA (Table 4-7) revealed a significant main effect of age, such that the young flies ($\bar{x}$=0.017, SD= 0.009) had significantly higher 2F1 responses than old flies ($\bar{x}$=0.01, SD=0.027). The main effect of masking was not significant: unmasked responses ($\bar{x}$=0.016, SD= 0.008) and masked responses ($\bar{x}$=0.014, SD=0.009) are not significantly different from each other. However, the interaction effect *was* significant. The unmasked responses were not different between young and old flies, *p*=0.6. The masked responses however, were significantly higher in the young flies compared to the old flies, *p*<0.001. In addition, early in life, the unmasked responses were not different from the masked

responses $p=0.18$ but later on, the unmasked responses were significantly greater than the masked responses, $p<0.001$ (Fig. 4-14).

Source	ANOVA Results
Age (young vs. old)	F= 18.8, df =1, **$p<0.001$**
Mask (unmasked vs. masked)	F= 3.5, df =1, $p>0.05$
Age * Mask	F= 13.3, df =1, **$p<0.001$**

Table 4-7: The results of performing a two-way ANOVA on the 2F1 masked responses of the kcc^{DHS1} flies.
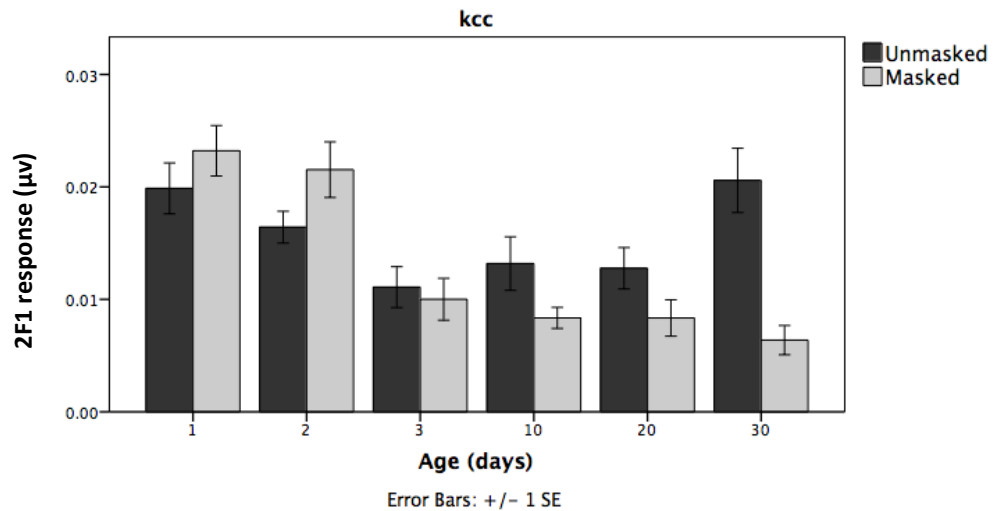
Figure 4-13: The maximum 2F1 values for the unmasked and masked responses of the kcc^{DHS1} flies. Young flies show no masking compared to old flies.

116
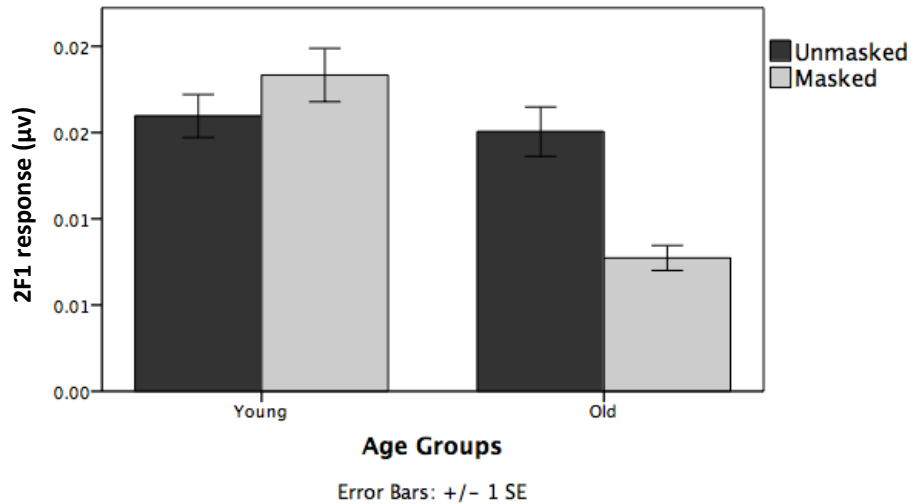
Figure 4-14: The maximum 2F1 values for the unmasked and masked responses of the *kcc^DHS1* flies. More masking is evident in older flies.

The increase in neuronal responses of the young *kcc^DHS1* flies is interesting. This increase corresponds to the reduced level of the KCC protein at this age. In the following section we compare the two genotypes (*w*-and *kcc^DHS1*) at the neuronal level.

4.3.3.3 The difference in the unmasked 2F1 responses between *w*- and *kcc^DHS1* flies

In addition to studying the effect of age and masking on each genotype individually, we compared the neuronally-generated 2F1 responses (unmasked) between the two genotypes (*w*- vs. *kcc^DHS1*) as a function of age. For the 2F1 responses a two-way ANOVA (Table 4-8) revealed a significant effect of genotypes. The control (*w*-) flies showed significantly higher 2F1 responses ($\bar{x}$=0.02, SD=0.005) than *kcc^DHS1* flies ($\bar{x}$=0.016, SD=0.008). The effect of age was not significant. Again, there was a significant interaction between genotype and age. The unmasked 2F1 responses of the young and old *w*- flies were higher than that of *kcc^DHS1* flies, $p<0.001$. In addition, there was a significant difference between the young and old *w*- flies, p <0.0, but not significant difference for the *kcc^DHS1* flies, p =0.54, (Fig. 4-15).

117

Source	ANOVA Results
Genotype (kcc^{DHS1} vs. w-)	F= 50.6, df =1, **$p<0.001$**
Age (young vs. old)	F= 1.9, df =1, $p>0.05$
Genotype * Age	F= 5.2, df =1, **$p<0.05$**

Table 4-8: The results of performing a two-way ANOVA on the 2F1 unmasked responses of the kcc^{DHS1} and w- flies.
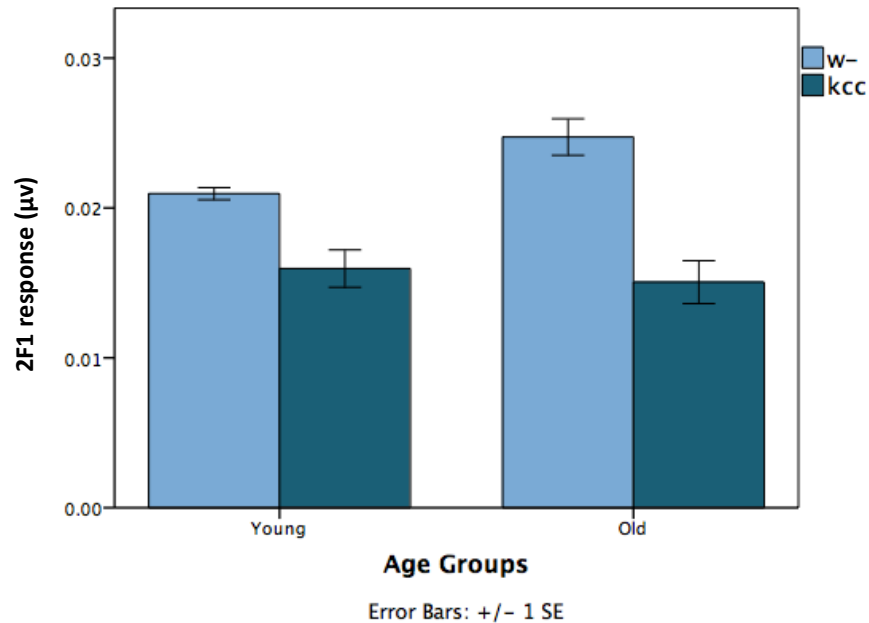
Figure 4-15: The maximum 2F1 values for the unmasked responses of the kcc^{DHS1} flies and w- flies. The w- flies show greater responses. Young and old kcc^{DHS1} flies show no significant difference.

In general, we find an overall reduction in neuronal responses for the kcc^{DHS1} flies compared to the w- flies. The amplitude of the 2F1 responses in both genotypes is lower than that of the 1F1 responses (see Fig. 4-10). It seems that the kcc^{DHS1} have reduced responses in both 1F1 and

2F1 compared to the *w- flies*. Because photoreceptors drive the neurons, and thus the neural activity must depend on photoreceptor activity. In general, we expect the *kcc* mutation to cause a deficit in neuronal processing and so we are interested in knowing how active the neural processing is in these animals

4.3.4 Hyperexcitability of young *kcc*^{DHS1} flies

To measure neuronal sensitivity and gain control while accounting for the amplitude of the photoreceptor responses, we must account for the amplitude of the 1F1 response when analysing the 2F1 response. A straightforward ratio (2F1/1F1) would be unstable (prone to division by very small numbers at times) and so we compute the amount of signal that we see in the neuronal responses (2F1) as a fraction of the total signal that we measure (2F1+1F1): $\frac{2F1}{(2F1+1F1)}$. Because *kcc*^{DHS1} flies are models of juvenile epilepsy, we hypothesised that these young flies have relatively increased neural responses, and therefore the ratio will be high.

For the control flies, the unmasked and masked neural responses are stable across all ages, accounting for about 30% of the total response at day 1. The neural responses then decrease to account for approximately 20% (Fig. 4-16). For the *kcc*^{DHS1} flies, however, the neural responses are not stable and significantly depend on the age of the fly. For day 1 flies, the unmasked neural responses accounts for approximately 83% of the total, and for day 2 flies this ratio decreases to about 60%. This can be thought of as a representation of the hyperexcitability of the neurons at these very young ages. By day 3, *kcc*^{DHS1} flies the ratio dramatically dropped accounting for only about 30% of the total – becoming very similar to *w-* responses.
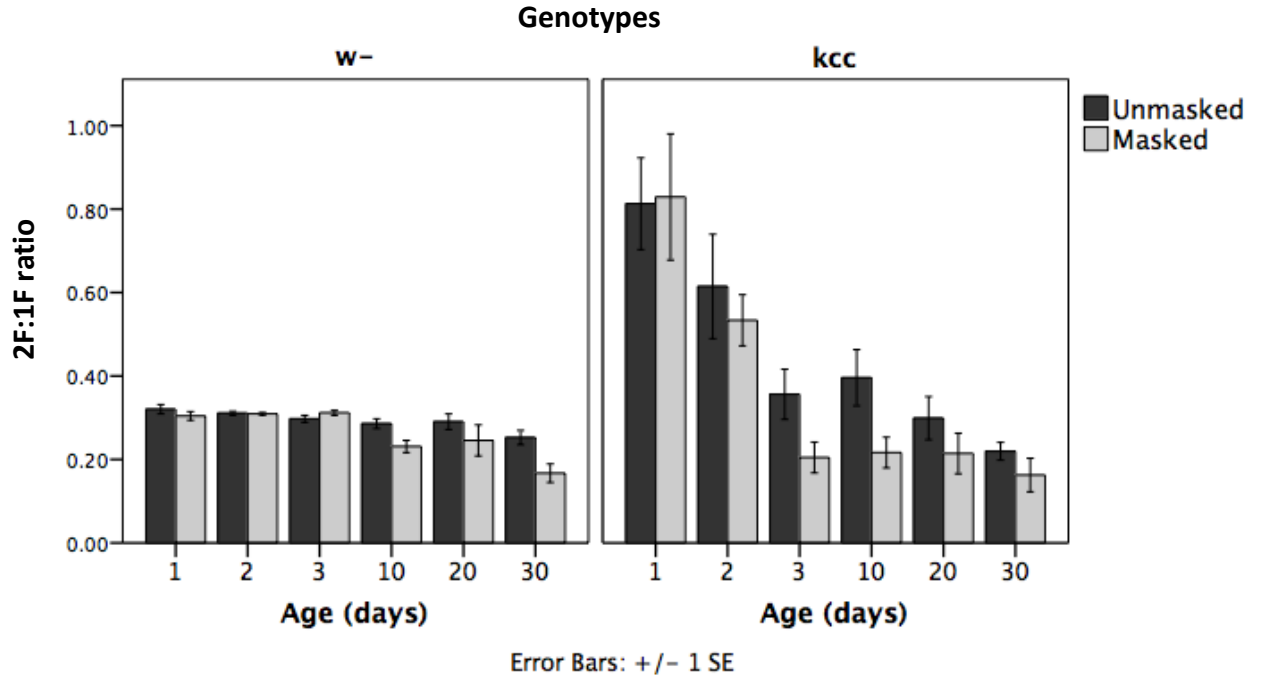
Figure 4-16: The ratio of the masked and unmasked responses for the w- and kcc^{DHS1} flies aged 1, 2, 3, 10, 20 and 30, taken from the 1st repetition only. Clearly, young kcc^{DHS1} flies have increased responses.

4.3.4.1   Maximum 2F1 ratio responses of *w-* flies

Similar to what we did before for 1F1 and 2F1 responses, a two-way ANOVA was conducted (Table 4-9) to look at the differences between the unmasked and masked responses as a function of age. There was a significant main effect of age, such that the young flies ($\bar{x}$=0.31, SD= 0.03) had significantly higher ratio compared to old flies ($\bar{x}$=0.25, SD=0.086). The main effect of masking was also significant, such that the unmasked responses ($\bar{x}$=0.3, SD= 0.04) had significantly higher ratio compared to the masked responses ($\bar{x}$=0.28, SD= 0.7). The interaction effect between masking and age was significant. In brief, the unmasked responses ratios were higher in the young flies, $p<0.01$. Early in life, the masked responses were higher than that at

120

old age, $p<0.001$. Moreover, the difference between unmasked and masked responses was not significant early in life, p=0.9, compared to significant difference later on, p<0.001 (Fig. 4-17).

Source	ANOVA Results
Age (young vs. old)	F= 54.1, df =1, *p<0.001*
Mask (unmasked vs. masked)	F= 11.8, df =1, *p<0.05*
Age * Mask	F= 12.4, df =1, *p<0.01*

Table 4-9: The results of performing a two-way ANOVA on the 2F:1F ratio of masked and unmasked responses of the *w-* flies.

Error Bars: +/− 1 SE
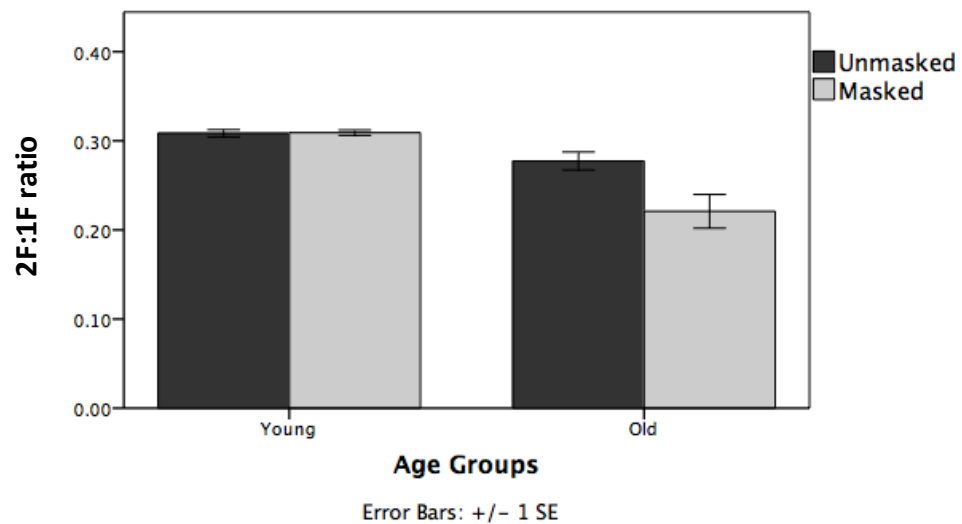
Figure 4-17: The 2F:1F ratio of the masked and unmasked responses for the *w-* flies. The young flies have increased responses compared to the old flies. More masking is evident in old flies.

4.3.4.2 The maximum 2F1 responses of *kcc^DHS1* flies

For the kcc^{DHS1} (Table 4-10), there was a significant effect of age, such that the young flies ($\bar{x}$=0.57, SD= 0.44) had significantly higher 2F1 ratio than old flies ($\bar{x}$=0.26, SD=0.17). However, the main effect of masking was not significant. The interaction effect was not significant. The unmasked and masked responses were significantly different between young and old flies, p<0.001. Young flies have more unmasked and masked responses compared to old flies. In addition, both early and later in life, the unmasked responses were insignificantly different from the masked responses p=0.38, p=0.19, respectively (Fig. 4-18).

Source	ANOVA Results
Age (young vs. old)	F= 29.6, df =1, **p<0.001**
Mask (unmasked vs. masked)	F= 2.5, df =1, p>0.05
Age * Mask	F= 1.6, df =1, p>0.05

Table 4-10: The results of performing a two-way ANOVA on the 2F:1F ratio of masked and unmasked responses of the *kcc^DHS1* flies.
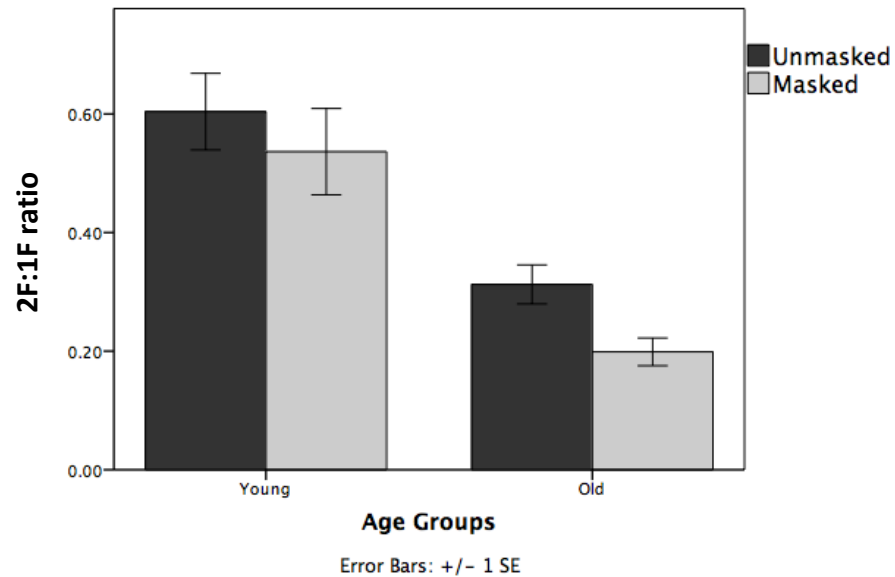
Figure 4-18: The ratio of the masked and unmasked responses for the kcc^{DHS1} flies. The young flies have increased responses compared to the old flies.

4.3.4.3 The difference in the unmasked 2F1 ratio responses between w- and kcc^{DHS1} flies

Studying the effect of age and masking on each genotype by comparing the unmasked 2F1 ratio response between the two genotypes (w- vs. kcc^{DHS1}) as a function of age using a two-way ANOVA (Table 4-11) revealed a significant effect of genotypes. The kcc^{DHS1} flies showed significantly higher 2F1 ratio ($\bar{x}$=0.48, SD=0.37) than w- flies ($\bar{x}$=0.3, SD=0.4). The effect of age was also significant. Finally, there was a significant interaction between the genotypes and age.

Briefly, the unmasked 2F1 ratio of young and old w- flies is not significantly different, p=0.54. However, young kcc^{DHS1} flies showed much higher neuronal responses compared to old flies, p<0.001 after accounting for photoreceptor activity. In addition, early in life, there was a highly significant difference between the w- and the kcc^{DHS1} flies, p <0.001, but no difference later on, p=0.54 (Fig. 4-19).

123

Source	ANOVA Results
Genotype (*kcc*^{DHS1} vs. *w*-)	F= 20.3, df =1, *p<0.001*
Age (young vs. old)	F= 19.3, df =1, *p<0.001*
Genotype * Age	F= 12.6, df =1, *p<0.01*

Table 4-11: The results of performing a two-way ANOVA on the unmasked ratio of the *kcc*^{DHS1} and *w*- flies.
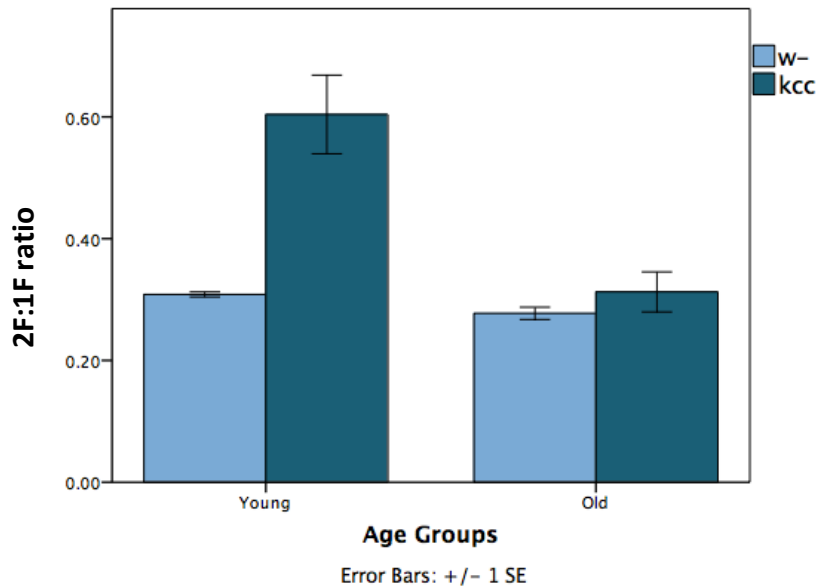
Figure 4-19: The ratio of the unmasked responses for the *w*- and *kcc*^{DHS1} flies. Clearly the young *kcc*^{DHS1} flies show increased responses compared to the *w*- flies.

In general, we find an overall increase in neuronal responses for the young the *kcc*^{DHS1} flies compared to the *w*- flies. This increase in neural activity of the *kcc*^{DHS1} flies return to the normal profile in old flies.

The findings support that prediction that the *kcc*^{DHS1} flies have abnormal visual responses early in life corresponding to the reduced KCC level at this early age..

4.4 Discussion

We have used the SSVEP technique to measure contrast-driven responses at multiple visual processing stages using a Drosophila model of epilepsy. Our data resembles to a great extent the previous studies on cats (Bonds, 1991), humans (Tsai et al., 2012) and Drosophila (Afsari et al., 2014). As in these studies, increasing contrast increased the responses to the probe, adding the mask generally reduced these responses. Because the kcc^{DHS1} mutation is age dependent, we expected to see abnormal gain control in young kcc^{DHS1} flies, and hypothesized that these abnormalities would recover to the normal profile as they get older. Due to the failure of our hyperbolic ratio fitting to accurately predict the R_{max} and C_{50}, we estimated the R_{max} by taking the mean value of the two highest contrast levels. This approach allows us to measure the R_{max} but without C_{50} it is not sufficient to describe the effect on the contrast response functions (CRFs), whether it is contrast gain control (a decrease in sensitivity) or response gain control (a reduction in the firing rate).

The primary reason for using this approach instead of the hyperbolic ratio is the fact that our response curves do not saturate. There are several possible reasons why this might be. Firstly, our stimulus is a zero-dimensional and therefore it cannot strongly drive the spatially tuned neurons (Afsari et al., 2014). Secondly, the light source used is blue, which is monochromatic with short wavelength. This might have affected the phototransduction cascade by slowing the reconversion process of metarhodopsin to rhodopsin, resulting in a reduction in the overall temporal sensitivity (Afsari et al., 2014; Hillman et al., 1983). Thirdly, our stimulus drove responses across much of the visual field resulting in the excitation of most of the neurons in the visual system to some extent. We show in Chapter 5 that wide-field excitation of this type is not an optimal stimulus for the SSVEP. Finally, as in humans, it is possible that masking in Drosophila is dependent on the spatial positions and orientations of the stimulus (Afsari et al., 2014; Cavanaugh et al., 2002) and thus changing the stimulus properties can lead to different contrast response functions (CRFs) combining both response and contrast gain effects (Reynolds and Heeger, 2009).

We found that flies expressing kcc^{DHS1} mutation were hypersensitive to contrast. This was particularly evident in the young kcc^{DHS1} flies. Our initial analysis was based on analyzing the

average of 5 repetitions. After inspecting the raw data, we noticed that the sensitivity of the kcc^{DHS1} flies is limited to the first repetition of the stimulus (Fig. 4-20). The main difference is related to the 2F1 ratio in the young kcc^{DHS1} flies. When taking the first repetition only the 2F1 ratio of the young kcc^{DHS1} flies (for both unmasked and masked responses) is significantly higher than that of the $w-$ flies indicating a neural excitability of these flies at this young age.

   The reason for this increased effect in the first repetition of the stimulus may be the refractory period following seizure episodes (Ganetzky and Wu, 1982). We believe that the kcc^{DHS1} flies might be experiencing mild seizures during the first stimulus epoch and then have increased their seizure threshold for the remainder of the experiment (Kuebler and Tanouye, 2000). If this were true, visual response abnormalities would be more evident if we analyzed the responses during just the first repetition.

   Analyzing only the first repetition demonstrated that the presence of kcc^{DHS1} mutation affects visual processing and contributed to the increased neural activity in the young kcc^{DHS1} flies. Firstly, control flies ($w-$) demonstrated steady (1F1) responses across all ages with the evidence that masking is a process that flies can develop with age. Because neurons are driven by photoreceptors, the $w-$ neural (2F1) responses mirror that of the 1F1 responses and thus the ratio of the 2F1 to 1F1 was very similar across all ages. On the contrary, kcc^{DHS1} flies have reduced 1F1 responses early in life and then start increasing with age. This coincides with the fact that KCC level is low when kcc^{DHS1} mutant flies are young and then the level increases as they get older. Unlike $w-$ flies, kcc^{DHS1} neural 2F1 responses show evidence of an additional variability caused by age-dependent changes in neuronal sensitivity. Very young kcc^{DHS1} flies have relatively high 2F1 responses and then become normal. What leads to this increased hypersensitivity in young animals? One hypothesis is failure of gain control. By looking at the masking data, we did not observe less instantaneous gain control in these animals: although kcc^{DHS1} flies showed very weak masking at young ages, this effect was also observed in the $w-$ flies. Thus, it is not failure of gain control *per se* that is responsible for the sensitivity increase although the absence of masking might contribute to this. Because the kcc^{DHS1} mutation is linked to Rdl GABA$_A$ receptor, we believe that the visual excitability seen in the young kcc^{DHS1} flies may be caused by reduced GABAergic inhibition. Observing a masking effect in these flies may

explain that GABA inhibition is not involved in masking (Katzner et al., 2011). Here we have shown not only that they are bang-sensitive earlier on, but also that their visual system neurons are hypersensitive shortly after eclosion and normalize late in life. The visual abnormalities seen in the young kcc^{DHS1} and then the recovery later on are associated with the increase of the production of the KCC protein as the kcc^{DHS1} flies get older (Afsari et al., 2014). This replicates a model of juvenile human epilepsy nicely.
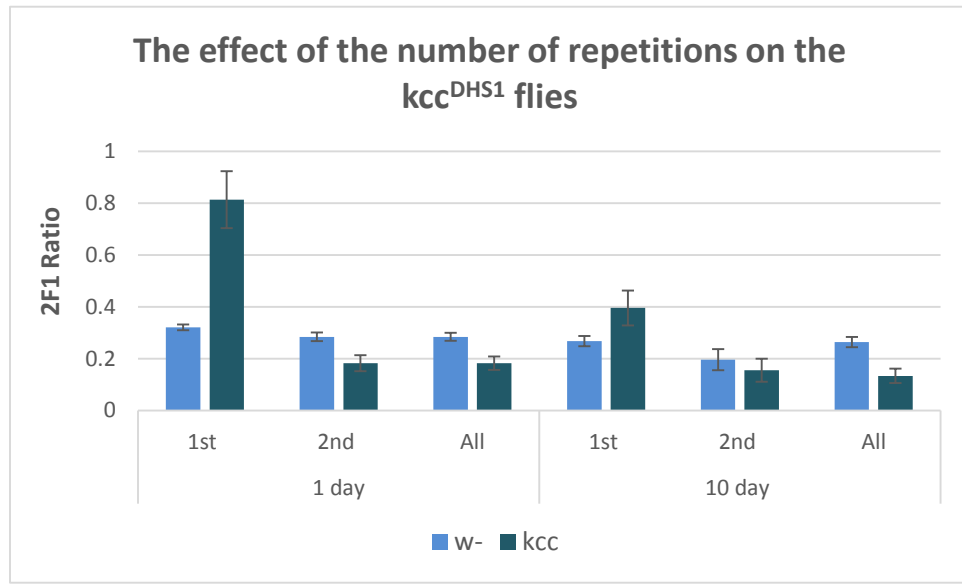
Figure 4-20: The 2F1 ratio of the unmasked responses taken from the 1st, 2nd and the average of the five repetitions compared between the young (day one old) and old (ten days old) flies. Note: the hyperexcitability observed in the young kcc^{DHS1} flies is only observed in the 1st repetition only. The amplitude of the w- flies are not greatly affected by this, indicating that this hypersensitivity of light is specific to young the kcc^{DHS1} flies.

4.5 Is the abnormality seen in the *kcc* flies specific to the *kcc^{DHS1}*?

In the previous section, we demonstrate that young kcc^{DHS1} flies have abnormally high neuronal sensitivity compared to *w-* animals. Comparisons between the kcc^{DHS1} and *w-* flies are possible because both genotypes have the same eye color. In the following section we describe attempts that we made to explore the kcc^{DHS1} genotype further. These attempts were complicated

127

by the fact that other mutant forms of the *kcc* gene, and the UAS-GAL4 system (Brand and Perrimon, 1993) that we used as a rescue mechanism altered the eye color of the flies and made comparisons with wild-type animals difficult.

In order to identify the extent of the *kcc* genotype seen in the kcc^{DHS1} flies, we have used several transgenic flies containing the kcc^{DHS1} in different background. Our aims were to understand the mechanism underlying the neural excitability of the kcc^{DHS1} flies and then try to rescue this genotype.

To assess the effect that kcc^{DHS1} mutation has on a specific part of the visual system, we took advantage of flies with p-elements in their genome. These flies had orange or red eyes as a consequence of the transgene (see Table 4-13). D672 is a group of red-eyed flies with the kcc^{DHS1} mutation. The difference between this and our original kcc^{DHS1} flies is the presence of the *1407-GAL4*, which carries a *w+* transgene, leading to the dark red eye color. If the eye color has no effect, we would expect to see that young D672 flies are hyperexcitable just as our original kcc^{DHS1} animals were.

We also used two other transgenic flies with p-elements inserted in the *kcc* gene, $kcc^{KG02390}$ and $kcc^{EY08304}$. The $kcc^{KG02390}$ stock carries a P-element insertion outside the coding sequence of the *kcc* gene, therefore the protein will be made with the same sequence as the wild type of kcc^{DHS1}. However the level of protein production may be different from the wild-type, and has not been determined. We crossed the females of this stock with the males of our original stock (D506), and we recorded from straight winged flies, $kcc^{KG02390}/kcc^{DHS1}$. $kcc^{KG02390}/kcc^{DHS1}$ flies have red eyes and were abbreviated kcc-P. In addition, $kcc^{EY08304}$ mutation results from a P-element insertion in the last exon of the *kcc* gene. We crossed the females from this stock with our original stock (D506), and we recorded from straight-winged flies, $kcc^{EY08304}/kcc^{DHS1}$. These flies have yellowish eyes and were labeled as *kcc-E*. Finally, we recoded from the light orange-eyed wild type flies (w^a) to have a control.

4.5.1 Fly stocks and methods

See (Table 4-12 and 4-13) for the detailed genotypes used and crosses made.

Stock No.	Genotype	Abbreviation	Source
148	Wild type (apricot eye colour)	w^a	Bloomington
D672	w; 1407, kcc^{DHS1}/CyO	D672	*A kind gift of Mark Tanouye*
13216	w[*]; P(y[+mDint2] w[BR.E.BR]=SUPor-P}kcc[KG02390]/CyOP(ry[+t7.2]=sevRas1.V12}FK1	kcc^{KG02390}	Bloomington
16887	y[1] w[67c23]; P(w[+mC] y[+mDint2]=EPgy2}kcc[EY08304]/CyO	kcc^{EY08304}	Bloomington

Table 4-12: The stock list used in this part of the experiment.

Female	Male	Progeny	Eye color of progeny		Abbreviation
kcc^{KG02390}	kcc^{DHS1}	kcc^{KG02390}/kcc^{DHS1}	Dark red		kcc-P
kcc^{EY08304}	kcc^{DHS1}	kcc^{EY08304}/kcc^{DHS1}	Yellow		kcc-E

Table 4-13: The crosses that performed to generate *kcc-P* and *kcc-E* flies.

4.5.1.1   Stimuli

The stimulus used in this experiment was identical to the previous one. The diffusing screen in front of the optic fiber is the only thing we modified. Previous experiments were done with the ground glass screen (see section 1.2) and these were done with a holographic 'light shaping diffuser' (http://www.luminitco.com/products/light-shaping-diffusers), which gives higher transmission of light. Changing the diffusing screen results in a more homogeneous illumination without a significant reduction in overall light output from the LED. We believe this should lead to more signal responses from the flies although our later experiments on punctate illumination of the Drosophila eye suggest that additional complexities may be involved in moving from a point- to a wide-field light source.

4.5.2 Results

4.5.2.1   The 1F and 2F responses depend on the color of the eyes

As seen in (Fig. 4-21), the eye color seems to have an impact on the *kcc* SSVEP phenotype. The wild type (w^a), D672 and *kcc-P* flies showed relatively stable unmasked and masked 1F responses across all ages. In contrast, the *kcc-E* flies showed low responses at day one, followed by increased responses at day 10 and 20.

4.5.2.1.1   The unmasked 1F1 responses

A two-way ANOVA was conducted (Table 4-14) that examined the effect of age and genotypes on the unmasked 1F1 responses. There was a significant effect of genotype. A significant effect of age and interaction were also shown. Briefly, at day one there was no significant difference between w^a, D672 and *kcc-P* flies, $p > 0.05$. However, the 1F1 responses of *kcc-E* was significantly lower than all genotypes, $p < 0.001$. At day 10, the *kcc-E* responses increased and showed no significant difference between any of the genotypes, $p > 0.05$, except the *kcc-P* flies, $p < 0.05$. At day 20, w^a and D672 flies are not different from each other, $p = 1.00$. The 1F1 responses of these flies are significantly lower than that of *kcc-P* and *kcc-E*, $p < 0.05$. Finally, *kcc-P* and *kcc-E* showed not significant difference, $p = 1.00$.

Moreover, the age difference did not affect the w^a, D672 and *kcc-P* flies, $p > 0.05$. For *kcc-E* flies, however, the age significantly affected the 1F1 responses, such that at day one, the responses were significantly lower than day 10 and 20, $p < 0.001$, and day 20 flies had higher 1F1 responses compared to both one and 10 day old flies, $p < 0.01$.

Source	ANOVA Results
Genotype	F= 33.8, df =3, **$p<0.001$**
Age	F= 24.5, df =2, **$p<0.001$**
Genotype * Age	F= 30.6, df =6, **$p<0.001$**

Table 4-14: The results of performing a two-way ANOVA on the unmasked 1F1 responses of all genotypes.

4.5.2.1.2   The masked 1F1 responses

For the masked 1F1 responses (Table 4-15), there was a significant effect of genotype. Significant effects of age and interaction were also present. Briefly, at day one there was no significant difference between w^a, D672 and *kcc-P* flies, $p > 0.05$. However, the 1F1 responses of *kcc-E* was significantly lower than all genotypes, $p < 0.001$. At day 10, the *kcc-E* responses increased and showed no significant difference between any of the genotypes, $p > 0.05$, except the *kcc-P* flies, $p < 0.05$. The observations at day one and ten are identical to that seen for the unmasked responses. At day 20, w^a, D672 and *kcc-E* flies are not different from each other, $p > 0.05$. The 1F1 responses of these flies are significantly lower than that of *kcc-P* and *kcc-E*, $p < 0.05$. Moreover, the age difference did not affect the w^a, D672 and *kcc-P* flies, $p > 0.05$. However, for *kcc-E* flies, the age significantly affected the 1F1 responses, such that at day one, the responses were significantly lower than day 10 and 20, $p < 0.001$, but no significant difference between day 10 and 20, $p > 0.05$.

131
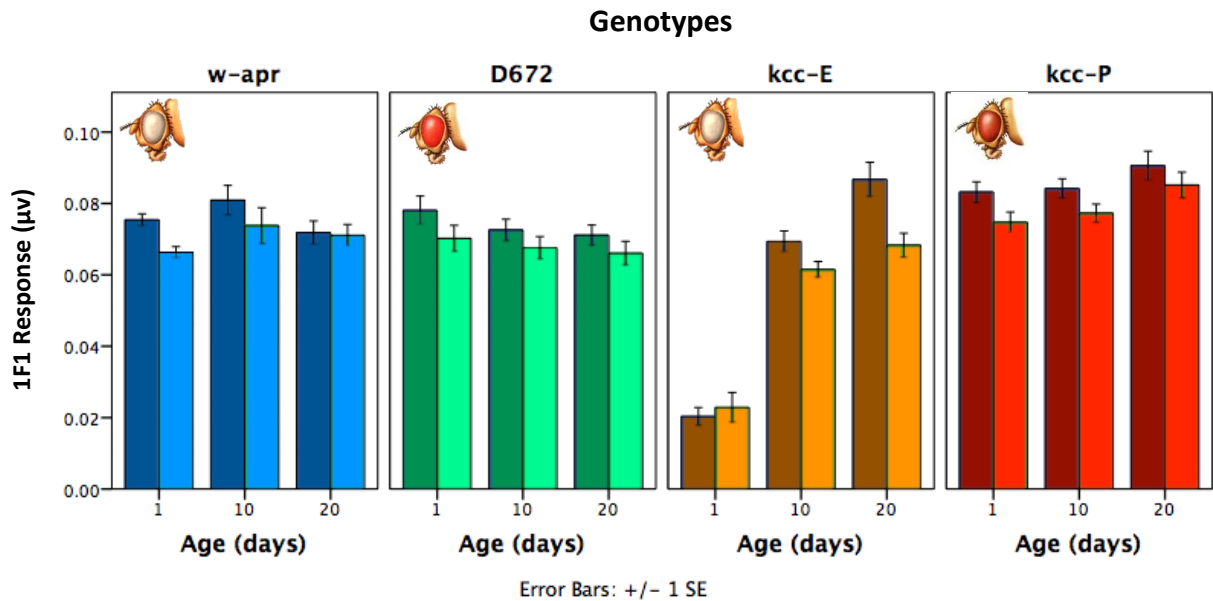
Figure 4-21: The maximum responses (unmasked and masked) at the 1F1 level for all genotypes. All flies show high 1F responses, except one-day old *kcc-E* flies.

Source	ANOVA Results
Genotype	F= 36.8, df =3, *p<0.001*
Age	F= 19.5, df =2, *p<0.001*
Genotype * Age	F= 13.3, df =6, *p<0.001*

Table 4-15: The results of performing a two-way ANOVA on the unmasked 1F1 responses of all genotypes.

In the final analyses of the 1F1 responses, we compared the difference between the unmasked and masked responses for each genotype across all ages using a two-way ANOVA (Table 4-16). For the w^a, there was no significant effect of age. However, there was an effect of masking, and the interaction effect was not obtained.

Simple effect analyses showed that the unmasked and masked responses were not significantly different across all ages, $p > 0.05$. In regard to the D672 flies, there was no significant effect of age and interaction between the age and masking. In short, the unmasked and masked responses were not significantly different across all ages, $p > 0.05$. For the *kcc-E* flies however, there was significant effect of age, masking and interaction. Post-hoc tests showed that the unmasked and masked responses were not significantly different at day 1 and 10, $p > 0.05$, but masking was present at day 20, $p < 0.01$. Finally, for the *kcc-P* flies, there was also a significant effect of age and masking, but no interaction effect was obtained. The unmasked and masked responses were not significantly different across all ages, $p > 0.05$, except higher unmasked responses at day 20, $p < 0.01$.

Genotype	Source	ANOVA Results
w^a	Age	F= 2.3, df =2, $p>0.05$
	Mask	F= 4.2, df =1, **$p<0.05$**
	Age * Mask	F= 0.8, df =2, $p>0.05$
D672	Age	F= 1.5, df =2, $p>0.05$
	Mask	F= 4.7, df =1, **$p<0.05$**
	Age * Mask	F= 0.1, df =2, $p>0.05$
$kcc\text{-}E$	Age	F= 150.6, df =2, $p<0.001$
	Mask	F= 7.7 df =1, **$p<0.05$**
	Age * Mask	F= 4.6, df =2, **$p<0.05$**
$kcc\text{-}P$	Age	F= 4.3, df =2, **$p<0.05$**
	Mask	F= 6.9, df =1, **$p<0.05$**
	Age * Mask	F= 4.6, df =2, $p>0.05$

Table 4-16: The results of performing a two-way ANOVA on the unmasked and masked 1F1 responses of all genotypes.

Overall, these results indicate that the photoreceptor responses in the colored-eyed kcc flies are not weak compared to the white-eyed kcc^{DHS1} flies (see Fig. 4-10). The pigment cells present in these colored-eyed kcc flies increased the responses of these flies. But we need to analyze the 2F1 responses in order to identify any increase in neuronal responses that was identified in the white-eyed kcc^{DHS1} flies.

4.5.2.1.3   The unmasked 2F1 responses

For the unmasked 2F1 responses (Fig. 4-21), there was a significant effect of genotype, age and interaction (Table 4-17). In short, at day one there was a significant difference between all genotypes, p <0.05. The w^a flies have the highest responses, followed by the *kcc-P* flies, and then the D672 flies. The *kcc-E* flies showed the lowest responses. At day 10, the *kcc-E* responses increased and showed no significant difference compared with w^a flies, p >0.05. These two genotypes had higher responses than *kcc-P* and D672 flies, which showed no significant difference between them. At day 20, the difference between all genotypes was significant, p <0.05, except between *kcc-P* and D672, p <0.05. The *kcc-E* flies showed the highest response, followed by the w^a, then the *kcc-P* flies. The D672 flies showed the lowest unmasked 2F1 responses. Moreover, the age difference did not affect the w^a flies, p >0.05. However, for the D672 flies, the age significantly affected the 1F1 responses, such that at day one, the responses were significantly higher than that at day 10, p <0.05, but not at day 20, p >0.05. For the *kcc-E* flies, one-day old flies showed the lowest responses, p <0.001, and 20-day old flies showed the highest responses, p <0.001. Finally, the *kcc-P* flies showed higher responses at day one, p <0.05, but not insignificant difference 10-day and 20-day old flies, p >0.05.

Source	ANOVA Results
Genotype	F= 93.4, df =3, *p<0.001*
Age	F= 12.2, df =2, *p<0.001*
Genotype * Age	F= 58.4, df =6, *p<0.001*

Table 4-17: The results of performing a two-way ANOVA on the unmasked 2F1 responses of all genotypes.

4.5.2.1.4   The masked 2F1 responses

For the masked 2F1 responses (Fig. 4-22), there was a significant effect of genotype, age and interaction (Table 4-18). Briefly, at day one, the w^a flies had higher responses than the *kcc-E* and the D672 flies, p <0.001, but not the *kcc-P* flies, p >0.05. The *kcc-E* and D672 flies were not different from each other, p >0.05. At day 10, the *kcc-E* responses increased and showed no significant difference compared with w^a flies, p >0.05. These two genotypes had higher responses than *kcc-P* and D672 flies, which again showed no significant difference between them. At day 20, the responses are identical to that at day 1. Moreover, the age difference did have any effect on any of the genotypes, p >0.05, except the *kcc-E* flies. Day-one old *kcc-E* flies showed lower responses compared to that at day 10 and 20, p <0.001. There was no difference between responses at day 10 and 20, p >0.05.

Source	ANOVA Results
Genotype	F= 30.5, df =3, p<0.001
Age	F= 5, df =2, p<0.01
Genotype * Age	F= 11.8, df =6, p<0.001

Table 4-18: The results of performing a two-way ANOVA on the masked 2F1 responses of all genotypes.
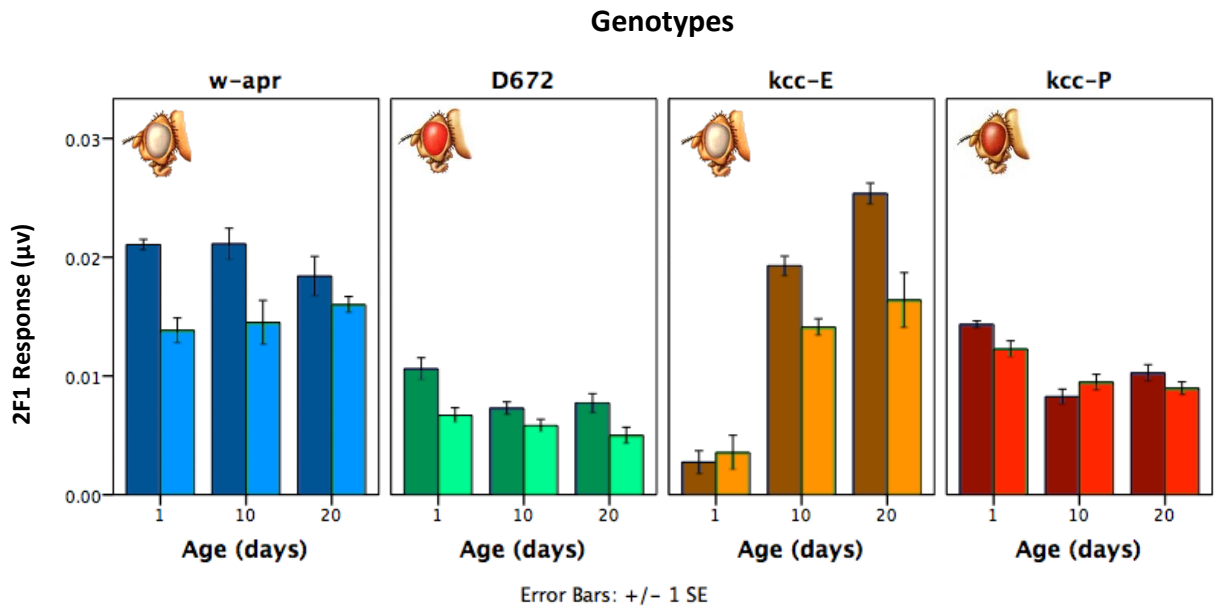
Figure 4-22: The maximum masked and unmasked responses at the 2F1 level for all genotypes. The Yellowish-eyed *kcc-E* flies show an increase in the 2F1 responses as they get older, resembling the control *w^a* flies. The red-eyed flies, D672 and *kcc-P*, show similar responses.

Finally, we compared the difference between the unmasked and masked responses for each genotype across all ages using a two-way ANOVA (Table 4-19). For the *w^a* flies, there was significant effect of masking, but no effect of age or interaction was obtained. Simple effect analyses showed that the unmasked responses were higher than the masked responses at day 1 and 10, $p < 0.01$. 20-day old flies showed no effect of masking, $p > 0.05$. In regard to the D672 flies, there was a significant effect of age and masking, but no interaction effect was obtained. In brief, the unmasked responses were significantly higher at day 1 and 20, $p < 0.01$. 10-day old flies showed no significant difference between the unmasked and masked responses, $p = 0.1$. For the *kcc-E* flies, there was significant effect of age, masking and interaction. Simple effect analyses showed that the unmasked responses were higher at day 10 and 20, $p < 0.01$, but not at day 1, $p = 0.6$. Finally, for the *kcc-P* flies, there was significant effect of age, masking and interaction. Simple effect analyses showed that the unmasked responses were higher at day 1

compared to the masked responses, $p < 0.05$, but no difference was obtained at day 10 and 20, $p > 0.05$.

Genotype	Source	ANOVA Results
w^a	Age	F= 0.1, df =2, $p>0.05$
	Mask	F= 27, df =1, **$p<0.05$**
	Age * Mask	F= 1.5, df =2, $p>0.05$
D672	Age	F= 6.5, df =2, **$p<0.01$**
	Mask	F= 22.2, df =1, **$p<0.001$**
	Age * Mask	F= 1.5, df =2, $p>0.05$
kcc-E	Age	F= 106, df =2, **$p<0.001$**
	Mask	F= 17.2 df =1, **$p<0.05$**
	Age * Mask	F= 7.4, df =2, **$p<0.01$**
kcc-P	Age	F= 27.5, df =2, **$p<0.001$**
	Mask	F= 6.9, df =1, **$p<0.05$**
	Age * Mask	F= 4, df =2, **$p<0.05$**

Table 4-19: The results of performing a two-way ANOVA on the unmasked and masked 2F1 responses of all genotypes.

In general, we find no evidence of increased neural activity of these colored-eyed *kcc* flies. In the following section we analyze the pure neuronal responses to confirm that.

4.5.2.2 The neural excitability seems to be confined to the white-eyed *kcc*^{DHS1} flies

As mentioned before, optical insulation by both the insulation of the individual ommatidia and the insulation of the entire compound eye provide better visual acuity of the Drosophila through preventing light rays from inappropriately activating photoreceptors. This optical insulation may provide some protection to the *kcc* mutants– most likely because they reduce the overall activity of the photoreceptors. To examine the excitability of neurons in the colored-eyed *kcc* flies we plotted the ratio as described in the previous section. Then we conducted a two-way ANOVA to test whether the colored-eyed flies would show any sign of neural excitability manifested as having high 2F1 ratio.

4.5.2.2.1 The unmasked 2F1 ratio responses

First of all, we will describe the unmasked responses (Fig. 4-23). There was no significant effect of age, but the effects of genotype an interaction were present (Table 4-20). In short, at day one, the w^a flies had higher responses than all other phenotypes, $p < 0.001$. The *kcc-E*, *kcc-P* and D672 flies were not different from each other, $p > 0.05$. At day 10 and 20, the *kcc-E* responses increased and showed no significant difference compared with w^a flies, $p > 0.05$. These two genotypes had higher responses than *kcc-P* and D672 flies, which again showed no significant difference between them. Moreover, the age difference did have any effect on the w^a and D672 flies, $p > 0.05$. Day-one old *kcc-E* flies showed lower responses compared to that at day 10 and 20, $p < 0.001$. There was no difference between responses at day 10 and 20, $p > 0.05$. Finally, Day-one old *kcc-P* flies showed higher responses than that at day 10 and 20, $p < 0.05$, but there was no difference between responses at day 10 and 20, $p > 0.05$.

Source	ANOVA Results
Genotype	F= 88.1, df =3, **$p<0.001$**
Age	F= 0.9, df =2, $p>0.05$
Genotype * Age	F= 20, df =6, **$p<0.001$**

Table 4-20: The results of performing a two-way ANOVA on the unmasked 2F1 ratio responses of all genotypes.

4.5.2.2.2 The masked 2F1 ratio responses

For the masked responses (Fig. 4-22), there was a significant effect of age, but the effects of genotype and interaction were not significant (Table 4-21). Briefly, at day one, the w^a flies had higher responses than all other genotypes, $p <0.001$, except the *kcc-P* flies, $p >0.05$. The *kcc-P*, *kcc-E* and D672 flies showed similar responses, $p >0.05$. At day 10 and 20, the *kcc-E* responses increased and showed no significant difference compared with w^a flies, $p >0.05$. These two genotypes had higher responses than *kcc-P* and D672 flies, which again showed no significant difference between them. Moreover, the age difference did have any effect on the w^a, *kcc-P* and D672 flies, $p >0.05$. Day-one old *kcc-E* flies showed lower responses compared to that at day 10 and 20, $p <0.001$, but was there was not difference between day 10 and 20, $p >0.05$.

Source	ANOVA Results
Genotype	F= 33.8, df =3, **$p<0.001$**
Age	F= 0.8, df =2, $p>0.05$
Genotype * Age	F= 7.2, df =6, **$p<0.001$**

Table 4-21: The results of performing a two-way ANOVA on the masked 2F1 ratio responses of all genotypes.
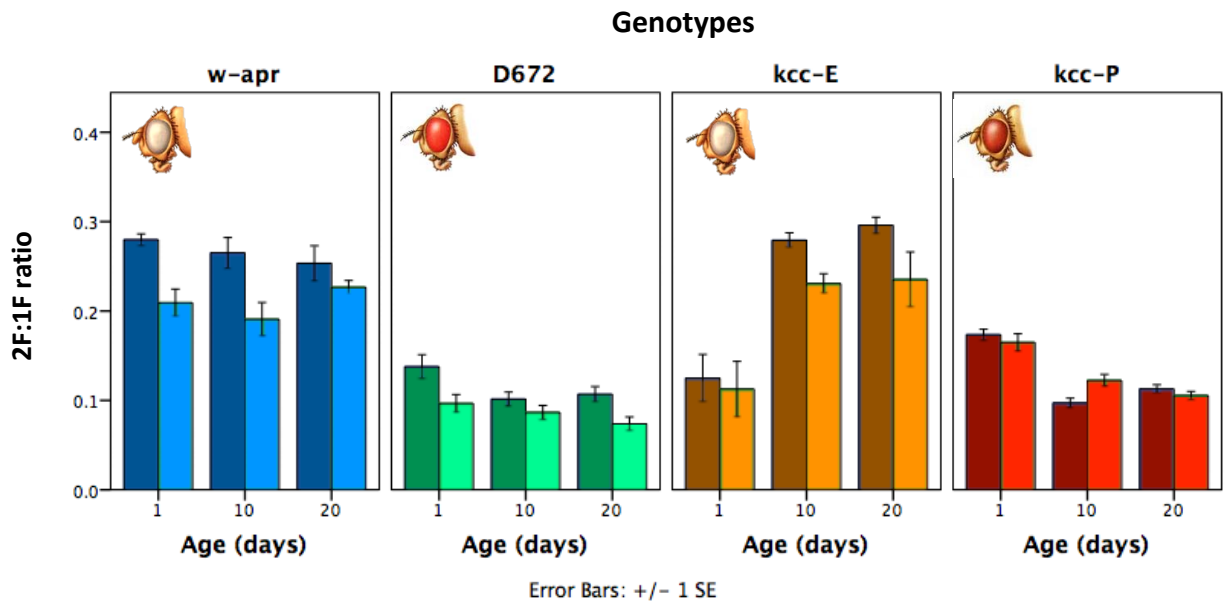
Figure 4-23: The ratio of the masked and unmasked responses for all genotypes. Non-of the flies have shown an increase in the 2F1 ratio. Red-eyed flies, show reduced responses compared to the yellowish-eyed flies. The *kcc-E* flies showed very similar responses to the control w^a flies, except at day 1.

Finally, we compared the difference between the unmasked and masked responses for each genotype across all ages using a two-way ANOVA (Table 4-22).

Genotype	Source	ANOVA Results
w^a	Age	F= 0.6, df =2, $p>0.05$
	Mask	F= 22, df =1, **$p<0.001$**
	Age * Mask	F= 1.5, df =2, $p>0.05$
D672	Age	F= 4.7, df =2, **$p<0.05$**
	Mask	F= 14.7, df =1, **$p<0.001$**
	Age * Mask	F= 1, df =2, $p>0.05$
kcc-E	Age	F= 26.5, df =2, **$p<0.001$**
	Mask	F= 4.6, df =1, **$p<0.05$**
	Age * Mask	F= 7.4, df =2, $p>0.05$
kcc-P	Age	F= 57, df =2, **$p<0.001$**
	Mask	F= 0.4, df =1, $p<0.05$
	Age * Mask	F= 5, df =2, **$p<0.05$**

Table 4-22: The results of performing a two-way ANOVA on the unmasked and masked 2F1 ratio.

For the w^a flies, there was significant effect of masking, but no effect of age or interaction was obtained. Simple effect analyses showed that the unmasked responses were higher than the masked responses at day 1 and 10, $p <0.01$. 20-day old flies showed no effect of masking, $p >0.05$. In regard to the D672 flies, there was a significant effect of age and masking, but no interaction effect was obtained. Simple effect analyses showed that the unmasked responses

were significantly higher at day 1 and 20, p <0.05. 10-day old flies showed no significant difference between the unmasked and masked responses, p =0.2. For the *kcc-E* flies, there was a significant effect of age and masking, but no interaction effect was obtained. Simple effect analyses showed that the unmasked and masked responses were not different across all ages, p >0.05. Finally, for the *kcc-P* flies, there was no significant effect of masking, but the effects of age and interactions were significant. In short, the unmasked responses were higher at day 10 compared to the masked responses, p <0.01, but no difference was obtained at day 1 and 20, p >0.05.

Overall, these results indicate that the neuronal responses in the colored-eyed *kcc* flies normal compared to the white-eyed *kcc*[DHS1] flies (see Fig. 4-19). Taken together, these results suggest that there is an association between the present of the pigment cells and the kcc phenotype.

4.5.3 Discussion

Repeating the previous experiment using transgenic and control flies expressing *kcc*[DHS1] mutation in different eye color background resulted in no increase in the neural activity – either as measured by a straightforward amplitude in young animals or when assayed by a ratio between photoreceptor and neuronal responses. This result suggests that the color of the eyes is essential for showing the hyperexcitability of the *kcc*[DHS1] flies. This is surprising, considering they have the same *kcc* mutation (D672) or have mutations that lead to even lower seizure threshold (*kcc-E* and *kcc-P*) (Hekmat-Scafe et al., 2006).

It has been shown that eye pigments improve the visual acuity by insulating each ommatidium so that light does not transfer laterally. Unlike white-eyed *kcc*[DHS1] flies, lateral transfer of light in colored-eyed *kcc* flies does not lead to an increase in the neural excitation. Because of that, we suggest that the visual abnormality, characterized by increased neural excitation, may be related to reduced lateral inhibition in the white-eyed *kcc*[DHS1] flies. Red eye pigments may also reduce the photon catch of each ommatidium in general, leading to corresponding reduction in overall photosensitivity. The eye pigment might also have other roles in the visual system that are still to be addressed.

143

In the following chapter (Chapter 5) we attempt to understand the relationship between neural excitation and lateral inhibition.

4.6 Conclusion

To conclude, the current study provides evidence that our Drosophila model of epilepsy, kcc^{DHS1}, has abnormal visual responses when young, mimicking a model of juvenile human epilepsy. This abnormality is believed to be caused by reduced GABAergic inhibition in these young flies rather than failure of other gain control mechanisms. Using transgenic flies in an attempt to rescue the *kcc* genotype was found to be a complicated task since more than one factor might have contributed to the absence of the hyper-excitability in these colored-eyed flies.

5 Chapter 5: Retinal signal processing in the *kcc^DHS1* flies

5.1 Introduction

In the previous chapter, we have seen that colored-eyed kcc^{DHS1} flies have normal responses (particularly at the neural level) compared to the white-eyed kcc^{DHS1} flies. This indicates that the eye color interacts with the *kcc* genotype. Our hypothesis is that the presence of insulating pigments surrounding the photoreceptors in the colored-eyed kcc^{DHS1} may be the reason why we do not see the visual abnormalities in these flies. The pigments may serve two purposes: to electrically insulate the photoreceptor like a plastic sheath around a wire, and also to optically insulate it and prevent stray light reaching other neighboring receptors (Tomlinson, 2012).

As mentioned before, the signal processing of visual information begins at the photoreceptors, where the light absorbed by the rhabdomere is converted into electrical signals. The electrical signals are then transmitted to the lamina. The lamina consists of two types of neurons; projection neurons that send their axons to the medulla, and local neurons (such as amacrine cells) that do not send their axons outside the lamina. Besides the local amacrine cells, the lamina contains 12 neuron classes including one type of photoreceptor terminal, R1-R6; two classes of long visual fiber from the ommatidium to the medulla, R7 and R8; the five classes of monopolar cells, L1-L5; the two classes of medulla cells, two centrifugal neurons C2 and C3, and a T1-type neuron (Meinertzhagen and O'Neil, 1991). Electron micrograph (EM) studies have shown that R1-R6 photoreceptors project to L1-L3 monopolar cells and amacrine cells, and receive feedback signals from L2, L4, amacrine cells, the lamina wide-field (Lawf) neurons and C3 cells (Hu et al., 2015) (Fig. 5-1). Stimulating Drosophila photoreceptors by light activates the phototransduction cascade leading to depolarization. The inhibitory neurotransmitter histamine is then released by the depolarized photoreceptors (Hardie, 1987). This hyperpolarizes the postsynaptic L1-L3 neurons and amacrine cells leading to the opening of their histamine-gated chloride channel, HisCl2 (Pantazis et al., 2008). To understand the feedback network that controls the photoreceptor output, Zheng and his colleagues showed, by intracellular recording, that L2 and amacrine cells, which are glutamatergic and/or cholinergic, receive inhibitory input from the R1-R6 axons (Zheng et al., 2006). This hyperpolarization of

L2 and amacrine cells lead to a reduction in the excitatory feedback to the photoreceptors. However, the physiological roles and underlying mechanisms of these excitatory feedback are still unknown. In addition, it is still unknown what types of excitatory neurotransmitter receptors are involved in the photoreceptors (Hu et al., 2015). Lateral interactions, which are responsible for enhancing the perception of edges and suppression of responses to spatially uniform intensity (Freifeld et al., 2013), constitute an essential part of neural processing in the visual system of both vertebrates and invertebrates (Dacey et al., 2000) providing a feedback signal to photoreceptors, and thus controlling their output gain (Fahrenfort et al., 2005; Razjouyan et al., 2009). Nearly all lamina neuron classes are assumed to have a role in these lateral interactions (Tuthill et al., 2013). Lateral inhibition generates the on-center off-surround and the off-center on-surround structures in a number of interneurons, including bipolar and ganglion cells in the vertebrates (Dacey et al., 2000), and the 1st order interneurons in flies (Dubs, 1982; Freifeld et al., 2013).

We hypothesize that the visual hyperexcitability of the white-eyed kcc^{DHS1} flies may be caused by abnormal lateral connections between their photoreceptors. To test this, we have investigated the difference between the wild type flies and the different kcc^{DHS1} flies, particularly looking at signals that must travel across the eye and how these might indicate abnormal feedback connections observed in the white-eyed kcc^{DHS1} flies.
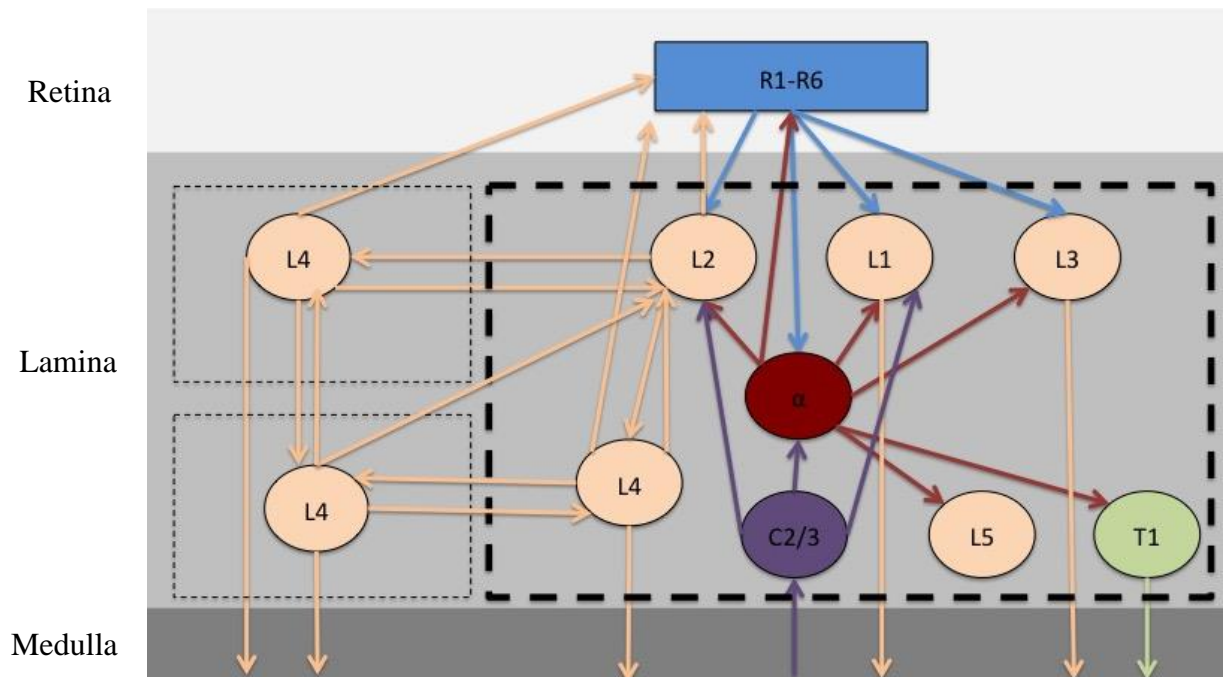
Figure 5-1: A diagram showing the information flow in the lamina. In each cartridge (indicated by the dotted lines, the thick line shows one cartridge), photoreceptors R1-R6 synapse directly with amacrine (α) and monopolar cells L1-L3. Lateral connections to other cartridges are provided through L2 and L4. Amacrine cells, L2 and L4, provide feedback signaling onto photoreceptors. The information is transferred to the medulla, and centrifugal cells C2/C3 provide feedback to the cartridge. Modified from (Meinertzhagen and O'Neil, 1991; Takemura et al., 2008)

5.2 Methods

5.2.1 Fly stocks

A list of Drosophila mutants used is given in Table 5-1. The flies were treated in the same way as in the experiments in the previous chapter. The visual responses were tested within 8-18 hours after eclosion (i.e. on day 1).

Stock No.	Genotype	Abbreviations	Source
148	Wild type (apricot eye colour)	w^a	Bloomington
13216	*w[*]; P(y[+mDint2] w[BR.E.BR]=SUPor-P}kcc[KG02390]/CyOP(ry[+t7.2]=sev Ras1.V12}FK1*	*kcc-P*	Bloomington
D506	*w; kcc^{DHS1}/CyO*	*kcc^{DHS1}*	*A generous gift from Mark Tanouye*
w^{1118}	*Wild type (White eyes)*	*w-*	*Elliott/Sweeney lab stock*
	Null mutation of hclA *(ort^{US6096})*	ort⁻	*A generous gift from Roger Hardie*

Table 5-1: The list of Drosophila mutants used in this experiment.

5.2.2 Flash ERG recording

Visually evoked potentials were recorded from one-day old flies using DasyLAB (Measurement Computing Corporation, 2012) following a flash of light of 0.5 second. The data were then saved to disk and analyzed in Matlab. These recordings were performed using the apparatus described in Chapter 4 and are presented here because they illustrate a novel and important feature of the ERG response in kcc^{DHS1} flies: Rapid oscillations following light transients. It was the presence of these transients that led us to investigate lateral interactions in kcc^{DHS1} flies in more detail.

5.2.3 Flash ERG analysis

Rapid oscillations were evident by visual inspection of individual ERG traces taken from kcc^{DHS1} flies. These are illustrated in (Fig. 5-4A). To analyze these further we performed a time/frequency analysis on the waveforms using a spectrogram (Fig. 5-4B) with a window size of 200 ms and a spectral resolution of 5 Hz. To quantify the frequency and size of the oscillations, we computed the RMS (root mean squared) power in different time intervals using an FFT-based approach. All spectral analysis was performed in Matlab.

5.2.4 Arduino-based SSVEP recording

The SSVEP experiments in this chapter were conducted on a new, smaller version of the equipment used in previous chapters. The visual stimulus in these experiments is based on LEDs driven by an open-source Arduino microcontroller prototyping platform similar to that used by Teikari et al (Teikari et al., 2012). The stimuli were produced by a single-channel LED (Kingbright KAF-5060PBESEEVGC, maximum blue emission wavelength 465 nm) controlled by an Arduino Due board. The spectral output of the LED was checked using an Oceanoptics USB2000 photospectrometer. The LED channel was centered at 467 nm and thus only rhodopsin 1 (Rh1), expressed in R1-R6 photoreceptors, was driven by our stimulus. Linearity was controlled using pulse-width modulation (PWM) of the LED outputs with a bit resolution of 12 bits (1 part in 4096). In three out of four conditions, the LED was attached to a fiber and an electrode was attached to the end of that fiber. The fiber electrode was placed near the upper medial edge of the left eye. The recording electrode was then positioned in three different

149

locations: 1) close to the fiber electrode, 2) in the middle of the eye, and 3) on the other side of the eye (ventral side). In a final, fourth condition, we used full-field stimulation instead of using the fiber-coupled LED. A reference electrode was placed in the mouth to provide an electrical contact and more movement restriction (Fig. 5-2).

Similar to the previous experiment, the stimuli consisted of 11-second trials (11 x 1 second 'bins' each with the first bin discarded during analysis to avoid onset transients). In each trial, the LED was modulated temporally. The temporal modulation was determined by adding together two sine wave modulations with two different frequencies, 12 Hz and 15 Hz, F1 (or probe) and F2 (or mask) respectively. We then examined responses to 7 contrast levels ranging from 0% to 69% contrast in equal steps. Trials were randomized and the entire sequence of 14 trials was repeated 5 times. The total data acquisition time was approximately 12 minutes. In this experiment, the stimuli were modulated in a sine wave rather than a square wave pattern. We later learned that square wave modulation generates far more masking. The masking effect was, therefore, weak in these experiments and we did not analyze it further. Recent modifications to the stimulus system include the option to perform both types of modulation.

The quality and stability of the electrical contacts was verified by running the program on the test mode. The visual responses of the flies were checked by manually turning the LED on and off. Only flies that showed high and maintained responses were accepted.
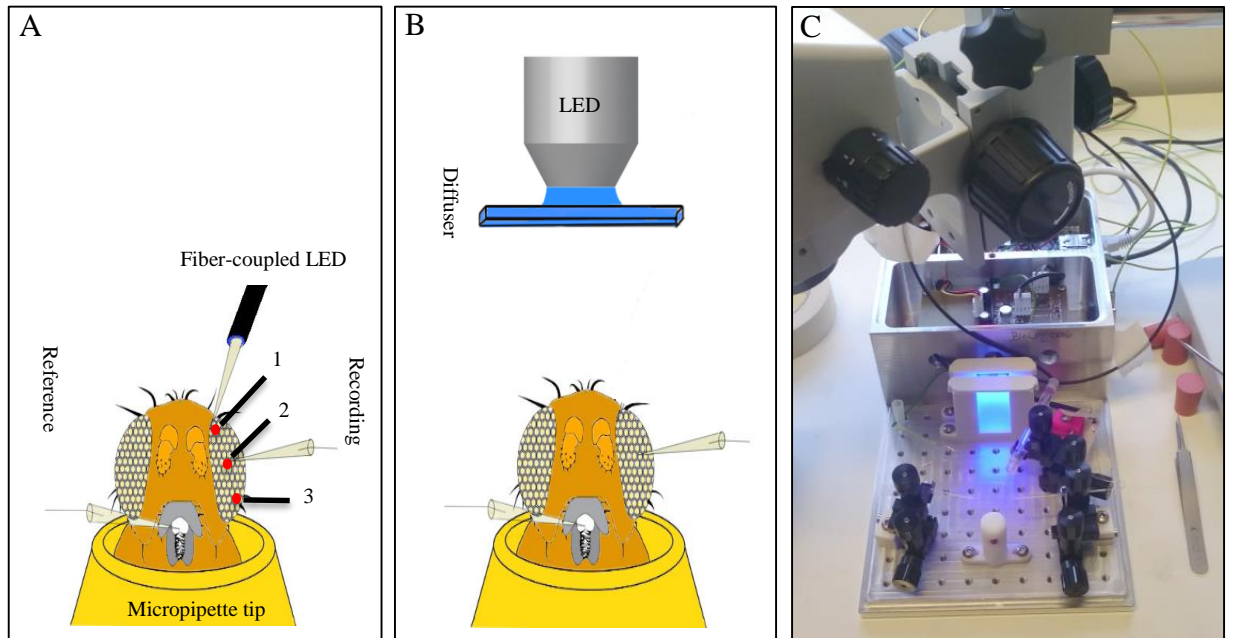
Figure 5-2: Diagram of a Drosophila positioned in the opening of a micropipette tip. The opening has been cut to allow the head to fit through, yet keep the thorax, wings and legs secure within the pipette. Nail polish was also used to restrict the movement further. A sharp reference electrode is inserted into the mouth while a recording electrode is inserted into the left eye. (A) Shows the localized stimulations using a fibre-coupled LED attached to an electrode and then inserted in the medial edge of the left eye. The red dots indicate the positions of the recording electrode; 1 (close), 2 (middle) and 3 (far). (B) Shows the full-field stimulation using a diffusing screen positioned at 7cm.

5.2.5 SSVEP analysis

The analysis used in this experiment is very similar to that used in the previous chapter. The only difference is that because responses were generally more stable, we used the highest contrast level as our measure of the maximum value instead of taking the mean of the two highest contrast levels.

5.2.6 Statistical analysis

The comparison between the groups was performed by two-way ANOVA using SPSS software (IBM SPSS Statistics, version 22). Matlab code was used to analyze the raw data before exporting to SPSS for the final analyses.

5.3 Results

5.3.1 Detection of high-frequency oscillatory events

Using the ERG apparatus used in the previous chapter, the ERG of a wild-type fly (*w-*) subjected to a flash of light of long duration (0.5 second) comprises a fast positive "on transient", a sustained negative wave which last for the whole period of illumination, a fast negative "off transient", and finally a decay of the sustained negative wave (Fig 5-3A).

In wild-type animals (*w-*), the ERG trace is relatively stable after the onset and offset transients. However, in our model of epilepsy, kcc^{DHS1}, we observe high frequency oscillatory events that begin immediately after the onset of light and a second set of oscillations that appear to be triggered by light offset (Fig. 5-4A).

We quantified these high frequency oscillations, identified in the time domain, by analyzing them in the frequency domain using MATLAB (Fig 5-3B and 5-4B). The wild type flies show no sustained frequency responses apart from a broadband increase in the intensity during the light onset and offset (Fig 5-3B) due to the square wave edge of the light onset transient. For the kcc^{DHS1} flies, the spectrogram shows a dominant high frequency band (50-100 Hz) during the illumination period, and another relatively low frequency band (20-25 Hz) during the decay period (Fig 5-4B). These high and low frequency bands can be regarded as biomarkers for the kcc^{DHS1} flies.

To understand the mechanism behind these rapid oscillations in the white-eyed *kcc^DHS1* flies, we set up a new tabletop Arduino-based LED stimulator system (Teikari et al., 2012). Our hypothesis was that the rapid oscillations seen in the white-eye *kcc^DHS1* flies are caused by reduced lateral inhibition from amacrine cells.
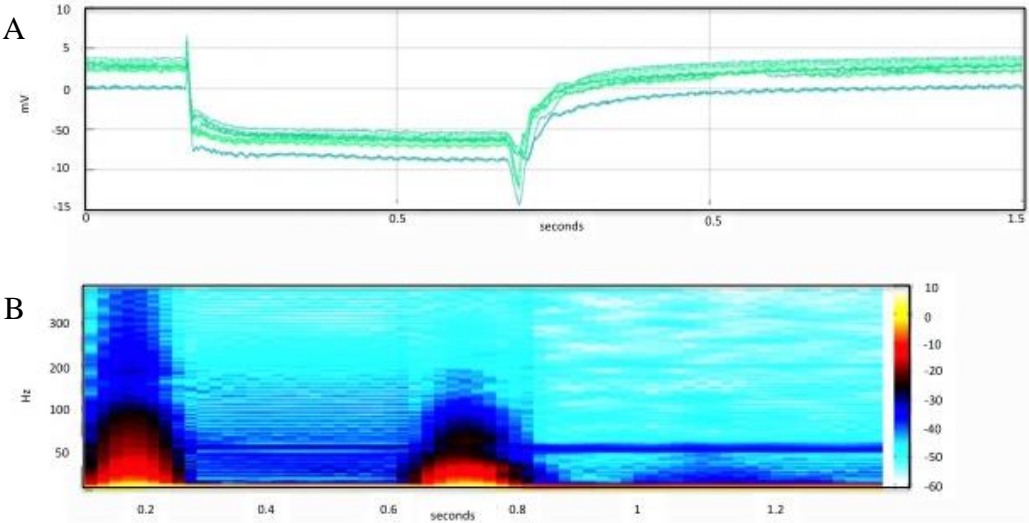
Figure 5-3: (A) The ERG trace for the *w-* flies. (B) The spectrogram of the ERG trace. No. of flies= 20 (one trace each).
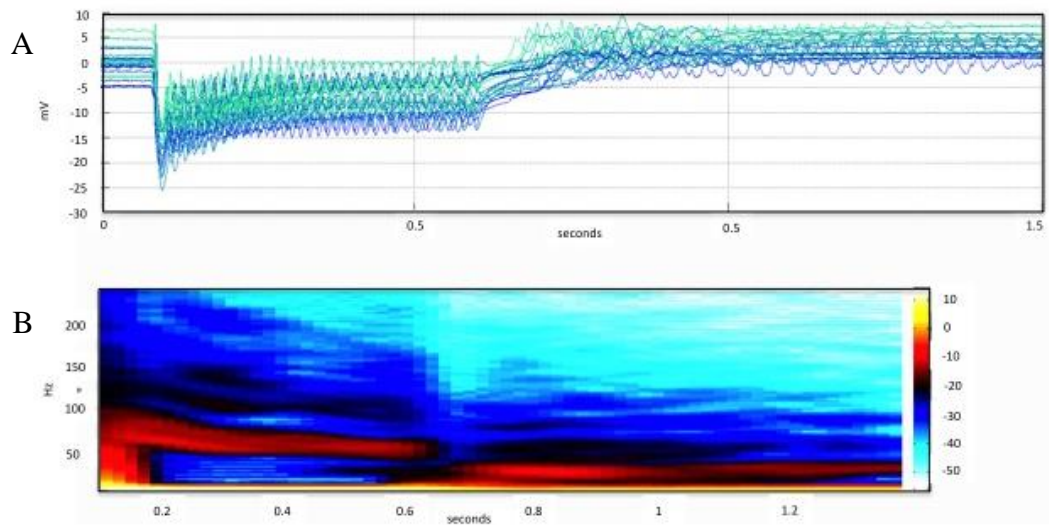
Figure 5-4: (A) The ERG trace for the *kcc^DHS1* flies. (B) The spectrogram of the ERG trace. The high and low frequency bands are present. No. of flies= 20 (one trace each).

To investigate whether the presence of insulating pigments have a role in preventing abnormal visual responses seen in the white-eyed *kcc^DHS1* flies, The red-eyed *kcc-P* flies were used. The flash ERG recording resulted in no rapid oscillations in the waveforms (Fig. 5A), and thus no high frequency was detected in the spectrogram (Fig. 5B). Our hypothesis is that the presence of insulating pigments surrounding the photoreceptors in these flies may protect them somehow – perhaps by preventing stray light reaching multiple photoreceptors or by insulating photoreceptors from each other and dampening electrical oscillations across the retina.
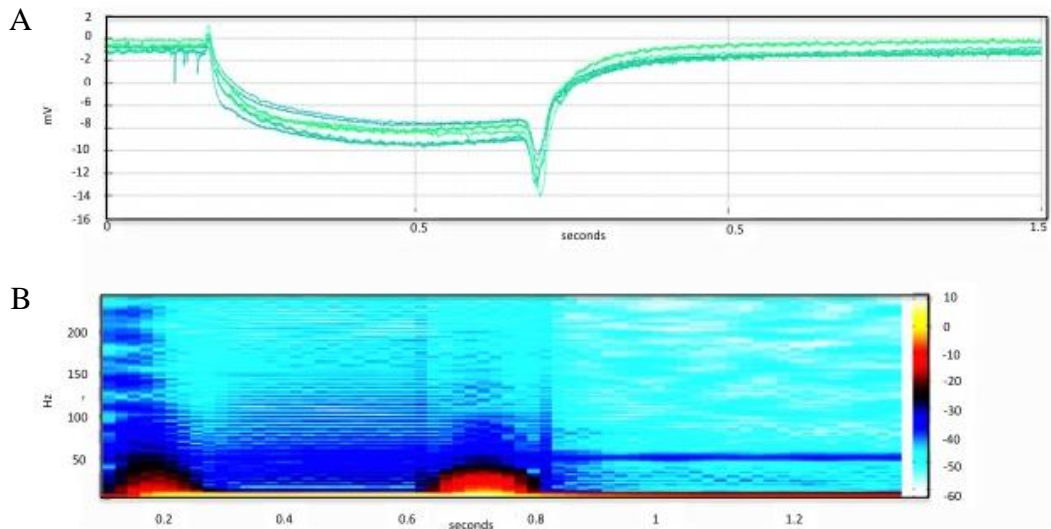
Figure 5-5: (A) The ERG trace for the *kcc-P* flies. (B) The spectrogram of the ERG trace. No. of flies= 20 (one trace each).

5.3.2 The reduced lateral inhibitory interaction in the white-eyed *kcc*^{DHS1} flies is responsible for the increased neural responses in these flies

To examine our initial assumption that the white-eyed *kcc*^{DHS1} flies have reduced lateral inhibition, we recorded from wild type and mutant flies using both a fiber-based small-field stimulus and a full-field stimulus. We hypothesized that for wild type flies we would see significant differences between localized small-field stimulation and wide-field stimulation because lateral inhibitory mechanisms would normalize responses for the latter but not the former. For the *kcc*^{DHS1} flies, we hypothesized that the small-field and full-field stimulations would be more similar because these lateral inhibitory mechanisms may be reduced or absent.

Source	ANOVA Results
Genotype	F=25, df=1, **p<0.001**
Stimulation Type	F=5.3, df=3, **p<0.01**
Genotype * Stimulation Type	F=3.3, df=3, **p<0.05**

Table 5-2: A two-way ANOVA to examine the effect of stimulation types (close, middle, far and full-field) on the *kcc^DHS1* and wild-type flies at the 1F1 level.

Source	ANOVA Results
Genotype	F=23, df=1, **p<0.001**
Stimulation Type	F=5.4, df=3, **p<0.01**
Genotype * Stimulation Type	F=3.5, df=3, **p<0.05**

Table 5-3: A two-way ANOVA to examine the effect of stimulation types (close, middle, far and full-field) on *kcc^DHS1* and wild-type flies at the 2F1 level.

First of all, a two-way ANOVA was conducted to examine the effect of the type of stimulation on the genotypes (kcc^{DHS1} and w-) and revealed overall significant main effects of the stimulation type, genotype as well as interactions between genotype and stimulation type (Table 5-2 and Table 5-3). At both the 1F1 (photoreceptor) and 2F1 (neuronal) levels (Fig. 5-6 and 5-7), the position of the small-field stimulations had no effect on any of the genotypes, p >0.05. However, the full-field stimulation (which stimulates a large fraction of the photoreceptors at once – including, potentially, the ones directly underneath the recording electrode) resulted in dramatically different responses. Because the small-field stimulations had no obvious effect in our data, we grouped all types of small field stimulations in one category (small-field stimulation), and then conducted a two-way ANOVA (Table 5-4 and 5-5). The

white-eyed wild type flies, *w-*, have decreased full-field responses compared to the small-field stimulations, $p < 0.05$ (Fig. 5-8), while the white-eyed kcc^{DHS1} flies (Fig. 5-9) have no change in the responses between the small-field stimulations and the full-field stimulation, $p > 0.05$.
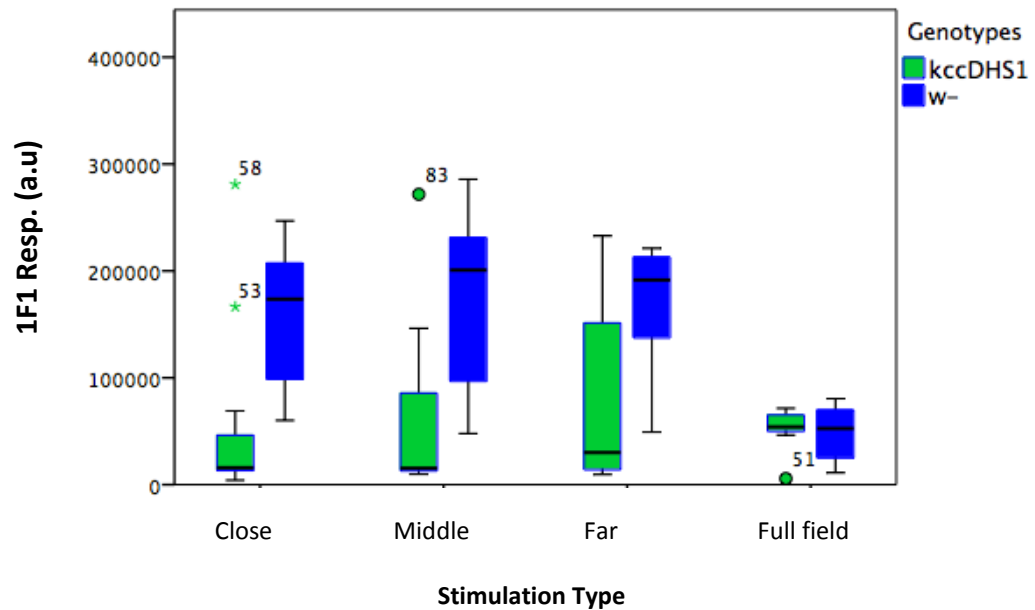
Figure 5-6: The 1F1 responses of kcc^{DHS1} and $w-$ flies. The kcc^{DHS1} flies don't show any significant difference between the conditions. The $w-$ flies, on the other hand, show reduced responses during the full-field stimulation compared to the small-field stimulations (close, middle and far).The stray numbers above and below the boxplots represent the outliers in our data. kcc^{DHS1}, N= 11 and $w-$, N= 10.

157
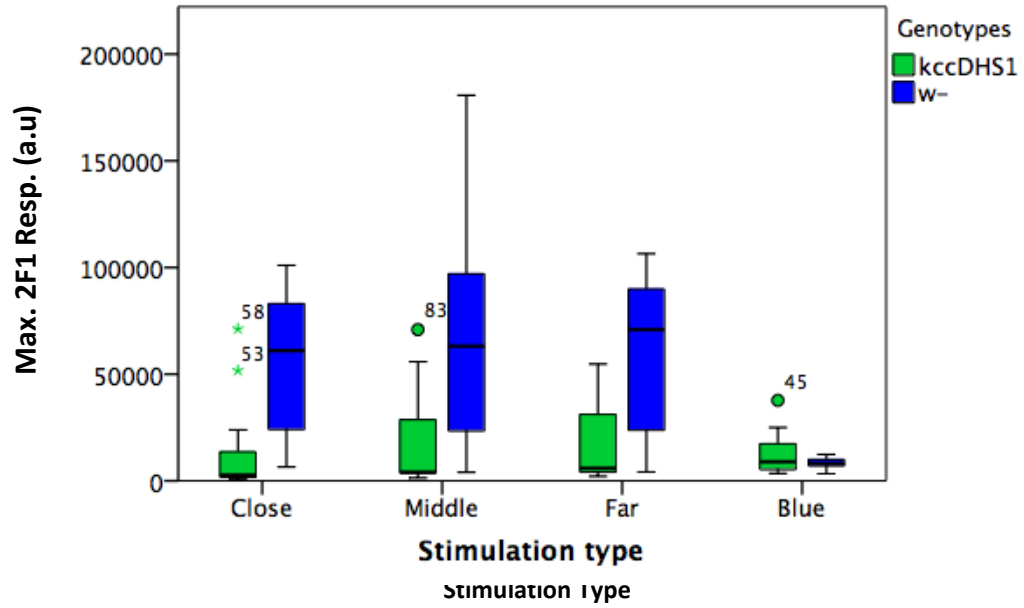
Figure 5-7: The 2F1 responses of kcc^{DHS1} and w - flies. The kcc^{DHS1} flies don't show any significant difference between the conditions. The w- flies, on the other hand, show reduced responses during the full-field stimulation compared to the small-field stimulations (close, middle and far). The stray numbers above and below the boxplots represent the outliers in our data. kcc^{DHS1}, N= 11 and w-, N= 10.
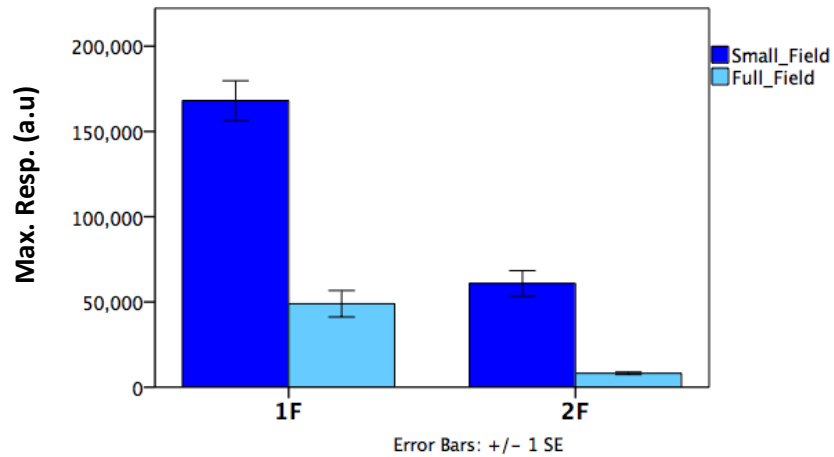
Figure 5-8: The maximum responses of the small field and full-field stimulations for the *w-* flies at the 1F1 and 2F1 levels. The small-field stimulation shows larger responses compared to the full field stimulation at 1F1 as well as 2F1.

Error Bars: +/- 1 SE

Figure 5-9: The maximum responses of the small field and full-field stimulations for the *kcc^{DHS1}* flies at the 1F and 2F levels. The small-field stimulation shows similar responses to the full field stimulations at 1F1 as well as 2F1.

Source	ANOVA Results
Genotype	F=8.1, df=1, *p<0.01*
Stimulation Type	F=15.9, df=1, *p<0.001*
Genotype * Stimulation Type	F=9.7, df=1, *p<0.01*

Table 5-4: A two-way ANOVA to examine the effect of stimulation types (small-field and full-field) on the *kcc^{DHS1}* and wild-type flies at the 1F1 level.

159

Source	ANOVA Results
Genotype	F=6.8, df=1, *p<0.05*
Stimulation Type	F=15.6, df=1, *p<0.001*
Genotype * Stimulation Type	F=10.6, df=1, *p<0.01*

Table 5-5: A two-way ANOVA to examine the effect of stimulation types (small-field and full-field) on the *kcc^{DHS1}* and wild-type flies at the 2F1 level.

We also compared the small-field and full-field stimulations of the 2F responses for each genotype (Fig. 5-7). The results were identical to that at the 1F level (Fig. 5-8 and 5-9). In addition, we looked at each stimulation type across all genotypes (Fig. 5-10 and 5-11). At both the 1F and 2F levels, the small-field stimulation resulted in greater responses for the *w-* flies compared to the *kcc^{DHS1}* flies, $p<0.05$. However, during full-field stimulation both genotypes show similar responses, $p>0.05$.

160
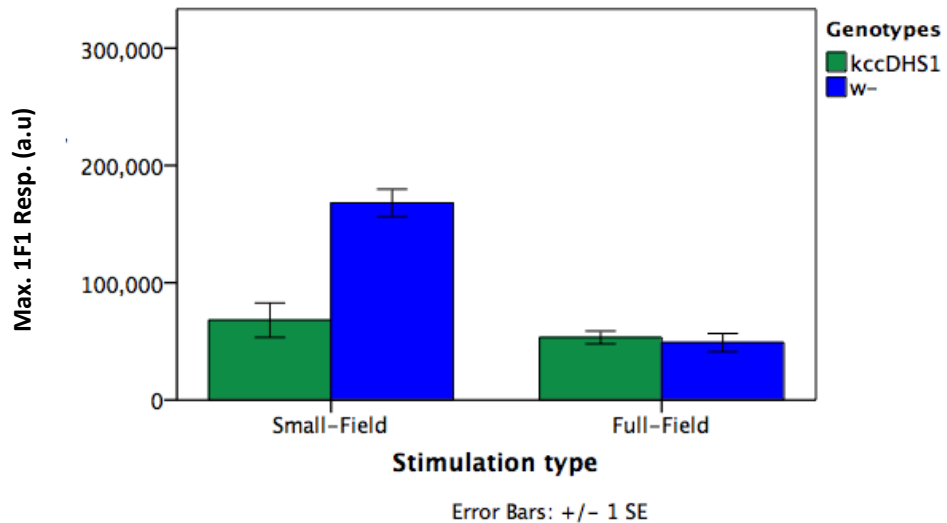
Figure 5-10: The maximum responses of the small field and full-field stimulations for the kcc^{DHS1} **and** *w-* **flies at the 1F1. The w- and** kcc^{DHS1} **show similar responses during the full-field stimulation.**
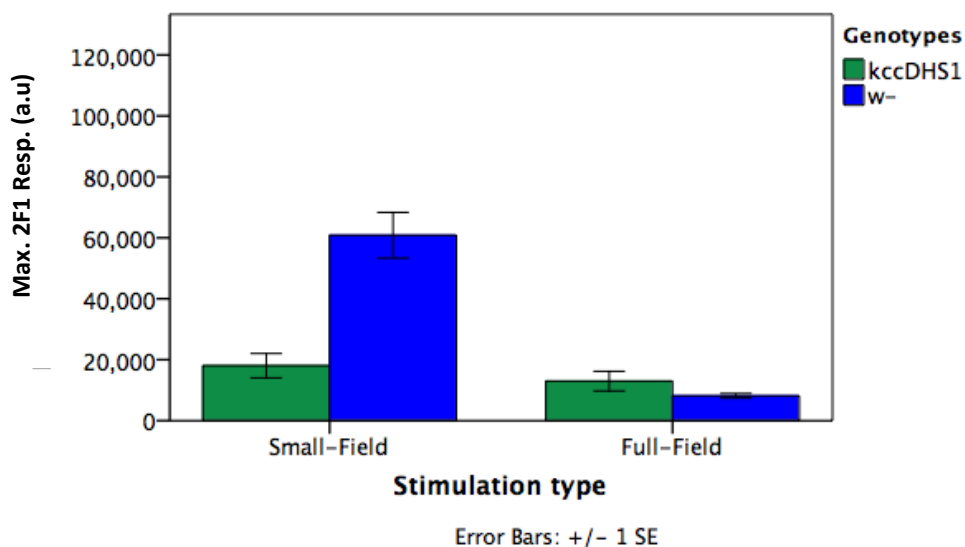
Figure 5-11: The maximum responses of the small field and full-field stimulations for the kcc^{DHS1} **and** *w-* **flies at the 2F1 level. The w- and** kcc^{DHS1} **show similar responses during the full-field stimulation.**

The most remarkable feature of the datasets described above is the significant reduction in response to full-field stimulation in the *w-* flies. Adding in vastly more light to the eye led to a huge reduction in visual response measured at a single photoreceptor. Why should this be? The answer, we hypothesize, is the presence of lateral suppressive interactions somewhere in the wild-type Drosophila visual system. We note that this suppression was almost entirely absent from the *kcc* genotype.

We then asked where the site of the lateral interactions might be? There are two obvious possibilities: direct coupling between photoreceptors (perhaps through gap junctions) or neuronal inhibition (via amacrine cells or even at the level of the lamina). To investigate the

difference between small-field stimulations and full-field stimulation we recorded from the homozygous ort- null flies, which have significantly reduced neural responses as their photoreceptors are blocked by the histamine receptor mutation (Afsari et al., 2014; Pantazis et al., 2008). Thus, if the small-field stimulations originate from interneurons whose responses are altered by this mutation, *ort-* flies should show very low responses compared to the full-field stimulation.

The results showed a complete loss of 1F1 responses following the small-field stimulations (Fig. 5-12 and 5-14), indicating that the responses we measure are mediated by neuronal transmission. However, after the full-field stimulation we still see an increase in the response. One-way ANOVA (Table 5-6) revealed that full-field stimulation is significantly higher than small-field stimulation at the 1F1 level, $p<0.001$. However, at the 2F1 level, *ort-* flies have lost the responses to both small-field and full-field stimuli, $p >0.05$ (Fig. 5-13 and 5-14). This suggests that the small-field stimulations are mediated by early, lateral interaction, potentially among amacrine cells or 2nd and 3rd order neurons.
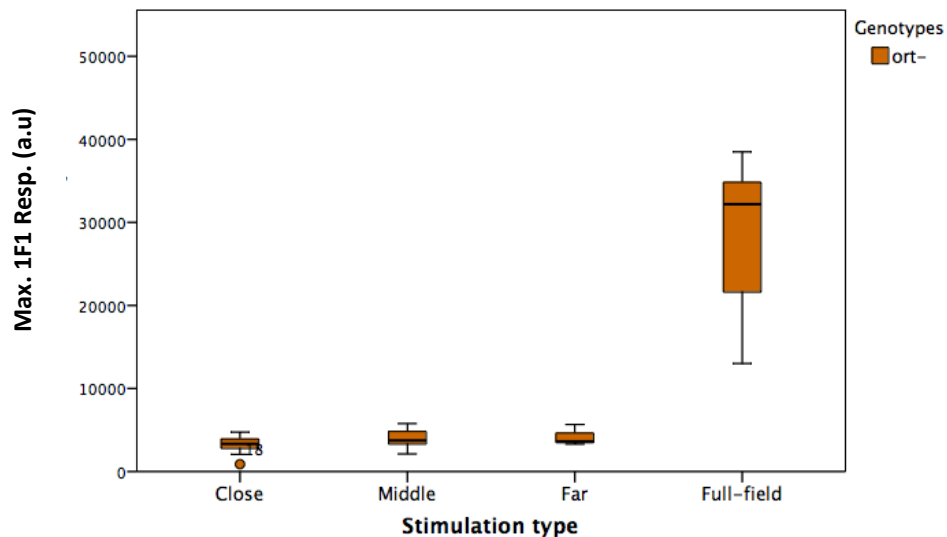
Figure 5-12: The 1F1 responses *ort-* flies. The small field stimulations show no responses. However, during the full-field stimulation, the ort= flies showed a significant response. *ort*⁻, N= 10.

162
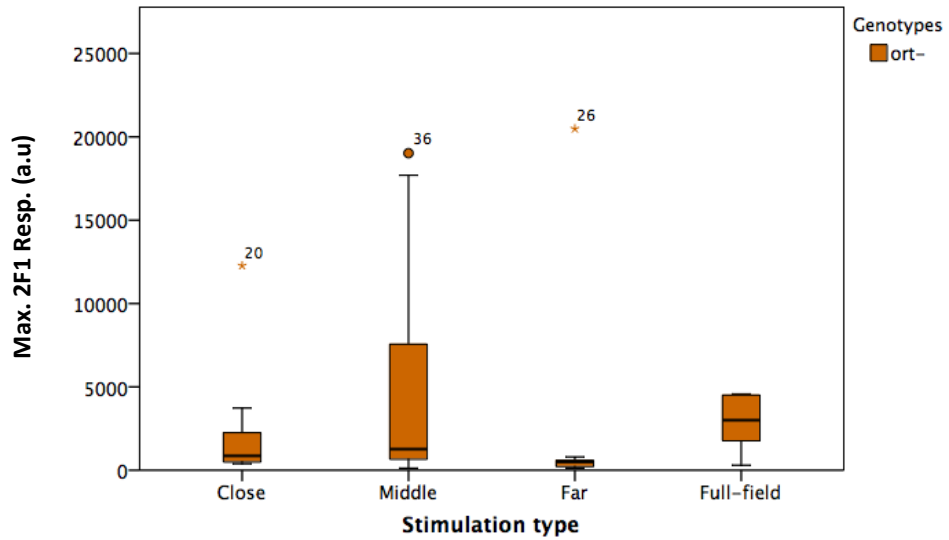
Figure 5-13: The 2F1 responses *ort-* flies. The small field stimulations and the full-field stimulation show no reliable responses at all. *ort⁻*, N= 10.

Source	Level	ANOVA Results
Stimulation Type	1F1	F=289.6, df=1, **p<0.001**
(Small-field vs. Full-field)	2F1	F=0.06, df=1, p>0.05

Table 5-6: A one-way ANOVA to examine the effect of stimulation types (small-field and full-field) on the ort flies at the 1F1 and 2F1 levels.
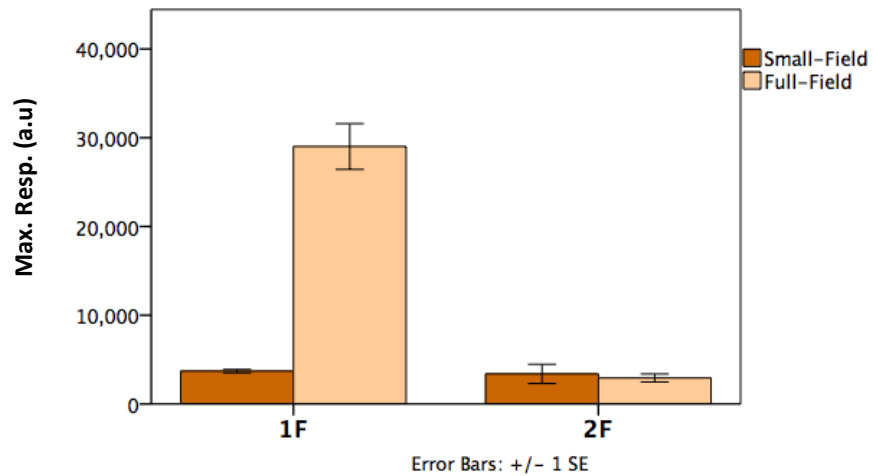
Figure 5-14: The maximum responses of the small field and full-field stimulations for the *ort* flies at the 1F1 and 2F1 levels. At the 1F1 level, the small-field stimulation shows lower responses compared to the full field stimulation. However, at the 2F1 level, both types of stimulation are similar.

Finally, we investigated the effect of local small-field stimulations and full-field stimulation on the red-eyed *kcc-P* flies. Because these flies have red pigments and do not show any visual abnormalities, it is interesting to see whether their responses differ from those of the w- animals. Similar to the *kcc^{DHS1}*, *w-* and *ort-* flies, the type of small-field stimulations did not show any significant effect in the *kcc-P* flies at the 1F1 and 2F1 levels (Fig. 5-15 and 5-16). Having all types of small-field stimulations under one category and then conducting a one-way ANOVA (Table 5-7) revealed a significant increase of responses during full-field stimulation compared to small-field stimulation at both 1F1 and 2F1 levels (Fig. 5-17), $p < 0.05$.
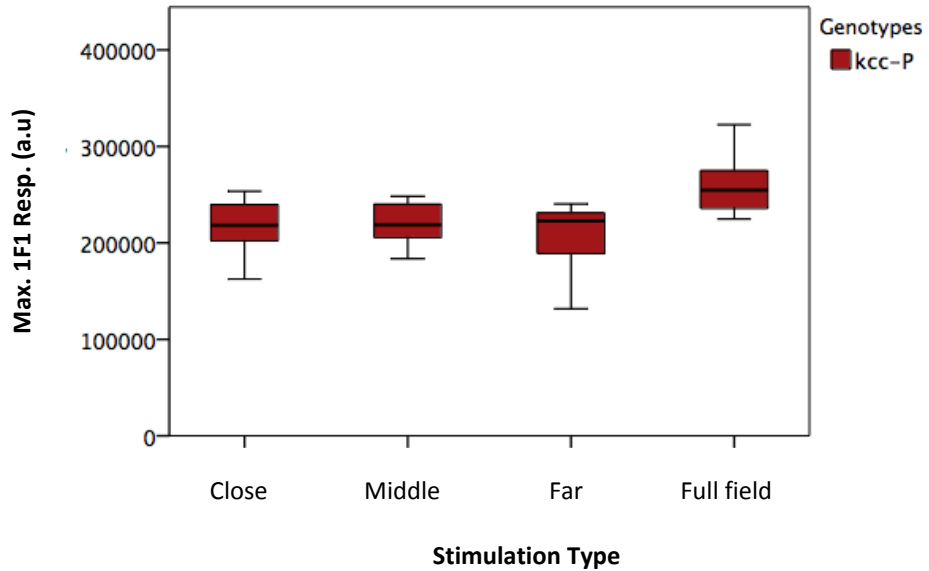
Figure 5-15: The 1F1 responses _kcc-P_ flies. The small-field stimulations are not significantly different from each other. During the full-field stimulation, the responses significantly increased. _kcc-P_, _N_= 8.
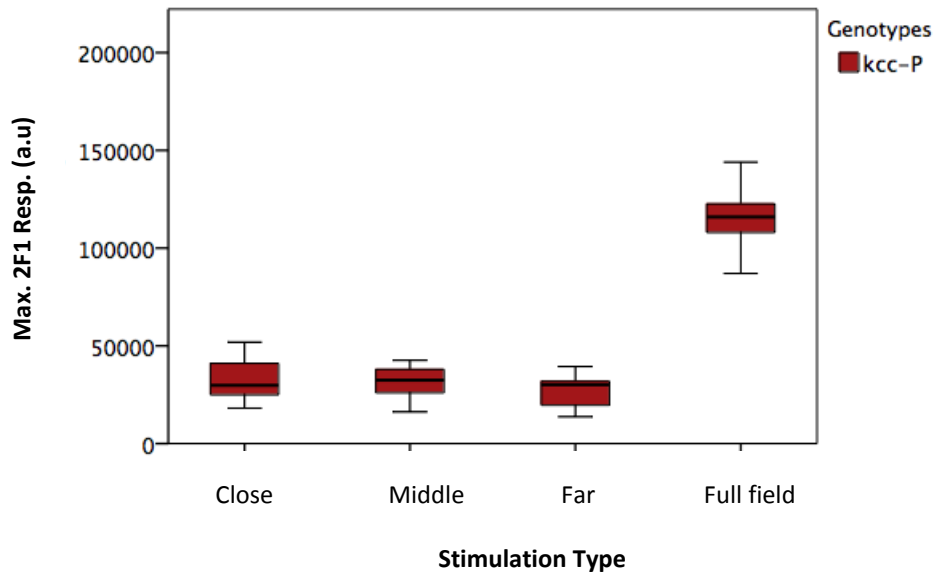
Figure 5-16: The 2F1 responses _kcc-P_ flies. The small-field stimulations are not significantly different from each other. During the full-field stimulation, the responses significantly increased. _kcc-P_, _N_= 8.

Source	Level	ANOVA Results
Stimulation Type	1F1	F=13.8, df=1, *p<0.01*
(Small-field vs. Full-field)	2F1	F=325.3, df=1, *p<0.001*

Table 5-7: A one-way ANOVA to examine the effect of stimulation types (small-field and full-field) on the *kcc-P* flies at the 1F1 and 2F1 levels.
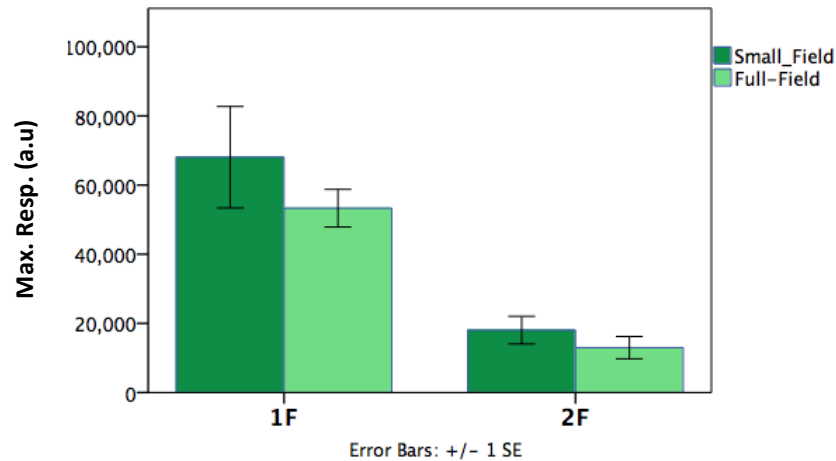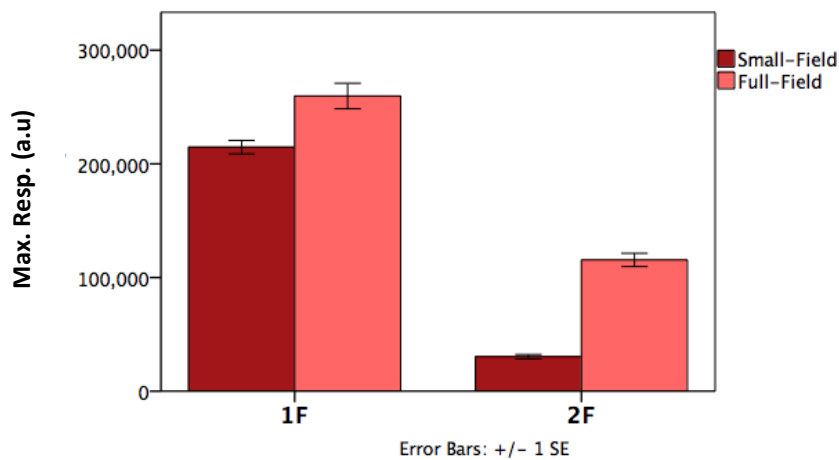

Figure 5-17: The maximum responses of the small field and full-field stimulations for the *kcc-P* flies at the 1F and 2F levels. The full-field stimulation shows greater responses compared to the small field stimulations at 1F as well as 2F.

This result suggests that the pigments surrounding the photoreceptors protect these flies somehow. The increased responses during the full-field stimulation indicate that photoreceptors did not inhibit each other, suggesting that each ommatidium is responding independently from the neighboring ommatidia – again, lateral suppressive interactions appear to be absent in some way.

166

5.3.3 Phase shifts

If the responses we measured in the small field stimulation were propagated across the eye by slow, lateral connections, we might expect to see a relative phase lag in the SSVEP response as we move from close to far conditions. In our analysis (Fig. 5-18 and 5-19), we find that the temporal phase of both the 1F1 and 2F1 responses were constant across all small-field conditions for all genotypes. The *ort-* flies have very small responses, and thus the phase data were not reliable. Moreover, the white-eyed *kcc*^{DHS1} and the red-eyed *kcc-P* flies have similar phase shifts, compared to probably faster responses for the *w-* flies. Finally, the full-field stimulation resulted in completely different phase shifts. It is difficult to tell if this full-field stimulation resulted in faster or slower responses compared to the small-field stimulations owing to the fact that the phase might have been inverted in this polar representation of the phase responses.
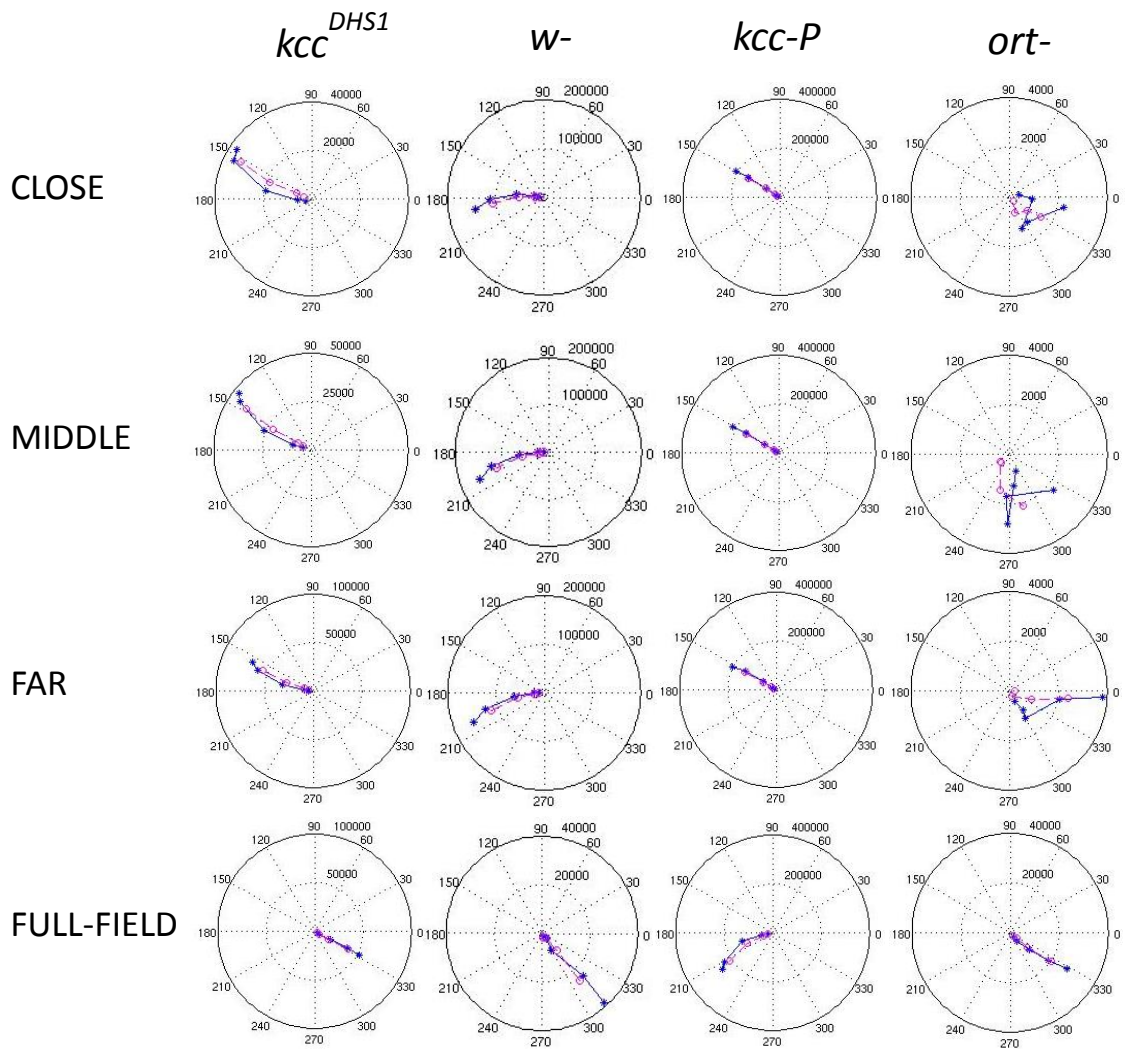
Figure 5-18: The phase data at the 1F1 level for the small-field stimulations (close, middle and far) and full-field stimulation. The red line represents the unmasked data, whereas the blue represent the masked data. kcc^{DHS1}, N= 11; *w-*, N= 10; *ort*, N= 10; *kcc-P*, N= 8.
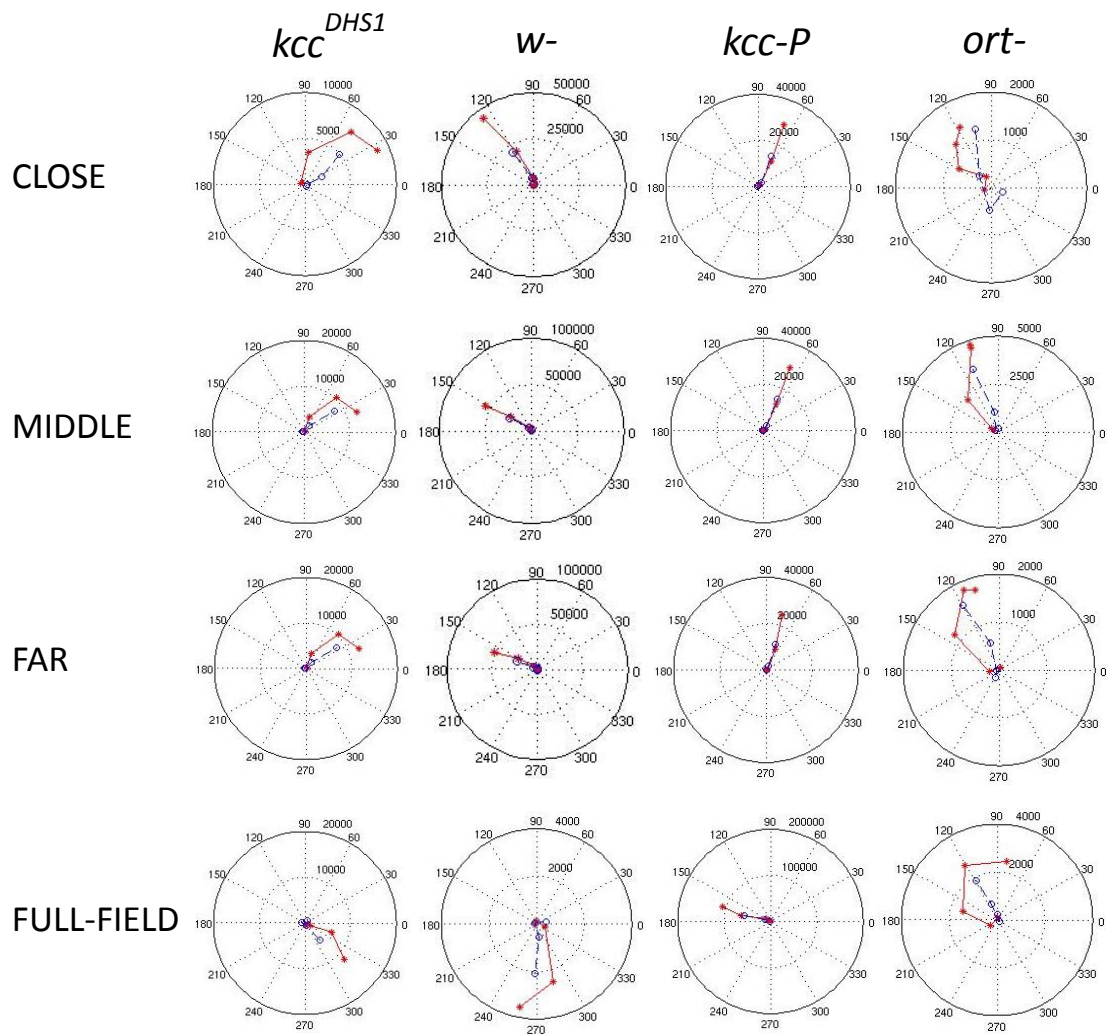
Figure 5-19: The phase data at the 2F1 level for the small-field stimulations (close, middle and far) and full-field stimulation. The red line represents the unmasked data, whereas the blue represent the masked data. *kcc^DHS1*, N= 11; *w-*, N= 10; *ort*, N= 10; *kcc-P*, N= 8.

5.4 Discussion

This study set out to explore the mechanism underlying the rapid oscillations observed only in the white-eyed kcc^{DHS1} flies during light stimulations. We hypothesized that wild-type animals might have more lateral inhibition, which would damp down the oscillations. We tested the amount of oscillations we saw by measuring responses across the retina at different distances in *w-* and also in red-eyed flies. Our hypothesis was that the rapid oscillations we see in the white-eyed kcc^{DHS1} during the sustained negative wave are due to the reduced lateral inhibitory interactions. Specifically, we hypothesized that flies that recruit strong lateral inhibition would exhibit relatively weak responses to full-field stimulation compared to the small-field stimulations. We stimulated single ommatidia by using fiber-coupled LED and measured the responses from three different electrode locations (close, middle and far) as well as a response to full field stimulation.

Since lateral interactions suppress responses to spatially uniform intensity (Freifeld et al., 2013), the white-eyed wild type flies (*w-*) were expected to have increased inhibition and subsequently reduced responses during full-field stimulation. Because the *w-* flies lack the insulating pigments, the effect of lateral interactions is weak or not present during the small-field stimulations marked by increased visual responses, but has a significant effect during the spatially uniform stimulation characterized by a drop in the visual responses. In comparison, the red-eyed *kcc-P* flies, in which the neighboring neurons are optically separated, have increased responses during the full-field stimulation indicating that lateral interactions are minimized in these flies. Finally, in the white-eyed kcc^{DHS1} flies, there was no significant difference between full field and localized stimulations indicating an abnormality in the lateral interaction mechanism in these flies.

One explanation for the decrease is that neighboring neurons (in the Lamina) inhibit each other. With a single input, there is no response in neighboring neurons and hence no inhibition. With full-field stimulation, all the neighbors are stimulated and everything inhibits everything else. Specifically, we hypothesized that the signals might be coming from the lateral interaction, potentially among amacrine cells (Hu et al., 2015) and 2nd and 3rd order neurons, rather than from lateral signal transmission across the retina. To confirm this, we used the homozygous *ort*

null mutant. *ort* is a gene encoding a histamine receptor subunit in L1 and L2 (Gengs et al., 2002). These flies show significantly reduced neural responses (Afsari et al., 2014), and if the spread of small-field stimulations is mediated by amacrine cells, we would expect to see no responses following small-field stimulations at the 1F1 level and no responses from both the small-field and the full-field stimulations at 2F1.

Using the *ort* null flies to examine the source of the signals after small-field and full-field stimulations suggested that responses to small-field stimulations are mediated by lateral interactions. These interactions are likely to arise in the amacrine cells (Hu et al., 2015), and 2nd and 3rd order neurons. Responses to the full-field stimulations are, presumably, mediated by the same mechanisms but with the additional major contribution of a response from the photoreceptors contacted directly by the recording electrode.

Contrary to expectations, this study did not show phase lags among the small-field stimulations to prove the hypothesis that signal propagation across the eye is mediated by lateral connections. A possible explanation for this might be that the stimulus frequency used in this study (12Hz) is not sufficient to show the shift in the phase data. Increasing the frequency may make it more noticeable but it would also reduce the amplitude of the responses. In practice, it might not be possible to measure phase shifts of the duration expected here using a pure steady-state technique.

The scope of this study was limited in terms of showing which class of neurons responsible for the differences observed between the stimulus types. In Chapter 8, we propose some experiments that may help to tackle this problem.

5.5 Conclusion

To conclude, this chapter set out to assess the visual abnormalities seen in the white-eyed *kcc^{DHS1}* flies characterized by increased neural responses and high frequency oscillatory events during light stimulation. The presence of pigment cells has been found to prevent these rapid oscillations. The contribution of this study has been to suggest that these visual abnormalities in these animals are probably due to weak lateral inhibition rather than abnormal gain control.

6 Chapter 6: Contrast adaptation abnormalities in Drosophila model of epilepsy

6.1 Introduction

Contrast is essential for detecting edges that can define borders and lighting conditions. Perceptual and physiological studies showed that the visual system has self-calibration mechanisms for adjusting its sensitivity to contrast based on the most recent stimulus history: This is known as contrast adaptation (see Kohn, 2007 for a review).

Psychophysical and electrophysiological experiments have shown contrast adaptation to a range of stimuli in the sensory cortices including the visual cortex. Psychophysical studies have demonstrated that prolonged exposure to high contrast stimuli results in a reduction in the perceived contrast of the test stimuli (Blakemore et al., 1973; Hammett et al., 1994; Snowden and Hammett, 1996), (see Graham, 1989 for a review). Electrophysiological studies examining the effect of contrast adaptation on the cats and primates visual systems have shown that a contrast response function is shifted rightward and/or downward after a prolonged exposure to high contrast gratings (Bonds, 1991; Gardner et al., 2005; Ohzawa et al., 1982; Sclar et al., 1989, 1985). This neural effect of contrast adaptation is attributed to either a reduction in firing rate due to a deleterious fatigue, or to a reduction in contrast sensitivity. Even though both effects can be seen in the primary visual cortex (V1), the reduction in contrast sensitivity is believed to be dominant (Albrecht et al., 1984; Bonds, 1991; Crowder et al., 2006; Movshon and Lennie, 1979; Ohzawa et al., 1982; Sclar et al., 1989). This readjustment of sensitivity centers the contrast response functions to the contrast of the adapting stimulus. Based on this fact, adaptation is considered as a form of gain control.

Having directly investigated the effect of gain control in the spatial domain (i.e. masking) in Chapter 4, this Chapter uses the same technique (SSVEPs) to investigate the effect of the temporal aspect of gain control by examining contrast adaptation in the kcc^{DHS1} and w- flies. A great deal is known about the effect of contrast adaptation on the visual systems of cats and primates, however, it is not well understood how fruit flies would respond to contrast adaptation, especially our fly model of epilepsy kcc^{DHS1} flies. Because gain control was found to be

abnormal in kcc^{DHS1} flies, one might speculate that contrast adaptation is abnormal in these flies too.

In the first experiment we used the SSVEP technique to measure the effect of contrast adaptation on kcc^{DHS1} and w- flies at different stages of their lives. In the second experiment we examined the role of GABAergic activity on the Drosophila visual system using mutant flies that express transgenes in specific subsets of neurons.

6.1.1 Methods

6.1.1.1   Fly stocks

White-eye wild type (w-) and kcc^{DHS1} flies were used in this experiment, and the flies were handled in the same way as in the previous chapters.

6.1.1.2   ERG recording

The ERG recording was almost identical to our experiments in Chapter 4, except in this experiment we did not use the diffusing screen in front of the fiber optic, and also we recorded from only one fly at a time. A number of kcc^{DHS1} and w- flies aged 1, 5, and 10 days were used in this experiment.

6.1.1.3   Stimuli

Our stimulus consists of a 20-second adaptation period of either 0% or 80% temporal contrast, and 4 probes of 2-seconds each (Fig. 6-1). The probe preceded the 20-second adaptor period was termed Probe1. The following probes were termed Probe2 (immediately after the adaptor), Probe3 (10 second after the adaptor) and Probe4 (18 seconds after the adaptor), respectively. During the probe period, a flickering light was presented at one of 6 different contrast levels (0%, 5%, 10%, 20%, 40% and 80%). The lights were generated using a single square wave, flickering at 6 Hz.

The stimulus consists of 12 trials, and in each trial the same contrast level was presented at each probe following both 0% and 80% adaptor. To avoid order effects of trials, the contrast levels of probes and adaptor were randomized in a counterbalanced manner.
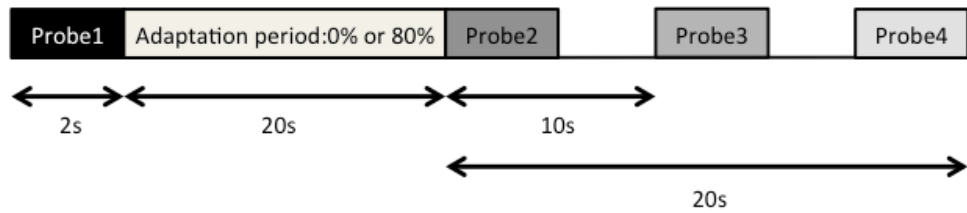
Figure 6-1: A schematic representation of the stimulus in a single trial. The stimulus started with the pre-adaptation period for 2 seconds (Probe 1), followed by an adaptation period for 20 seconds. Immediately after the adaptor, Probe 2 was presented. 10 seconds and 18 seconds after the offset of the adaptor, Probe 3 and Probe 4 were presented, respectively, to look at the recovery from adaptation.

6.1.1.4   Analysis

The software and the analysis concept to extract the photoreceptor and the neural responses used in this experiment are identical to that used in our experiment in Chapter 4.

To measure the adaptation effect, we initially subtracted the responses to Probe2 (to look at the effect immediately after the adaptor was turned off) from Probe1, for both 1F1 and 2F1. To measure the effect of high contrast adaptation specifically, rather than the probe order in itself, we subtracted the differences found in trials following the 80% adaptor from those following 0% adaptor; we termed this "mean difference" (Fig. 6-2). If the mean difference (1FDiff and 2FDiff) is greater than zero, it means we have an effect of adaptation. We also looked at what time the system will recover from adaptation by measuring the responses to Probe3 as well as Probe4 in the same way as we explained above for Probe2. The mean differences were plotted as a function of probe contrast and the maximum values were also plotted for all probes.

174
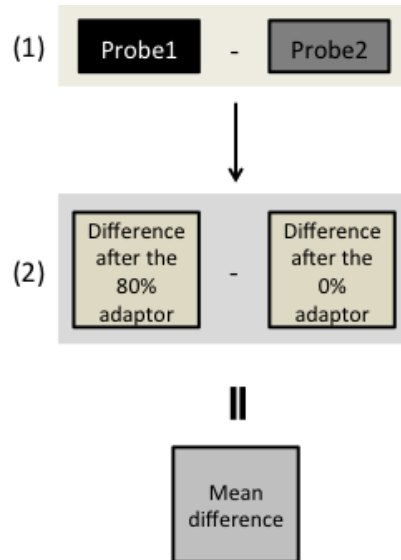
Figure 6-2: A schematic representation of the analysis steps. First of all, we subtracted Probe 2 responses from Probe 1. Then subtracted the differences found in trials followed the 80% adaptor from those following the 0% adaptor. We termed this (mean difference). If the mean difference (1FDiff and 2FDiff) is greater than zero, it means we have an effect of adaptation

6.1.2 Results

6.1.2.1   Evidence of adaptation effect in the *w-* flies

CRFs of both the photoreceptor (1F) and neural (2F) responses for *w-* flies are shown in (Fig. 6-3). Firstly, SSVEPs generate reliable CRFs with the highest amplitude corresponding to the highest contrast level. Secondly, responses following 80% adaptation period are weaker, especially at high contrast levels, compared to that following the 0% adaptation period. This is true for both 1F and 2F.

Because we were interested in the effect of contrast adaptation rather than the probes order per se, we analyzed the responses by measuring the mean differences (see Analysis). A two-way ANOVA was conducted that examined the effect of age and contrast on both 1FDiff and 2FDiff for *w-* flies. There was a statistically significant effect of age and contrast on 1FDiff, but the interaction effect was not significant (Table 6-1). Briefly, at day one and five, the increase

in contrast levels did not have any effect on the 1FDiff. At day 10, however, there was a significant difference between the 5% contrast and the rest of contrast levels. Moreover, the age effect did not have any significant difference at any of the contrast levels.

Source	1FDiff	2FDiff
Age	F= 6.7, df=2, **$p<0.01$**	F= 0.4, df=2, $p>0.05$
Contrast	F=7.1, df=4, **$p<0.001$**	F=13.2, df=4, **$p<0.001$**
Age * Contrast	F=0.6, df=8, $p>0.05$	F=0.3, df=8, $p>0.05$

Table 6-1: A two-way ANOVA to examine the effect of age and contrast levels on the *w-* flies.

For 2FDiff, on the contrary, there was significant effect of contrast levels but no effect of age and no significant interaction between age and contrast levels were obtained (Table 6-1). Briefly, the age effect did not have any significant difference at any of the contrast levels. Moreover, at day one and ten, the 80% contrast resulted in greater responses than the other contrast levels.

Because the sample size in our data is not large enough, we cannot assume that the data is normally distributed. Thus, we have conducted the non-parametric test, Wilcoxon signed rank test, to ask whether the 1FDiff or 2FDiff is greater than zero (Fig. 6-4), and therefore whether an adaptation effect was present. At day one, the test revealed that the 1FDiff is significantly higher than zero across all contrast levels, $p < 0.05$. The 2FDiff, however, is only significant at high contrast levels (20%, 40% and 80%). At day 5, the 1FDiff demonstrated significance at all contrast levels except the 5% contrast, $p < 0.05$. For the 2FDiff, the adaptation is only present at high contrast levels. In addition, 10 days old flies showed significant 1FDiff at all contrast levels, $p < 0.01$. However, in 2FDiff the effect is only significant at high contrast levels, $p < 0.05$.
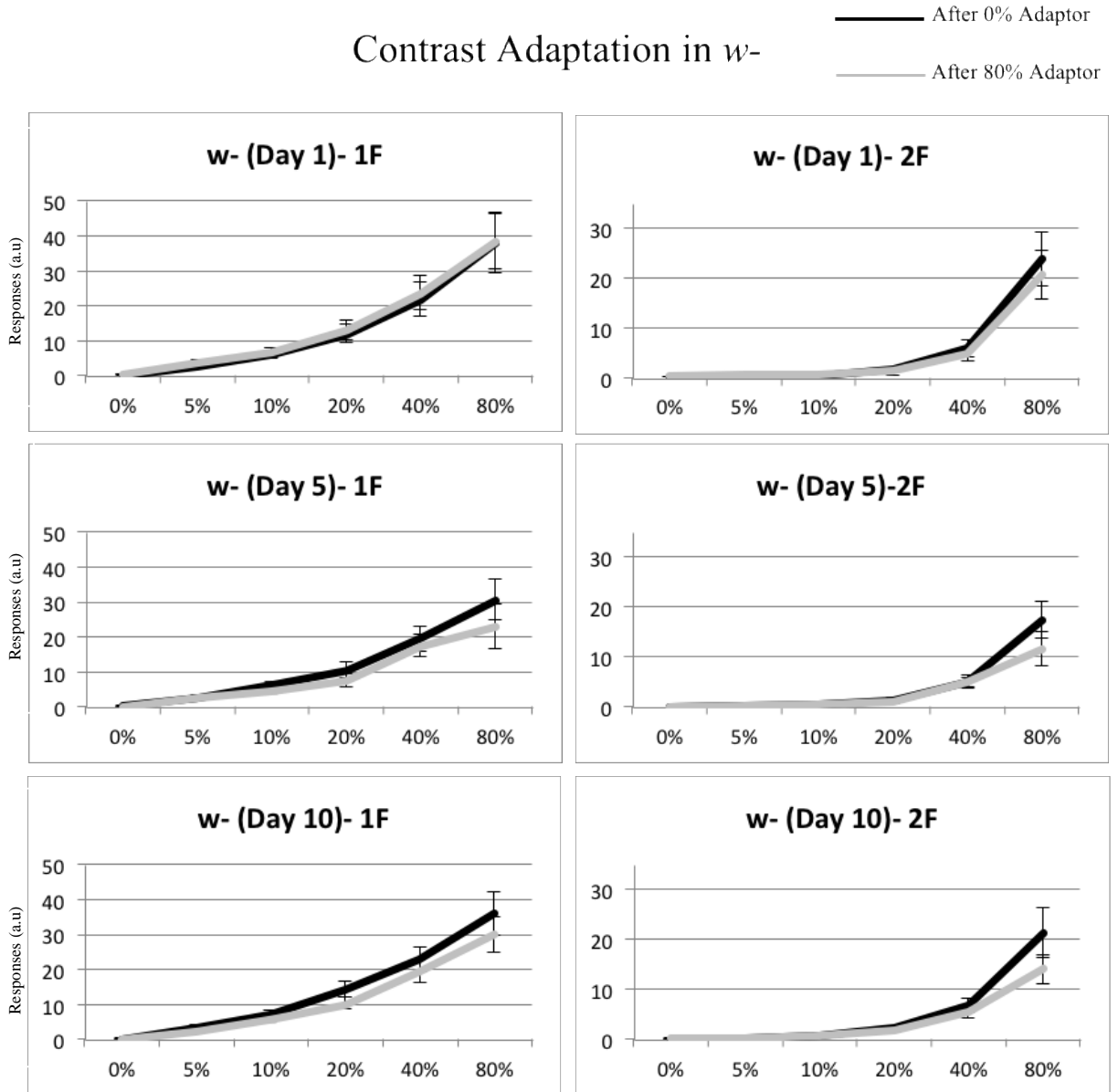
Figure 6-3: CRFs taken from Probe2 for *w-* flies aged 1, 5 and 10 days. SSVEPs generated reliable CRFs with the highest amplitude corresponding to the highest contrast level. In addition, responses following 80% adaptation period are weaker, especially at high contrast levels, compared to that following the 0% adaptation period.

w-

Day 1
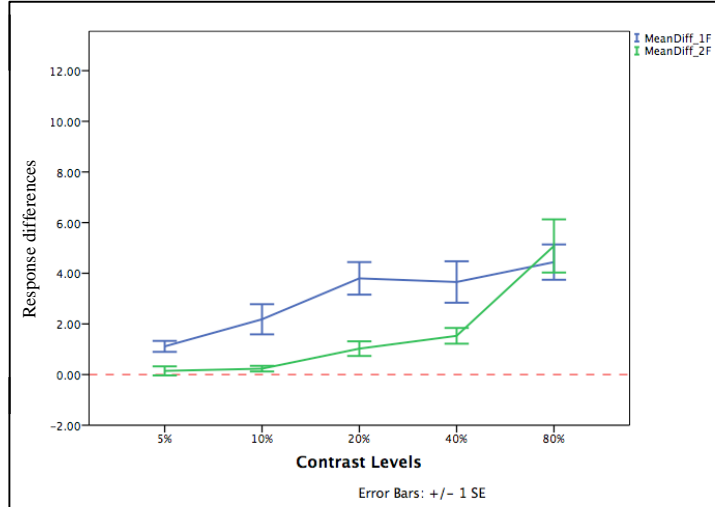
Day 5
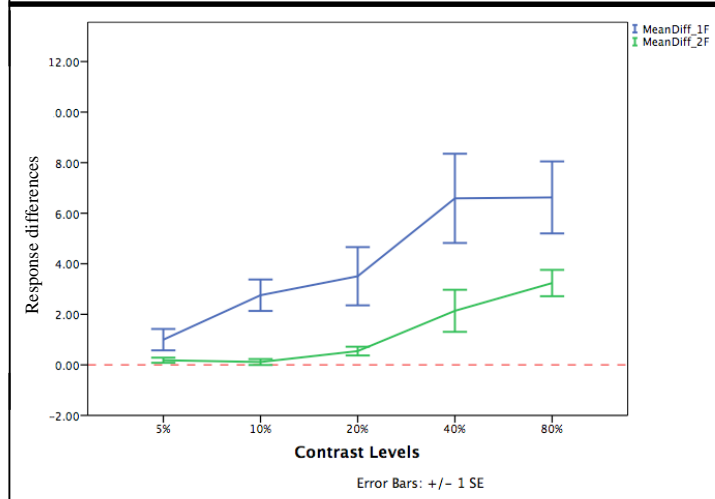
Day 10
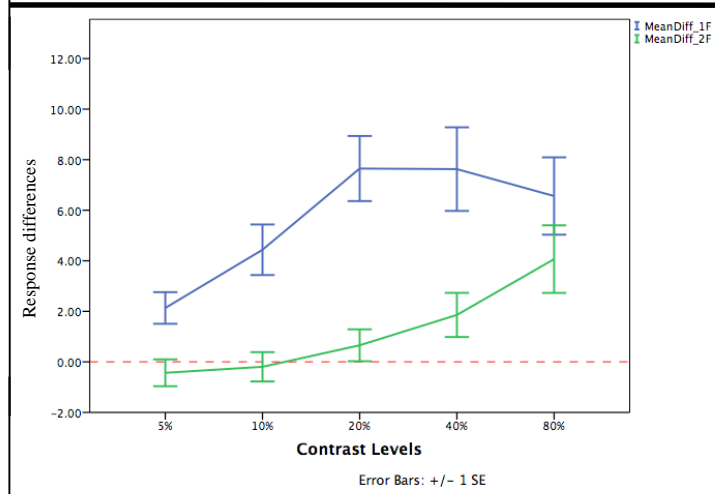
Figure 6-4: The mean differences (1FDiff and 2FDiff) as a function of contrast for *w-* flies aged 1, 5 and 10 days.

6.1.2.2   Evidence of adaptation effect in the *kcc^{DHS1}* flies

CRFs of both the photoreceptor (1F) and neural (2F) responses for *kcc^{DHS1}* flies are shown in (Fig. 6-5). First of all, 1-day old flies had weak SSVEPs, and then became stronger at 5-days and 10-days old flies, with the highest amplitude corresponding to the highest contrast level. In addition, at 1F and 2F levels, responses following the 80% adaptation period were weaker compared to that following the 0% adaptation period.

A two-way ANOVA was conducted that examined the effect of age and contrast levels on both 1FDiff and 2FDiff (Fig. 6-6). There was a statistically significant effect of age on 1FDiff but no significant effect of contrast and no significant interaction between age and contrast levels were obtained (Table 6-2). The only significant difference was observed for 20% contrast probes in day-one flies responses where responses were significantly reduced compared to day-five and ten flies. In short, we did not find any significant effect of age at any of the contrast levels. In addition, increasing the contrast level did not have any effect on any of the *kcc^{DHS1}* flies at this level.

For 2FDiff, on the contrary, there was a significant effect of contrast and age, but no significant interaction between the two (Table 6-2). Briefly, at day one, increasing the contrast level did not have any effect on these flies. However, at day five, there was a significant difference between the 80% contrast and low contrast levels (5%, 10% and 20%). At day ten, the 40% contrast was significantly higher than 5% and 10% contrast levels. In addition, we did not find any effect of age at any of the contrast levels.

Analyzing the data using a Wilcoxon signed rank test showed that at day one, the 1FDiff is not significantly greater than zero across all contrast levels, $p > 0.05$. However, the 2FDiff was only significant at (80%), $p < 0.05$. At day 5, both the 1FDiff and 2FDiff demonstrated significance across all contrast levels, $p < 0.05$, except at 10% contrast for the 2FDiff. Finally, the 1FDiff at day 10 showed an adaptation effect across all contrast levels, $p < 0.05$, except the

10%. The 2FDiff, on the other hand, showed the effect only at the high contrast levels (20%, 40% and 80%), $p < 0.05$.

Source	1FDiff	2FDiff
Age	F= 6.5, df=2, *p<0.01*	F= 8.3, df=2, *p<0.001*
Contrast	F=1.8, df=4, *p>0.05*	F=7.5, df=4, *p<0.01*
Age * Contrast	F=0.8, df=8, *p>0.05*	F=0.9, df=8, *p>0.05*

Table 6-2: A two-way ANOVA to examine the effect of age and contrast levels on the *kcc^{DHS1}* flies.

These results suggest that the kcc^{DHS1} flies have weak adaptation early in life, which gets stronger in older flies. This increase in adaptation might be different from that of the w⁻ flies. In the next section, we described the difference in adaptation between the kcc^{DHS1} and w⁻ flies.

Contrast Adaptation in kcc^{DHS1}
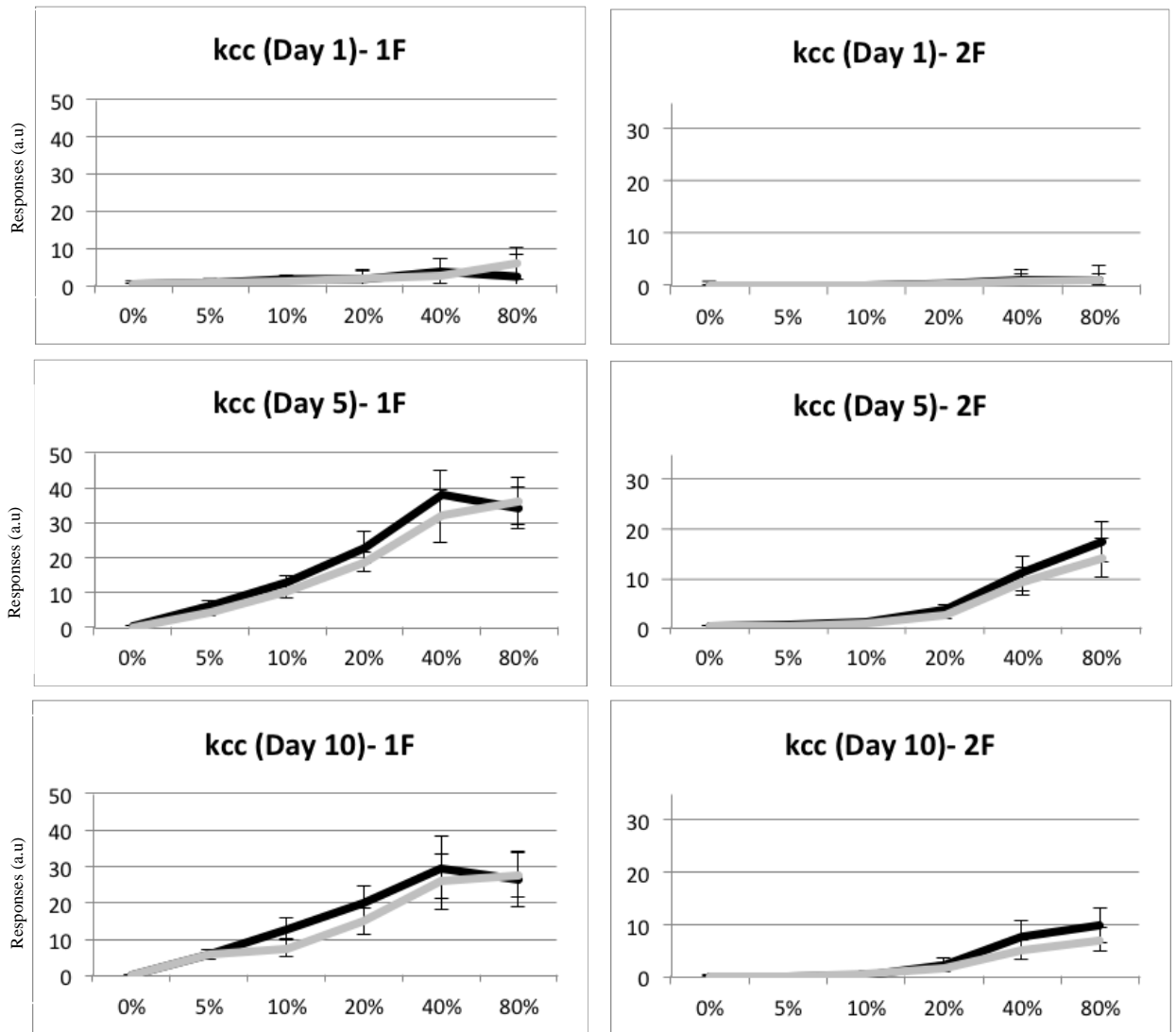
Figure 6-5: CRFs taken from Probe2 for kcc^{DHS1} flies aged 1, 5 and 10 days.

$$kcc^{DHS1}$$

Day 1
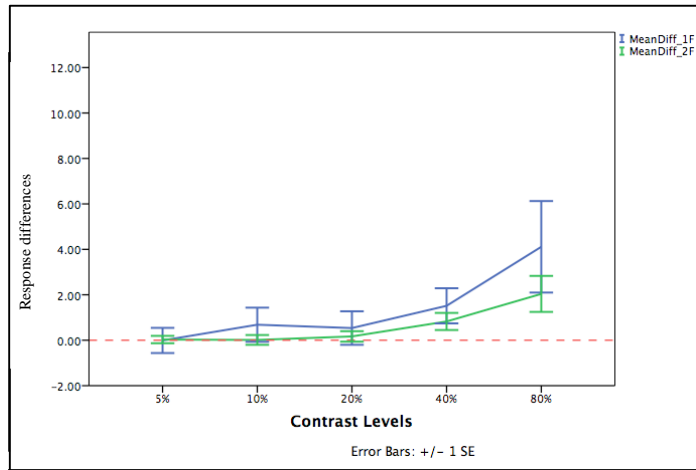
Day 5
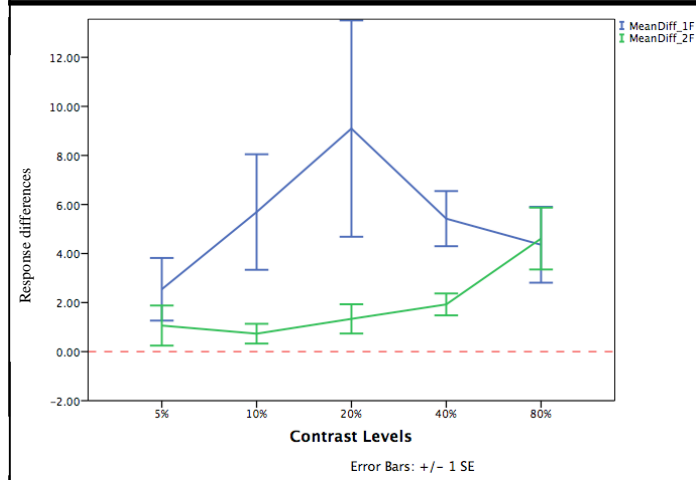
Day 10
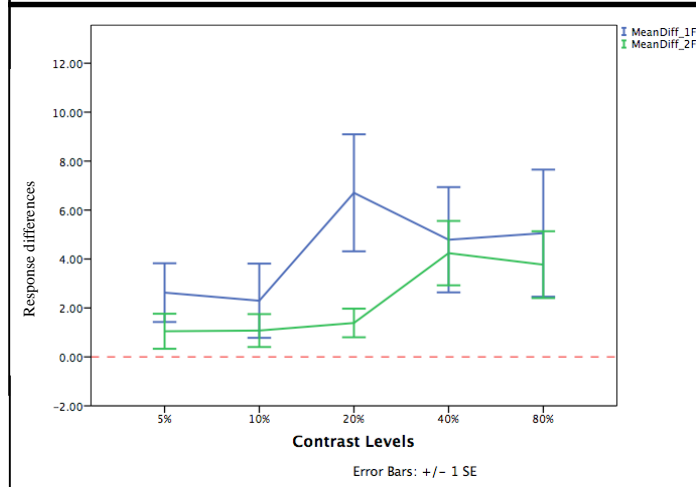
Figure 6-6: The mean differences (1FDiff and 2FDiff) as a function of contrast for *kcc^DHS1* flies aged 1, 5 and 10 days.

6.1.2.3 The mean difference (1FDiff and 2FDiff) of *kcc^{DHS1}* vs. *w-* flies

1FDiff (Fig. 6-7) and 2FDiff (Fig. 6-8) values were then compared between the genotypes (*kcc^{DHS1}* and *w-*) at day one in a bootstrapped two-way ANOVA. We found a significant effect of contrast for the 1FDiff but only a marginally significant effect of genotype. There was no interaction between the genotype and contrast levels (Table 6-3). The difference between the two genotypes appears to be large but because the small sample size of the data, ANOVA cannot detect the effect of the genotype. Removing the 80% contrast from our data for its high variance points, revealed a highly significant effect of genotypes, $p = 0.001$, particularly at the 20% contrast. More data would be needed to confirm the effect of genotype unambiguously.

For the 2FDiff, there was a significant effect of contrast. However, we again found no effect of genotype and no interaction between genotype and contrast (Table 6-3).

Source	1FDiff	2FDiff
Genotype	F= 3.8, df=1, **$p=0.056$**	F= 2.4, df=1, $p>0.05$
Contrast	F=5.4, df=4, **$p<0.01$**	F=9.4, df=4, **$p<0.001$**
Genotype * Contrast	F=1.1, df=4, $p>0.05$	F=0.6, df=4, $p>0.05$

Table 6-3: A two-way ANOVA to examine the effect of genotype and contrast levels at day 1.

We have also conducted the non-parametric Mann-Whitney test owing to our small size data. The test indicated that the 1FDiff was significantly greater for the *w-* flies (Median=1.9) than for the *kcc^{DHS1}* flies (Median=0.9), $U = 812$, $p = 0.02$. The 2FDiff, however, revealed no significant difference between the two genotypes, $U = 899$, $p = 0.09$.
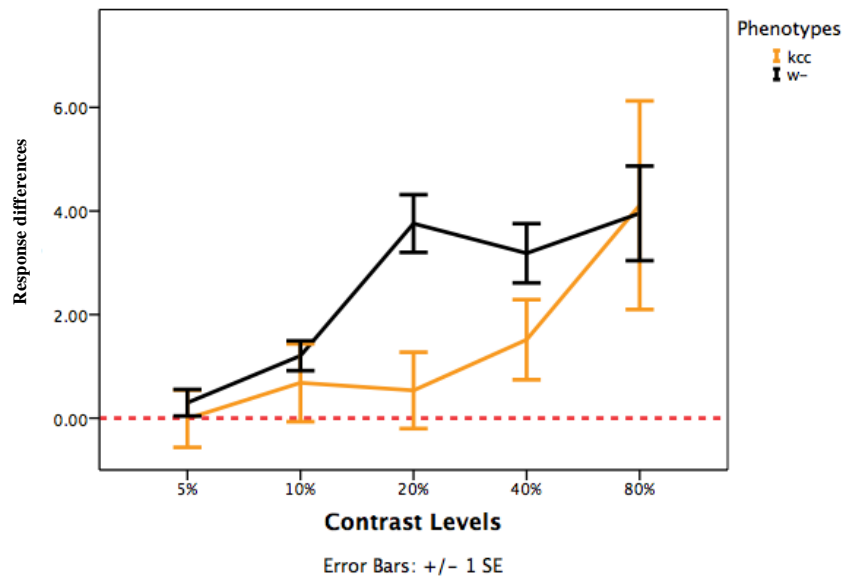
Figure 6-7: 1FDiff for *kcc*^{DHS1} and *w-* flies at day one. The w-flies show more adaptation particularly at the 20% contrast level.
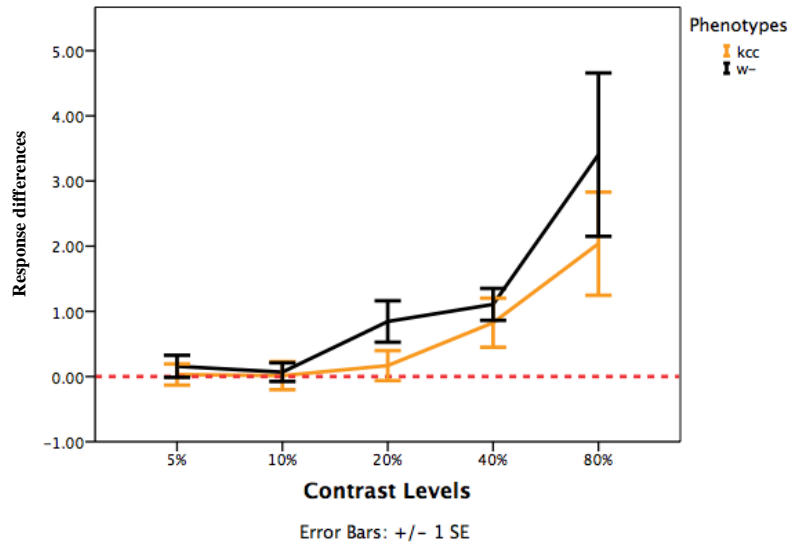
Figure 6-8: 2FDiff for *kcc*^{DHS1} and *w-* flies at day one. This shows no difference between the *kcc*^{DHS1} and *w-* flies.

A two-way ANOVA was then used to compared 1FDiff (Fig. 6-9) and 2FDiff (Fig. 6-10) between kcc^{DHS1} and w- at day 5. We found no significant difference of 1FDiff between the kcc^{DHS1} and w, no significant effect of contrast, and no significant effect of interaction between genotypes and contrast levels (Table 6-4). In addition, the 2FDiff showed a significant effect of contrast. However, the genotypes and interaction between the kcc^{DHS1} and w- and the contrast level were found to be not significant (Table 6-4).

Source	1FDiff	2FDiff
Genotype	F= 1.1, df=1, $p>0.05$	F= 2.8, df=1, $p>0.05$
Contrast	F=0.1, df=4, $p>0.05$	F=5.2, df=4, $p<0.001$
Genotype * Contrast	F=1.2, df=4, $p>0.05$	F=0.4, df=4, $p>0.05$

Table 6-4: A two-way ANOVA to examine the effect of genotype and contrast levels at day 5.

We then compared 1FDiff and 2FDiff between the two genotypes using a Mann-Whitney test. The test indicated that both the 1FDiff and 2FDiff were not significantly different between the two genotypes ($U =700$, $p >0.05$, $U =608$, $p >0.05$, respectively).

185
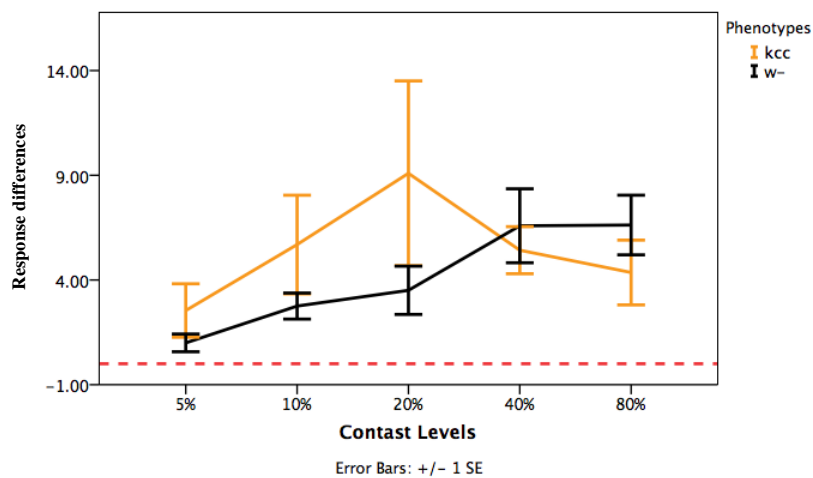
Figure 6-9: 1FDiff for *kcc^DHS1* and *w-* flies at day 5. This shows no difference between the *kcc^DHS1* and *w-* flies.
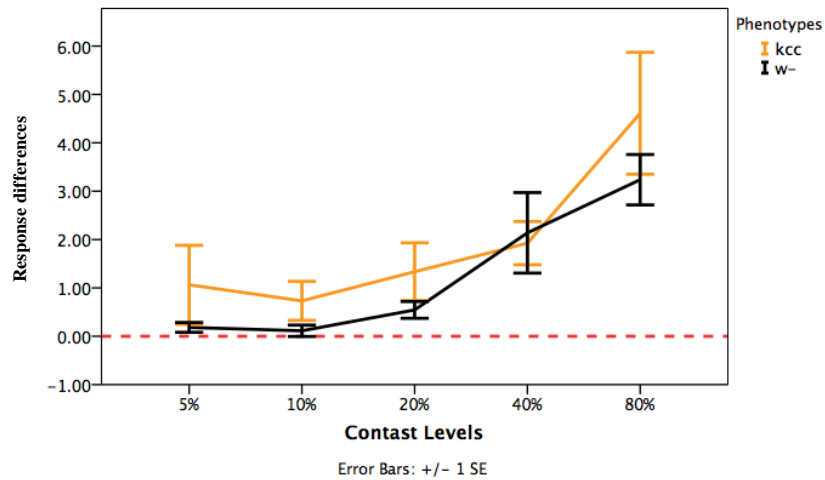
Figure 6-10: 2FDiff for *kcc^DHS1* and *w-* flies at day 5. This shows no difference between the *kcc^DHS1* and *w-* flies.

Finally, we compared 1FDiff (Fig. 6-11) and 2FDiff (Fig. 6-12) between *kcc^DHS1* and *w-* at day 10. We found no significant effect of genotype in 1FDiff. However, the contrast and interaction showed significant effects (Table 6-5). The *w-* and *kcc^DHS1* flies did not show any significant difference at any of the contrast levels. Moreover, changes in contrast levels showed no increased in adaptation. For the 2FDiff, we found a significant effect of contrast, and, again, no significant effect of genotype and no interaction effects (Table 6-5). The *w-* and *kcc^DHS1* flies did not show any significant difference at any of the contrast levels.

186

Source	1FDiff	2FDiff
Genotype	F= 1.9, df=1, $p>0.05$	F= 1.9, df=1, $p>0.05$
Contrast	F=3.2, df=4, ***$p<0.05$***	F=6.1, df=4, ***$p<0.001$***
Genotype * Contrast	F=3.1, df=4, $p>0.05$	F=0.6, df=4, $p>0.05$

Table 6-5: A two-way ANOVA to examine the effect of genotype and contrast levels at day 10.

The Mann-Whitney test indicated that the 1FDiff was significantly greater for the *w-* flies (Median= 4.9) than for the kcc^{DHS1} flies (Median= 1.8), $U=1285, p=0.03$. The 2FDiff, however, revealed no significant difference between the two genotypes, $U=1486, p=0.28$.
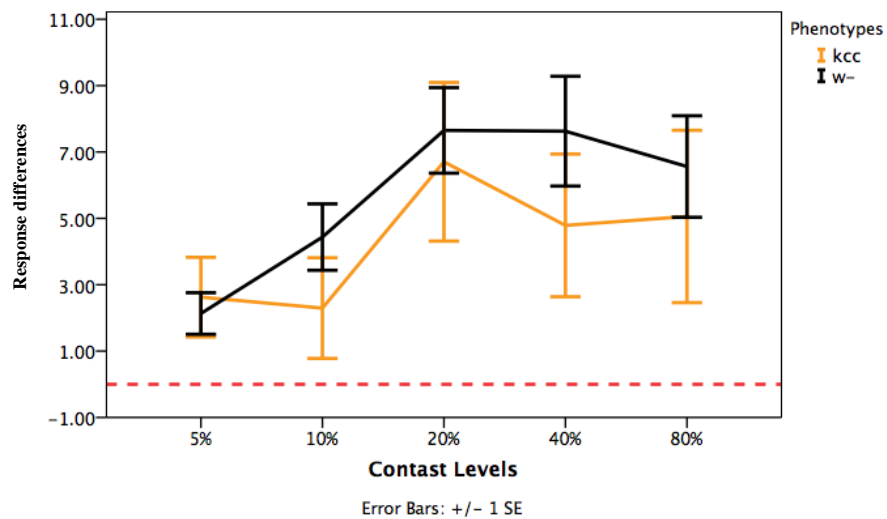
Figure 6-11: 1FDiff for kcc^{DHS1} and *w-* flies at day 10. The w- flies show more adaptation than the kcc^{DHS1} flies.

187
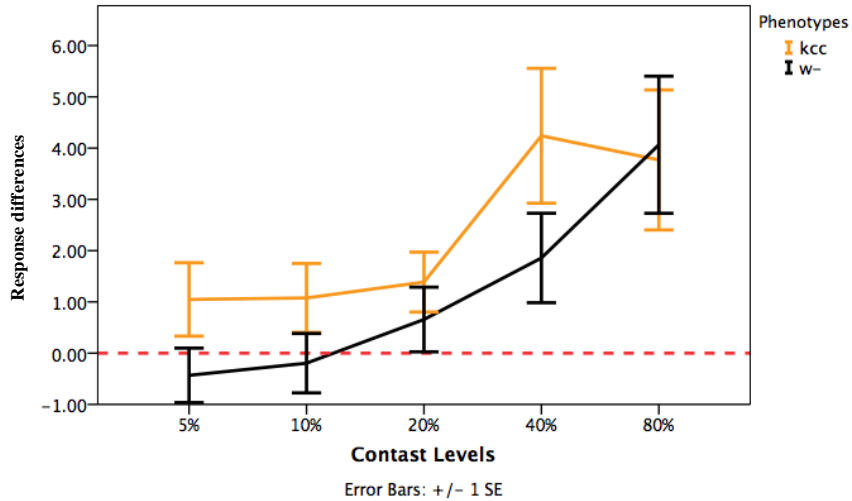
Figure 6-12: 2FDiff for kcc^{DHS1} and *w-* flies at day 10. This shows no difference between the kcc^{DHS1} and *w-* flies.

6.1.2.4   Modeling contrast response function

Most studies (Albrecht et al., 1984; Sclar et al., 1990) that characterized CRFs used the hyperbolic ratio equation of Naka and Rushton (1966):

$$R = R_{max} \frac{C^n}{C^n + C_{50}^n},$$

This equation provides values for 4 parameters; R_{max}, C_{50} and the exponent n (see Chapter 2). To produce a good fit for this type of neuronal data, the exponent n was restricted to a small range (1.5-2.5) (Busse et al., 2009) – a range that is commonly encountered in both human and animal electrophysiology.

Unfortunately, our results, particularly one-day old flies, are very unstable. Specifically, the responses did not saturate at high contrast levels, and therefore the R_{max} and C_{50} cannot be estimated accurately. In (Fig. 6-13), we have presented an example of our fitting for five-days old w⁻ flies. This figure demonstrated the effect of adaptation by the rightward shift in the CRF for Probe 2 and then the recovery from adaptation in Probe 3 and Probe 4.
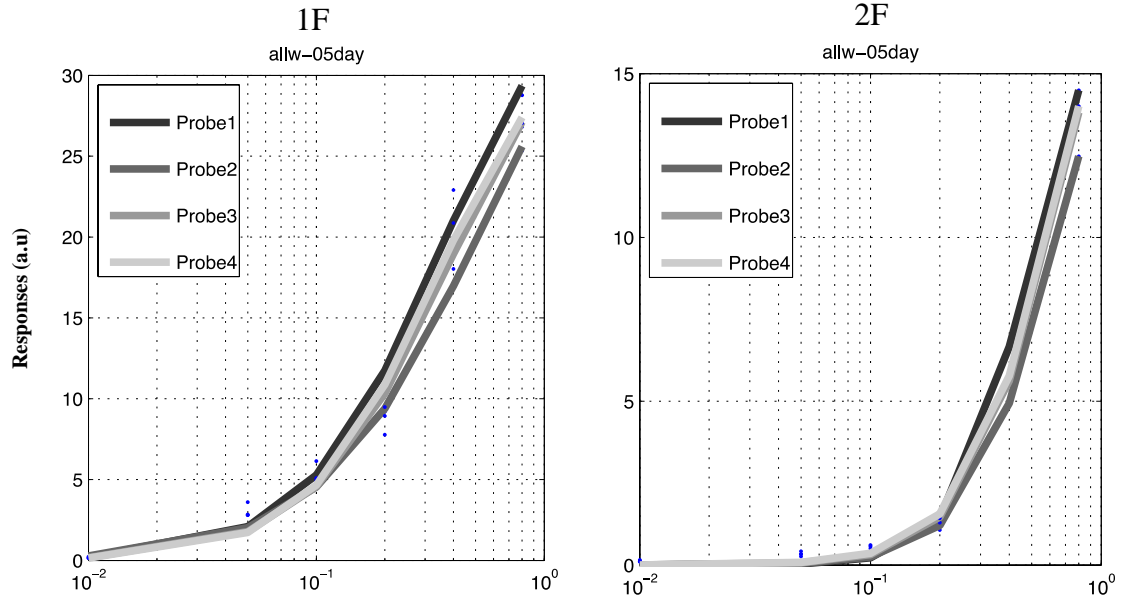
Figure 6-13: The contrast response functions were fitted with hyperbolic ratio for both 1F and 2F for _w-_ at day 5.

6.1.2.5   1F-Rmax

To determine whether there is an adaptation effect or not, we took the ratio of adaptation by dividing Probe2, Probe3 and Probe4 by Probe1 (which is indicated by the dotted red line in Fig. 6-14). Because some of our data are not normally distributed, we used the Wilcoxon signed rank test to ask whether the adapted responses (Probe2, Probe3 and Probe4) are lower than the unadapted responses (Probe1).

For kcc^{DHS1} at day 1, we found that Probe1 is not significantly different from any of the other probes (Probe2, Probe3 or Probe4), $p > 0.05$. In addition, kcc^{DHS1} at day 5 showed a sign of adaptation, with Probe2, Probe3 and Probe4 are significantly lower than Probe1, $p < 0.05$. 10-days old-kcc^{DHS1} flies showed that Probe2 is significantly lower than Probe1, $p < 0.01$, but Probe3 and Probe4 are not significantly different from Probe1, $p > 0.05$, a sign of recovery from adaptation.

189

For the *w-* flies at day 1, we found that Probe1 is not significantly different from any of the other probes (Probe2, Probe3 or Probe4), $p > 0.05$. At 5 days, we found that Probe1 is significantly lower than Probe2, $p < 0.05$, but not different from Probe3 and Probe4, $p > 0.05$. Finally, at day 10, we found that Probe2, Probe3 and Probe4 are significantly lower than Probe1, $p > 0.01$.

These findings show that young kcc^{DHS1} and *w-* flies have weak adaptation at the photoreceptor level, whereas older flies have strong adaptation. At this level, we cannot see any adaptation difference between the two genotypes.
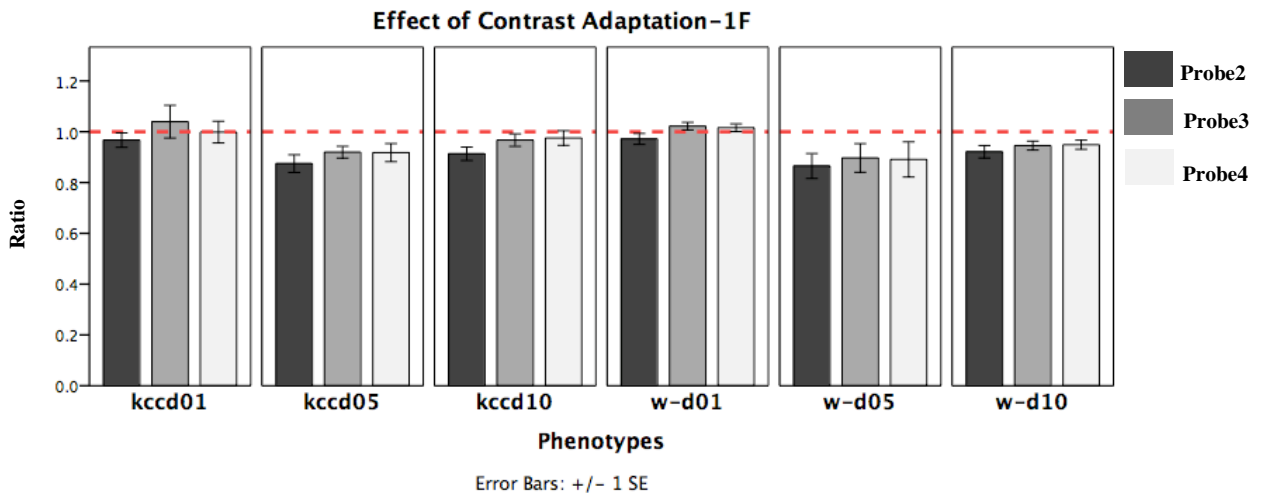
Figure 6-14: The effect of adaptation on the *w-* and k*cc^{DHS1}* flies aged 1, 5 and 10 days at the photoreceptor level.

6.1.2.6   2F-Rmax

We analyzed the maximum neural responses (2F-Rmax) (Fig. 6-15) in the same way we did for the maximum photoreceptor responses (1F-Rmax). For day-one-kcc^{DHS1}, we found that Probe1 is not significantly different from the other probes, $p > 0.05$. For day-5-kcc^{DHS1} flies, Probe1 is significantly higher than Probe2 and Probe3, $p < 0.05$, but not significantly different from Probe4, $p > 0.05$. In addition, 10 days kcc^{DHS1} flies were found to have all the post adapted probes to be significantly lower than Probe1, $p < 0.01$.

For the *w-* flies at day 1 and 5, we found that Probe2 is significantly lower than Probe1, *p* <0.01. However, Probe3 and Probe4 are not significantly different from Probe1, p>-0.05 (a sign of recovery from adaptation). For day-10-*w-* flies, we found all post-adapted probes to be significantly lower than Probe1, *p* <0.01.

These findings show that young *kcc*^{DHS1} flies have weak adaptation at the photoreceptor level, whereas young *w-* flies have strong adaptation. The *kcc*^{DHS1} flies become more sensitive to adaptation at older age resembling the responses of the *w-* flies.
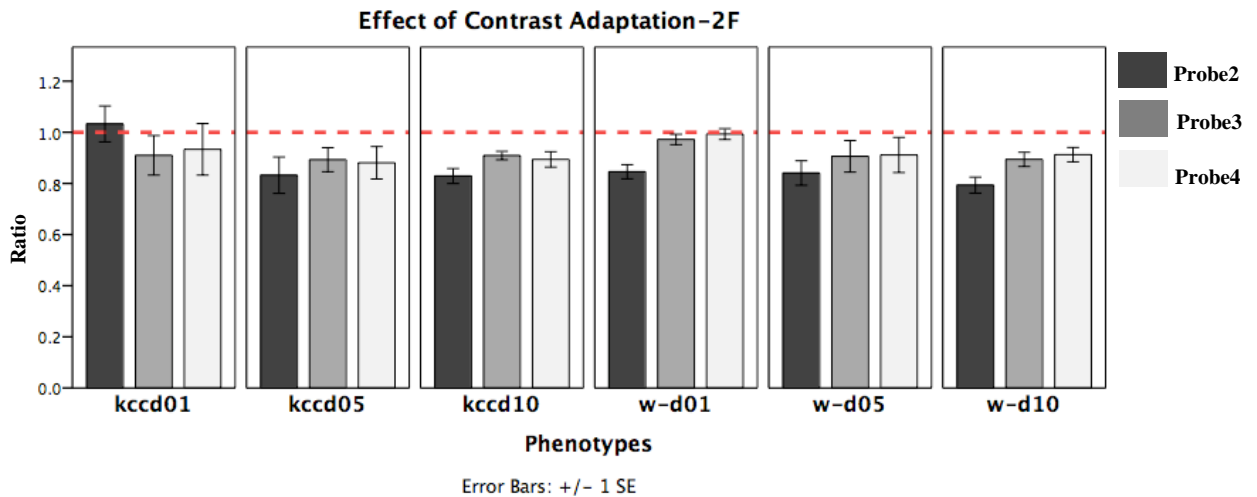
Figure 6-15: The effect of adaptation on the *w-* and kcc^{DHS1} flies aged 1, 5 and 10 days at the neural level.

6.1.3 Discussion

Using a stimulus similar to that usually used to investigate electrophysiological phenomena in humans, we found evidence that contrast adaptation, especially to high contrast stimuli, leads to decreased SSVEP responses in Drosophila at both the photoreceptor and neural levels. We found that control flies (*w-*) have significant adaptation at the photoreceptor level regardless of their age. At the neural level, unlike older flies, young *w-* flies do not seem to adapt at low contrast levels.

191

kcc^DHS flies showed an adaptation effect regardless of their age. Because age is a critical factor in the pathological effects of this genotype, as the KCC levels increase with age, and therefore the GABA effect shifts from excitatory to inhibitory (Hekmat-Scafe et al., 2006a), someone might expect to see a more severe gain control abnormalities in the young *kcc^DHS1* flies. Our finding showed that with respect to adaptation, *kcc^DHS1* and *w*-flies are not significantly different from each other, particularly at the neural level. This contradicts what we already know about the *kcc^DHS1* flies in terms of their hypersensitivity to light especially at young age (see Chapter 4). Because they are hypersensitive one might expect to see an absence of adaptation and gain control, particularly at the neural level and not the opposite.

What could explain our findings of weaker responses with partial adaptation in the one-day old animals? This experiment was the first we performed so we did not know that much about *kcc^DHS1* flies. We believe the reason the results presented in this chapter might be that the stimulus design did not take into account the extreme hypersensitivity of these flies (Chapter 4). Specifically, the design consisted of 6 contrast levels, and with each level, the 20-seconds adaptation period was presented once. Subsequently we presented probes at 20s lags after the adaptation and the cycle began again shortly afterwards. This large number of conditions and the short interval between the last probe in one series and the first probe in the next series might have resulted in early and constant adaptation in the *kcc^DHS1* animals. Probe1, which is our reference for the pre-adaptation period, may still be depressed by the effects of previous adaptation events. The adaptation effects we measure here in the *kcc^DHS1* flies are therefore likely to be 'riding' on a background of decreased activity that persists across the entire experiment. Because the contrast levels of probes were randomized in a counterbalance manner to avoid any order effects (see section 6.1.1.3), it is impossible to extract the maximum values of Probe 1 in the whole sequence. Having known about the hypersensitivity of the *kcc^DHS1* flies after finishing with the experiment, we only analyzed the data from the first run. Analyzing all data from the two runs resulted in an even lower response for the *kcc^DHS1* flies but not the *w*- flies, particularly at day 5 and 10 (Fig. 6-16 and 6-17). One-day old *kcc^DHS1* flies did not show any difference whether it is the first run only or the two runs. This suggests that at day one these flies are very sensitive to light, and even taking the first run is not enough to show the effect. To overcome this problem, we suggest that the stimulus probes should only have one high contrast level (e.g.

80%) for a short period of time, and then allow some recovery time before the second probe is applied. The decrease in responses after analyzing the two runs for day 5 and 10 flies suggests that these flies are still hypersensitive to light but much that this effect is less severe than at day 1.

In general, it may be that measuring adaptation in kcc^{DHS1} flies is difficult because of their hypersensitivity, the potential for light-triggered seizures and subsequent 'refractory' period in visual sensitivity. Other methods for measuring gain control in these animals might involve simultaneous masking using relatively low-contrast stimuli – masking was clearly present in kcc^{DHS1} flies in these experiments (see Chapter 4) but again, the magnitude was hard to assess because of the repetitive nature of the stimulus. A stimulus with long 'recovery' periods might be required to make these measurements more reliable.
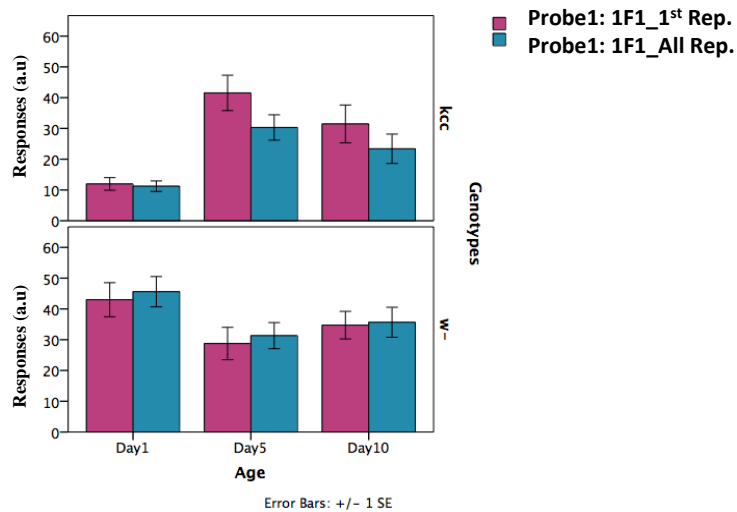
Figure 6-16: The difference between the first run and the mean of the two runs of the stimulus at the 1F1 level. The kcc^{DHS1} flies at day 1 have similar responses during the first repetition and all repetitions. At day 5 and 10, all repetitions showed lower responses compared to the responses during the first repetition only. The w- flies show no difference in responses between the two conditions across all ages.

193
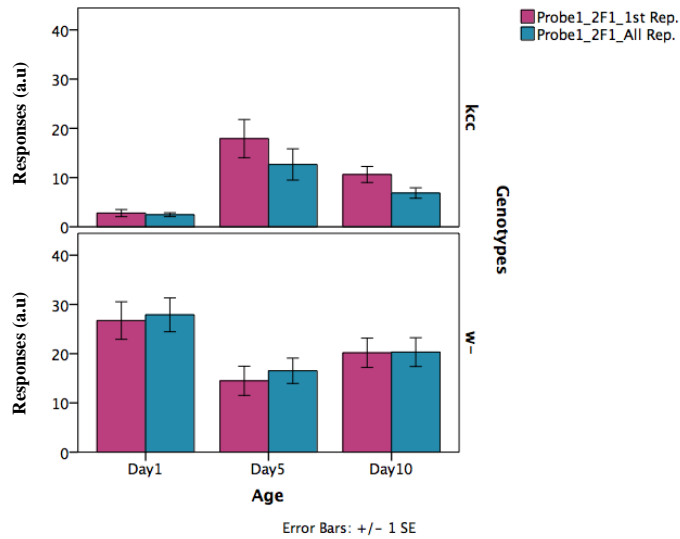
Figure 6-17: The difference between the first run and the mean of the two runs of the stimulus at the 2F1 level. The *kcc^DHS1* flies at day 1 have similar responses during the first repetition and all repetitions. At day 5 and 10, all repetitions showed lower responses compared to the responses during the first repetition only. The *w-* flies show no difference in responses between the two conditions across all ages.

6.2 Does contrast adaptation depend on GABAergic activity?

The importance of using Drosophila in this thesis is that it allows us to understand how different classes of neurons contribute to the function of the nervous system. GABAergic neurons, which are primarily responsible for synaptic inhibition, can be disrupted to investigate their role in adaptation.

It is been known for decades that overexpression of genes encoding the potassium channels can suppress neuronal electrical activity (Johns et al., 1999; Jones and Ribera, 1994; Kaang et al., 1992). In addition, a mutation in the genetically engineered Drosophila Shaker K+ channel also has the same effect. This channel is known as electrical knock-out (EKO, shaker[220]) channel (White et al., 2001). On the other hand, using a combination of dominant negative transgenes for *shaker* (*Sh*) and *ether a go-go* (*eag*) potassium channel proteins, electrical knock-in (EKI), inhibits potassium currents (Duch et al., 2008; Hindle et al., 2013). Since EKI and EKO

194

constructs affect neural membrane dynamics by increasing or decreasing shaker K+ channel activity, we would expect to see a change in the GABAergic activity particularly in neurons expressing GABA receptors. Flies expressing the EKO transgene have increased K+ currents leading to reduced firing of action potentials and consequently reduced activity of neurons expressing GABA receptors. However, flies expressing the EKI transgene have reduced K+ currents leading to increased firing of action potentials and consequently increased activity in neurons expressing GABA receptors. Due to the functional interaction between the kcc^{DHS1} mutation and Rdl-GABA receptors, we speculated that GABA might have a role in contrast gain control. We therefore tried to test this using EKI and EKO flies which mimic lower- and higher-levels of GABAergic activity in neurons expressing GABA$_A$ receptor, respectively.

We expressed the EKO and EKI genes under control of the Drosophila Gal4/UAS system (Brand and Perrimon, 1993). This system consists of two parts: the Gal4 gene, which is the driver that provides tissue-specific Gal4 expression, and the upstream activating sequence (UAS), which is the responder that carries the coding sequence of the gene of interest. Mating of the UAS responder flies with flies carrying a Gal4 driver results in progeny flies that express the UAS gene in the tissue of interest. This provides a powerful tool for tracing Drosophila trans-synaptic neural pathways.

Female flies carrying the UAS-EKO or UAS-EKI were mated with male flies carrying the *Rdl*-GAL4. In this way, we ensure that EKI or EKO are expressed only in cells that also express *Rdl*: the gene encoding the RDL subunit of the Drosophila GABA receptor. *Rdl*-Gal4; UAS-EKO flies have reduced activity in neurons expressing GABA receptors, while *Rdl*-Gal4; UAS-EKI have increased activity.

6.2.1 Methods

Flies carrying Rdl-Gal4 were crossed with either UAS-EKO or UAS-EKO lines and placed in vials containing yeast-sucrose-agar fly food. Their progeny were transferred into new vials every day and were kept at 25°C on a 12 hours light on and 12 hours light off. The flies were transferred again into new vials after 7 days to prevent overlapping of generations.

6.2.2 Results

6.2.2.1   *Rdl-EKO* vs. *Rdl-EKI*

To examine the role of GABAergic activity for neurons expressing $GABA_A$ receptor on contrast adaptation we compared the two genotypes above. Firstly, we compared the 1FDiff and 2FDiff between the two genotypes in a two-way ANOVA. We found a significant difference of 1FDiff between the *Rdl-EKO* and *Rdl-EKI,* a significant effect of contrast, but no effect of interaction between genotypes and contrast levels (Table 6-6). Briefly, we found no difference between the two genotypes at any of the contrast levels (Fig. 6-18 and 6-19).

Similarly, for the 2FDiff we found a significant effect of contrast, but no significant difference of genotype and no effect of interaction between genotypes and contrast levels (Table 6-6). Similar to 1FDiff, we found no significant difference between the two genotypes at any of the contrast levels (Fig. 18 and 20).

Source	1FDiff	2FDiff
Genotype	F= 4.4, df=1, ***p*<0.05**	F= 1.1, df=1, *p*>0.05
Contrast	F=18.8, df=4, ***p*<0.05**	F=17.2, df=4, ***p*<0.001**
Genotype * Contrast	F=0.2, df=4, *p*>0.05	F=0.3, df=4, *p*>0.05

Table 6-6: A two-way ANOVA to examine the effect of age and contrast levels on the *Rdl-EKO* and *Rdl-EKI* flies.
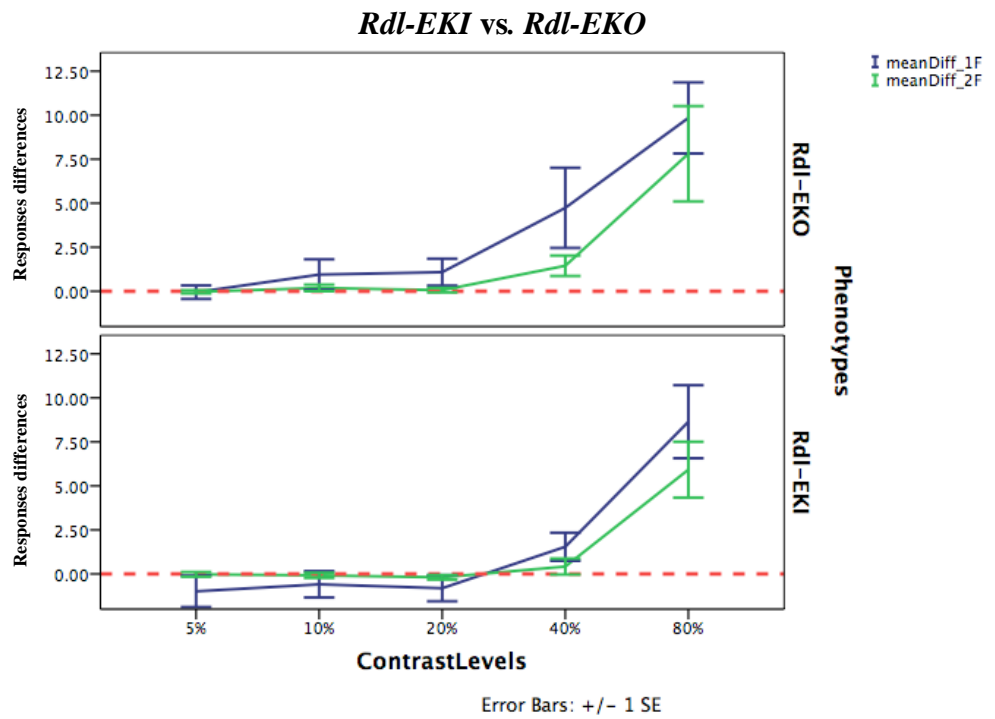
Figure 6-18: The mean differences (1FDiff and 2FDiff) as a function of contrast for _Rdl-EKI_ and _Rdl-EKO_ flies aged 5 days.
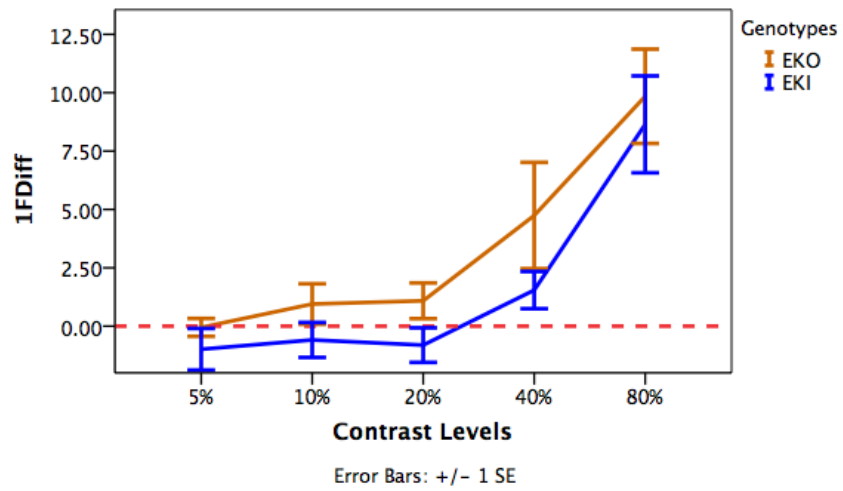
Figure 6-19: The mean differences (1FDiff) as a function of contrast for _Rdl-EKI_ and _Rdl-EKO_ flies aged 5 days.
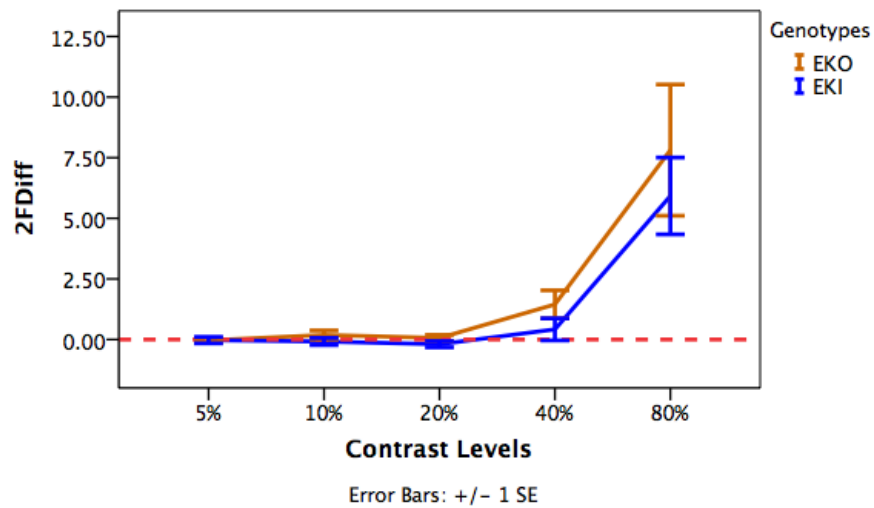
Figure 6-20: The mean differences (2FDiff) as a function of contrast for *Rdl-EKI* and *Rdl-EKO* flies aged 5 days.

Because our fits may not give good estimates of activity at high contrast levels, we extracted the maximum values from each genotype. At 1F level (Fig. 6-21), it is clear that *Rdl-EKI* flies have reduced responses compared to *Rdl-EKO*. In addition, Probe2 in both genotypes showed reduced responses compared to Probe1, a sign for adaptation. Furthermore, Probe3 and Probe4 showed an increase in the responses, a sign for a recovery from adaptation.

The maximum values for each probe of the two genotypes were examined using an independent t-test. At the photoreceptor level, 1F, (Fig. 6-21), we found no significant difference between the two genotypes for any of the probes, $p > 0.05$. To examine the percentage of adaptation in these genotypes (Fig. 6-22), we subtracted the post-adapted responses (Probe2, Probe3 and Probe4) from the pre-adapted responses (Probe1). In addition, we asked if the percentage of adaptation is significantly different in these genotypes using an independent t-test. Again, we found no significant difference between the genotypes for any of the probes, $p > 0.05$.
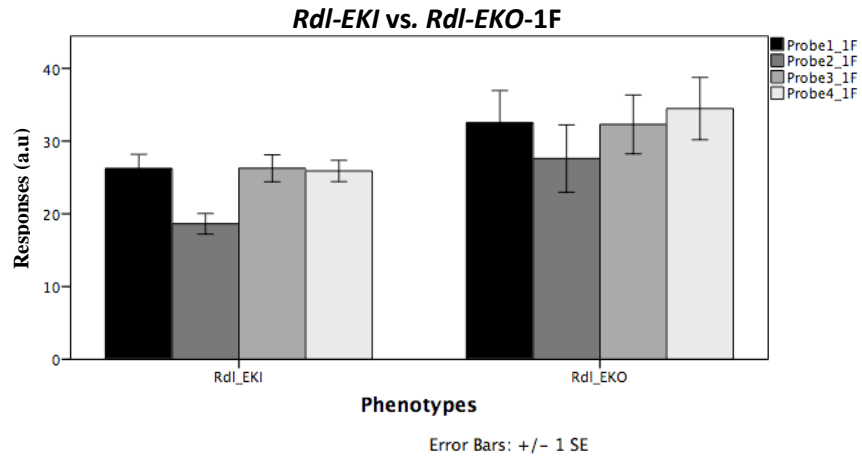
Figure 6-21: The maximum responses for all four probes at the photoreceptor level.
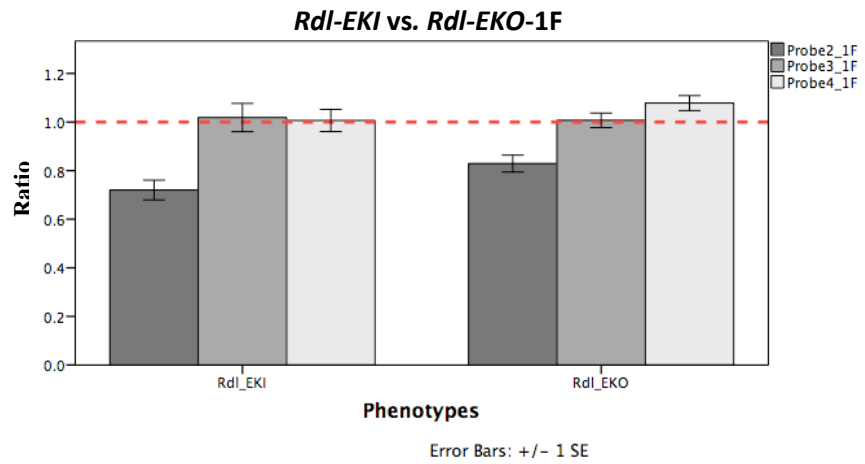
Figure 6-22: The effect of adaptation on the *Rdl-EKI* and *Rdl-EKO* flies aged 5 days at the photoreceptor level.

At 2F level (Fig. 6-23), it appears that *Rdl-EKI* flies have also reduced responses compared to *Rdl-EKO*. Similar to 1F, Probe2 showed a sign of adaptation, and Probe3 and Probe4 a recovery from adaptation.

The maximum values for each probe of the two genotypes were also examined using an independent t-test. We found no significant difference between the two genotypes for any of the probes, $p>0.05$. To examine the percentage of adaptation in these genotypes (Fig. 6-24), we also subtracted the post-adapted responses (Probe2, Probe3 and Probe4) from the pre-adapted responses (Probe1). In addition, we examined if the percentage of adaptation is significantly different in these genotypes using an independent t-test. We found no significantly difference between the genotypes for any of the probes, $p>0.05$.
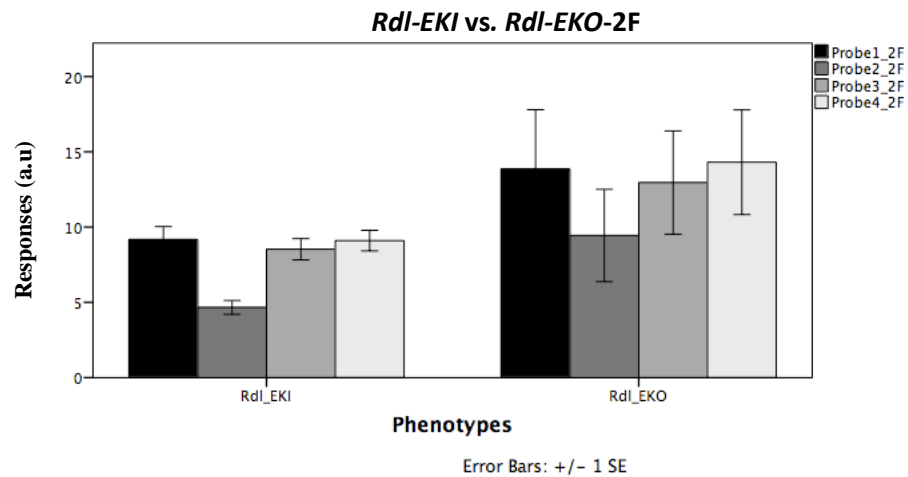
Figure 6-23: The maximum responses for all four probes at the neural level.
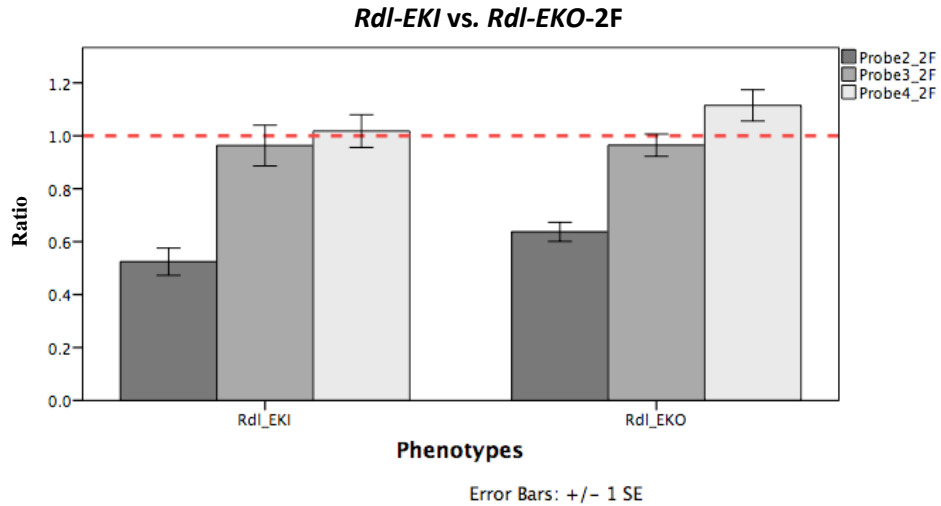
Figure 6-24: The effect of adaptation on the *Rdl-EKI* and *Rdl-EKO* flies aged 5 days at the neural level.

6.2.3 Discussion

Using *Rdl-EKI* and *Rdl-EKO* to investigate the role of neural activity expressing $GABA_A$ receptors on contrast adaptation, we found no evidence in the mean difference at the 1F or 2F levels. These findings suggest that activity in neurons expressing $GABA_A$ receptors played no role in contrast adaptation. This result is similar to previous electrophysiological studies on vertebrates (DeBruyn and Bonds, 1986; Vidyasagar, 1990) suggesting that contrast adaptation in Drosophila may be controlled by mechanisms similar to those operating in vertebrates.

We have also found no significant difference in the maximum responses when comparing the two genotypes. This is surprising as one might expect to see an increase in the overall responses in the *Rdl-EKO* flies due to the reduced inhibition in these flies. However, on inspection of (Fig. 6-21 and 6-23) does suggest a slight relative increase in responsivity in EKO flies that does not meet statistical significance. It is possible that further experiments using more flies will expose a real effect of GABA activity in the Drosophila visual system and other adaptation mechanisms might also be at play since we have not identified them in this $GABA_A$ experiment. Moreover, our experiment was investigating the effect of only one subunit, RDL,

201

of GABA$_A$ receptor. Other subunits such as GRD and LCCH3 (see Chapter 1 for more details) might compensate for the increase or the decrease in the activity of RDL subunit.

The most important limitation lies in the fact that we manipulated the activity of the RDL subunit of GABA$_A$ receptor. Because this can be GABAergic and/or glutamergic, GABA activity may have not been affected. An alternative technique would be to manipulate the GABA biosynthetic enzyme glutamic acid decarboxylase via the Gad1^{L352F} null mutation (Hekmat-Scafe et al., 2006).

6.3 Conclusion

To conclude, this chapter provides evidence that both the wild-type *w-* flies and the *kcc^{DHS1}* flies have strong contrast adaptation at both the photoreceptor and neural levels. Adaptation seems to be higher in the w- flies for young and old flies at the photoreceptor level but not at the neural level. Investigating the role of GABA receptors, particularly the RDL subunit, on contrast adaptation suggested that another mechanism might be responsible of this phenomenon. In line with the previous chapters, the present dataset highlights that the *kcc^{DHS1}* flies are hypersensitive to light and therefore a special care should be taken into account when designing visual stimuli.

7 Chapter 7: The interaction between contrast adaptation and attention in humans

7.1 Introduction

Studying visual abnormalities in Drosophila can reveal important information but eventually we need to link any visual abnormalities observed in animal models to humans. If we wish to use contrast gain control to examine neurological disease in humans, we must be able to both measure CRFs in humans and also measure subtle changes in those CRFs due to some manipulation or external influence. Here, we attempted to measure subtle changes in gain control in humans due to the effect of both adaptation and attention. This is a manipulation that links to our work on adaptation in Drosophila in the previous chapters but which also extends the use of gain control measurements to a domain (attention), which is difficult to address in invertebrates.

Several influential studies using fMRI have demonstrated that the amplitude of the BOLD signal can be influenced by contrast (G. M. Boynton et al., 1996), chromaticity (Engel et al., 1997), temporal frequency (Liu and Wandell, 2005) attention (Boynton, 2009; Buracas and Boynton, 2007; Gouws et al., 2014; Li et al., 2008) and contrast adaptation (Gardner et al., 2005).

Adaptation and attention are two mechanisms that enhance visual performance. Adaptation enhances visual performance by normalizing neuronal operating ranges to the mean of the environment. This tends to recentre the steepest part of the neurons' response curves around the mean, providing the greatest sensitivity at this point. This, in turn, allows neurons to encode contrasts that are relevant to the scene being viewed efficiently. This adaptation effect has been reported in many electrophysiological studies in e.g. cats (Bonds, 1991; Ohzawa et al., 1982) and monkeys (Carandini et al., 1997; Sclar et al., 1989), as well as in human fMRI work (Engel and Furmanski, 2001; Gardner et al., 2005).

Attention enhances visual performance by increasing neural activity to attended stimuli while decreasing them to unattended stimuli. The neuronal mechanisms of attentional modulation is still unclear with some reporting changes in response gain (Kim et al., 2007; Lee and Maunsell,

2010), while others reported that attention only enhances the intermediate contrast stimuli in a manner consistent with a contrast gain mechanism (Martínez-Trujillo and Treue, 2002; Reynolds et al., 2000b). Some studies suggested that a combination of different gain modulations may occur as a result of attention (Buracas and Boynton, 2007; Lauritzen et al., 2010; Pestilli et al., 2011). A recent, influential theory of attentional modulation suggests that it is, fundamentally, an early contrast gain control mechanism and that some of the confusion in the field is due to the relationship between attentional field size and stimulus size. Attention to a large field can modulate both the stimulus and surrounding gain pool and the joint effect can lead to changes in contrast response functions that vary smoothly between response- and contrast-gain control (Reynolds and Heeger, 2009) – see Fig. 7-1.

Investigating the relationship between adaptation and attention is a continuing concern within the field. Recently, investigators have examined this effect (Anton-Erxleben et al., 2013; Ling and Carrasco, 2006; Pestilli et al., 2007). One strong hypothesis from the work of Reynolds and Heeger is that if attention acts early, then it should interact with adaptation in the cortex. In other words, attended regions should appear to have higher contrast and should generate more adaptation.

Although extensive research has been carried out on this relationship, no single study exists which adequately cover the effect of attention on contrast adaptation using the fMRI technique, and whether the normalization model of attention (Fig. 7-1) would correctly predict it. In this chapter, we attempted to understand how attention and adaptation interact by using a similar approach to that of Gardner and his colleagues (2005), with attention as an additional measure.
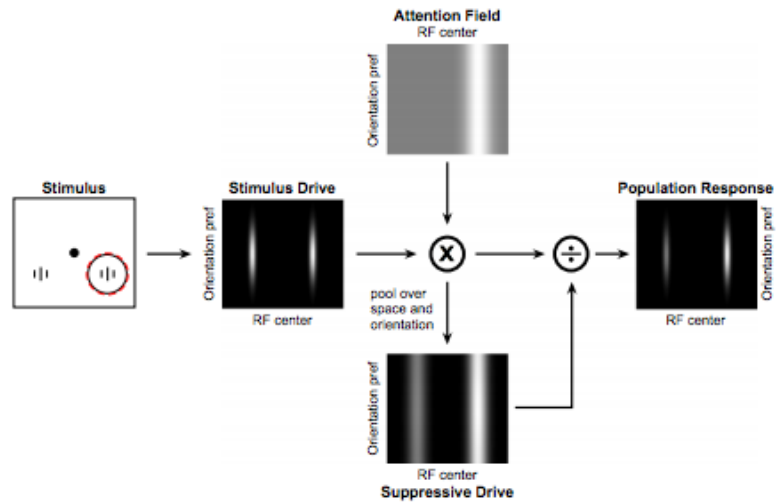
Figure 7-1: The normalization model of attention. The stimulus drive, which represent the stimulation to the field alone, is multiplied by the attention field, indicated by the dashed red circle, and divided by the suppressive field, which pools over a wide range of spatial locations and features than the stimulation field. The population response shows that the response to the attended stimulus is greater than the unattended one, adopted from (Reynolds and Heeger, 2009). Note that the attention field acts early in the processing hierarchy – at a point that could, potentially, be before primary visual cortex.

Based on work by Gardner and his colleagues, we hypothesized that adaptation modulates neural sensitivity to the steepest part of the response curve towards the adapting contrast. We then asked whether attending to an adaptor would alter the magnitude of this shift. Our overall hypothesis was that the contrast response functions in the adapted, attended region would shift towards a higher level that those in the adapted but unattended region.

We measured BOLD contrast response functions for a 22% adaptation contrast using an event-related stimulus paradigm (Fig. 7-2). Then we tested contrast responses at different contrast levels (0%, 5%, 22%, 30% and 80%). The stimulus was split into four quadrants, avoiding the fovea and vertical and horizontal meridian to help with the retinotopic mapping

since the boundaries of cortical visual areas tend to lie along these meridians. We adapted locations in two quadrants of the visual field and instructed the participants to perform a task in only one of those quadrants during the adaptation period. The other two 'unadapted' quadrants were the control locations in our experiment. We assumed that attention would enhance the adaptation effect and therefore the probe contrast of 22% would move to the right for the attended region compared to the adapted-only region (Rezec et al., 2004).

7.2 Materials and Methods

7.2.1 Participants

Ten healthy subjects (five female and five male; mean age, 35.3 years) with normal or corrected-to-normal vision participated in the study after giving informed consent. The study approved by the York Neuroimaging Centre Research Governance Committee (Department of Psychology, University of York).

7.2.2 Visual stimuli

All stimuli were generated using Psykinematix and were rear-projected (Dukane Image Pro 8942 LCD projector) onto an acrylic screen in the bore of the MRI scanner. Lying supine, subjects viewed the stimuli via a front-silvered mirror placed above the head coil.

7.2.2.1   Localizer and inplane scans

Before the functional data were collected we acquired anatomical 'localizers' to help us prescribe the functional planes and a set of T1-weighted 'inplanes' in the same location as the functional data to assist with subsequent anatomical alignment and processing.

7.2.2.2   Experimental scan

The stimuli were presented in the configuration shown in (Fig. 7-2). Stimuli consisted of sinusoidal gratings (spatial frequency=2 cycles per degree, frequency=6 Hz and radius, 2º). Briefly, the stimuli began with an initial adaptation period for 30 seconds. This initial adaptation was only presented at the beginning of each scan. The adaptors were presented in the top right and bottom left of the screen. During this period, the participants were instructed to fixate at the

center of the screen. While fixating, the participants were instructed to maintain fixation in the center of the screen but to perform a demanding contrast modulation detection task in the upper right quadrant (shown by the arrow in Fig. 7-2). In this region, the adaptor changed at random between 24% and 20% (the mean adaptation contrast is 22%), and subjects had to click a mouse button to indicate this change. Psychophysical tests outside the scanner indicated that subjects performed at 75% on this task. During all adaptation periods therefore, subjects adapted to two stimuli: upper right and bottom left but attended to only one (upper right).

Following the initial 30 seconds adaptation period, the participants were presented with a blank screen for 6 seconds. After that, probe stimuli at one of five contrast levels (0%, 5%, 22%, 30% and 80%) were presented at the four positions (top right, top left, bottom right and bottom left). The participants were instructed to maintain central fixation without attending to any of the probes. Then, another blank screen was presented for four seconds. Finally, a top-up adaptation period identical to the initial adaptation was presented for 10 seconds. The block was repeated for 10 times so that each probe contrast level was presented twice. Prior to scanning, each participant was trained on the task.

Initial adaptation
(30 s)

Blank
(6 s)

Probe
(4 s)

Blank
(4 s)

Top-up adaptation
(10 s)

UU

AA

AU

UU
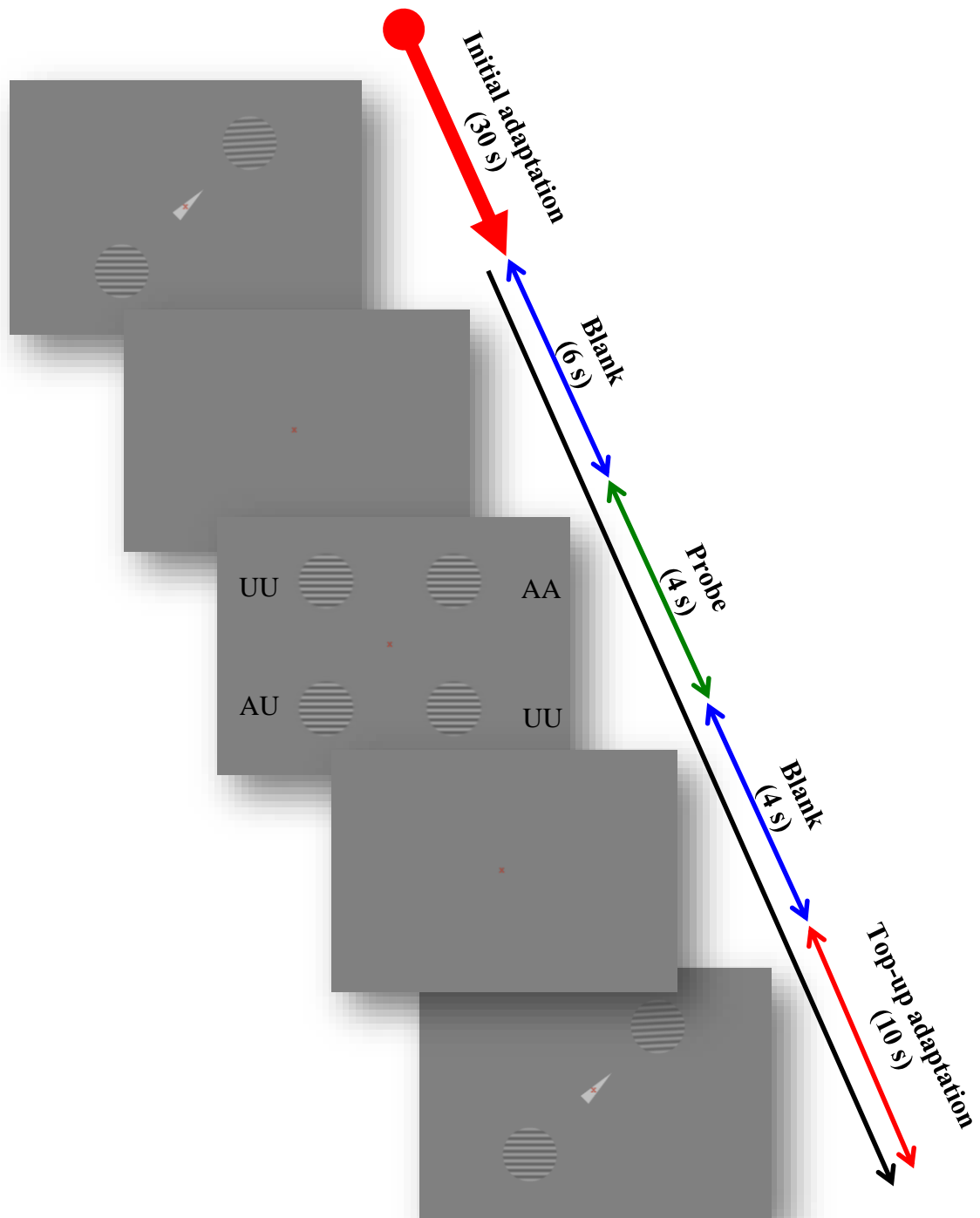
Figure 7-2: fMRI experimental stimulus. The experiment starts with a 30-seconds initial adaptation period, followed by blank screen for 6 seconds. The probes then were presented for 4 seconds at one of five contrast levels (0%, 5%, 22%, 30% and 80%) at the four positions (top right, top left, bottom right and bottom left). This is followed by another blank screen before the top-up adaptation period begins for 10 seconds. The entire block was repeated 10 times so that each probe contrast level was presented twice within each scan. Abbreviations: (UU= Unadapted Unattended region), (AU= Adapted-Unattended region) and (AA= Adapted-Attended region). Multiple scans were collected on each subject.

7.2.3 fMRI protocol

Functional and anatomical data were acquired using a 3 Tesla MRI scanner (GE Signa Excite) using a 16-channel phased-array head coil at the York Neuroimaging Centre. To minimize head movement during acquisition, a careful head fixation (conventional restraining straps, CRS) was used when positioning each participant's head.

Anatomical data: T1-weighted sagittal images (TR= 7.8 ms; TE= 3 ms; Flip angle= 20°; Matrix size=256 x 256, Slices; Slice thickness= 1 mm, Voxel size= 1 x 1 x 1 mm) were acquired to provide a high-resolution, whole-brain anatomical images and a reference to which all other functional and anatomical volumes were aligned.

Functional data: gradient echo EPI sequences were used to measure T2* BOLD data (TR= 3000 ms, TE=30 ms, flip angle= 90°; 128 x 128 matrix size; 32 contiguous slices with 2 mm slice thickness and voxel size = 1.5x 1.5 x 2 mm). The slice orientation was coronal (perpendicular to the calcarine sulcus) to cover the occipital lobes. 97 image volumes ('TRs') per time series were acquired, plus five dummies to allow magnetization to reach steady state (see Chapter 3). The localizer parameters were identical to the adaptation experiment except that we only collected 64 image volumes per time series. Proton density weighted scans were acquired at the start of each session for each subject at the same slice orientation used to acquire

the functional data (TR= 2520; TE=35; Flip angle=90; Matrix size=512 x 512; Slice thickness= 2 mm, Voxel size= 0.375 x 0.375 x 2 mm).

7.2.4 fMRI data analysis

We analyzed the data in Matlab using mrVISTA fMRI software package (see Chapter 3). Functional data were corrected for both motion and spatial inhomogeneity. To allow the functional data to be visualized on the inflated cortical areas, the EPI images were initially aligned to high-resolution T1-weighted images manually and refined with automated procedures afterwards. A general linear model (GLM) was used for data analysis to determine which areas of cortex were differentially active during each condition and to extract beta weights for each condition and voxel. Statistical threshold at p <0.001 was used for statistical maps. Beta weights for the 0% contrast value were subtracted from all other weights to provide a baseline measure.

7.3 Results

7.3.1 Retinotopic maps

In this study we attempted to recruit participants who already have retinotopic maps. Some participants, however, did not have the retinotopic maps and consequently retinotopic mapping was carried out in a separate session or in the same session using standard procedures (see Chapter 3) (Fig. 7-3 and 7-4).
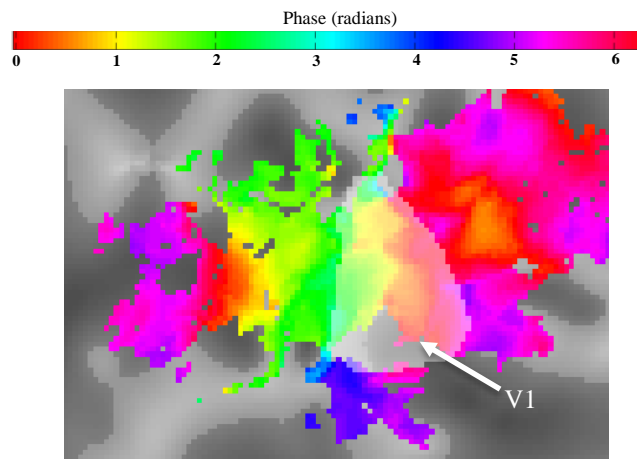
Figure 7-3: The retinotopic maps (wedges) of the right hemisphere. The primary visual cortex is drawn in white. V1 contains a full hemifield map (containing half a full stimulus cycle). The boundaries of V1 (at dorsal and ventral V2) are indicated by reversals in the polar angle phase map.
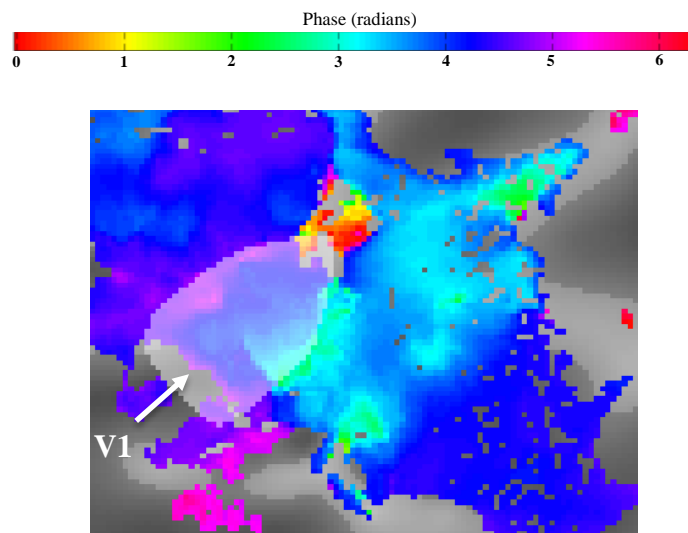
Figure 7-4: The retinotopic maps (wedges) of the left hemisphere. The primary visual cortex is drawn in white. This hemisphere contains a representation of the right visual field– again, the borders of V1 are indicated by reversals in the phase map.

7.3.2 Identifying the regions of interest (ROIs)

The ROIs used in our experiment were identified using the localizer scan described in Chapter 3. These ROIs were located in the left ventral, left dorsal, right ventral and right dorsal of the primary visual cortex (Fig. 7-5 and 7-6). Before drawing the ROIs, we made sure that the ROIs corresponded to the localizer by looking at the time series of each ROI (Fig. 7-7 and 7-8). Finally, the ROIs were visualized and inspected in the inflated surface reconstruction of the right and left hemispheres (Fig. 7-9). Ultimately, they were defined on the flattened representation of the cortex.
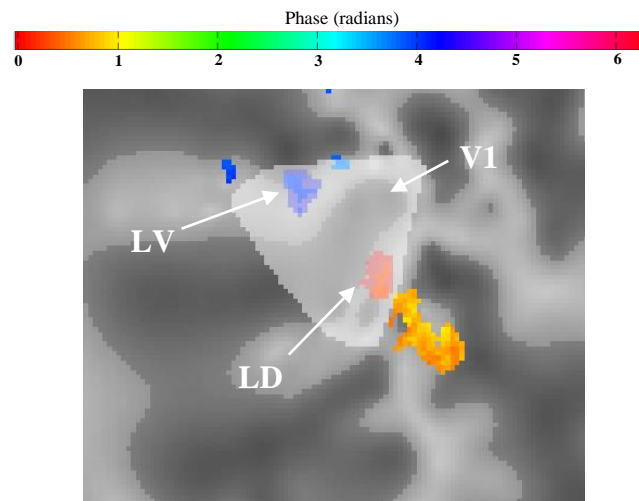
Figure 7-5: The left ventral (blue) and left dorsal (orange) are identified by the localizer scan. The primary visual cortex (V1) is drawn in white. It is clear that the localizer identified these two ROIs in V1 and additional representations of the localizer in V2 and beyond. Abbreviations: LV: left ventral, LD: left dorsal.
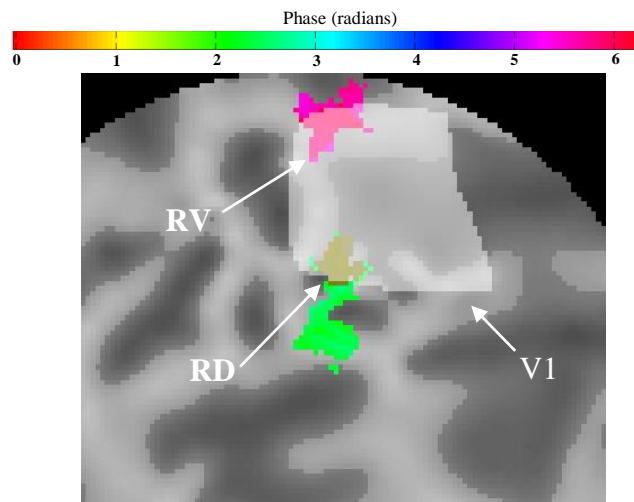
Figure 7-6: The right ventral (pink) and right dorsal (green) are identified by the localizer scan. The primary visual cortex (V1) is drawn in white. Again, it is clear that the localizer identified these two ROIs in V1. Abbreviations: LV: left ventral, LD: left dorsal.
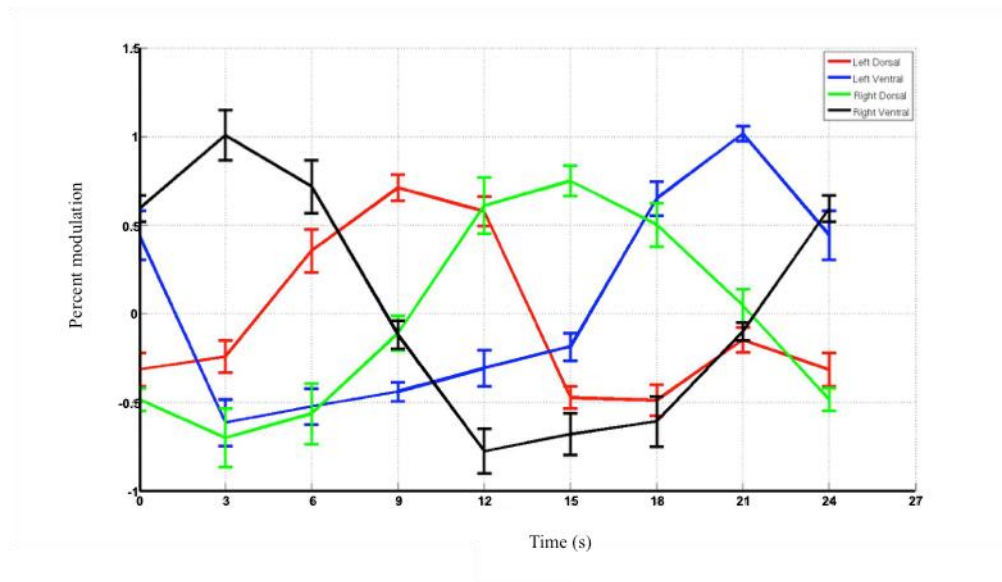
Figure 7-7: An average time series for each ROI. This was plotted for each subject to ensure that the ROIs correspond to the localizer. The first stimulus lasted for six seconds and activated the left ventral region of the brain. This was followed by a stimulus in the bottom left field of view, which activated the right dorsal region of the brain. The third stimulus was presented in the bottom left and activated the right dorsal region of the brain. The final stimulus was presented in the top right field, and activated the left ventral region of the brain. The time courses measured in the four ROIs therefore have a similar amplitude but are 6 seconds (or ¼ of a cycle) lagged from each other.
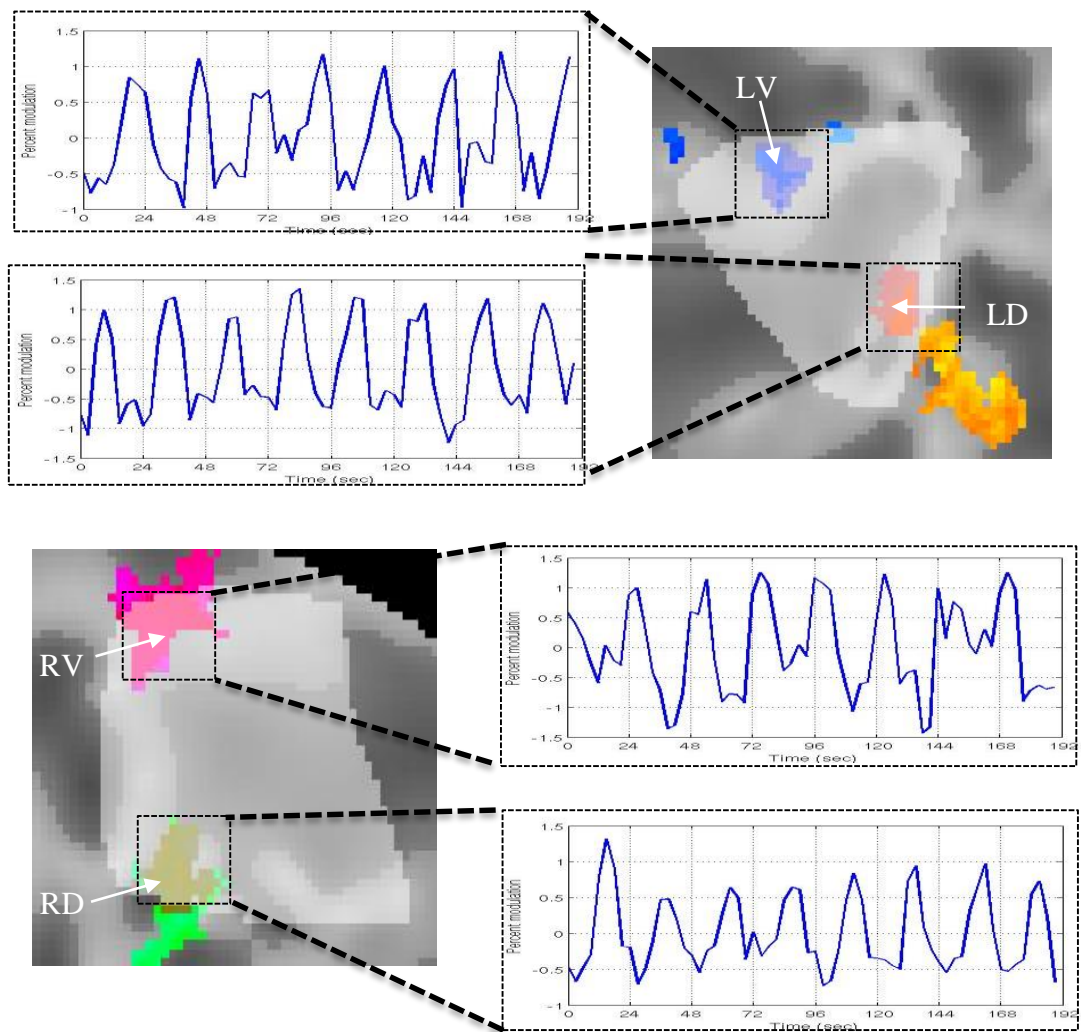
Figure 7-8: The time series for all ROIs. Each ROI has 8 cycles corresponding to 8 repetitions for the localizer. Abbreviations: LV: left ventral, LD: left dorsal, RD: right dorsal, RV: right ventral
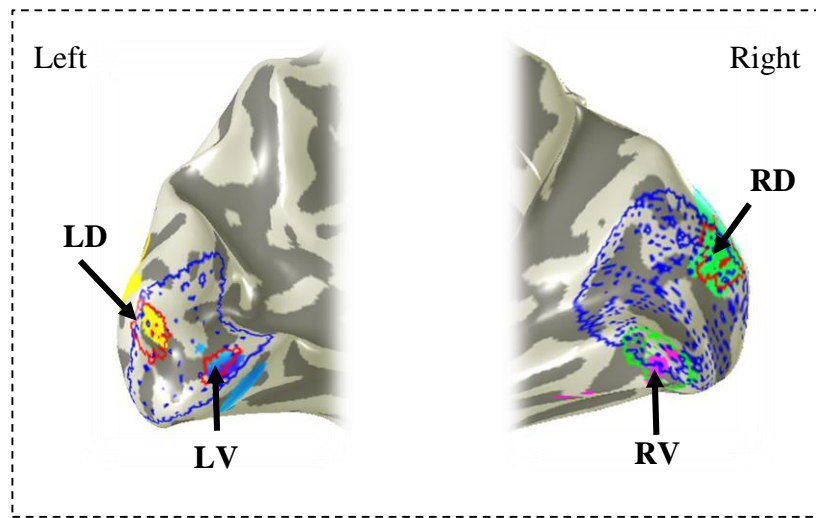
Figure 7-9: Inflated surface reconstruction of the left and right hemispheres showing the ROIs in the V1. Abbreviations: LV: left ventral, LD: left dorsal, RD: right dorsal, RV: right ventral

7.3.3 Event-related data

The aim of this study was to find the relationship between contrast adaptation and attention. The results as shown in (Fig. 7-10), indicate that the responses showed an increase with contrast. In the unadapted-unattended regions (left dorsal side and right ventral side of the brain), the responses to the probes showed similar responses. However, when we looked at the responses during the adaptation period we see that the effect of the adaptor is twice as big in the left dorsal side (which corresponds to the attentional side of the screen) compared to the right ventral side. All 10 subjects showed negative BOLD in the non-stimulated left dorsal region whereas 8 subjects showed negative BOLD in the non-stimulated right ventral region.

The adapted-attended region (left ventral side of the brain) and the adapted-unattended region (right dorsal side of the brain) showed similar responses with a tendency to have more responses in the attended region, particularly at high contrast levels as well as during the adaptation period.

We then looked at the effect of our data on the CRFs and found that the attended region (LV) showed a tendency towards contrast gain by shifting into the left side, compared to the adapted-only region (RD) (Fig. 7-11).

A two-way ANOVA was performed to look at the effect of adaptation and attention on the visual responses. There was a significant main effect of probe contrast, but no significant main effect of ROI and interaction between probe contrast and ROIs (Table 7-1). Using a post-hoc test (Bonferroni) for multiple comparisons we found no significant difference between the ROIs at any of the contrast levels, $p>0.05$.

Source	ANOVA Results
Contrast	F= 9.3, df =3, **$p<0.001$**
ROI	F= 2, df =3, $p>0.05$
Contrast x ROI	F= 0.3, df =9, $p>0.05$

Table 7-1: The results of performing a two-way ANOVA to look at the effect of adaptation and attention on the visual responses.

Finally, we compared the responses to the adaptors for all ROIs using pair-samples t-test. We found no significant difference between the stimulated regions, the adapted-attended region and the adapted-only, $p>0.05$. We also found no significant difference between the non-stimulated LD in the attended side and RV in the adapted-only side, $p>0.05$.

Error Bars: +/− 1 SE
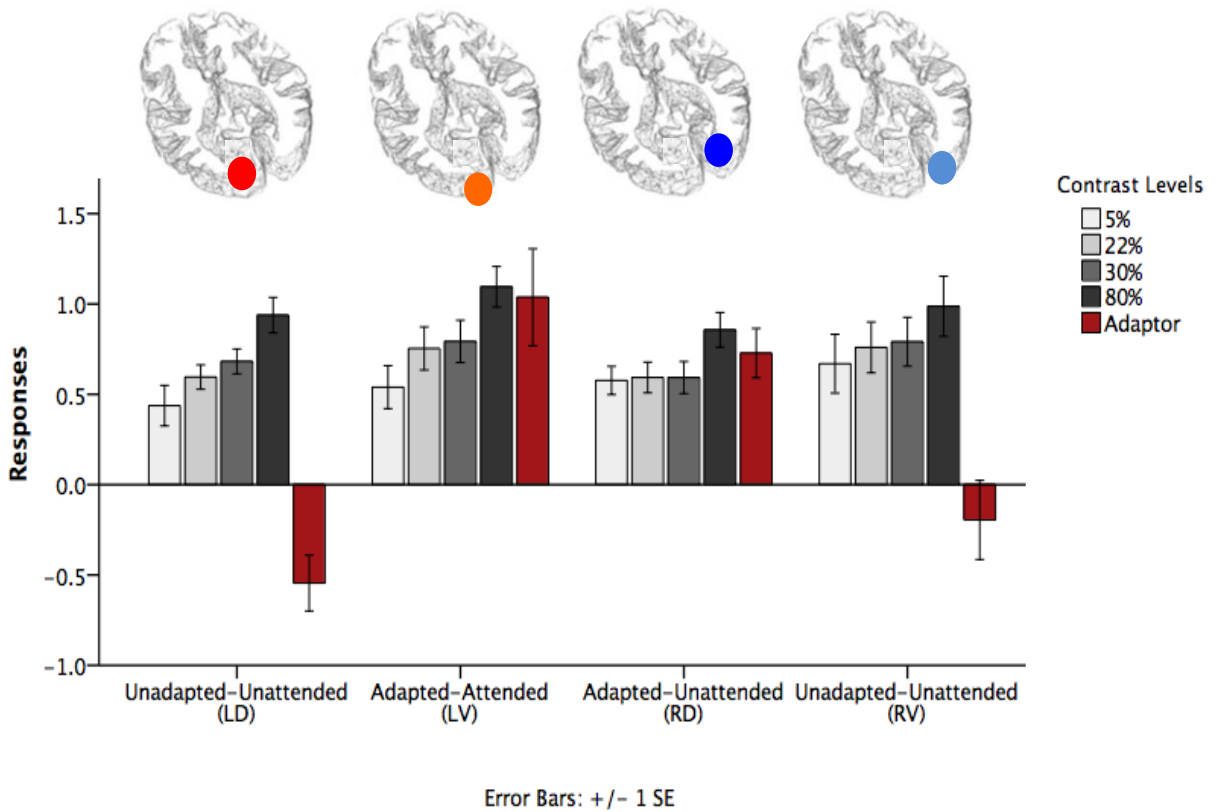
Figure 7-10: The effect of contrast adaptation on attention. The graph shows that the attention does not seem to have any effect of the contrast levels, but it tends to increase the negative BOLD on the same side (Left dorsal, LD). The circle spots indicate the ROIs positions. Red corresponds to the Left dorsal region, orange is the left ventral region, blue is the right dorsal region and light blue is the right ventral region of the brain.
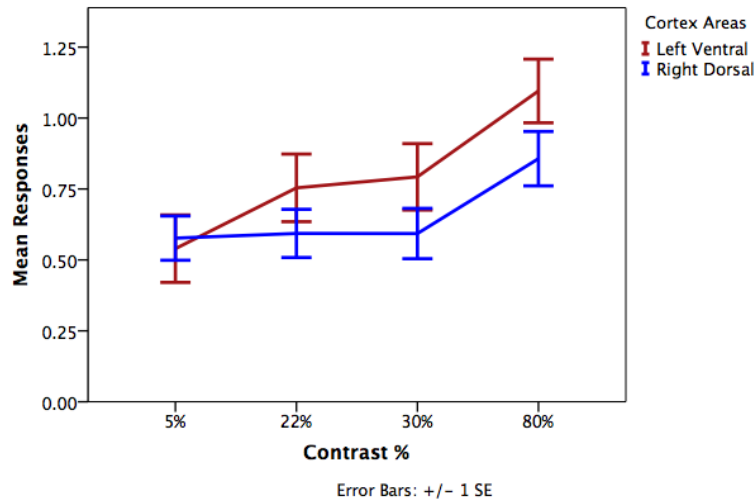
Figure 7-11: CRFs for the attended-adapted region (LV - red) and the unattended, adapted-only region (RD –blue). The attended region showed a sign of leftward shift but the effect is statistically non-significant.

7.4 Discussion

The data presented in this chapter do not support the interaction between attention and contrast adaptation that we initially hypothesized. Our data demonstrated significant effects of contrast (we measured robust contrast vs. response functions) but those functions were not altered in a consistent manner by adaptation and we found no significant interaction between adaptation and attention.

This was not because the adaptors were ineffective. The BOLD responses during the adaptor periods were highly robust. Adapted regions showed large responses during the adaptation period while unadapted regions showed strong negative BOLD responses (Gouws et al., 2014; Shmuel et al., 2006; Smith et al., 2004; Wade and Rowland, 2010). Attending to the adaptor appeared to increase the BOLD response in that location by a small but non-significant amount (and similarly increased the magnitude of the NBR by a small but insignificant amount). But this strong response during the adaptation period had no subsequent effect on the response to the probe in the same location.

It is possible that increasing the number of subjects would reveal subtle effects of adaptation or attention that were masked by noise in the current set of experiments. The number of subjects used here (10) was more than used in other, similar fMRI experiments on contrast responses in human cortex (for example, (Shmuel et al., 2006) used 9 subjects in their study, (Smith et al., 2004) used only five in their study and (Wade and Rowland, 2010) used 9 subjects) but a recent study on the interaction between attention and the NBR used as many as 20 subjects in one of the experiments (Gouws et al., 2014). To pursue this topic further would, however, require significantly more scanning resources that we used in the experiment described here.

Other groups have reported profound changes in BOLD responses caused by spatial attention (Gandhi et al., 1999; Kastner and Ungerleider, 2000; Tootell et al., 1998) but it is possible that the configuration of our stimuli worked against us in this case. Specifically, we hypothesize that the relatively small size of our probes might have caused an interaction between the classical central receptive fields in cortex and the suppressive surrounds that could have renormalized some of our response variation away.

Specifically: Classical receptive fields in visual cortex are often accompanied by 'silent' suppressive surrounds that can act to reduce responses to stimuli that activate both regions (Solomon et al., 2002; Solomon and Kohn, 2014). The adaptor stimuli that we used in our experiment were larger than the probes and may have adapted both the central CRFs and suppressive surrounds. While adaptation of the central field would be expected to lead to a reduction in the CRF response, adaptation of the surround might lead to dis-inhibition (a reduction of suppression) that might act in the opposite direction. The result might be a relative stability of the responses from the central region, or even a slight increase in their responses after adaptation similar to what we observed in the study described here. This logic is described in detail in the recent review article by Solomon and Kohn (Solomon and Kohn, 2014). To test this hypothesis, we would need to alter the relative size of the adaptor and probe regions – an experiment described in more detail in Chapter 8.

Finally, one further explanation might be that attention acts largely on inhibitory rather than excitatory mechanisms. Our data show profound effects of negative BOLD and there appears to be a trend towards increased NBR in the hemisphere that receives attention. This negative

219

BOLD has been observed in a number of studies (Gouws et al., 2014; Smith et al., 2004; Wade and Rowland, 2010) and it seems that negative BOLD responses reflect active suppression of neural activity and not just decreased local blood flow ('blood stealing') from nearby vessels. It is possible therefore, that attention might increase suppression in the non-stimulated regions rather than increasing responses in the attended region – a hypothesis that was made explicit by (Gouws et al., 2014) in their recent paper.

This can be thought of as inverting the model of attention made by Reynolds and Heeger (2009). Reynolds and Heeger proposed that attention act by increasing the response to the attended region without affecting the other regions. Gouws et al (and we) propose that attention works by suppressing the other regions without affecting the attended region. In the end, the results from both models (ours and Reynolds and Heeger) would be computationally similar: making the response to the attended regions relatively higher. In a block design study where attended and unattended conditions are interleaved, the two hypotheses would predict identical effects. Earlier studies (using block design paradigms) would therefore have observed a relatively increased response to attended stimuli but our event-related paradigm might have been unable to detect an increase because it was largely driven by suppression of the unattended region.

7.5 Conclusion

The main goal of this study was to examine the relationship between spatial attention and contrast adaptation. Even though our data did not show any significant interaction between attention and adaptation, the results presented here suggest that that negative BOLD responses observed in the non-stimulated regions may have a role in suppressing responses in spatial attention. Further studies need be carried out in order to validate this are proposed in the next chapter.

8   Conclusion

The original goal of this project was to investigate visual gain control in an animal model of disease and show how this work might be extended to humans. I chose the model organism Drosophila because of its powerful genetics and ease of application. I focused on the disease of epilepsy – specifically a mutation in the *kcc* gene that has been linked to juvenile epilepsy in humans.

In **Chapter 4**, I measured the way that visual responses in Drosophila changed with contrast and compared these to responses in wild-type animals. I also examined the possible effects of contrast masking in these models. I found that young mutant (kcc^{DHS1}) flies have increased neural activity that recovers to the normal profile as they get older. We have also found that these kcc^{DHS1} flies are hypersensitive to light, particularly when young. These two findings are consistent with the fact that the level of the KCC protein increases with age (Hekmat-Scafe et al., 2006).

As part of our preliminary measurements on kcc^{DHS1} animals we noticed that they generate high frequency oscillations in their ERGs in response to abrupt light onsets and offsets. In our standard kcc^{DHS1} animals this was a reliable biomarker of the disease gene and we hypothesized that the oscillations may result from abnormal gain control mechanisms operating within the retina: a failure of feedback that would normally dampen the response. To investigate this, in **Chapter 5**, we performed measurements of ERG responses due to spot illuminations at different distances from the electrode as well as full-field illumination. We found that spot illuminations at different distances have no apparent differences on the individual genotypes used. Full-field illumination, however, results in a drop in the responses for the wild-type flies, but has no effect on the kcc^{DHS1} flies. Using the ort$^{-/-}$ knockout mutation that inactivates the histamine A receptor and therefore prevent photoreceptors from transmitting signals to deeper structures revealed that the high frequency oscillations seen in the young kcc^{DHS1} flies are probably due to reduced lateral inhibition.

Adaptation can be considered to be another form of gain control. In **Chapter 6** we examined the effects of contrast adaptation in kcc^{DHS1} and wild-type animals while in **Chapter 7** we

attempted to translate these types of experiments to humans – while also investigating a third manifestation of gain control that is more reliable to measure in vertebrates: spatial attention. The data from **Chapter 6** showed that it was possible to measure contrast adaptation in both wild-type and kcc^{DHS1} animals: Responses after a long period of adaptation were lower than those measured before the adaptation period. Although we also saw profound differences in the overall response amplitudes in kcc^{DHS1} and wild-type animals, it is possible that these were due to refractory periods after visually evoked seizures in the kcc^{DHS1} flies.

In our human work in **Chapter 7**, we used fMRI to measure responses in four regions of primary visual cortex defined through a retinotopic mapping procedure. Each of these regions generated a contrast response function when probed with flickering grating stimuli. Although our data indicated that both attention and adaptation might influence the responses independently, statistical analysis indicated that neither of these effects reached significance. Although surprising, these results are in line with recent work from other members of our group (Gouws et al., 2014) suggesting that attention in early visual pathways largely affects the level of suppression in non-stimulated regions around the adaptor rather than responses to the probe itself.

8.1 Future work

The changes in CRFs between wild-type and kcc^{DHS1} animals are intriguing. Overall, future work should take into account the extreme sensitivity of kcc^{DHS1} animals at young ages. Reliable responses can be measured at relatively low contrast levels in wild-type animals and these low-contrast regimes are also preferable for experiments in kcc^{DHS1} animals because they are unlikely to lead to photic seizures. We anticipate that our future work will take place entirely at low contrast levels for this reason.

Perhaps the most interesting results were obtained from the single-point experiments measuring responses to stimuli at different distances from the retinal electrode. These data showed profound interactions between the stimulus type (distance from the electrode, or full-field illumination) and genotype. We would like to pursue the idea that many of these differences are driven by feedback from deeper layers and the genetic flexibility of Drosophila means that

we could selectively knock out individual classes of neurons (for example, Amacrine cells, L1 or L2) to test this hypothesis.

In terms of the contrast adaptation experiment presented in Chapter 6, we propose repeating the same experiment with slight adjustments to the stimulus design (particularly longer gaps between the probes, and perhaps a weaker adaptor. Additionally, because the fly visual system is sensitive to motion and other groups have reported relatively strong adaptation effects using motion rather than flicker stimuli (Harris et al., 2000; O'Carroll, 2001), it would be of interest to look at the differences between adaptation using drifting gratings compared to flickering low-frequency LEDs or contrast reversing patterns..

In humans, our fMRI results demonstrate that we can measure clean, spatially localized responses driven by distinct probe types (as well as negative responses associated with high-contrast probes in remote parts of the visual field) and analyse these on a per-area basis across subjects. Our paradigm could be extended in two ways: Firstly, given work by Gardner and others it should be possible to measure frank adaptation effects within V1. Our results here were weak, possibly because we chose relatively small probe sizes and adapting stimuli that were 'blurred' over visual cortex due to the limited resolution of fMRI. We could either attempt to improve the resolution of our imaging procedures (for example, by measuring at a higher field strength or for longer to gain an improved SNR) or we could increase the size of our stimuli to cover more cortex and, importantly, vary the relative sizes of adaptor and probe fields parametrically. The observations of both Solomon and Kohn (2014) and Reynolds and Heeger (2009) that the local gain pool influences the effects of both attention and adaptation has not been well-explored in fMRI and these experiments provide a paradigm that could be extended to study these effects.

With respect to attention, the work by (Gouws et al., 2014) also leads us to suspect that many of the attentional effects we are pursuing are in fact more evident in the negative responses around the stimuli-driven region – perhaps driven exclusively by the suppressive surrounds that are a feature of many neuronal receptive fields. Although our experiments did include adaptation stimuli in unattended locations, the effects of negative BOLD responses are likely to be weaker in these regions because they appear in the opposite hemisphere and visual hemifield. An

experiment that explicitly placed two larger adaptation/ probe regions closer to each other would have more chance of measuring an interaction between stimulus-driven responses, adaptation and attention (Fig. 8-1).
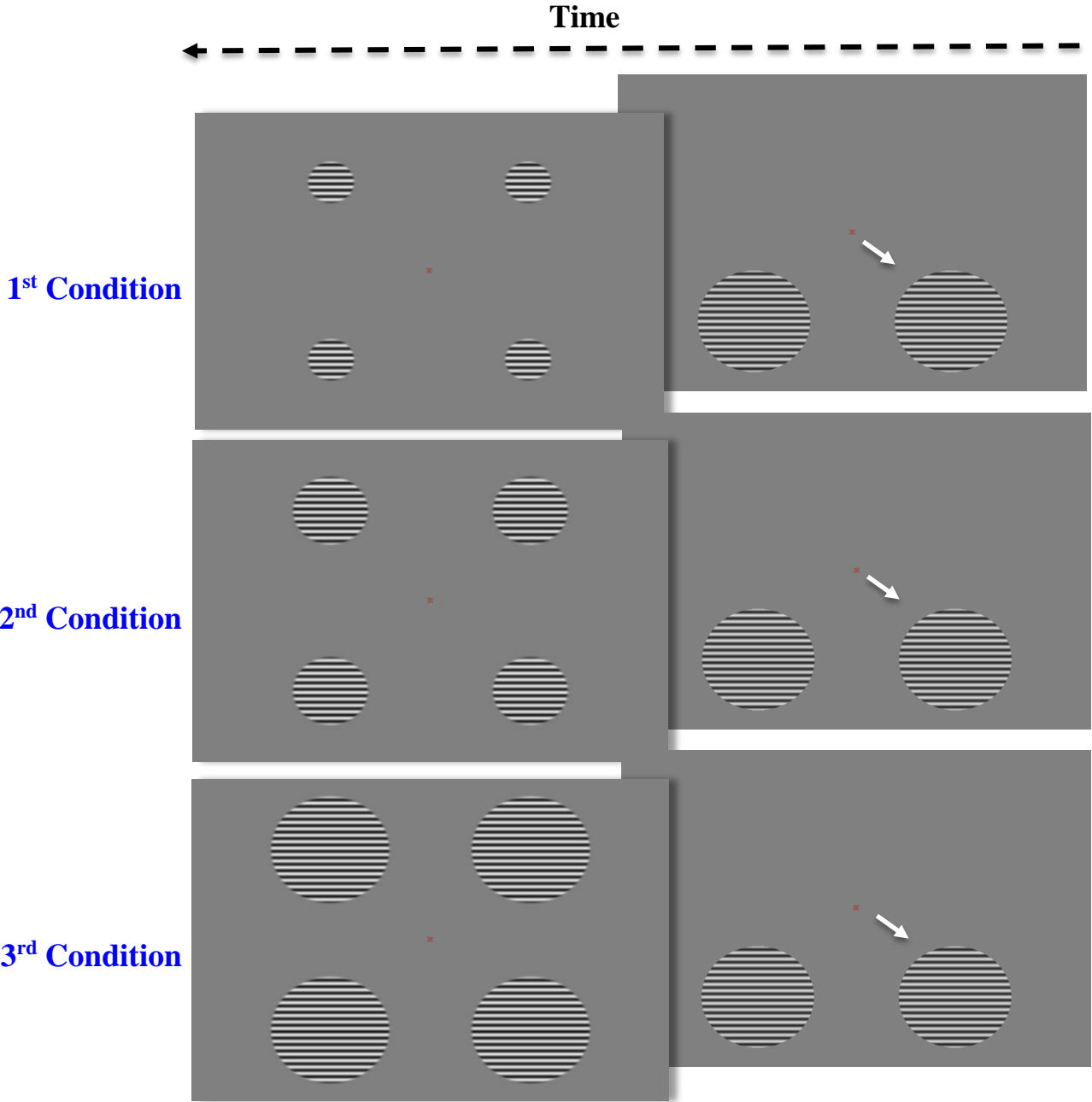
Figure 8-1: The proposed experiment to tackle the issue of surround inhibition. In the 1ˢᵗ condition, the size of the probes is very small compared to the adaptors. In the 2ⁿᵈ condition, the size of the probes is larger than that in the 1ˢᵗ condition but it is still smaller than the adaptors. In the 3ʳᵈ condition, the size of the probes is identical to that of the adaptors. The arrows in the adaptors indicate the attended region.

To conclude: The general principle we have investigated in this thesis is the way that gain control can alter visual responses in both animal models and humans. In animal models we show that changes in gain control provide insights into a common genetic model of neurological disease. In humans, we have tested a paradigm for measuring the effects of attention and adaptation across a range of contrasts and spatial positions. Because these two phenomena are both hypothesised to depend on gain control mechanisms, further work in this area might provide a sensitive measure of other neurological diseases and disorders based on subtle abnormalities in fMRI BOLD responses.

References

Abbott, L.F., Varela, J.A., Sen, K., Nelson, S.B., 1997. Synaptic depression and cortical gain control. Science 275, 220–224.

Adams, M.D., Celniker, S.E., Holt, R.A., Evans, C.A., Gocayne, J.D., Amanatides, P.G., Scherer, S.E., Li, P.W., Hoskins, R.A., Galle, R.F., George, R.A., Lewis, S.E., Richards, S., Ashburner, M., Henderson, S.N., Sutton, G.G., Wortman, J.R., Yandell, M.D., Zhang, Q., Chen, L.X., Brandon, R.C., Rogers, Y.H., Blazej, R.G., Champe, M., Pfeiffer, B.D., Wan, K.H., Doyle, C., Baxter, E.G., Helt, G., Nelson, C.R., Gabor, G.L., Abril, J.F., Agbayani, A., An, H.J., Andrews-Pfannkoch, C., Baldwin, D., Ballew, R.M., Basu, A., Baxendale, J., Bayraktaroglu, L., Beasley, E.M., Beeson, K.Y., Benos, P.V., Berman, B.P., Bhandari, D., Bolshakov, S., Borkova, D., Botchan, M.R., Bouck, J., Brokstein, P., Brottier, P., Burtis, K.C., Busam, D.A., Butler, H., Cadieu, E., Center, A., Chandra, I., Cherry, J.M., Cawley, S., Dahlke, C., Davenport, L.B., Davies, P., de Pablos, B., Delcher, A., Deng, Z., Mays, A.D., Dew, I., Dietz, S.M., Dodson, K., Doup, L.E., Downes, M., Dugan-Rocha, S., Dunkov, B.C., Dunn, P., Durbin, K.J., Evangelista, C.C., Ferraz, C., Ferriera, S., Fleischmann, W., Fosler, C., Gabrielian, A.E., Garg, N.S., Gelbart, W.M., Glasser, K., Glodek, A., Gong, F., Gorrell, J.H., Gu, Z., Guan, P., Harris, M., Harris, N.L., Harvey, D., Heiman, T.J., Hernandez, J.R., Houck, J., Hostin, D., Houston, K.A., Howland, T.J., Wei, M.H., Ibegwam, C., Jalali, M., Kalush, F., Karpen, G.H., Ke, Z., Kennison, J.A., Ketchum, K.A., Kimmel, B.E., Kodira, C.D., Kraft, C., Kravitz, S., Kulp, D., Lai, Z., Lasko, P., Lei, Y., Levitsky, A.A., Li, J., Li, Z., Liang, Y., Lin, X., Liu, X., Mattei, B., McIntosh, T.C., McLeod, M.P., McPherson, D., Merkulov, G., Milshina, N.V., Mobarry, C., Morris, J., Moshrefi, A., Mount, S.M., Moy, M., Murphy, B., Murphy, L., Muzny, D.M., Nelson, D.L., Nelson, D.R., Nelson, K.A., Nixon, K., Nusskern, D.R., Pacleb, J.M., Palazzolo, M., Pittman, G.S., Pan, S., Pollard, J., Puri, V., Reese, M.G., Reinert, K., Remington, K., Saunders, R.D., Scheeler, F., Shen, H., Shue, B.C., Sidén-Kiamos, I., Simpson, M., Skupski, M.P., Smith, T., Spier, E., Spradling, A.C., Stapleton, M., Strong, R., Sun, E., Svirskas, R., Tector, C., Turner, R., Venter, E., Wang, A.H., Wang, X., Wang, Z.Y., Wassarman, D.A., Weinstock, G.M., Weissenbach, J., Williams, S.M., WoodageT, null, Worley, K.C., Wu, D., Yang, S., Yao, Q.A., Ye, J., Yeh, R.F., Zaveri, J.S., Zhan, M., Zhang, G., Zhao, Q., Zheng, L., Zheng, X.H., Zhong, F.N., Zhong, W., Zhou, X., Zhu, S., Zhu, X., Smith, H.O., Gibbs, R.A., Myers, E.W., Rubin, G.M., Venter, J.C., 2000. The genome sequence of Drosophila melanogaster. Science 287, 2185–2195.

Adelöw, C., Andersson, T., Ahlbom, A., Tomson, T., 2012. Hospitalization for psychiatric disorders before and after onset of unprovoked seizures/epilepsy. Neurology 78, 396–401. doi:10.1212/WNL.0b013e318245f461

Afsari, F., Christensen, K.V., Smith, G.P., Hentzer, M., Nippe, O.M., Elliott, C.J.H., Wade, A.R., 2014. Abnormal visual gain control in a Parkinson's disease model. Hum. Mol. Genet. 23, 4465–4478. doi:10.1093/hmg/ddu159

Agam, K., Campenhausen, M. von, Levy, S., Ben-Ami, H.C., Cook, B., Kirschfeld, K., Minke, B., 2000. Metabolic Stress Reversibly Activates the DrosophilaLight-Sensitive Channels TRP and TRPL In Vivo. J. Neurosci. 20, 5748–5755.

Agarwal, A., Boyd, S., Drews, R.C., 2011. Diagnostic and Imaging Techniques in Ophthalmology. JP Medical Ltd.

Albrecht, D.G., Farrar, S.B., Hamilton, D.B., 1984. Spatial contrast adaptation characteristics of neurones recorded in the cat's visual cortex. J. Physiol. 347, 713–739.

Albrecht, D.G., Geisler, W.S., 1991. Motion selectivity and the contrast-response function of simple cells in the visual cortex. Vis. Neurosci. 7, 531–546.

Albrecht, D.G., Hamilton, D.B., 1982. Striate cortex of monkey and cat: contrast response function. J. Neurophysiol. 48, 217–237.

Anton-Erxleben, K., Herrmann, K., Carrasco, M., 2013. Independent effects of adaptation and attention on perceived speed. Psychol. Sci. 24, 150–159. doi:10.1177/0956797612449178

Avidan, G., Harel, M., Hendler, T., Ben-Bashat, D., Zohary, E., Malach, R., 2002. Contrast sensitivity in human visual areas and its relationship to object recognition. J. Neurophysiol. 87, 3102–3116.

Baulac, S., Huberfeld, G., Gourfinkel-An, I., Mitropoulou, G., Beranger, A., Prud'homme, J.F., Baulac, M., Brice, A., Bruzzone, R., LeGuern, E., 2001. First genetic evidence of GABA(A) receptor dysfunction in epilepsy: a mutation in the gamma2-subunit gene. Nat. Genet. 28, 46–48. doi:10.1038/88254

Beaudoin, D.L., Borghuis, B.G., Demb, J.B., 2007. Cellular Basis for Contrast Gain Control over the Receptive Field Center of Mammalian Retinal Ganglion Cells. J. Neurosci. 27, 2636–2645. doi:10.1523/JNEUROSCI.4610-06.2007

Belmonte, M., 2000. Abnormal Attention in Autism Shown by Steady-State Visual Evoked Potentials. Autism 4, 269–285. doi:10.1177/1362361300004003004

Belusic, G., 2011. ERG in Drosophila, in: Belusic, G. (Ed.), Electroretinograms. InTech.

Ben-Ari, Y., 2002. Excitatory actions of gaba during development: the nature of the nurture. Nat. Rev. Neurosci. 3, 728–739. doi:10.1038/nrn920

Bettler, B., Kaupmann, K., Mosbacher, J., Gassmann, M., 2004. Molecular structure and physiological functions of GABA(B) receptors. Physiol. Rev. 84, 835–867. doi:10.1152/physrev.00036.2003

Betts, L.R., Sekuler, A.B., Bennett, P.J., 2009. Spatial characteristics of center-surround antagonism in younger and older adults. J. Vis. 9, 25.1-15. doi:10.1167/9.1.25

Bex, P.J., Mareschal, I., Dakin, S.C., 2007. Contrast gain control in natural scenes. J. Vis. 7, 12.1-12. doi:10.1167/7.11.12

Biervert, C., Schroeder, B.C., Kubisch, C., Berkovic, S.F., Propping, P., Jentsch, T.J., Steinlein, O.K., 1998. A potassium channel mutation in neonatal human epilepsy. Science 279, 403–406.

Birca, A., Carmant, L., Lortie, A., Vannasing, P., Lassonde, M., 2008. Gamma frequency SSVEP components differentiate children with febrile seizures from normal controls. Epilepsia 49, 1946–1949. doi:10.1111/j.1528-1167.2008.01878.x

Blaesse, P., Airaksinen, M.S., Rivera, C., Kaila, K., 2009. Cation-chloride cotransporters and neuronal function. Neuron 61, 820–838. doi:10.1016/j.neuron.2009.03.003

Blakemore, C., Muncey, J.P., Ridley, R.M., 1973. Stimulus specificity in the human visual system. Vision Res. 13, 1915–1931.

Boas, D.A., Jones, S.R., Devor, A., Huppert, T.J., Dale, A.M., 2008. A vascular anatomical network model of the spatio-temporal response to brain activation. NeuroImage 40, 1116–1129. doi:10.1016/j.neuroimage.2007.12.061

Boggs, J.G., 2004. Mortality Associated with Status Epilepticus. Epilepsy Curr. 4, 25–27. doi:10.1111/j.1535-7597.2004.04110.x

Bonds, A.B., 1991. Temporal dynamics of contrast gain in single cells of the cat striate cortex. Vis. Neurosci. 6, 239–255.

Bonhoeffer, T., Grinvald, A., 1991. Iso-orientation domains in cat visual cortex are arranged in pinwheel-like patterns. Nature 353, 429–431. doi:10.1038/353429a0

Bonin, V., Mante, V., Carandini, M., 2005. The Suppressive Field of Neurons in Lateral Geniculate Nucleus. J. Neurosci. 25, 10844–10856. doi:10.1523/JNEUROSCI.3562-05.2005

Bowman, S.M., Aitken, M.E., Sharp, G.B., 2010. Disparities in hospital outcomes for injured people with epilepsy/seizures. Epilepsia 51, 862–867. doi:10.1111/j.1528-1167.2009.02492.x

Boynton, G.M., 2009. A framework for describing the effects of attention on visual responses. Vision Res. 49, 1129–1143. doi:10.1016/j.visres.2008.11.001

Boynton, G.M., Demb, J.B., Glover, G.H., Heeger, D.J., 1999. Neuronal basis of contrast discrimination. Vision Res. 39, 257–269.

Boynton, G.M., Engel, S.A., Glover, G.H., Heeger, D.J., 1996. Linear Systems Analysis of Functional Magnetic Resonance Imaging in Human V1. J. Neurosci. 16, 4207–4221.

Brand, A.H., Perrimon, N., 1993. Targeted gene expression as a means of altering cell fates and generating dominant phenotypes. Dev. Camb. Engl. 118, 401–415.

Brewer, A., Barton, B., 2012. Visual Field Map Organization in Human Visual Cortex, in: Molotchnikoff, S. (Ed.), Visual Cortex - Current Status and Perspectives. InTech.

Brouwer, G.J., Heeger, D.J., 2011. Cross-orientation suppression in human visual cortex. J. Neurophysiol. 106, 2108–2119. doi:10.1152/jn.00540.2011

Bubl, E., Tebartz Van Elst, L., Gondan, M., Ebert, D., Greenlee, M.W., 2009. Vision in depressive disorder. World J. Biol. Psychiatry Off. J. World Fed. Soc. Biol. Psychiatry 10, 377–384. doi:10.1080/15622970701513756

Buckingham, S.D., Biggin, P.C., Sattelle, B.M., Brown, L.A., Sattelle, D.B., 2005. Insect GABA receptors: splicing, editing, and targeting by antiparasitics and insecticides. Mol. Pharmacol. 68, 942–951. doi:10.1124/mol.105.015313

Buracas, G.T., Boynton, G.M., 2007. The effect of spatial attention on contrast response functions in human visual cortex. J. Neurosci. Off. J. Soc. Neurosci. 27, 93–97. doi:10.1523/JNEUROSCI.3162-06.2007

Busse, L., Wade, A.R., Carandini, M., 2009. Representation of Concurrent Stimuli by Population Activity in Visual Cortex. Neuron 64, 931–942. doi:10.1016/j.neuron.2009.11.004

Campbell, F.W., Cooper, G.F., Enroth-Cugell, C., 1969. The spatial selectivity of the visual cells of the cat. J. Physiol. 203, 223–235.

Candy, T.R., Skoczenski, A.M., Norcia, A.M., 2001. Normalization Models Applied to Orientation Masking in the Human Infant. J. Neurosci. 21, 4530–4541.

Carandini, M., Ferster, D., 1997. A Tonic Hyperpolarization Underlying Contrast Adaptation in Cat Visual Cortex. Science 276, 949–952. doi:10.1126/science.276.5314.949

Carandini, M., Heeger, D.J., 2012. Normalization as a canonical neural computation. Nat. Rev. Neurosci. 13, 51–62. doi:10.1038/nrn3136

Carandini, M., Heeger, D.J., Movshon, J.A., 1997. Linearity and Normalization in Simple Cells of the Macaque Primary Visual Cortex. J. Neurosci. 17, 8621–8644.

Carandini, M., Heeger, D.J., Senn, W., 2002. A synaptic explanation of suppression in visual cortex. J. Neurosci. Off. J. Soc. Neurosci. 22, 10053–10065.

Carrasco, M., Ling, S., Read, S., 2004. Attention alters appearance. Nat. Neurosci. 7, 308–313. doi:10.1038/nn1194

Casagrande, V.A., Guillery, R.W., Sherman, S.M., 2005. Cortical Function: A View from the Thalamus. Gulf Professional Publishing.

Cavanaugh, J.R., Bair, W., Movshon, J.A., 2002. Selectivity and Spatial Distribution of Signals From the Receptive Field Surround in Macaque V1 Neurons. J. Neurophysiol. 88, 2547–2556. doi:10.1152/jn.00693.2001

Chance, F.S., Abbott, L.F., Reyes, A.D., 2002. Gain modulation from background synaptic input. Neuron 35, 773–782.

Charlier, C., Singh, N.A., Ryan, S.G., Lewis, T.B., Reus, B.E., Leach, R.J., Leppert, M., 1998. A pore mutation in a novel KQT-like potassium channel gene in an idiopathic epilepsy family. Nat. Genet. 18, 53–55. doi:10.1038/ng0198-53

Cherubini, E., Gaiarsa, J.L., Ben-Ari, Y., 1991. GABA: an excitatory transmitter in early postnatal life. Trends Neurosci. 14, 515–519.

Clare, S., 1997. Functional Magnetic Resonance Imaging: Methods and Applications. University of Nottingham.

Clayton, G.H., Owens, G.C., Wolff, J.S., Smith, R.L., 1998. Ontogeny of cation-Cl-cotransporter expression in rat neocortex. Brain Res. Dev. Brain Res. 109, 281–292.

Cohen, I., Navarro, V., Clemenceau, S., Baulac, M., Miles, R., 2002. On the origin of interictal activity in human temporal lobe epilepsy in vitro. Science 298, 1418–1421. doi:10.1126/science.1076510

Cook, T., Desplan, C., 2001. Photoreceptor subtype specification: from flies to humans. Semin. Cell Dev. Biol. 12, 509–518. doi:10.1006/scdb.2001.0275

Crowder, N.A., Price, N.S.C., Hietanen, M.A., Dreher, B., Clifford, C.W.G., Ibbotson, M.R., 2006. Relationship Between Contrast Adaptation and Orientation Tuning in V1 and V2 of Cat Visual Cortex. J. Neurophysiol. 95, 271–283. doi:10.1152/jn.00871.2005

Dacey, D., Packer, O.S., Diller, L., Brainard, D., Peterson, B., Lee, B., 2000. Center surround receptive field structure of cone bipolar cells in primate retina. Vision Res. 40, 1801–1811.

Dakin, S., Carlin, P., Hemsley, D., 2005. Weak suppression of visual context in chronic schizophrenia. Curr. Biol. CB 15, R822-824. doi:10.1016/j.cub.2005.10.015

Dawson, G.D., 1954. A summation technique for the detection of small evoked potentials. Electroencephalogr. Clin. Neurophysiol. 6, 65–84. doi:10.1016/0013-4694(54)90007-3

DeBruyn, E.J., Bonds, A.B., 1986. Contrast adaptation in cat visual cortex is not mediated by GABA. Brain Res. 383, 339–342.

Demb, J.B., 2002. Multiple mechanisms for contrast adaptation in the retina. Neuron 36, 781–783.

Devor, A., Tian, P., Nishimura, N., Teng, I.C., Hillman, E.M.C., Narayanan, S.N., Ulbert, I., Boas, D.A., Kleinfeld, D., Dale, A.M., 2007. Suppressed Neuronal Activity and Concurrent Arteriolar Vasoconstriction May Explain Negative Blood Oxygenation Level-Dependent Signal. J. Neurosci. Off. J. Soc. Neurosci. 27, 4452–4459. doi:10.1523/JNEUROSCI.0134-07.2007

DeYoe, E.A., Bandettini, P., Neitz, J., Miller, D., Winans, P., 1994. Functional magnetic resonance imaging (FMRI) of the human brain. J. Neurosci. Methods 54, 171–187.

Dolph, P., Nair, A., Raghu, P., 2011. Electroretinogram recordings of Drosophila. Cold Spring Harb. Protoc. 2011, pdb.prot5549.

Dougherty, R.F., Koch, V.M., Brewer, A.A., Fischer, B., Modersitzki, J., Wandell, B.A., 2003. Visual field representations and locations of visual areas V1/2/3 in human visual cortex. J. Vis. 3, 1–1. doi:10.1167/3.10.1

Dubs, A., 1982. The spatial integration of signals in the retina and lamina of the fly compound eye under different conditions of luminance. J. Comp. Physiol. 146, 321–343. doi:10.1007/BF00612703

Duch, C., Vonhoff, F., Ryglewski, S., 2008. Dendrite Elongation and Dendritic Branching Are Affected Separately by Different Forms of Intrinsic Motoneuron Excitability. J. Neurophysiol. 100, 2525–2536. doi:10.1152/jn.90758.2008

Duffy, J.B., 2002. GAL4 system in Drosophila: a fly geneticist's Swiss army knife. Genes. N. Y. N 2000 34, 1–15. doi:10.1002/gene.10150

Enell, L., Hamasaka, Y., Kolodziejczyk, A., Nässel, D.R., 2007. gamma-Aminobutyric acid (GABA) signaling components in Drosophila: immunocytochemical localization of GABA(B) receptors in relation to the GABA(A) receptor subunit RDL and a vesicular GABA transporter. J. Comp. Neurol. 505, 18–31. doi:10.1002/cne.21472

Engel, S.A., Furmanski, C.S., 2001. Selective adaptation to color contrast in human primary visual cortex. J. Neurosci. Off. J. Soc. Neurosci. 21, 3949–3954.

Engel, S.A., Glover, G.H., Wandell, B.A., 1997. Retinotopic organization in human visual cortex and the spatial precision of functional MRI. Cereb. Cortex 7, 181–192. doi:10.1093/cercor/7.2.181

Engel, S.A., Rumelhart, D.E., Wandell, B.A., Lee, A.T., Glover, G.H., Chichilnisky, E.J., Shadlen, M.N., 1994. fMRI of human visual cortex. Nature 369, 525. doi:10.1038/369525a0

Engel, S.A., Zhang, X., Wandell, B.A., 1997. Color tuning in human visual cortex measured using functional magnetic resonance imaging. Nature.

Escayg, A., MacDonald, B.T., Meisler, M.H., Baulac, S., Huberfeld, G., An-Gourfinkel, I., Brice, A., LeGuern, E., Moulard, B., Chaigne, D., Buresi, C., Malafosse, A., 2000. Mutations of SCN1A, encoding a neuronal sodium channel, in two families with GEFS+2. Nat. Genet. 24, 343–345. doi:10.1038/74159

Fahrenfort, I., Klooster, J., Sjoerdsma, T., Kamermans, M., 2005. The involvement of glutamate-gated channels in negative feedback from horizontal cells to cones. Prog. Brain Res. 147, 219–229. doi:10.1016/S0079-6123(04)47017-4

Ffrench-Constant, R.H., Roush, R.T., 1991. Gene mapping and cross-resistance in cyclodiene insecticide-resistant Drosophila melanogaster (Mg.). Genet. Res. 57, 17–21.

Finger, T.E., 2009. International Symposium on Olfaction and Taste. John Wiley & Sons.

Flatman, P.W., 2008. Cotransporters, WNKs and hypertension: an update. Curr. Opin. Nephrol. Hypertens. 17, 186–192. doi:10.1097/MNH.0b013e3282f5244e

Foley, J.M., 1994. Human luminance pattern-vision mechanisms: masking experiments require a new model. J. Opt. Soc. Am. A Opt. Image Sci. Vis. 11, 1710–1719.

Freifeld, L., Clark, D.A., Schnitzer, M.J., Horowitz, M.A., Clandinin, T.R., 2013. GABAergic Lateral Interactions Tune the Early Stages of Visual Processing in Drosophila. Neuron 78, 1075–1089. doi:10.1016/j.neuron.2013.04.024

Friston, K.J., Holmes, A.P., Poline, J.B., Grasby, P.J., Williams, S.C., Frackowiak, R.S., Turner, R., 1995. Analysis of fMRI time-series revisited. NeuroImage 2, 45–53. doi:10.1006/nimg.1995.1007

Frucht, M.M., Quigg, M., Schwaner, C., Fountain, N.B., 2000. Distribution of seizure precipitants among epilepsy syndromes. Epilepsia 41, 1534–1539.

Gabis, L., Pomeroy, J., Andriola, M.R., 2005. Autism and epilepsy: cause, consequence, comorbidity, or coincidence? Epilepsy Behav. EB 7, 652–656. doi:10.1016/j.yebeh.2005.08.008

Gadsby, D.C., 2009. Ion channels versus ion pumps: the principal difference, in principle. Nat. Rev. Mol. Cell Biol. 10, 344–352. doi:10.1038/nrm2668

Gandhi, S.P., Heeger, D.J., Boynton, G.M., 1999. Spatial attention affects brain activity in human primary visual cortex. Proc. Natl. Acad. Sci. 96, 3314–3319. doi:10.1073/pnas.96.6.3314

Ganetzky, B., Wu, C.F., 1982. Indirect Suppression Involving Behavioral Mutants with Altered Nerve Excitability in DROSOPHILA MELANOGASTER. Genetics 100, 597–614.

Garcia, G., 2008. High frequency SSVEPs for BCI applications. Comput.-Hum. Interact.

Gardner, J.L., Sun, P., Waggoner, R.A., Ueno, K., Tanaka, K., Cheng, K., 2005. Contrast adaptation and representation in human early visual cortex. Neuron 47, 607–620. doi:10.1016/j.neuron.2005.07.016

Gengs, C., Leung, H.-T., Skingsley, D.R., Iovchev, M.I., Yin, Z., Semenov, E.P., Burg, M.G., Hardie, R.C., Pak, W.L., 2002. The Target of Drosophila Photoreceptor Synaptic Transmission Is a Histamine-gated Chloride Channel Encoded byort (hclA). J. Biol. Chem. 277, 42113–42120. doi:10.1074/jbc.M207133200

Glover, G.H., 2011. Overview of Functional Magnetic Resonance Imaging. Neurosurg. Clin. N. Am. 22, 133–139. doi:10.1016/j.nec.2010.11.001

Goldsmith, T.H., Barker, R.J., Cohen, C.F., 1964. SENSITIVITY OF VISUAL RECEPTORS OF CAROTENOID-DEPLETED FLIES: A VITAMIN A DEFICIENCY IN AN INVERTEBRATE. Science 146, 65–67.

Gouws, A.D., Alvarez, I., Watson, D.M., Uesaki, M., Rogers, J., Morland, A.B., 2014. On the Role of Suppression in Spatial Attention: Evidence from Negative BOLD in Human Subcortical and Cortical Structures. J. Neurosci. 34, 10347–10360. doi:10.1523/JNEUROSCI.0164-14.2014

Graham, N.V.S., 1989. Visual Pattern Analyzers. Oxford University Press.

Gray, M., Kemp, A.H., Silberstein, R.B., Nathan, P.J., 2003. Cortical neurophysiology of anticipatory anxiety: an investigation utilizing steady state probe topography (SSPT). NeuroImage 20, 975–986. doi:10.1016/S1053-8119(03)00401-4

Hammett, S.T., Georgeson, M.A., Bedingham, S., Barbieri-Hesse, G.S., 2003. Motion sharpening and contrast: gain control precedes compressive non-linearity? Vision Res. 43, 1187–1199.

Hammett, S.T., Snowden, R.J., Smith, A.T., 1994. Perceived contrast as a function of adaptation duration. Vision Res. 34, 31–40.

Hara, Y., Pestilli, F., Gardner, J.L., 2014. Differing effects of attention in single-units and populations are well predicted by heterogeneous tuning and the normalization model of attention. Front. Comput. Neurosci. 8. doi:10.3389/fncom.2014.00012

Hardie, R.C., 1987. Is histamine a neurotransmitter in insect photoreceptors? J. Comp. Physiol. [A] 161, 201–213.

Hardie, R.C., Raghu, P., 2001. Visual transduction in Drosophila. Nature 413, 186–193. doi:10.1038/35093002

Harris, R.A., O'Carroll, D.C., Laughlin, S.B., 2000. Contrast Gain Reduction in Fly Motion Adaptation. Neuron 28, 595–606. doi:10.1016/S0896-6273(00)00136-7

Harvey, R.J., Schmitt, B., Hermans-Borgmeyer, I., Gundelfinger, E.D., Betz, H., Darlison, M.G., 1994. Sequence of a Drosophila ligand-gated ion-channel polypeptide with an unusual amino-terminal extracellular domain. J. Neurochem. 62, 2480–2483.

Haug, K., Warnstedt, M., Alekov, A.K., Sander, T., Ramírez, A., Poser, B., Maljevic, S., Hebeisen, S., Kubisch, C., Rebstock, J., Horvath, S., Hallmann, K., Dullinger, J.S., Rau, B., Haverkamp, F., Beyenburg, S., Schulz, H., Janz, D., Giese, B., Müller-Newen, G., Propping, P., Elger, C.E., Fahlke, C., Lerche, H., Heils, A., 2003. Mutations in CLCN2 encoding a voltage-gated chloride channel are associated with idiopathic generalized epilepsies. Nat. Genet. 33, 527–532. doi:10.1038/ng1121

Heeger, D.J., 1992. Normalization of cell responses in cat striate cortex. Vis. Neurosci. 9, 181–197.

Heeger, D.J., Ress, D., 2002. What does fMRI tell us about neuronal activity? Nat. Rev. Neurosci. 3, 142–151. doi:10.1038/nrn730

Heimel, J.A., Saiepour, M.H., Chakravarthy, S., Hermans, J.M., Levelt, C.N., 2010. Contrast gain control and cortical TrkB signaling shape visual acuity. Nat. Neurosci. 13, 642–648. doi:10.1038/nn.2534

Heisenberg, M., 1971. Separation of receptor and lamina potentials in the electroretinogram of normal and mutant Drosophila. J. Exp. Biol. 55, 85–100.

Hekmat-Scafe, D.S., Lundy, M.Y., Ranga, R., Tanouye, M.A., 2006. Mutations in the K+/Cl-cotransporter gene kazachoc (kcc) increase seizure susceptibility in Drosophila. J. Neurosci. Off. J. Soc. Neurosci. 26, 8943–8954. doi:10.1523/JNEUROSCI.4998-05.2006

Henderson, J.E., Soderlund, D.M., Knipple, D.C., 1993. Characterization of a putative gamma-aminobutyric acid (GABA) receptor beta subunit gene from Drosophila melanogaster. Biochem. Biophys. Res. Commun. 193, 474–482. doi:10.1006/bbrc.1993.1648

Herzog, A.G., Harden, C.L., Liporace, J., Pennell, P., Schomer, D.L., Sperling, M., Fowler, K., Nikolov, B., Shuman, S., Newman, M., 2004. Frequency of catamenial seizure exacerbation in women with localization-related epilepsy. Ann. Neurol. 56, 431–434. doi:10.1002/ana.20214

Hillman, P., Hochstein, S., Minke, B., 1983. Transduction in invertebrate photoreceptors: role of pigment bistability. Physiol. Rev. 63, 668–772.

Hindle, S., Afsari, F., Stark, M., Middleton, C.A., Evans, G.J.O., Sweeney, S.T., Elliott, C.J.H., 2013. Dopaminergic expression of the Parkinsonian gene LRRK2-G2019S leads to non-autonomous visual neurodegeneration, accelerated by increased neural demands for energy. Hum. Mol. Genet. 22, 2129–2140. doi:10.1093/hmg/ddt061

Hirtz, D., Thurman, D.J., Gwinn-Hardy, K., Mohamed, M., Chaudhuri, A.R., Zalutsky, R., 2007. How common are the "common" neurologic disorders? Neurology 68, 326–337. doi:10.1212/01.wnl.0000252807.38124.a3

Holtzschue, L., 2011. Understanding Color: An Introduction for Designers, 4th Edition edition. ed. John Wiley & Sons, Hoboken, NJ.

Hosie, A., Sattelle, D., Aronstein, K., ffrench-Constant, R., 1997. Molecular biology of insect neuronal GABA receptors. Trends Neurosci. 20, 578–583. doi:10.1016/S0166-2236(97)01127-2

Hotta, Y., Benzer, S., 1969. Abnormal electroretinograms in visual mutants of Drosophila. Nature 222, 354–356.

Hou, F., Huang, C.-B., Liang, J., Zhou, Y., Lu, Z.-L., 2013. Contrast gain-control in stereo depth and cyclopean contrast perception. J. Vis. 13. doi:10.1167/13.8.3

Hu, W., Wang, T., Wang, X., Han, J., 2015. Ih Channels Control Feedback Regulation from Amacrine Cells to Photoreceptors. PLoS Biol 13, e1002115. doi:10.1371/journal.pbio.1002115

Hubel, D.H., Wiesel, T.N., 1977. Ferrier lecture. Functional architecture of macaque monkey visual cortex. Proc. R. Soc. Lond. B Biol. Sci. 198, 1–59.

Hubel, D.H., Wiesel, T.N., 1968. Receptive fields and functional architecture of monkey striate cortex. J. Physiol. 195, 215–243.

Hubel, D.H., Wiesel, T.N., 1965. Receptive Fields and Functional Architecture in Two Nonstriate Visual Areas (18 and 19) of the Cat. J. Neurophysiol. 28, 229–289.

Hubel, D.H., Wiesel, T.N., 1962. Receptive fields, binocular interaction and functional architecture in the cat's visual cortex. J. Physiol. 160, 106–154.2.

Hubel, D.H., Wiesel, T.N., 1959. Receptive fields of single neurones in the cat's striate cortex. J. Physiol. 148, 574–591.

Hübner, C.A., Stein, V., Hermans-Borgmeyer, I., Meyer, T., Ballanyi, K., Jentsch, T.J., 2001. Disruption of KCC2 reveals an essential role of K-Cl cotransport already in early synaptic inhibition. Neuron 30, 515–524.

Hutcheon, B., Yarom, Y., 2000. Resonance, oscillation and the intrinsic frequency preferences of neurons. Trends Neurosci. 23, 216–222. doi:10.1016/S0166-2236(00)01547-2

Jacob, B., Hache, J.C., Pasquier, F., 2002. [Dysfunction of the magnocellular pathway in Alzheimer's disease]. Rev. Neurol. (Paris) 158, 555–564.

Johns, D.C., Marx, R., Mains, R.E., O'Rourke, B., Marbán, E., 1999. Inducible genetic suppression of neuronal excitability. J. Neurosci. Off. J. Soc. Neurosci. 19, 1691–1697.

Jones, S.M., Ribera, A.B., 1994. Overexpression of a potassium channel gene perturbs neural differentiation. J. Neurosci. Off. J. Soc. Neurosci. 14, 2789–2799.

Kaang, B.K., Pfaffinger, P.J., Grant, S.G., Kandel, E.R., Furukawa, Y., 1992. Overexpression of an Aplysia shaker K+ channel gene modifies the electrical properties and synaptic efficacy of identified Aplysia neurons. Proc. Natl. Acad. Sci. U. S. A. 89, 1133–1137.

Kahle KT, Khanna A, Clapham DE, Woolf CJ, 2014. THerapeutic restoration of spinal inhibition via druggable enhancement of potassium-chloride cotransporter kcc2–mediated chloride extrusion in peripheral neuropathic pain. JAMA Neurol. 71, 640–645. doi:10.1001/jamaneurol.2014.21

Kaila, K., Price, T.J., Payne, J.A., Puskarjov, M., Voipio, J., 2014. Cation-chloride cotransporters in neuronal development, plasticity and disease. Nat. Rev. Neurosci. 15, 637–654. doi:10.1038/nrn3819

Kastner, S., Ungerleider, L.G., 2000. Mechanisms of Visual Attention in the Human Cortex. Annu. Rev. Neurosci. 23, 315–341. doi:10.1146/annurev.neuro.23.1.315

Katzner, S., Busse, L., Carandini, M., 2011. GABAA inhibition controls response gain in visual cortex. J. Neurosci. Off. J. Soc. Neurosci. 31, 5931–5941. doi:10.1523/JNEUROSCI.5753-10.2011

Kemp, A.H., Gray, M.A., Silberstein, R.B., Armstrong, S.M., Nathan, P.J., 2004. Augmentation of serotonin enhances pleasant and suppresses unpleasant cortical electrophysiological responses to visual emotional stimuli in humans. NeuroImage 22, 1084–1096. doi:10.1016/j.neuroimage.2004.03.022

Kim, Y.J., Grabowecky, M., Paller, K.A., Muthu, K., Suzuki, S., 2007. Attention induces synchronization-based response gain in steady-state visual evoked potentials. Nat. Neurosci. 10, 117–125. doi:10.1038/nn1821

Kohn, A., 2007. Visual Adaptation: Physiology, Mechanisms, and Functional Benefits. J. Neurophysiol. 97, 3155–3164. doi:10.1152/jn.00086.2007

Kuebler, D., Tanouye, M., 2002. Anticonvulsant valproate reduces seizure-susceptibility in mutant Drosophila. Brain Res. 958, 36–42.

Kuebler, D., Tanouye, M.A., 2000. Modifications of seizure susceptibility in Drosophila. J. Neurophysiol. 83, 998–1009.

Kuebler, D., Zhang, H., Ren, X., Tanouye, M.A., 2001. Genetic suppression of seizure susceptibility in Drosophila. J. Neurophysiol. 86, 1211–1225.

Kumar, J.P., 2001. Signalling pathways in Drosophila and vertebrate retinal development. Nat. Rev. Genet. 2, 846–857. doi:10.1038/35098564

Lauritzen, T.Z., Ales, J.M., Wade, A.R., 2010. The effects of visuospatial attention measured across visual cortex using source-imaged, steady-state EEG. J. Vis. 10. doi:10.1167/10.14.39

Lee, H., Chen, C.X.-Q., Liu, Y.-J., Aizenman, E., Kandler, K., 2005. KCC2 expression in immature rat cortical neurons is sufficient to switch the polarity of GABA responses. Eur. J. Neurosci. 21, 2593–2599. doi:10.1111/j.1460-9568.2005.04084.x

Lee, J., Maunsell, J.H.R., 2010. The effect of attention on neuronal responses to high and low contrast stimuli. J. Neurophysiol. 104, 960–971. doi:10.1152/jn.01019.2009

Lee, J., Wu, C.-F., 2002. Electroconvulsive seizure behavior in Drosophila: analysis of the physiological repertoire underlying a stereotyped action pattern in bang-sensitive mutants. J. Neurosci. Off. J. Soc. Neurosci. 22, 11065–11079.

Li, X., Lu, Z.-L., Tjan, B.S., Dosher, B.A., Chu, W., 2008. Blood oxygenation level-dependent contrast response functions identify mechanisms of covert attention in early visual areas. Proc. Natl. Acad. Sci. U. S. A. 105, 6202–6207. doi:10.1073/pnas.0801390105

Line, P., Silberstein, R.B., Wright, J.J., Copolov, D.L., 1998. Steady state visually evoked potential correlates of auditory hallucinations in schizophrenia. NeuroImage 8, 370–376. doi:10.1006/nimg.1998.0378

Ling, S., Carrasco, M., 2006. When sustained attention impairs perception. Nat. Neurosci. 9, 1243–1245. doi:10.1038/nn1761

Liu, J., Wandell, B.A., 2005. Specializations for chromatic and temporal signals in human visual cortex. J. Neurosci. Off. J. Soc. Neurosci. 25, 3459–3468. doi:10.1523/JNEUROSCI.4206-04.2005

Logothetis, N.K., Pauls, J., Augath, M., Trinath, T., Oeltermann, A., 2001. Neurophysiological investigation of the basis of the fMRI signal. Nature 412, 150–157. doi:10.1038/35084005

Mackenzie, S.M., Brooker, M.R., Gill, T.R., Cox, G.B., Howells, A.J., Ewart, G.D., 1999. Mutations in the white gene of Drosophila melanogaster affecting ABC transporters that determine eye colouration. Biochim. Biophys. Acta BBA - Biomembr. 1419, 173–185. doi:10.1016/S0005-2736(99)00064-4

Macpherson, H., Pipingas, A., Silberstein, R., 2009. A steady state visually evoked potential investigation of memory and ageing. Brain Cogn. 69, 571–579. doi:10.1016/j.bandc.2008.12.003

Malonek, D., Grinvald, A., 1996. Interactions between electrical activity and cortical microcirculation revealed by imaging spectroscopy: implications for functional brain mapping. Science 272, 551–554.

Mante, V., Frazor, R.A., Bonin, V., Geisler, W.S., Carandini, M., 2005. Independence of luminance and contrast in natural scenes and in the early visual system. Nat. Neurosci. 8, 1690–1697. doi:10.1038/nn1556

Martínez-Trujillo, J.C., Treue, S., 2002. Attentional Modulation Strength in Cortical Area MT Depends on Stimulus Contrast. Neuron 35, 365–370. doi:10.1016/S0896-6273(02)00778-X

Marx, M., Bodis-Wollner, I., Bobak, P., Harnois, C., Mylin, L., Yahr, M., 1986. Temporal frequency-dependent vep changes in Parkinson's disease. Vision Res. 26, 185–193. doi:10.1016/0042-6989(86)90080-5

Matić, T., Laughlin, S.B., 1981. Changes in the intensity-response function of an insect's photoreceptors due to light adaptation. J. Comp. Physiol. 145, 169–177. doi:10.1007/BF00605031

Mbuba, C.K., Newton, C.R., 2009. Packages of Care for Epilepsy in Low- and Middle-Income Countries. PLoS Med 6, e1000162. doi:10.1371/journal.pmed.1000162

Meinertzhagen, I.A., O'Neil, S.D., 1991. Synaptic organization of columnar elements in the lamina of the wild type in Drosophila melanogaster. J. Comp. Neurol. 305, 232–263. doi:10.1002/cne.903050206

Minke, B., 1982. Light-induced reduction in excitation efficiency in the trp mutant of Drosophila. J. Gen. Physiol. 79, 361–385. doi:10.1085/jgp.79.3.361

Mishkin, M., Ungerleider, L.G., Macko, K.A., 1983. Object vision and spatial vision: two cortical pathways. Trends Neurosci. 6, 414–417. doi:10.1016/0166-2236(83)90190-X

Mitchell, S.J., Silver, R.A., 2003. Shunting inhibition modulates neuronal gain during synaptic excitation. Neuron 38, 433–445.

Montell, C., 2012. Drosophila visual transduction. Trends Neurosci. 35, 356–363. doi:10.1016/j.tins.2012.03.004

Morante, J., Desplan, C., 2008. The color-vision circuit in the medulla of Drosophila. Curr. Biol. CB 18, 553–565. doi:10.1016/j.cub.2008.02.075

Morante, J., Desplan, C., 2005. Photoreceptor axons play hide and seek. Nat. Neurosci. 8, 401–402. doi:10.1038/nn0405-401

Morgan, S.T., Hansen, J.C., Hillyard, S.A., 1996. Selective attention to stimulus location modulates the steady-state visual evoked potential. Proc. Natl. Acad. Sci. U. S. A. 93, 4770–4774.

Morgan, T.H., 1910. SEX LIMITED INHERITANCE IN DROSOPHILA. Science 32, 120–122. doi:10.1126/science.32.812.120

Morrone, M.C., Burr, D.C., Speed, H.D., 1987. Cross-orientation inhibition in cat is GABA mediated. Exp. Brain Res. 67, 635–644.

Movshon, J.A., Lennie, P., 1979. Pattern-selective adaptation in visual cortical neurones. Nature 278, 850–852.

Murray, S.O., 2008. The effects of spatial attention in early human visual cortex are stimulus independent. J. Vis. 8, 2.1-11. doi:10.1167/8.10.2

Naka, K.I., Rushton, W.A., 1966. S-potentials from luminosity units in the retina of fish (Cyprinidae). J. Physiol. 185, 587–599.

Ngugi, A.K., Bottomley, C., Kleinschmidt, I., Sander, J.W., Newton, C.R., 2010. Estimation of the burden of active and life-time epilepsy: a meta-analytic approach. Epilepsia 51, 883–890. doi:10.1111/j.1528-1167.2009.02481.x

Nippe, O., 2015. Drosophila melanogaster clock gene mutants exhibit a circadian rhythm in visual contrast response (mscresearch). University of York.

Norcia, A.M., Appelbaum, L.G., Ales, J.M., Cottereau, B.R., Rossion, B., 2015. The steady-state visual evoked potential in vision research: A review. J. Vis. 15. doi:10.1167/15.6.4

O'Carroll, D.C., 2001. Motion Adaptation and Evidence for Parallel Processing in the Lobula Plate of the Bee-Fly Bombylius major, in: Zanker, J.M., Zeil, J. (Eds.), Motion Vision. Springer Berlin Heidelberg, pp. 381–394.

O'Connor, D.H., Fukui, M.M., Pinsk, M.A., Kastner, S., 2002. Attention modulates responses in the human lateral geniculate nucleus. Nat. Neurosci. 5, 1203–1209. doi:10.1038/nn957

Odom, J.V., Bach, M., Barber, C., Brigell, M., Marmor, M.F., Tormene, A.P., Holder, G.E., Vaegan, null, 2004. Visual evoked potentials standard (2004). Doc. Ophthalmol. Adv. Ophthalmol. 108, 115–123.

Offner, S., 1996. A Plain English Map of the Chromosomes of the Fruit Fly Drosophila Melanogaster. Am. Biol. Teach. 58, 462–469. doi:10.2307/4450212

Ogawa, S., Lee, T.M., Kay, A.R., Tank, D.W., 1990. Brain magnetic resonance imaging with contrast dependent on blood oxygenation. Proc. Natl. Acad. Sci. U. S. A. 87, 9868–9872.

Ohzawa, I., Sclar, G., Freeman, R.D., 1985. Contrast gain control in the cat's visual system. J. Neurophysiol. 54, 651–667.

Ohzawa, I., Sclar, G., Freeman, R.D., 1982. Contrast gain control in the cat visual cortex. Nature 298, 266–268. doi:10.1038/298266a0

Owens, D.F., Boyce, L.H., Davis, M.B.E., Kriegstein, A.R., 1996. Excitatory GABA Responses in Embryonic and Neonatal Cortical Slices Demonstrated by Gramicidin Perforated-Patch Recordings and Calcium Imaging. J. Neurosci. 16, 6414–6423.

Pandey, U.B., Nichols, C.D., 2011. Human Disease Models in Drosophila melanogaster and the Role of the Fly in Therapeutic Drug Discovery. Pharmacol. Rev. 63, 411–436. doi:10.1124/pr.110.003293

Pantazis, A., Segaran, A., Liu, C.-H., Nikolaev, A., Rister, J., Thum, A.S., Roeder, T., Semenov, E., Juusola, M., Hardie, R.C., 2008. Distinct Roles for Two Histamine Receptors (hclA and hclB) at the Drosophila Photoreceptor Synapse. J. Neurosci. 28, 7250–7259. doi:10.1523/JNEUROSCI.1654-08.2008

Pauling, L., Coryell, C.D., 1936. The Magnetic Properties and Structure of Hemoglobin, Oxyhemoglobin and Carbonmonoxyhemoglobin. Proc. Natl. Acad. Sci. U. S. A. 22, 210–216.

Payne, J.A., Rivera, C., Voipio, J., Kaila, K., 2003. Cation-chloride co-transporters in neuronal communication, development and trauma. Trends Neurosci. 26, 199–206. doi:10.1016/S0166-2236(03)00068-7

Pestilli, F., Carrasco, M., Heeger, D.J., Gardner, J.L., 2011. Attentional enhancement via selection and pooling of early sensory responses in human visual cortex. Neuron 72, 832–846. doi:10.1016/j.neuron.2011.09.025

Pestilli, F., Viera, G., Carrasco, M., 2007. How do attention and adaptation affect contrast sensitivity? J. Vis. 7, 9.1-12. doi:10.1167/7.7.9

Petrov, Y., Carandini, M., McKee, S., 2005. Two distinct mechanisms of suppression in human vision. J. Neurosci. Off. J. Soc. Neurosci. 25, 8704–8707. doi:10.1523/JNEUROSCI.2871-05.2005

Plioplys, S., Dunn, D.W., Caplan, R., 2007. 10-year research update review: psychiatric problems in children with epilepsy. J. Am. Acad. Child Adolesc. Psychiatry 46, 1389–1402. doi:10.1097/chi.0b013e31815597fc

Porciatti, V., Bonanni, P., Fiorentini, A., Guerrini, R., 2000. Lack of cortical contrast gain control in human photosensitive epilepsy. Nat. Neurosci. 3, 259–263. doi:10.1038/72972

Porciatti, V., Pizzorusso, T., Maffei, L., 1999. The visual physiology of the wild type mouse determined with pattern VEPs. Vision Res. 39, 3071–3081. doi:10.1016/S0042-6989(99)00022-X

Powell, J., 1997. Progress and Prospects in Evolutionary Biology : The Drosophila Model: The Drosophila Model. Oxford University Press, USA.

Prescott, S.A., De Koninck, Y., 2003. Gain control of firing rate by shunting inhibition: roles of synaptic noise and dendritic saturation. Proc. Natl. Acad. Sci. U. S. A. 100, 2076–2081. doi:10.1073/pnas.0337591100

Priebe, N.J., Ferster, D., 2002. A new mechanism for neuronal gain control (or how the gain in brains has mainly been explained). Neuron 35, 602–604.

Raghu, S.V., Claussen, J., Borst, A., 2013. Neurons with GABAergic phenotype in the visual system of Drosophila. J. Comp. Neurol. 521, 252–265. doi:10.1002/cne.23208

Razjouyan, J., Gharibzadeh, S., Fallah, A., 2009. Organizational Role of Retina Horizontal Cells. J. Neuropsychiatry Clin. Neurosci. 21, 479–480. doi:10.1176/jnp.2009.21.4.479

Regan, D., 1966. Some characteristics of average steady-state and transient responses evoked by modulated light. Electroencephalogr. Clin. Neurophysiol. 20, 238–248. doi:10.1016/0013-4694(66)90088-5

Reiter, L.T., Potocki, L., Chien, S., Gribskov, M., Bier, E., 2001. A Systematic Analysis of Human Disease-Associated Gene Sequences In Drosophila melanogaster. Genome Res. 11, 1114–1125. doi:10.1101/gr.169101

Renganathan, R., Delanty, N., 2003. Juvenile myoclonic epilepsy: under-appreciated and under-diagnosed. Postgrad. Med. J. 79, 78–80.

Reynolds, E.R., Stauffer, E.A., Feeney, L., Rojahn, E., Jacobs, B., McKeever, C., 2004. Treatment with the antiepileptic drugs phenytoin and gabapentin ameliorates seizure and paralysis of Drosophila bang-sensitive mutants. J. Neurobiol. 58, 503–513. doi:10.1002/neu.10297

Reynolds, J.H., Heeger, D.J., 2009. The normalization model of attention. Neuron 61, 168–185. doi:10.1016/j.neuron.2009.01.002

Reynolds, J.H., Pasternak, T., Desimone, R., 2000. Attention Increases Sensitivity of V4 Neurons. Neuron 26, 703–714. doi:10.1016/S0896-6273(00)81206-4

Rezec, A., Krekelberg, B., Dobkins, K.R., 2004. Attention enhances adaptability: evidence from motion adaptation experiments. Vision Res. 44, 3035–3044. doi:10.1016/j.visres.2004.07.020

Rivera, C., Voipio, J., Payne, J.A., Ruusuvuori, E., Lahtinen, H., Lamsa, K., Pirvola, U., Saarma, M., Kaila, K., 1999. The K+/Cl|[minus]| co-transporter KCC2 renders GABA hyperpolarizing during neuronal maturation. Nature 397, 251–255. doi:10.1038/16697

Salcedo, E., Huber, A., Henrich, S., Chadwell, L.V., Chou, W.H., Paulsen, R., Britt, S.G., 1999. Blue- and green-absorbing visual pigments of Drosophila: ectopic expression and physiological characterization of the R8 photoreceptor cell-specific Rh5 and Rh6 rhodopsins. J. Neurosci. Off. J. Soc. Neurosci. 19, 10716–10726.

Sander, J.W., 2003. The epidemiology of epilepsy revisited. Curr. Opin. Neurol. 16, 165–170. doi:10.1097/01.wco.0000063766.15877.8e

Sanes, J.R., Zipursky, S.L., 2010. Design principles of insect and vertebrate visual systems. Neuron 66, 15–36. doi:10.1016/j.neuron.2010.01.018

Sang, J.H., 1982. A handbook of Drosophila development. Trends Biochem. Sci. 7, 341–342. doi:10.1016/0968-0004(82)90276-6

Schneider, B.A., Parker, S., Murphy, D., 2011. A model of top-down gain control in the auditory system. Atten. Percept. Psychophys. 73, 1562–1578. doi:10.3758/s13414-011-0097-7

Sclar, G., Lennie, P., DePriest, D.D., 1989. Contrast adaptation in striate cortex of macaque. Vision Res. 29, 747–755.

Sclar, G., Maunsell, J.H., Lennie, P., 1990. Coding of image contrast in central visual pathways of the macaque monkey. Vision Res. 30, 1–10.

Sclar, G., Ohzawa, I., Freeman, R.D., 1985. Contrast gain control in the kitten's visual system. J. Neurophysiol. 54, 668–675.

Shapley, R.M., Victor, J.D., 1981. How the contrast gain control modifies the frequency responses of cat retinal ganglion cells. J. Physiol. 318, 161–179.

Shmuel, A., Augath, M., Oeltermann, A., Logothetis, N.K., 2006. Negative functional MRI response correlates with decreases in neuronal activity in monkey visual area V1. Nat. Neurosci. 9, 569–577.

Shorrocks, B., 1972. Drosophila. Ginn.

Shorvon, S., 2014. The concept of symptomatic epilepsy and the complexities of assigning cause in epilepsy. Epilepsy Behav. EB 32, 1–8. doi:10.1016/j.yebeh.2013.12.025

Shorvon, S., Tomson, T., 2011. Sudden unexpected death in epilepsy. Lancet Lond. Engl. 378, 2028–2038. doi:10.1016/S0140-6736(11)60176-1

Shorvon, S.D., 2011. The etiologic classification of epilepsy. Epilepsia 52, 1052–1057. doi:10.1111/j.1528-1167.2011.03041.x

Shorvon, S.D., Perucca, E., Jr, J.E., 2009. The Treatment of Epilepsy. John Wiley & Sons.

Silberstein, R.B., Nunez, P.L., Pipingas, A., Harris, P., Danieli, F., 2001. Steady state visually evoked potential (SSVEP) topography in a graded working memory task. Int. J. Psychophysiol. Off. J. Int. Organ. Psychophysiol. 42, 219–232.

Smith, A.T., Williams, A.L., Singh, K.D., 2004. Negative BOLD in the visual cortex: evidence against blood stealing. Hum. Brain Mapp. 21, 213–220. doi:10.1002/hbm.20017

Smith, K.R.M., Matson, J.L., 2010. Psychopathology: differences among adults with intellectually disabled, comorbid autism spectrum disorders and epilepsy. Res. Dev. Disabil. 31, 743–749. doi:10.1016/j.ridd.2010.01.016

Smith, M.A., Bair, W., Movshon, J.A., 2006. Dynamics of Suppression in Macaque Primary Visual Cortex. J. Neurosci. 26, 4826–4834. doi:10.1523/JNEUROSCI.5542-06.2006

Snowden, R.J., Hammett, S.T., 1996. Spatial frequency adaptation: threshold elevation and perceived contrast. Vision Res. 36, 1797–1809.

Solomon, S.G., Kohn, A., 2014. Moving Sensory Adaptation beyond Suppressive Effects in Single Neurons. Curr. Biol. 24, R1012–R1022. doi:10.1016/j.cub.2014.09.001

Solomon, S.G., White, A.J.R., Martin, P.R., 2002. Extraclassical receptive field properties of parvocellular, magnocellular, and koniocellular cells in the primate lateral geniculate nucleus. J. Neurosci. Off. J. Soc. Neurosci. 22, 338–349.

Song, J., Tanouye, M.A., 2008. From bench to drug: Human seizure modeling using Drosophila. Prog. Neurobiol. 84, 182–191. doi:10.1016/j.pneurobio.2007.10.006

Squire, 2008. Fundamental Neuroscience, 4 edition. ed. Academic Press, Amsterdam ; Boston.

Stafstrom, C.E., Tempel, B.L., 2000. Epilepsy genes: The link between molecular dysfunction and pathophysiology. Ment. Retard. Dev. Disabil. Res. Rev. 6, 281–292. doi:10.1002/1098-2779(2000)6:4<281::AID-MRDD7>3.0.CO;2-9

Steer, S., Pickrell, W.O., Kerr, M.P., Thomas, R.H., 2014. Epilepsy prevalence and socioeconomic deprivation in England. Epilepsia 55, 1634–1641. doi:10.1111/epi.12763

Talairach JT, L.T., 1988. Co-Planar Stereotaxic Atlas of the Human Brain: An Approach to Cerebral Imaging.

Tan, J.S., Lin, F., Tanouye, M.A., 2004. Potassium bromide, an anticonvulsant, is effective at alleviating seizures in the Drosophila bang-sensitive mutant bang senseless. Brain Res. 1020, 45–52. doi:10.1016/j.brainres.2004.05.111

241

Tanaka, H., Ohzawa, I., 2009. Surround suppression of V1 neurons mediates orientation-based representation of high-order visual features. J. Neurophysiol. 101, 1444–1462. doi:10.1152/jn.90749.2008

Tanis, J.E., Bellemer, A., Moresco, J.J., Forbush, B., Koelle, M.R., 2009. The potassium chloride cotransporter KCC-2 coordinates development of inhibitory neurotransmission and synapse structure in Caenorhabditis elegans. J. Neurosci. Off. J. Soc. Neurosci. 29, 9943–9954. doi:10.1523/JNEUROSCI.1989-09.2009

Teikari, P., Najjar, R.P., Malkki, H., Knoblauch, K., Dumortier, D., Gronfier, C., Cooper, H.M., 2012. An inexpensive Arduino-based LED stimulator system for vision research. J. Neurosci. Methods 211, 227–236. doi:10.1016/j.jneumeth.2012.09.012

Ting, C.-Y., Lee, C.-H., 2007. Visual circuit development in Drosophila. Curr. Opin. Neurobiol. 17, 65–72. doi:10.1016/j.conb.2006.12.004

Tomlinson, A., 2012. The Origin of the Drosophila Subretinal Pigment Layer. J. Comp. Neurol. 520, 2676–2682. doi:10.1002/cne.23063

Tootell, R.B., Reppas, J.B., Kwong, K.K., Malach, R., Born, R.T., Brady, T.J., Rosen, B.R., Belliveau, J.W., 1995. Functional analysis of human MT and related visual cortical areas using magnetic resonance imaging. J. Neurosci. Off. J. Soc. Neurosci. 15, 3215–3230.

Tootell, R.B.H., Hadjikhani, N., Hall, E.K., Marrett, S., Vanduffel, W., Vaughan, J.T., Dale, A.M., 1998. The Retinotopy of Visual Spatial Attention. Neuron 21, 1409–1422. doi:10.1016/S0896-6273(00)80659-5

Tsai, J.J., Norcia, A.M., Ales, J.M., Wade, A.R., 2011. Contrast gain control abnormalities in idiopathic generalized epilepsy. Ann. Neurol. 70, 574–582. doi:10.1002/ana.22462

Tsai, J.J., Wade, A.R., Norcia, A.M., 2012. Dynamics of Normalization Underlying Masking in Human Visual Cortex. J. Neurosci. 32, 2783–2789. doi:10.1523/JNEUROSCI.4485-11.2012

Tsai, J.J., Wade, A.R., Norcia, A.M., 2012c. Dynamics of Normalization Underlying Masking in Human Visual Cortex. J. Neurosci. 32, 2783–2789. doi:10.1523/JNEUROSCI.4485-11.2012

Tuchman, R., Rapin, I., 2002. Epilepsy in autism. Lancet Neurol. 1, 352–358. doi:10.1016/S1474-4422(02)00160-6

Tuthill, J.C., Nern, A., Holtz, S.L., Rubin, G.M., Reiser, M.B., 2013. Contributions of the 12 Neuron Classes in the Fly Lamina to Motion Vision. Neuron 79, 128–140. doi:10.1016/j.neuron.2013.05.024

Van Essen, D.C., Anderson, C.H., 1995. Information processing strategies and pathways in the primate visual system. Introd. Neural Electron. Netw. 2, 45–76.

Van Swinderen, B., 2012. Competing visual flicker reveals attention-like rivalry in the fly brain. Front. Integr. Neurosci. 6, 96. doi:10.3389/fnint.2012.00096

Vermeulen, J., Kalitzin, S., Parra, J., Dekker, E., Vossepoel, A., da Silva, F.L., 2008. Non-provocative diagnostics of photosensitivity using visual evoked potentials. Clin.

Neurophysiol. Off. J. Int. Fed. Clin. Neurophysiol. 119, 842–852. doi:10.1016/j.clinph.2007.11.177

Vialatte, F.-B., Maurice, M., Dauwels, J., Cichocki, A., 2010. Steady-state visually evoked potentials: Focus on essential paradigms and future perspectives. Prog. Neurobiol. 90, 418–438. doi:10.1016/j.pneurobio.2009.11.005

Vidyasagar, T.R., 1990. Pattern adaptation in cat visual cortex is a co-operative phenomenon. Neuroscience 36, 175–179.

Wade, A.R., Rowland, J., 2010. Early suppressive mechanisms and the negative BOLD response in human visual cortex. J. Neurosci. Off. J. Soc. Neurosci. 30, 5008–5019. doi:10.1523/JNEUROSCI.6260-09.2010

Wallace, R.H., Marini, C., Petrou, S., Harkin, L.A., Bowser, D.N., Panchal, R.G., Williams, D.A., Sutherland, G.R., Mulley, J.C., Scheffer, I.E., Berkovic, S.F., 2001. Mutant GABA(A) receptor gamma2-subunit in childhood absence epilepsy and febrile seizures. Nat. Genet. 28, 49–52. doi:10.1038/88259

Wallace, R.H., Wang, D.W., Singh, R., Scheffer, I.E., George, A.L., Phillips, H.A., Saar, K., Reis, A., Johnson, E.W., Sutherland, G.R., Berkovic, S.F., Mulley, J.C., 1998. Febrile seizures and generalized epilepsy associated with a mutation in the Na+-channel beta1 subunit gene SCN1B. Nat. Genet. 19, 366–370. doi:10.1038/1252

Wandell, B.A., Winawer, J., 2011. Imaging retinotopic maps in the human brain. Vision Res., Vision Research 50th Anniversary Issue: Part 1 51, 718–737. doi:10.1016/j.visres.2010.08.004

Wang, R., 2013. Projection from retina to V1. URL http://fourier.eng.hmc.edu/e180/lectures/v1/node2.html (accessed 2.17.16).

Webster, M.A., De Valois, R.L., 1985. Relationship between spatial-frequency and orientation tuning of striate-cortex cells. J. Opt. Soc. Am. A 2, 1124–1132.

Westbrook, C., Roth, C.K., 2011. MRI in Practice. John Wiley & Sons.

White, B.H., Osterwalder, T.P., Yoon, K.S., Joiner, W.J., Whim, M.D., Kaczmarek, L.K., Keshishian, H., 2001. Targeted Attenuation of Electrical Activity in Drosophila Using a Genetically Modified K+ Channel. Neuron 31, 699–711. doi:10.1016/S0896-6273(01)00415-9

Wiederman, S.D., O'Carroll, D.C., 2013. Selective Attention in an Insect Visual Neuron. Curr. Biol. 23, 156–161. doi:10.1016/j.cub.2012.11.048

Williams, J.R., Sharp, J.W., Kumari, V.G., Wilson, M., Payne, J.A., 1999. The neuron-specific K-Cl cotransporter, KCC2. Antibody development and initial characterization of the protein. J. Biol. Chem. 274, 12656–12664.

Williford, T., Maunsell, J.H.R., 2006. Effects of spatial attention on contrast response functions in macaque area V4. J. Neurophysiol. 96, 40–54. doi:10.1152/jn.01207.2005

Wilson, H.R., Kim, J., 1998. Dynamics of a divisive gain control in human vision. Vision Res. 38, 2735–2741.

Wong, M., 2010. Too Much Inhibition Leads to Excitation in Absence Epilepsy. Epilepsy Curr. 10, 131–132. doi:10.1111/j.1535-7511.2010.01379.x

Yoon, J.H., Maddock, R.J., Rokem, A., Silver, M.A., Minzenberg, M.J., Ragland, J.D., Carter, C.S., 2010. GABA concentration is reduced in visual cortex in schizophrenia and correlates with orientation-specific surround suppression. J. Neurosci. Off. J. Soc. Neurosci. 30, 3777–3781. doi:10.1523/JNEUROSCI.6158-09.2010

Zheng, L., Polavieja, G.G. de, Wolfram, V., Asyali, M.H., Hardie, R.C., Juusola, M., 2006. Feedback Network Controls Photoreceptor Output at the Layer of First Visual Synapses in Drosophila. J. Gen. Physiol. 127, 495–510. doi:10.1085/jgp.200509470